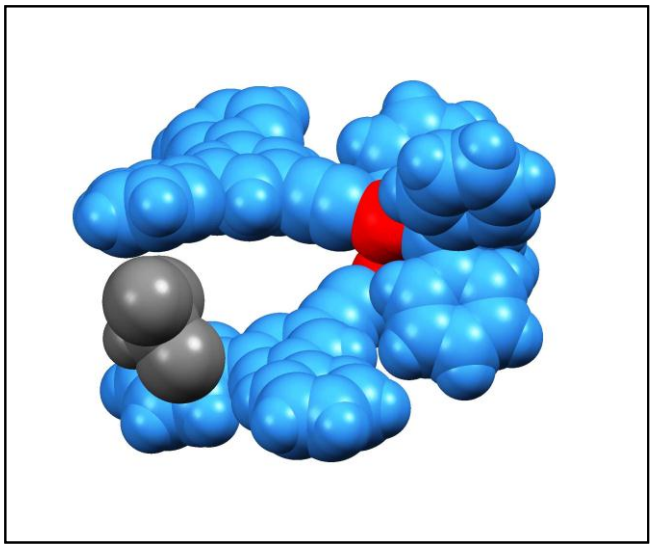

# Gold-Decorated Ligands with Photoactive Properties

PhD thesis of Marzena Kocik

# Gold-Decorated Ligands with Photoactive Properties

## Inauguraldissertation

zur

Erlangung der Würde eines Doktors der Philosophie

vorgelegt der

Philosophisch-Naturwissenschaftlichen Fakultät

der Universität Basel

von

**Marzena Kocik**

aus Polen

**Basel, 2011**

Genehmigt von der Philosophisch-Naturwissenschaftlichen Fakultät auf Antrag
Von

Prof. Dr. Catherine Housecroft  Prof. Dr. Andreas Pfaltz

Basel, den 20.09.2011

Prof. Dr. Martin Spiess
Dekan

creative commons

**Namensnennung-Keine kommerzielle Nutzung-Keine Bearbeitung 2.5 Schweiz**

---

## Sie dürfen:

das Werk vervielfältigen, verbreiten und öffentlich zugänglich machen

## Zu den folgenden Bedingungen:

**Namensnennung**. Sie müssen den Namen des Autors/Rechteinhabers in der von ihm festgelegten Weise nennen (wodurch aber nicht der Eindruck entstehen darf, Sie oder die Nutzung des Werkes durch Sie würden entlohnt).

**Keine kommerzielle Nutzung**. Dieses Werk darf nicht für kommerzielle Zwecke verwendet werden.

**Keine Bearbeitung**. Dieses Werk darf nicht bearbeitet oder in anderer Weise verändert werden.

- Im Falle einer Verbreitung müssen Sie anderen die Lizenzbedingungen, unter welche dieses Werk fällt, mitteilen. Am Einfachsten ist es, einen Link auf diese Seite einzubinden.
- Jede der vorgenannten Bedingungen kann aufgehoben werden, sofern Sie die Einwilligung des Rechteinhabers dazu erhalten.
- Diese Lizenz lässt die Urheberpersönlichkeitsrechte unberührt.



Quelle: http://creativecommons.org/licenses/by-nc-nd/2.5/ch/ Datum: 3.4.2009

Mojej mamie Renacie Kocik

To my mum, Renata Kocik

# Abstract

A series of new phosphinegold(I) decorated ligands was obtained *via* multi-step synthesis. The luminescent properties of the unique molecular system consisting of the π-electron rich 4,4'-diethynyl-2,2'-bipyridine or 4'-ethynyl-2,2':6',2"-terpyridine substituted by phosphinegold(I) units can be tuned by the coordination of different transition metal-ions to polypyridine moieties or even quenched as in the case of the Fe(II) complexes.

Eleven ligands **L1**-**L11**, six of $(R_3PAu{-}{\equiv})_2$bpy type and five of $PR_3Au{-}{\equiv}{-}$tpy type, were synthesised and their characterisation (excluding two) by NMR, UV-Vis, fluorescence spectroscopies and X-ray diffraction is described in chapters 3 and 4. The emission spectra of the ligands have been measured, demonstrating the luminescent properties of these kinds of compounds and studies of their crystal structures reveal an interesting relationship between the steric hindrance of the phosphine moieties and the existence of aurophilic interactions for **L1**-**L9.**

Complexes of these ligands with Zn(II), Fe(II) and Ru(II) are discussed in chapter 5 and their NMR spectra show characteristic changes of the chemical shifts of the proton peaks caused by complexation. Preliminary studies of Fe(II) and Zn(II)-complexes with a bridging ligand (**L8**) show the possibility of macrocycle formation consisting of two ligands and two metal-ions and they are also described in this chapter.

Potentially, compounds **L1**-**L9** with regards to their luminescent properties and anticipated (but not tested), bioactive properties as in the case of many other gold(I) compounds (see chapter 1) may find applications in the antiviral and ani-tumor therapy.

# Acknowledgements

First and foremost, I would like to thank Prof. Dr. Catherine Housecroft and Prof. Dr. Edwin Constable for giving me the chance to do my PhD in Switzerland, for their support and for helping me to solve every problem over the last few years.

I would like to thank Prof. Dr. Andreas Pfaltz for being my co-referee and co-examiner.

I would like to thank the Constable/Housecroft group members both past and present for their help and friendship (in alphabetical order):

Dr. Jonathon Beves, Dr. Imenne Bouamaied, Dr. Biljana Bozic-Weber, Sven Brauchli, Dr. Conor Brennan, Andreas Bünzli, Dr. Anne Chamayou, Dr. Paulina Chwalisz, Dr. Emma Dunphy, Sebastian Fürer, Dr. Stefan Graber, Dr. Ana Hernandez, Dr. Kate Harris, Dr. Marc Häusler, Nik Hostettler, Dr. Swarna Kokatam, Peter Kopecky, Dr. William Kylberg, Dr. Colin Martin**,** Dr. Elaine Medlycott, Dr. Niamh Murray, Dr. Jason Price, Dr. Pirmin Rosel, Jennifer Rudd, Ralf Schmitt, Gabriel Schneider, Ewald Schönhofer, Jonas Schönle, Alexandra Senger, Liselotte Siegfried, Marketa Smidkova, Dr. Umut Soydaner, Dr. David Vonlanthen, Dr. Iain Wright, Dr. Jennifer Zampese and Dr. Guoqi Zhang.

I would like to thank the people who corrected my thesis for their patience and all valuable comments: Prof. Dr. Catherine Housecroft, Karolina Langowska, Dr. Iain Wright, Dr. Niamh Murray, Jennifer Rudd, Dr. Małgorzata Hołynska, Dr. Jennifer Zampese and Dr. Kate Harris.

I would like to thank my family and all my friends for their support and help, especially: my mum Renata Kocik, my brother Paweł Kocik, my aunt Marzena Magarewitsch and Irena Simkowa, Natalia Woźniak, Karolina Langowska, Dr. Paulina Chwalisz, Dr. Małgorzata Hołynska, Natalia Wisłowska-Szkudlarek and Katarzyna Kijek.

I would like to thank people who work at University of Basel and have helped me to solve a lot problems, especially: Beatrice Erismann, Markus Hauri and Dr. Bernhard Jung.

Last but not least I would like thank the Swiss National Science Foundation and the University of Basel for financial support.

# Contents

**ABBREVIATIONS**

**1. GENERAL:**

| | |
|---|---|
| A1-A8 | Symbol of centroids in X-Ray |
| AcBr | Acetyl bromide |
| AcOH | Acetic acid |
| bpy | 2,2'-Bipyridine |
| bpyl | 2,2'-Bipyridin-5-yl |
| *t*-Bu | *tert*-Butyl |
| DIPA | N,N-Diisopropylamine or Bis(isopropyl)amine |
| dmmp | Bis(dimethyphosphinomethyl)methylphosphine |
| dmpm | Bis(dimethylphosphino)methane |
| DMSO | Dimethyl sulfoxide |
| dpmp | Bis(diphenylphosphinomethyl)phenylphosphine |
| dppa | Bis(diphenylphosphanyl)acetylene |
| dppb | 1,4-Bis(diphenylphosphino)butane |
| dppd | 1,10-Bis(diphenylphosphino)decane |
| dppe | 1,2-Bis(diphenylphosphino)ethane |
| dppf | 1,1'-Bis(diphenylphosphino)ferrocene |
| dppip | Bis(diphenylphosphanyl)isopropane |
| dppm | 1,2-Bis(diphenylphosphino)methane |
| dppp | 1,3-Bis(diphenylphosphino)propane |
| Et | Ethyl |
| Hacac | Acetylacetone |
| Hhfac | Hexafluoroacetylacetonate |
| HOMO | Highest occupied molecular orbital |
| IL | Intraligand |
| LC | Ligand-centered |
| LUMO | Lowest occupied molecular orbital |
| MC | Metal-centered |
| MeOH | Methanol |
| Mes | 2,4,6-Trimethylphenyl |
| MLCT | Metal-to-ligand charge transfer |
| MMLCT | Metal-metal-to-ligand charge transfer |
| Ph | Phenyl |
| Pip | Piperidine |
| *i*-Pr | *iso*-Propyl |

| | |
|---|---|
| Tf | Tri(fluoromethyl)sulfonyl |
| TFMSA | Trifluoromethanesulfonic anhydride |
| THF | Tetrahydrofuran |
| TPA | 1,3,5-Triaza-7-phosphaadamantane |
| tht | Tetrahydrotiophen |
| TMS | trimethylsilanyl |
| *m*-Tol | *meta*-Tolyl |
| *o*-Tol | *orto*-Tolyl |
| *p*-Tol | *para*-Tolyl |
| tpy | 2,2':6',2"-Terpyridine |
| Xy | 2,6-Dimethylphenyl |

## 2. EXPERIMENTAL METHODS:

- *Mass Spectrometry (MS ):*

| | |
|---|---|
| ESI-MS | Electrospray Ionization Mass Spectroscopy |
| m/z | Mass to charge ratio |
| MALDI-MS | Matrix assisted laser desorption ionisation Mass Spectroscopy |

- *Elemental Analysis (EA) :*

| | |
|---|---|
| *calc* | Calculated |

- *Fluorescence Spectroscopy:*

| | |
|---|---|
| $\lambda_{ex}$ | Excitation wavelength [nm] |
| $\lambda_{em}$ | Emission wavelength [nm] |
| [a.u.] | Arbitrary unit |

- *Nuclear Magnetic Resonance (NMR) Spectroscopy:*

| | |
|---|---|
| $^{13}$C NMR | $^{13}$C Nuclear Magnetic Resonance |
| $^{1}$H NMR | $^{1}$H Nuclear Magnetic Resonance |
| $^{31}$P NMR | $^{31}$P Nuclear Magnetic Resonance |
| COSY | Correlated Spectroscopy |
| DEPT | Distortionless Enhancement by Polarisation Transfer |
| HMBC | Heteronuclear Multiple Bond Correlation |
| HMQC | Heteronuclear Multiple Quantum Correlation |
| NOESY | Nuclear Overhauser Effect Spectroscopy |

| | |
|---|---|
| br | Broad |
| δ | Chemical shift (ppm) |
| d | Doublet |
| dd | Doublet of doublets |
| ddd | Doublet of doublet of doublets |
| ddt | Doublet of doublet of triplets |
| dq | Doublet of quartets |
| dt | Doublet of triplets |
| dτ | Delay time |
| *J* | Coupling constant [Hz] |
| m | Multiplet |
| NS | Number of scans |
| s | Singlet |
| t | Triplet |
| td | Triplet of doublets |

- *Ultraviolet-Visible (UV-VIS) Spectroscopy :*

| | |
|---|---|
| ε | Extinction coefficient [$dm^3mol^{-1}cm^{-1}$] |
| $\lambda_{max}$ | Wavelength at which maximum absorption occurs [nm] |

## GENERAL EXPERIMENTAL

- *NMR spectroscopy*

$^{1}H$, $^{13}C$, $^{31}P$ NMR spectra were recorded on Bruker Avance DRX 400 or DRX 500 MHz spectrometers.

- *Mass spectrometry*

Electrospray ionization (ESI) mass spectra were recorded with Finnigan MAT LCQ or Bruker esquire $3000^{plus}$ spectrometers. MALDI-TOF mass spectra were recorded using PerSeptive Biosystems Voyager mass spectrometer.

- *Ultraviolet-Visible (UV-VIS) Spectroscopy*

Electronic absorption spectra were recorded with a Varian-Cary 5000 spectrophotometer.

- *Fluorescence Spectroscopy*

Emission spectra were recorded with a Shimadzu RF-5301 PC spectrofluorometer.

- *X-Ray*

Data was collected with a Bruker-Nonius Kappa CCD or Stoe IPDS diffractometer.

- *Microwave reactions*

Microwave reactions were performed under argon in a Biotage Initiator 8 reactor.

# 1. Introduction

## 1.1. Gold

Gold has been present in our culture since ancient times. As a symbol of wealth, it was used in the decoration of temples (e.g. golden calves, ritual vessels), in the production of jewellery, cloths (gold threads) and coins [1], [2], [3].

Gold was such a desirable raw material that alchemists spent all their life searching for the philosopher's stone, which in their opinion could transmute the base metals (especially lead) into gold [1]. Even though the alchemists never achieved the transmutation of base metals to gold, their contributions to science were crucial to the development of the field of chemistry.

The dreams of alchemists came true in 1980 when Glenn Seaborg - Nobel Laureate in Chemistry obtained a small amount of gold from lead. There are also reports that this happened earlier in 1972 in the Soviet Union. Soviet physicists found out that the lead shielding of an experimental nuclear reactor had changed to gold. Even though nuclear experiments have successfully transmuted lead into gold, the expense of this process far exceeds the value of the gold obtained this way [2].

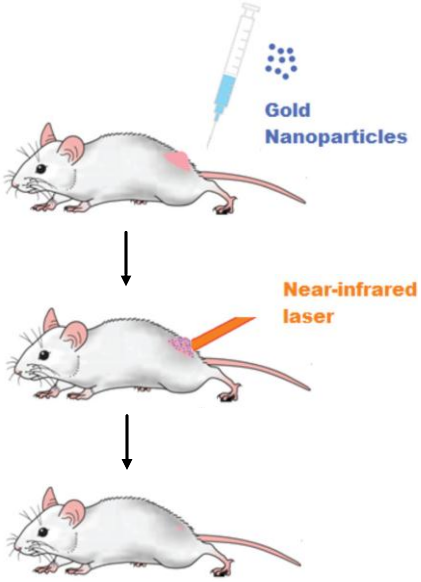


**Figure 1.1** Gold nanoparticle thermal therapy [5].

Gold has been used as a drug in China since 2500 BC but the first *in vitro* antibacterial activity of gold was discovered by Robert Koch in 1890, who observed the inhibition of the tuberculosis bacteria growth [3], [4].

Nowadays, gold containing compounds are widely investigated with regards to their bacteriostatic, antiviral and antitumor properties [5]-[7]. Gold being a soft acid (using Pearson's definition [8]) is known to bind strongly with soft bases like thiols. Proteins including cysteine and lysine residues are unique ligands for binding to metal nanoparticles such as gold and this alters their biological activities [4]. One of the promising antitumoral therapies is gold nanoparticle thermal therapy (**Figure 1.1**), which provides an opportunity for effective treatment against chemotherapy-resistant cancers [5], [9], [10].

Gold as an inert metal is used in surface engineering [11], while gold nanoparticles and gold containing compounds have many other applications including DNA detection,

biosensors, clinical laboratory diagnostics, integrated photothermal nanodiagnostics and nanotherapy as mentioned previously, microemulsions, drugs, catalysis, electrochemical nanobiosensors and fingerprint detection [6], [10], [12]-[14].

With such a wide range of potential applications, the basic investigations of gold containing compounds is a very important field of research.

## 1.2. Aurophilicity and aurophilic interactions

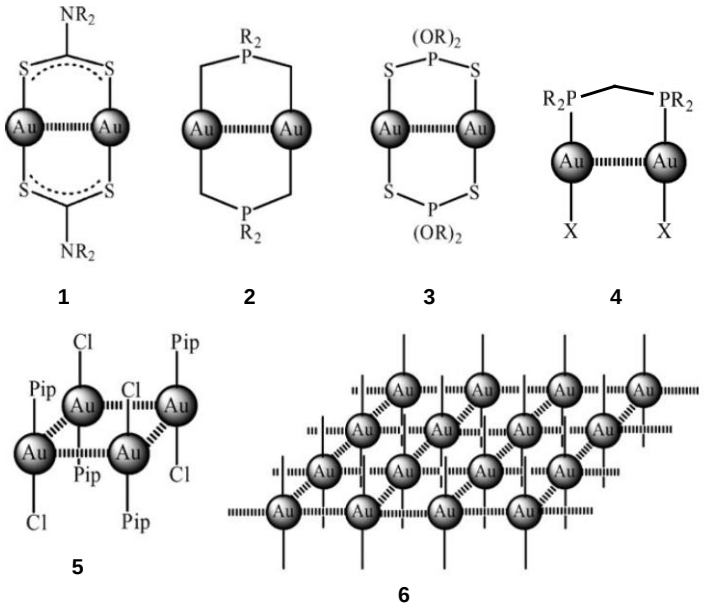


**Figure 1.2** Au-Au interactions in: dimeric gold(I) dithiocarbamates (**1**), dialkylphosphonium-bismethylides (**2**) dialkyldithiophosphates (**3**), R= Ph, X= Cl, $(dppm)(AuCl)_2$ (**4**), a tetramer of (piperidine)AuCl (**5**), a sheet of aggregated (MeNC)AuCN (**5**) [15].

Short Au-Au bonds and unexpected twists in the crystal structure of gold containing compounds have been observed over many years. The first reported compounds demonstrating Au-Au interactions are illustrated in **Figure 1.2** [16]-[21]. Compounds **5** and **6** show the arrangement of gold atoms in a square (**5**) and these squares form gold sheets in the case of **6,** suggesting the existence of some interactions responsible for this unusual crystal packing.

Schmidbaur and Schier in their review define aurophilicity as follows:

"Aurophilicity appears to be operative between closed-shell gold centres in the formal oxidation state Au(I) (with the valence electronic configuration $5d^{10}$) and in the linearly two-coordinate state. The low coordination number is an important prerequisite since it minimizes steric repulsions between ligands in the aggregates" [15].

**Aurophilic interactions** were classified as weak forces with bond energies in the range of **21-62 kJ/mol** and with a wide of range of distances **2.8-3.5 Å** [15]. Au-Au bonding, also called "super van der Waals bonding", is formed by 6s, 6p and 5d orbital mixing and cannot be explained by conventional valence theory [15].

In sections 3.7 and 4.7, the terms aurophilicy, aurophilic interaction and Au-Au contact will be used interchangeably.

## 1.2.1. Intramolecular Au-Au contacts

Intramolecular Au-Au interactions are present in a range of single molecules containing two Au atoms. Short Au-Au contacts from 2.59 (for **7**) to 3.12 (for **13**) Å in bridged phosphine gold halides (**Figure 1.3**) force these compounds into a Z-conformation (here, related with the positions of the Au atoms) [15], [22]–[29]. The shortest regular Au-Au bond is present in $Au_2$ (dimer) in the gas phase and is 2.47 Å in length [15], [30].

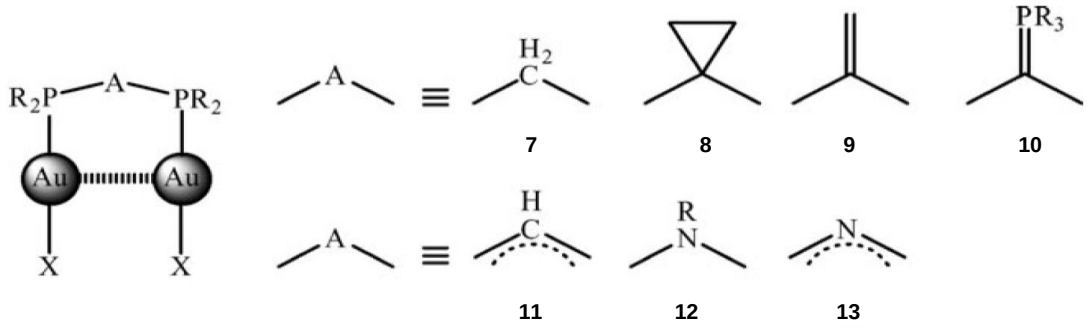


**Figure 1.3** Schematic structures of bridged phosphine gold(I) halides **7-13** [15].

Short Au-Au intermolecular interactions of 3.02 (**14**), 3.09 (**15**) and 3.05 (**16**) Å (**Figure 1.4**) were found in the analogues of compounds **7-13** and the slight increase of the bridge length (to two C-atoms between P-atoms) does not drastically influence the strength of these interactions. A Z-conformation is also preferred for these compounds [15], [31]-[33].

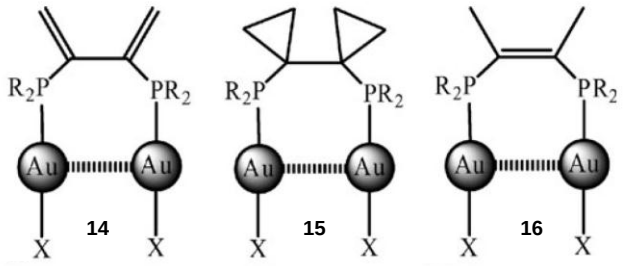


**Figure 1.4** Schematic structures of bridged phosphine gold(I) halides **14-16** [15].

The folding of macrocycle **17** (**Figure 1.5**) by twisting two xantphos moieties is caused by a short Au-Au interaction (2.86 Å). The conformation of **17** with two loops separated by a Au-Au bond is evidence for weak Au-Au forces. The crystal structure contains both right- and left-handed molecules of this compound [34].

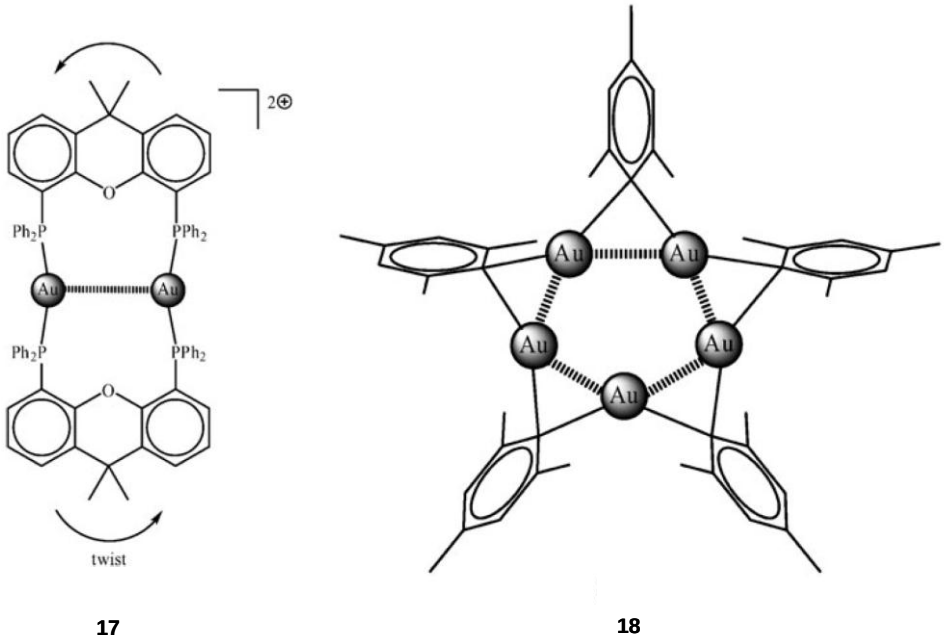


**Figure 1.5** Structures of the cation in $[Au_2(\mu\text{-xantphos})_2](NO_3)_2$ (**17**) and of complex $(AuMes)_5$ (**18**) [15].

Compound **18** (**Figure 1.5**) was synthesised by the reaction of AuCOCl with a stoichiometric amount of MesMgBr. The molecular structure of **18** shows the star-like shape of this complex supported by a pentagon of gold atoms. The linear geometry characteristic of Au(I) is puckered here by the Au-Au interactions (*ca*. 2.70 Å). Also, unusual stabilization of the metal-carbon bond may be caused by the presence of the Au-Au contacts [35].

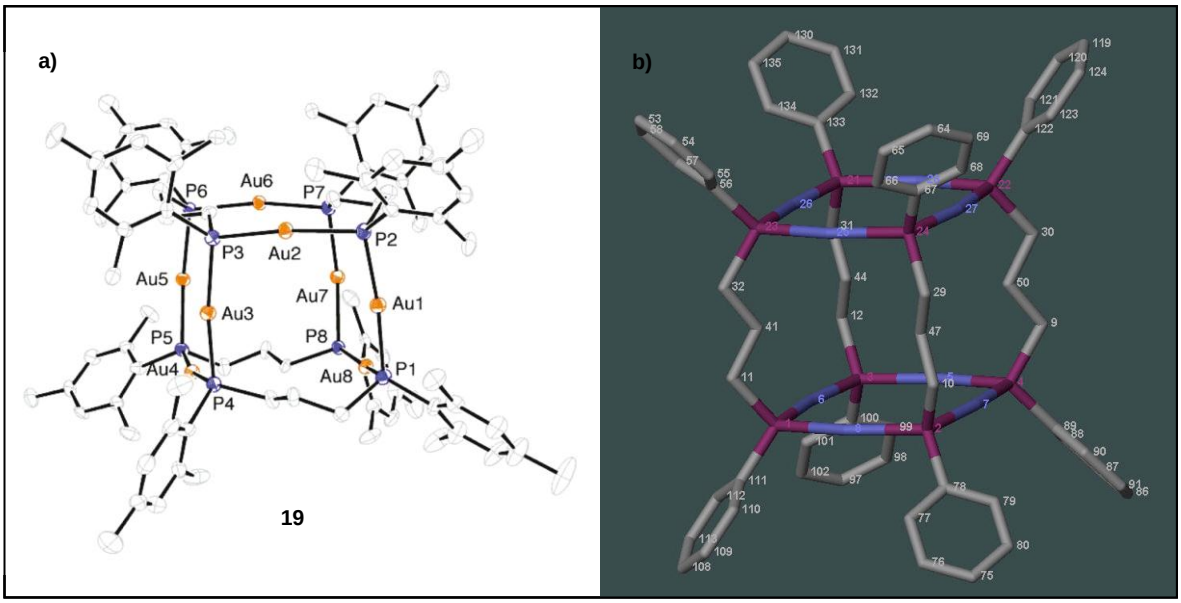


**Figure 1.6** ORTEP diagram of $[Au(PMes(CH_2)_3PMes)Au]_4$ (**a)**), DFT calculated structure of $[Au(PPh(CH_2)_3PPh)Au]_4$ (**b)**) [36].

Lane e*t al.* reported the cubic structure of $[Au(PMes(CH_2)_3PMes)Au]_4$ (**Figure 1.6**). DFT calculations for **19** (Ph instead of Mes substituents) show very good agreement with the crystal structure of this compound. The Au-Au distances are in the range of 3.49-3.66 Å and are longer than typical aurophilic interactions (2.8-3.5 Å). The nearly linear geometry of the P-Au-P rods in the crystal structure, forced by the Au-atom, confirms the lack of Au-Au interactions. Intramolecular Au-Au interactions in the molecular structure of **19** could also distort the cube structure of this compound [36].

## 1.2.2. Intermolecular Au-Au contacts

Au-Au intermolecular interactions are mostly found in gold complexes containing only one Au atom and in which ligands are not steric hindrances to this kind of interaction.

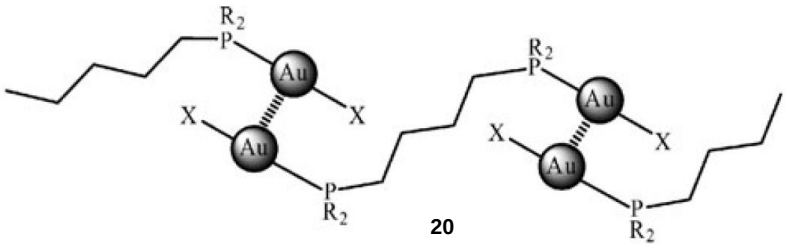


**Figure 1.7** Intermolecular Au-Au interactions for X= S(*p*-Tol), R = Ph [15].

Intermolecular interactions in bridged phosphine gold(I) halides are described in section 1.2.1. The extension of the phosphine bridge to four (**20**, **Figure 1.7**) or five atoms (instead of one or two) and the change of halides to 4-mercaptotolyl (4-methylthiophenyl) leads to intermolecular Au-Au contacts of lengths 3.09 and 3.20 Å, respectively. A characteristic "head-to-tail" motif can be singled out in the crystal structure and forming a zigzag pattern can be also observed in the crystal packing (**Figure 1.7**) [37].

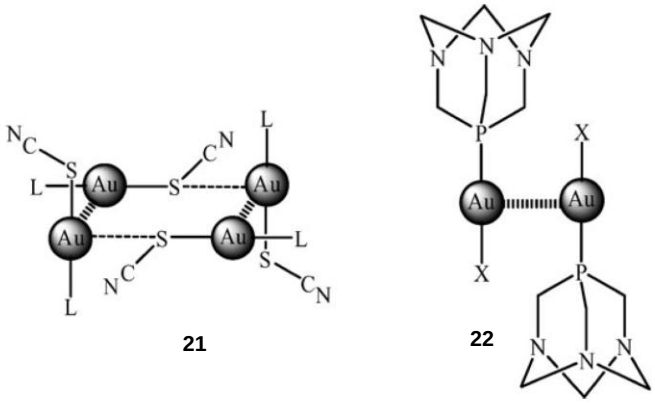


**Figure 1.8** Tetramer of $Me_3PAuSCN$ (**21**), dimer of TPAAuX, X=Cl (**22**) [15].

$Me_3PAuCl$ and $Me_3PAuCN$ containing a small, tertiary phosphine form chains connected by intermolecular Au-Au interactions with a length of *circa* 3.30 Å [38].

Intramolecular Au-Au interactions (3.10 Å) cause dimerisation of $Me_3PAuSCN$ (**21**) and the Au…S contact (3.77 Å) to neighbouring dimers furthers the assembly into tetramers (**Figure 1.8**) [39]. Also, the gold complex (**22**), which has an interesting cage type phosphine ligand associates into dimers *via* intermolecular Au-Au interactions. "Head-to-tail" positioning of the molecules in the dimer is the preferred conformation (**Figure 1.8**) [40].

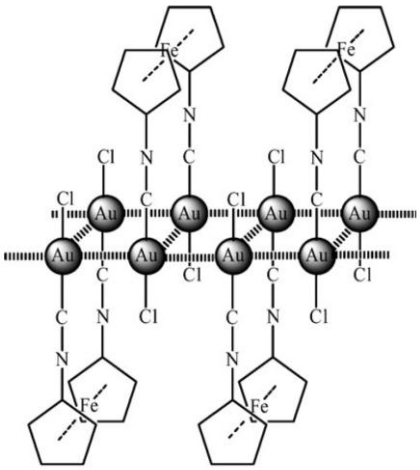

**Figure 1.9** View of the association of of 1,1'-diisocyanoferrocenegold(I)chloride (23) in the crystal structure [15].

For compounds containing two gold atoms in the molecular structure, both intra- and intermolecular aurophilic interactions can occur and usually these Au-Au contacts completely control the crystal structure packing. In many cases they form aggregates of molecules as for **23** (**Figure 1.9**) and **24** (**Figure 1.10**) [41], [42].

The crystal packing of **23** shows Au atoms aggregated in the corrugated ladder-like structure, in which intramolecular Au-Au bonds are the rungs of this ladder (Au-Au distance 3.34 Å) and intermolecular Au-Au bonds, length 3.48 and 3.35 Å, form the frame [41].

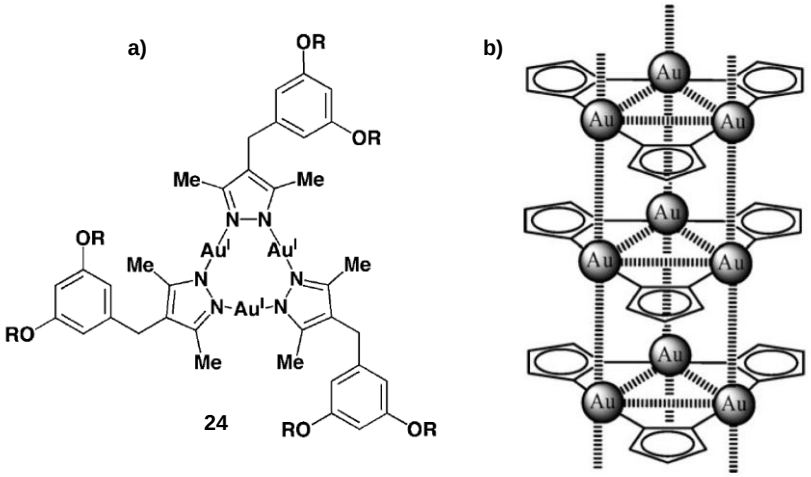


**Figure 1.10 a)** Trinuclear Au(I) pyrazolate complex, R = $C_{18}H_{37}$, **b)** schematic self-assembled structure of **24** [42],[15].

Au(I)-Au(I) metallophilic interactions cause a gelation of **24** (**Figure 1.10**) in hexane solution at room temperature. Additionally, when obtained this way, the gel emits red light, which changes to blue after the addition of a small amount of Ag(I). The process of gelation is thermoreversible, and the sol-gel changes can be repeated without decomposition of **24** [42]. The aurophilic short contacts form self-assembling structures (**Figure 1.10**, **b**) containing intra- and intermolecular Au-Au interactions.

## 1.3. Gold(I) complexes with phosphine ligands

Au…Au interactions influence the crystal packing (section 1.2.1, 1.2.2) but can also change the luminescent properties. Yam and Cheng reported two homoleptic gold(I) complexes $[Au_2(dmpm)_2](ClO_4)_2$ and $[Au_3(dmmp)_2](ClO_4)_3$, in which dual phosphorescence with bands $\lambda_{em}$ = 455 and 555 nm and $\lambda_{em}$ = 467 and 580 nm, respectively, are observed [43]. The increase of the number of linear aggregated intramolecular Au-Au interactions from two in $[Au_2(dmpm)_2](ClO_4)_2$ to three in $[Au_3(dmmp)_2](ClO_4)_3$ cause a red shift of bands in both the electronic and fluorescence spectra 269 nm→315 nm ($^1[d\sigma^*\rightarrow p\sigma]$) and 555 nm→570 nm ($^3[(d\delta^*)^1(p\sigma)^1]$), respectively. As is illustrated in **Figure 1.11** this can be explained by the reduction of the energy gap **(**dσ*-pσ and dδ*-pσ) [44].

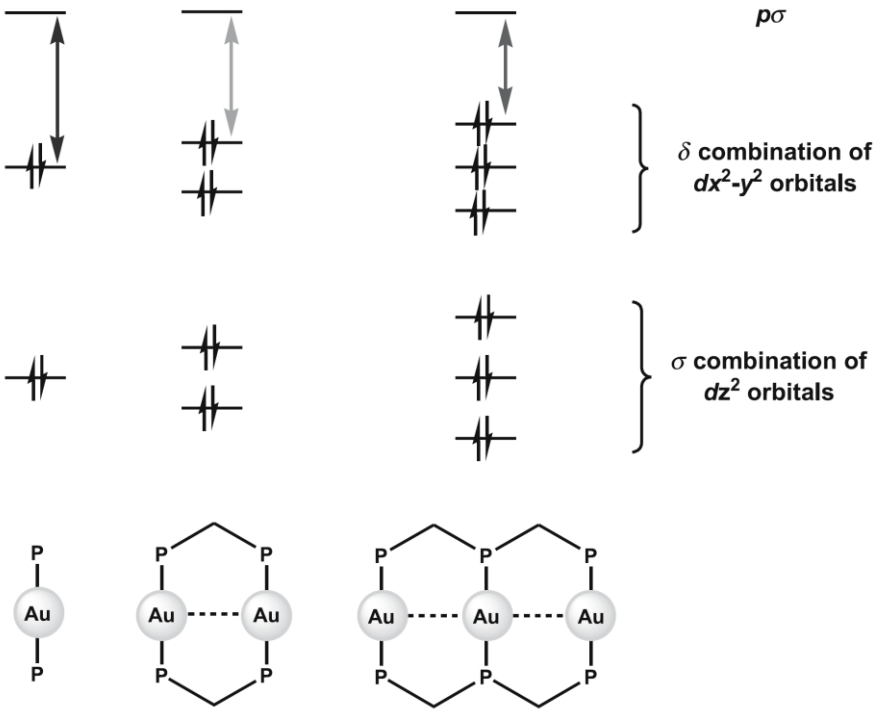


**Figure 1.11** Schematic molecular orbital diagram showing the effect of aurophilic contacts on the HOMO-LUMO energy gap of gold(I) phosphine complexes [44].

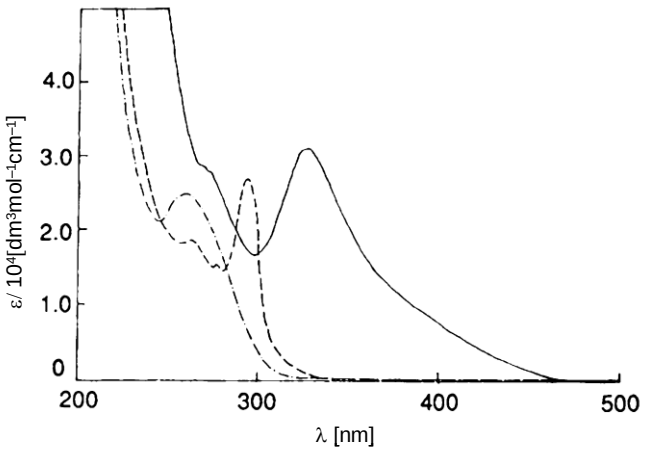


**Figure 1.12** Electronic absorption spectra of $[Au(PPh_3)_2]OTf$ (– · – · – ·), $[Au_2(dppm)_2](OTf)_2$ (– – –) and $[Au_3(dpmp)_2](SCN)_3$ (—) in MeCN at room temperature [44].

The same effect is observed in the case of $[Au(PPh_3)_2]OTf$, $[Au_2(dppm)_2](OTf)_2$ and $[Au_3(dpmp)_2](SCN)_3$. An increase in the number of linear aggregated Au-Au interactions decreases the energy gap between the hybridized Au orbitals and causes a red shift in the electronic absorption spectra (**Figure 1.12**).

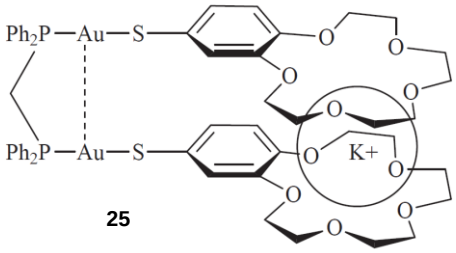


**25**

**Figure 1.13** A proposed binding mode in which a potassium ion is sandwiched between the benzo-15-crown-5 units of the dinuclear gold(I) complex (**25**) [45].

Dinuclear gold(I) crown-ether complex (**25**, **Figure 1.13**) also shows the strong dependence of the luminescent properties on Au-Au intramolecular interactions. Addition of $K^+$ causes a change to the sandwiched position of the two crown-ether units and decreases the Au-Au distance.

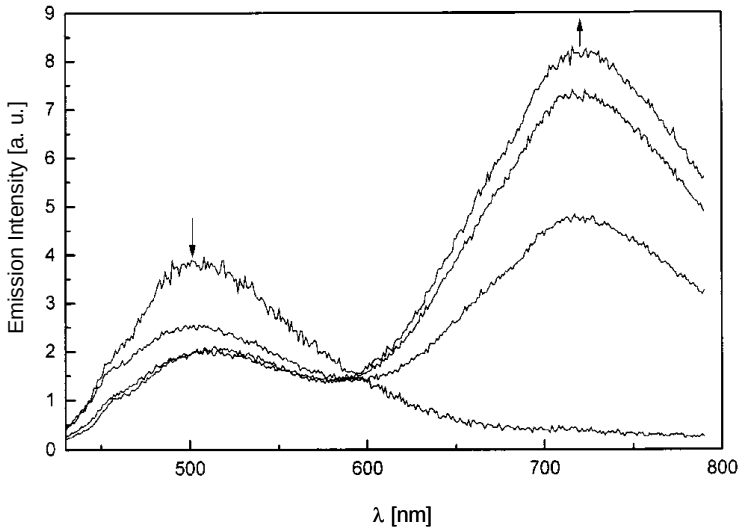


**Figure 1.14** Emission spectra of **25** (1.7 mM) upon addition of various concentrations of potassium ions in $CH_2Cl_2$–MeOH [45].

Weak Au-Au interactions reduce the energy gap between orbitals (**Figure 1.15**), which results in the growth of a new band about 720 nm (**Figure 1.14**) for this compound [45]. The authors claim that this lower energy transition (red emission) arises from a LMMCT (ligand-to-metal-metal bond charge transfer) from the thiolate ligand to the Au-Au bond [$RS^- \rightarrow Au_2$] excited state [46].

Compound **25** shows a high selectivity towards $K^+$ and one $K^+$ cation is sandwiched between two crown-ethers. This bonding causes a change in the luminescent properties, which can be applied to the development of sensing materials for different analytes [45].

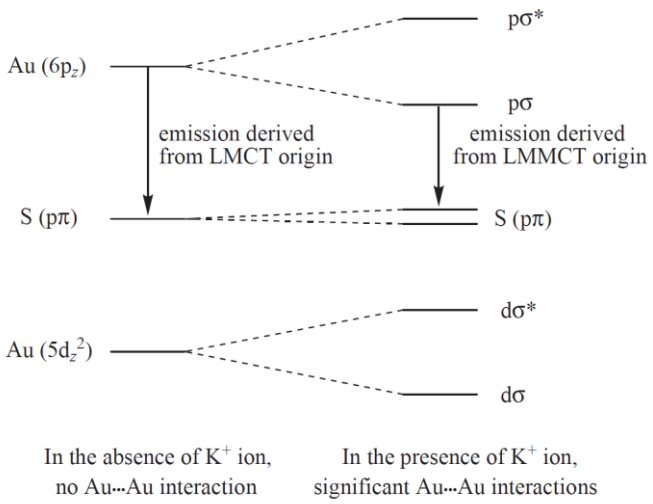


**Figure 1.15** A schematic representation of the orbital splittings in **25** in the absence and in the presence of potassium ion binding [45].

A lot of gold(I) phosphine complexes have recently been investigated with regards to their bioactive properties and their potential application as drugs [47]. Auranofin (**26**) is a well known drug for the treatment of rheumatoid arthritis, but *in vivo* studies on monkeys also show a reduction of the viral reservoir of HIV [48]. Au-Naphth-1 (**27**) is an analogue of **26** and was designed as a drug with improved cellular uptake and shows promising preclinical results in the treatment of cancer [49].

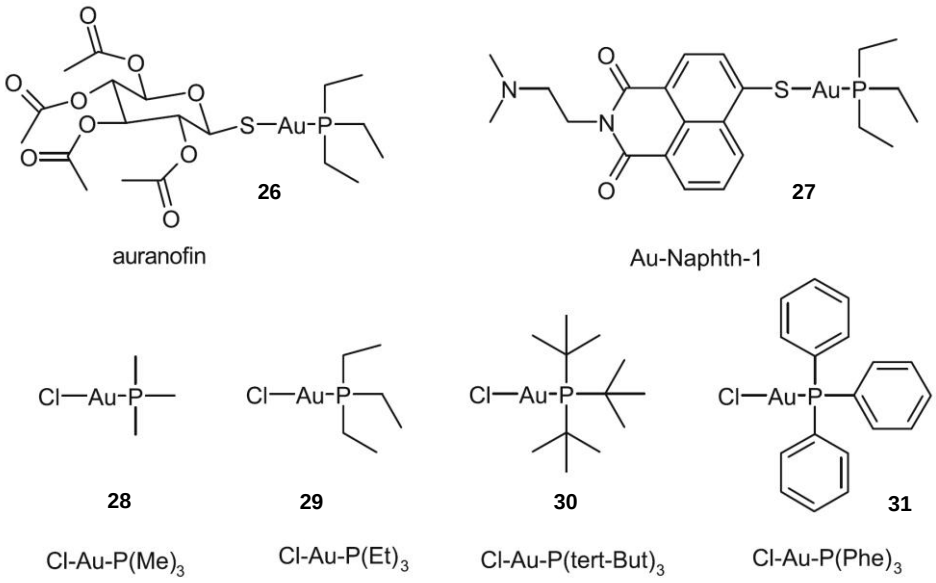


**Figure 1.16** Bioactive gold(I) phosphine complexes [47].

Compounds **28-31** (**Figure 1.16**) show antiproliferative effects against colon and breast cancer cells. However a currently unsolved problem with using gold(I) complexes as drugs is their rather low cytoselectivity [47].

## 1.4. Gold(I) alkynyl complexes

Gold(I) alkynyl complexes with the preferential linear geometry of gold(I) and (R—≡—H) unit are widely used as building blocks for molecular design and they find many applications as luminescent materials, optical switches, and in electronics, catalysis and molecular recognition [44], [50].

A structurally interesting, gold(I) alkynyl complex based on aurophilic interactions, is illustrated in **Figure 1.17**. Short Au-Au contacts in the range 3.25 to 3.30 Å allow a rod, which is placed inside this rotaxane, to be held. The system demonstrates a threefold symmetry, in which the rod of the rotaxane is the $C_3$ rotation axis [15], [51].

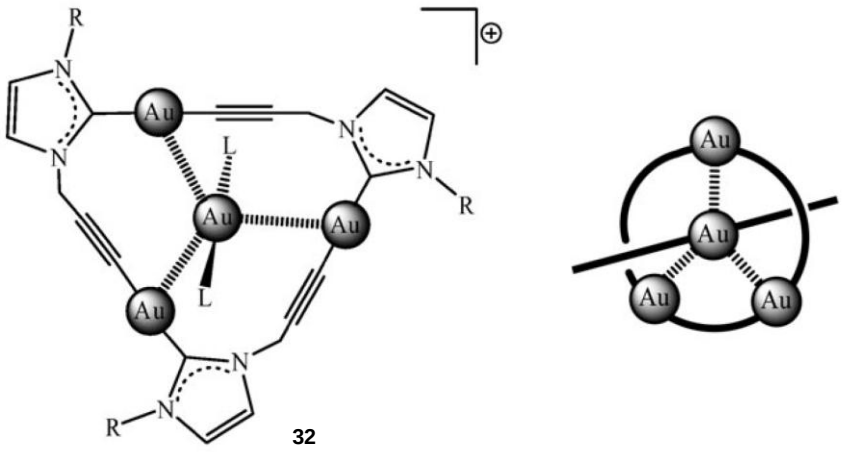


**Figure 1.17** The rotaxane ring composed of a cyclic trinuclear gold complex and the $Au(PMe_3)_2^+$ rod [15].

Luminescent properties of tetranuclear gold(I) alkynylcalixarene complexes **33** and **34** **(Figure 1.18)**, could be tuned by the addition of metal ions such as $K^+$ and $Na^+$ similarly to **25**. Au-Au contacts between adjacent gold atoms observed in the crystal structure of **33** are 3.1344(8) and 3.2048(8) Å and a narrowing of the HOMO–LUMO energy gap caused by intramolecular Au-Au interactions influences the emission this complex [44], [52].

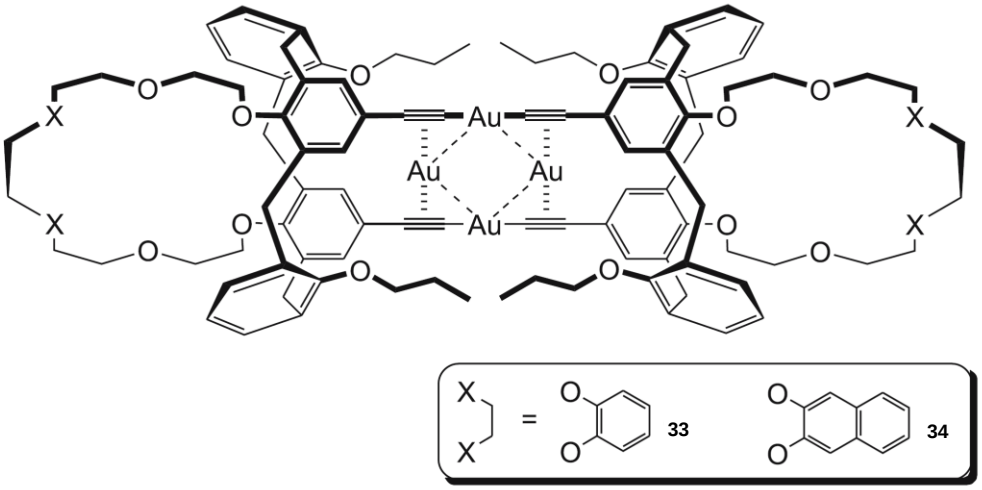


**Figure 1.18** Structure of the luminescent tetranuclear gold(I) alkynylcalixarene complexes **33** and **34** [44].

A series of gold(I) alkynyl complexes was reported by Vincente and co-workers, in which the pyridine ring is substituted in the 3,5-positions by gold(I) alkynyl phosphine chains as in **Figure 1.19** [53]. Unfortunately, the authors did not describe the luminescent properties of these compounds.

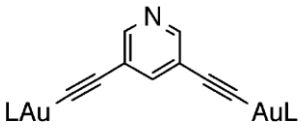


**L** = *t*-BuNC (**35**), $Me_3P$ (**36**), $Ph_3P$ (**37**), $(p\text{-Tol})_3P$ (**38**)

**Figure 1.19** Structures of **35**, **36**, **37**, **38** [53].

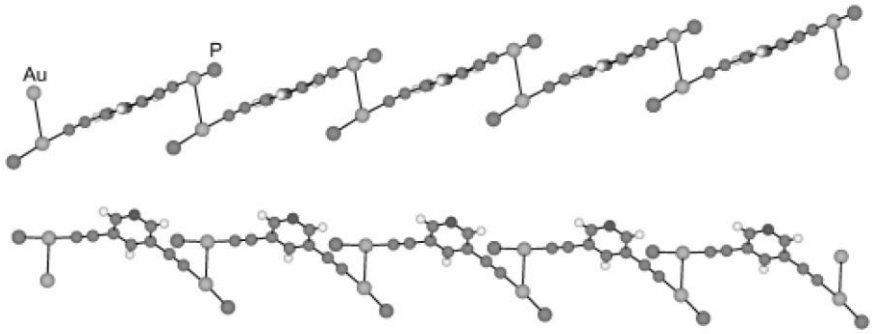


**Figure 1.20** Two different views of the aurophilic contacts in **38** giving rise to infinite chains. The tolyl groups and the hydrogen atoms have been omitted [53].

The crystal packing of **38** is very interesting (**Figure 1.20**). Molecules are arranged in a zigzag form, in which parallel layers are connected by Au-Au bonds (3.23 Å) [53].

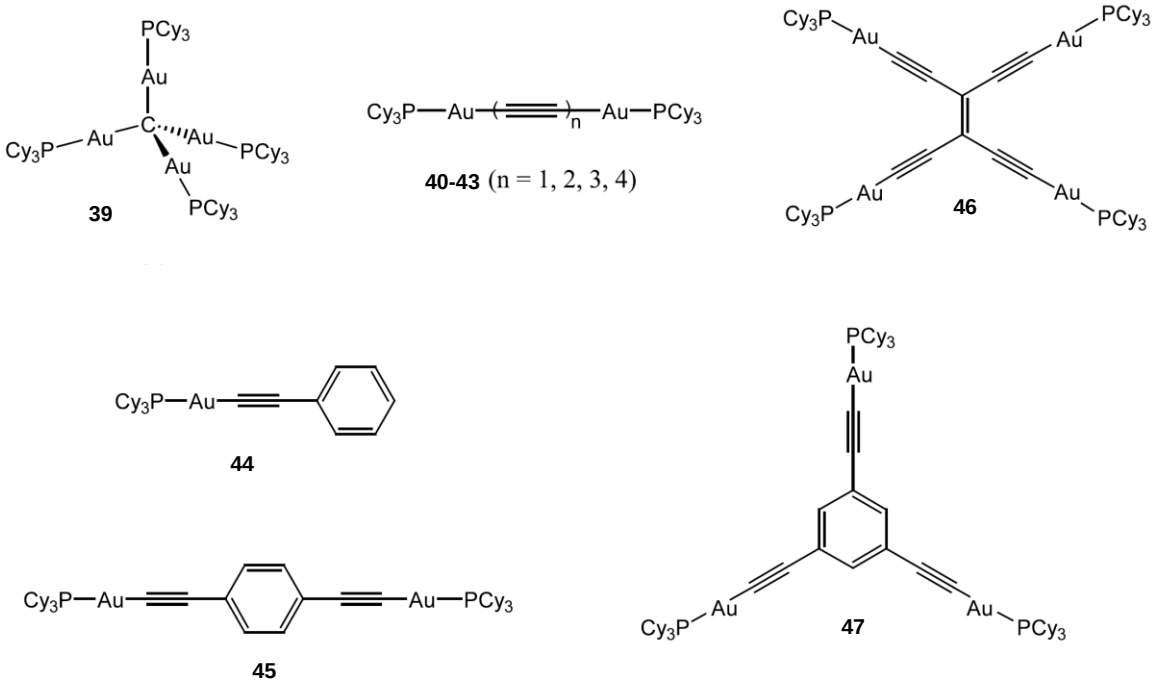


**Figure 1.21** Examples of gold(I) alkylyl complexes **39-47** [54].

Two carbon rich gold(I) acetylide complexes (**46**, **47**) illustrated in **Figure 1.21** were obtained by Lu and co-workers. Comparison of **39-47** leads to the conclusion that the spectroscopic nature of these compounds is strongly dependent on the carbon rich conjugated/cross-conjugated organic framework. As a result of this, **46** exhibits $^{1}(\pi\text{-}\pi^*)$ fluorescence at 413 nm and 428 nm whereas for **47,** $^{3}(\pi\text{-}\pi^*)$ phosphorescence at 446 nm and 479 nm can be observed [54].

A series of gold(I) ethynylpyridine complexes **48**-**56** was reported by Ferrer *et. al.* (**Figure 1.22**). All of these compounds demonstrate luminescent properties, excluding **55** (due to quenching by the ferrocenyl unit). Au-Au intramolecular interactions are present in the crystal structure of **50**, **51** and **56** of length 3.24, 2.98 and 3.38 Å, respectively. The Au-Au contact in **51** is the shortest compared with reported compounds, which are analogous to **51** [55].

It is worth mentioning that the metal–metal separation in metallic gold is 2.89 Å and the sum of the van der Waals radii is 3.6 Å [51].

For compounds **53** and **54** any Au-Au interactions are not observed while **52** forms an aurophilic chain *via* intramolecular Au-Au interactions. The range of this interaction is 3.38 Å (**Figure 1.23**).

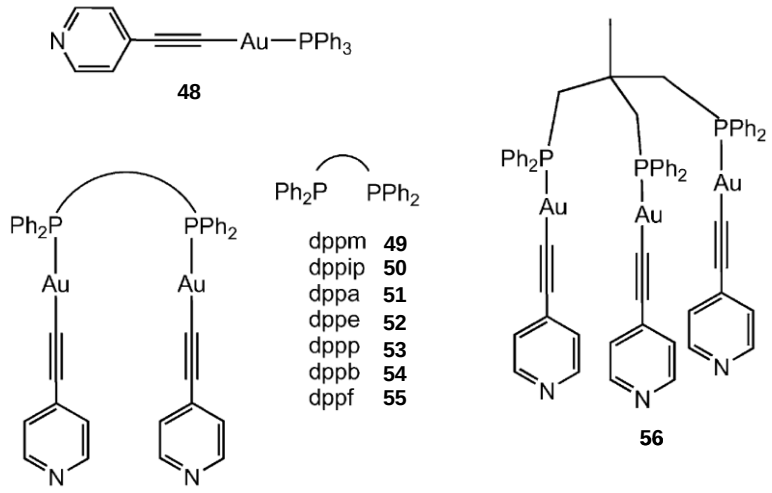


**Figure 1.22** Structures of gold(I) ethynylpyridine complexes **48-56** [55].

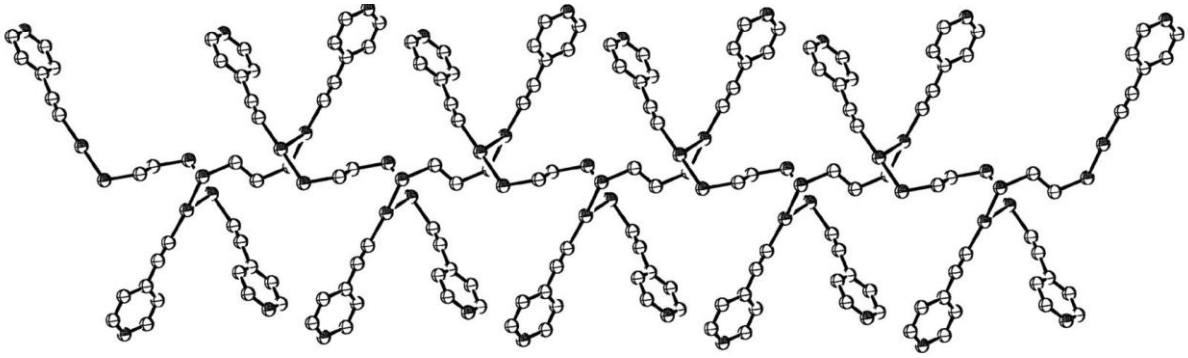

**Figure 1.23** Supramolecular association in **52** through intermolecular aurophilic contacts to form an infinite chain. The phenyl rigs of dppe are omitted for clarity [55].

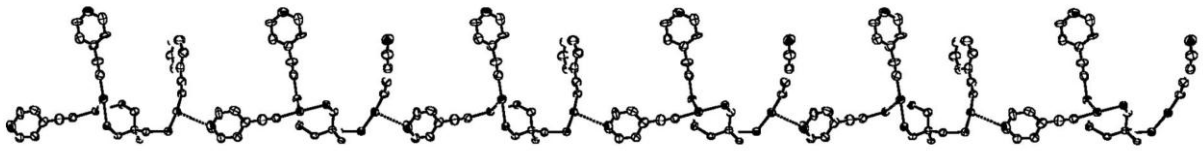

**Figure 1.24** Supramolecular association in **56** through intermolecular N···Au interactions to form an infinite chain. The phenyl rigs are omitted for clarity [55].

Intermolecular N…Au interactions (3.13 Å) can be observed in the crystal structure of **56** and cause it to assemble in a chain structure as shown in **Figure 1.24** [55].

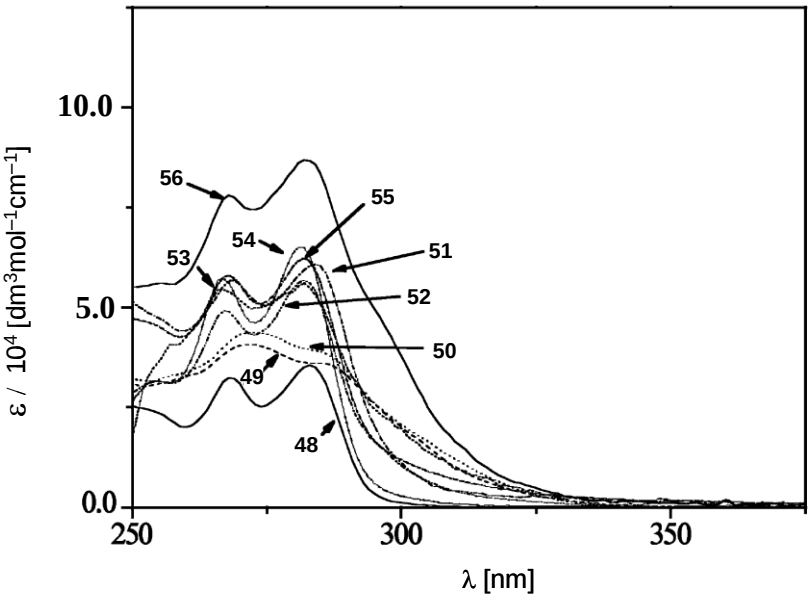


**Figure 1.25** Electronic absorption spectra of compounds **48**-**56** in $CH_2Cl_2$ ($10^{-6}$ M) [55].

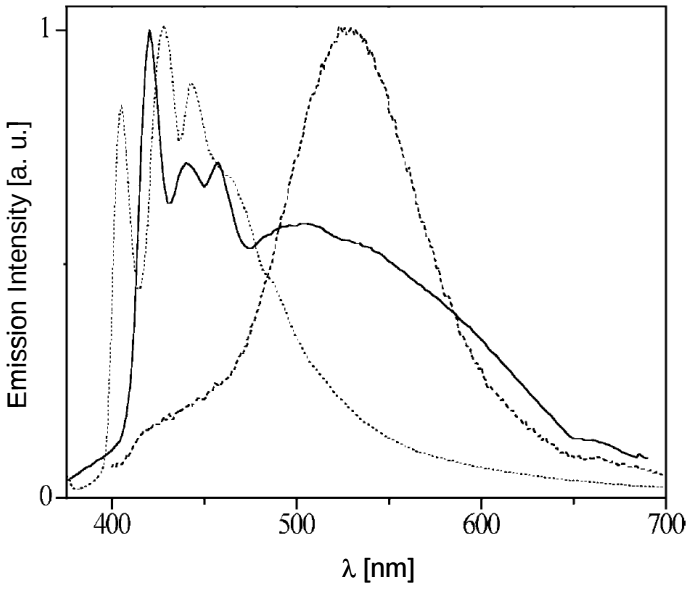


**Figure 1.26** Solid-state emission spectra of compounds **48** (dotted line), **50** (solid line) and **51** (dashed line) upon excitation at $\lambda_{ex}$ = 360 nm at room temperature [55].

**Figure 1.25** illustrates absorption spectra of compounds **48**-**56** and shows that the spectra of compounds **48**, **51**-**56** all exhibit similar features. Differences in the absorption spectra of **49** and **50** may be caused by Au-Au interactions existing in solution.

**Figure 1.26** emission spectra for **48**, **50**, **51**. The authors suggest that the emission bands arise from an intraligand $^3[\pi\text{-}\pi^*(\text{alkynyl})]$ and the $^3[\sigma(\text{Au–P})\rightarrow\pi^*(\text{C}\equiv\text{Cpy})]$ excited state transitions [55].

## 1.5. 2,2'-Bipyridine

2,2'-Bipyridine (bpy) is a molecule consisting of two pyridine rings connected by a single bond in the 2,2'-position. With regards to the possibility of rotation around this single bond, bpy can adopt two extreme positions, in which N-atoms are on the same side in relation to the mentioned single bond – *cis*-conformation (**Figure 1.27, b**) or with N-atoms on each sides the connecting single bond – *trans*-conformation (**Figure 1.27**, **a**). The latter conformation is energetically preferred for free ligands [56], [57].

2,2'-Bipyridine can be obtained in the homocoupling reaction of 2-bromopyridine in DMSO using $Pd(dppf)Cl_2$ as a catalyst with a yield about 100% [58]. Reacting 2-iodopyridine with palladium on carbon (Pd/C) as a catalyst also gives similar results [59].

As a bidentate chelating ligand in metal complexes, bpy assumes a *cis*-conformation in order to use the two N-atoms as donors. In both the free ligand and the complex, two pyridine rings usually lie in the same plane [60].

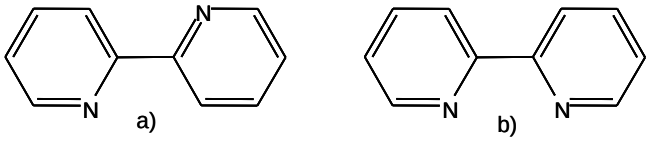


**Figure 1.27** *Trans* [a)] and *cis* [b)] conformers of 2,2'-bipyridine.

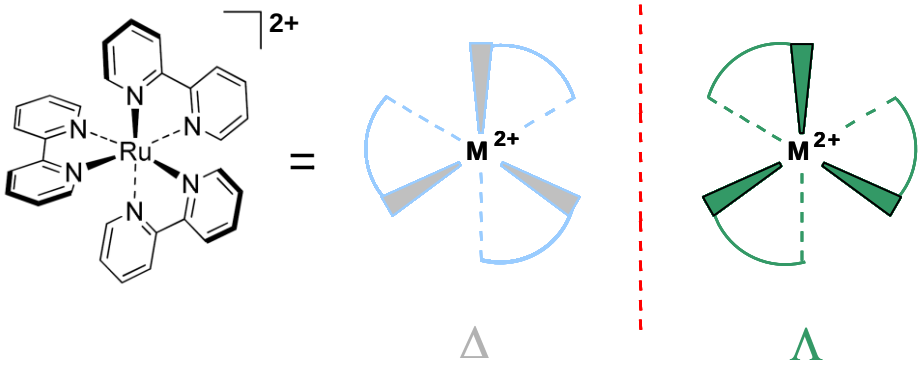


**Figure 1.28.** The Δ-isomer (right-handed enantiomer) and the Λ-isomer (left-handed enantiomer) of $[Ru(bpy)_3]^{2+}$.

Metal-ions, which prefer an octahedral geometry such Ru(II), Fe(II) form tris(bpy) complexes with high stability constants [60]-[62]. These complexes are chiral and mixtures of two enantiomers, Δ and Λ, are present in solution. Optically active ruthenium tris(bpy) and bis(bpy) complexes have found an application as selectively binding agents in chiral recognition and they are widely studied in the DNA-recognition field [63], [64].

The N-atoms of bpy-moieties can be protonated, forming mono- and dications, respectively. This process can be observed by measurement of the absorption spectra (**Figure 1.29**) [56], [65].

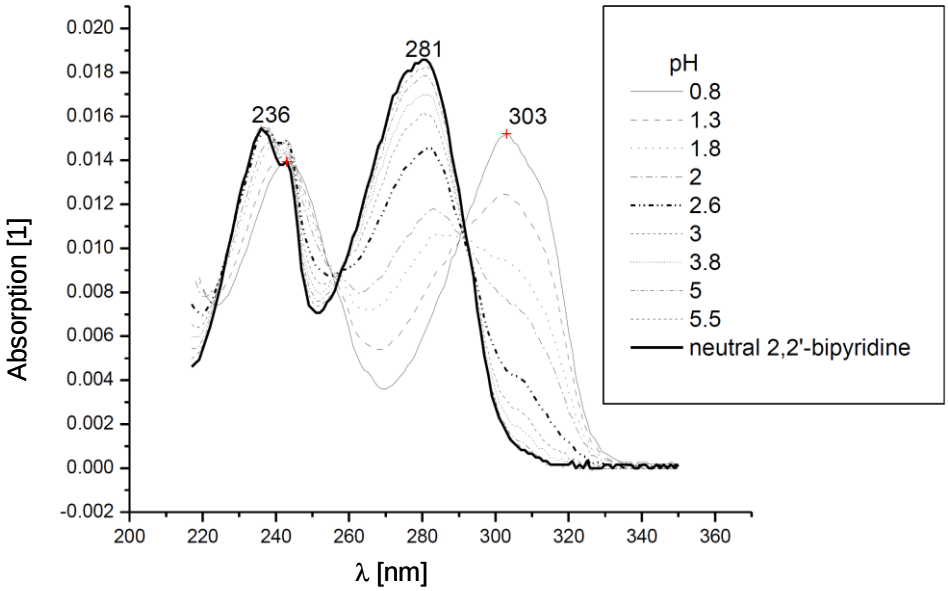


**Figure 1.29** Absorption spectra of 2,2'-bipyridine measured at different pH in acetonitrile [65].

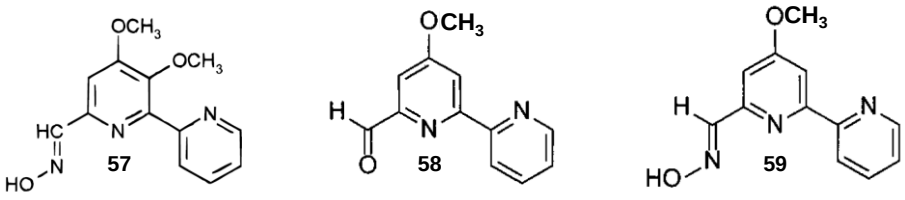


**Figure 1.30** Structures of Caerulomycins C (**57**), E (**58**) and A (**59**) [66], [67].

It is worth mentioning that derivatives of 2,2'-bipyridine have been found and isolated from bacteria *Streptomyces caeruleus* and their activity as natural antibiotics has been demonstrated (**Figure 1.30**) [66], [67].

Nowadays, 2,2'-bipyridine and its derivatives have found many applications and are still being investigated with regard to their potential properties. They can be used, for example as DNA-biosensors [68], in cancer therapy [69]-[71], in molecular design as building blocks [72]-[74], or in dye sensitized solar cells [75]-[77].

## 1.5.1. Gold(I) phosphine-decorated 2,2'-bipyridine

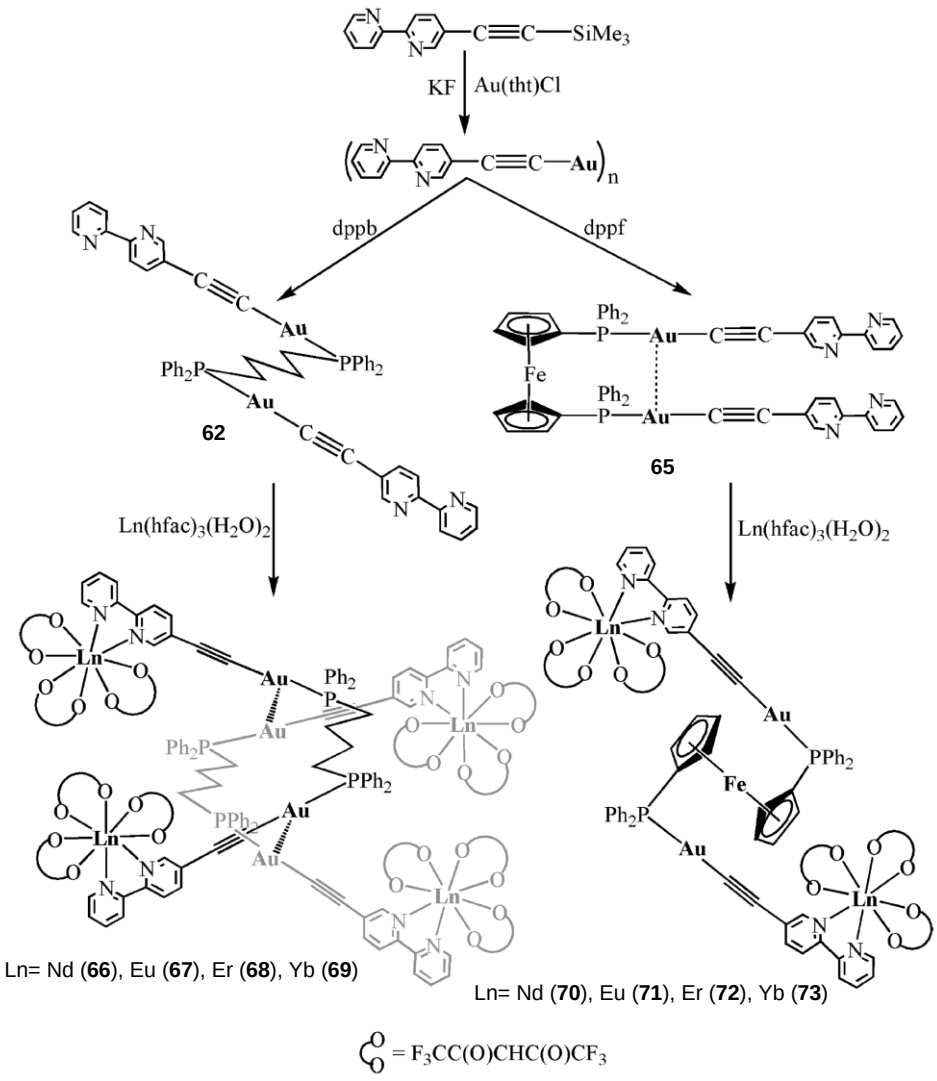


**Scheme 1.1** Synthetic routes of the Au-Ln heteronuclear complexes **66-73** [78].

A series of binuclear gold compounds (bpyC≡CAu)$_2$\{$\mu$-Ph$_2$P(CH$_2$)$_n$PPh$_2$\} (n = 2-6, **60-64**) or (bpyC≡CAu)$_2$($\mu$-dppf) (**65**) and their heteropolynuclear complexes (Au$_4$Ln$_4$ or Au$_2$Ln$_2$, **66-73**) with selected lanthanides (Ln = Nd, Eu, Er, Yb) was reported by Xu and co-workers [78].

X-ray studies of compounds **62** and **68,** and **65** and **72** (see **Scheme 1**) show an interesting correlation occurring between the supported Au-Au interactions and the conformation of the bpy-moieties as a result of complexation of **62** and **65**. After the complexation with Er, the *trans*-conformation of bpy-moieties in compound **62** changes to a *cis*-conformation due to the intermolecular Au-Au contacts (3.13 Å) for **68**. In the case of compounds **65** and **72** it is the other way round, the *cis*-orientation of the bpy-moieties in **65** with intramolecular Au-Au interactions (3.26 Å) rearranges to a *trans*-conformation in the Er-complex (**72**) [78].

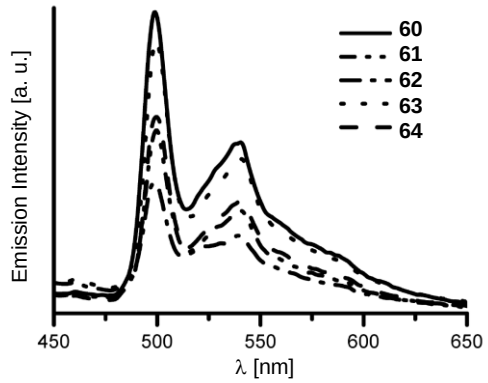


**Figure 1.31** Emission spectra of **60-64** in frozen $CH_2Cl_2$ at 77 K [78].

The binuclear gold compounds **60-64** are luminescent (**Figure 1.31**) and electronic transitions $^1(\pi\rightarrow\pi^*)$ from the excited-state of the alkynyl ligand and the $^3(\pi\rightarrow\pi^*)$ excited-state of the acetylide ligand are observed. These transitions may be influenced by the (Au-Au)→(C≡Cbpy) $^3$MMLCT transitions. Compound **65** is non-emissive due to luminescence quenching by the electron-rich ferrocenyl unit [78].

A series of luminescent alkynyl gold metallaligands containing 2,2'-bipyridine-5-yl donor groups was obtained by Vincente *et. al*. The synthetic strategy is illustrated in **Scheme 1.2**. The reaction of $[Au(C\equiv Cbpyl)]_n$ with a number different phosphines produced three asymetric ligands (**76-78**) and four ligands containing a phosphine bridge in their structure (**79-82**), (**Scheme 1.2**), [79].

Any intra- and intermolecular Au…Au interactions are not present in the crystal structures of **76** and **83**. Compounds **80** and **81,** with intermolecular Au-Au interactions 3.02 and 3.63 Å respectively, form infinite parallel chains in both cases. The Au-Au distance for **81** is longer than that usually observed Au-Au interactions (2.8-3.5 Å) [15], [79].

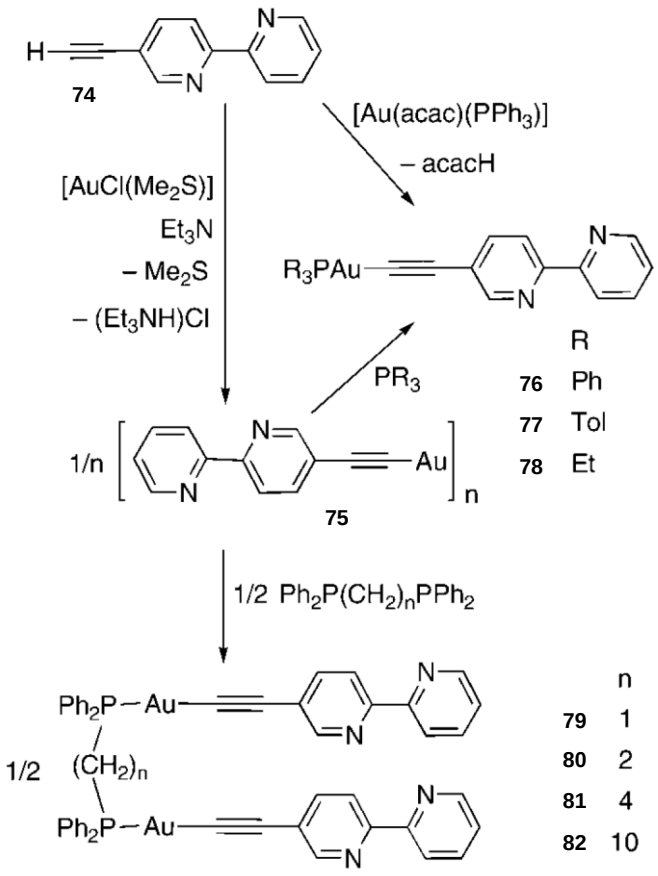


**Scheme 1.2** Synthesis of **76-78**, **79-82** [79].

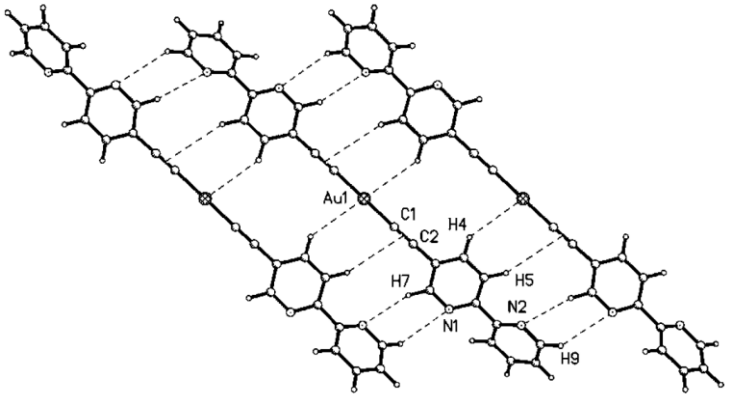


**Figure 1.32** Weak interactions in the structure R–≡–Au–≡–R, R= bpyl (**83**) are indicated by dashed lines [79].

Compound **83** was also reported in the same paper. Characteristic C-H…Au contacts can be observed in the crystal structure of this compound, which are marked in **Figure 1.32** [79].

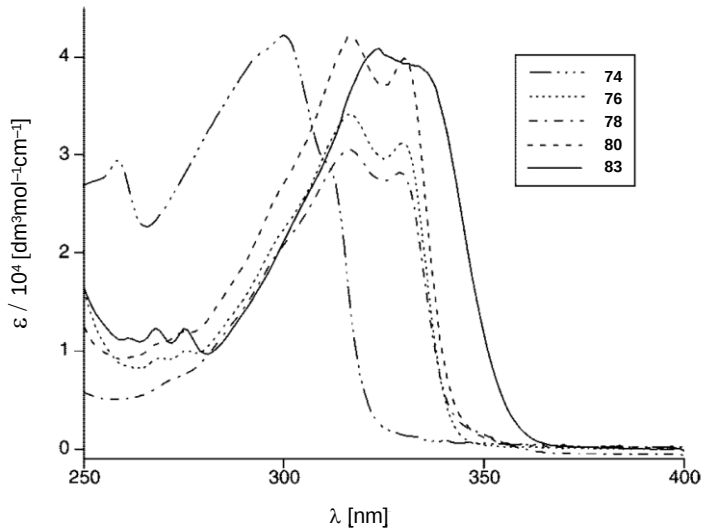


**Figure 1.33** Absorption spectra ($CH_2Cl_2$) of compounds **74**, **76**, **78**, **80**, and **83** [79].

The authors tentatively proposed that intraligand transitions [$\pi \rightarrow \pi^*$-(C≡CAr)], with some participation of Au orbital transitions are dominant for **74**, **76**, **78**, **80**, and **83**. The absorption spectra are illustrated in **Figure 1.33**. They claimed that metal-perturbed alkynyl ligand based transitions cause the emission of **74**, **76**, **78**, **80**, **83**. These emission spectra are shown in **Figure 1.34** [79].

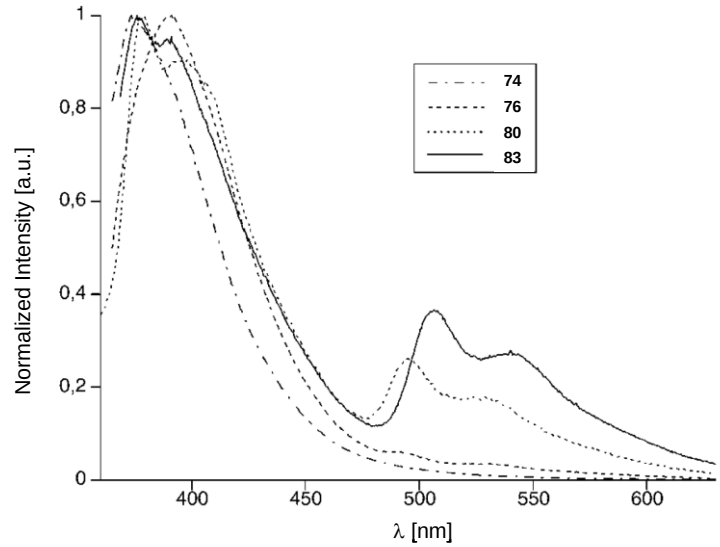


**Figure 1.34** Emission spectra ($CH_2Cl_2$, 298 K) of compounds **74**, **76**, **78**, **80**, **83** [79].

## 1.6. 2,2':6',2''-Terpyridine

The first report detailing 2,2':6',2''-terpyridine (tpy) in a reaction of pyridine with iron(II1) chloride was published by Morgan and Burstall. This bidentate or terdentate ligand from the oligopyridine family consists of three pyridine rings and adopts a *trans, trans* positions of N-atoms as this is energetically more favourable for free ligand (**Figure 1.35**) [80].

In its complexes 2,2':6',2''-terpyridine changes conformation to the *cis*, *cis* form as is illustrated in **Figure 1.35**. Protonation of the N-atoms is also possible, but is unfavourable in the case of reactions forming metal-complexes [80].

2,2':6',2''-Terpyridine as a ligand can coordinate to the majority of transition metals, similar to bpy, forming metal-complexes in many cases, with octahedral coordination geometries. Bis(terdentate) bonding mode observed in tpy-complexes is very stable with respect to ligands dissociation [80].

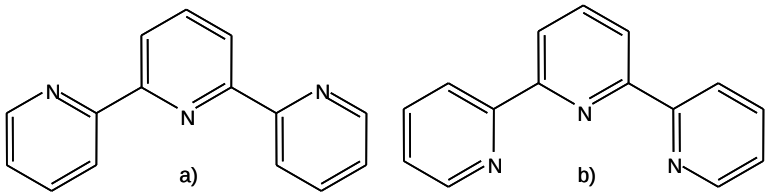


**Figure 1.35** *Trans*, *trans* [a)] and *cis*, *cis* [b)] conformers of 2,2':6',2''-terpyridine.

2,2':6',2''-Terpyridine and its derivatives and metal complexes have found a lot of applications for example, in the synthesis of metallodendrimers [81], [82] (example of tpy-dendrimers showed in **Figure 1.36**), in supramolecular chemistry: forming micelles [83], in self-assembly [84] as building blocks [85], in biological applications [86], [87] and in solar cells [88], [89].

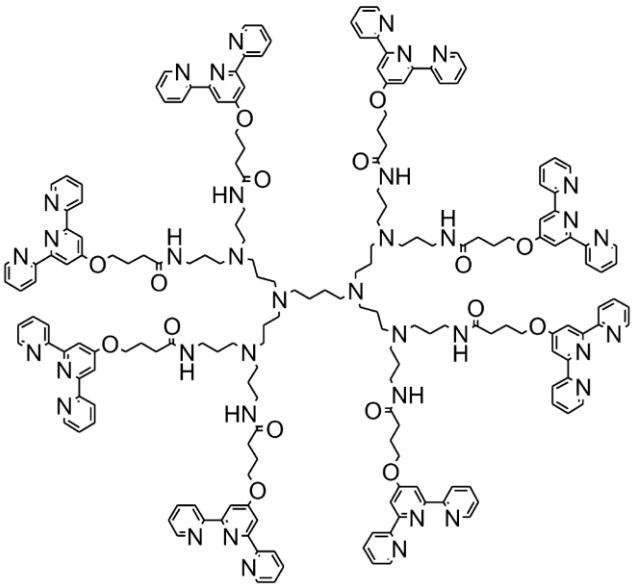

**Figure 1.36.** The terpyridinyl core dendrimer [82].

## 1.6.2. Gold(I) phosphine-decorated 2,2':6',2''-terpyridine

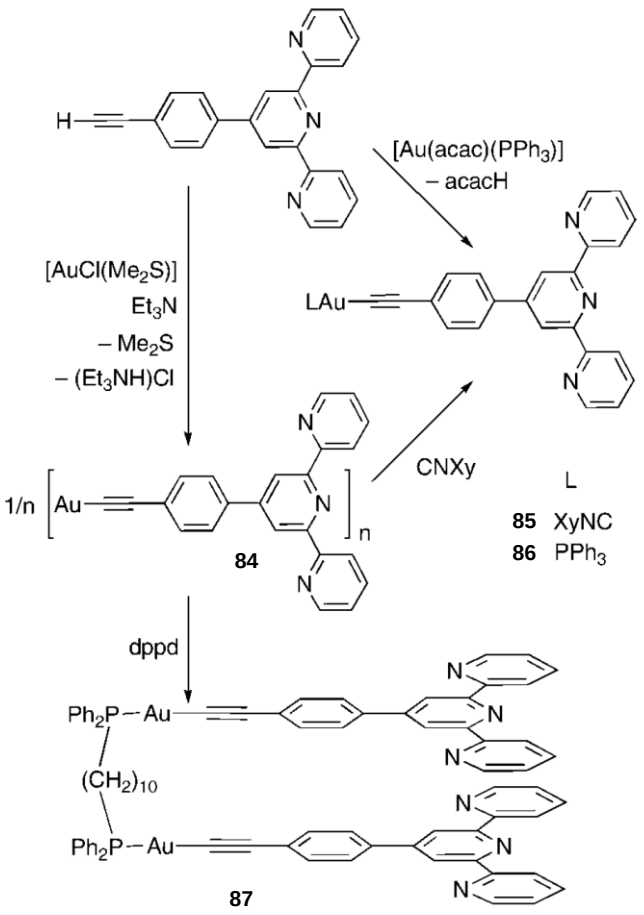


**Scheme 1.3** Synthesis of **85**, **86**, **87** [79].

The "acac" strategy, in which the weak ligand acetylacetone is protonated and replaced by a stronger nucleophile, was used to obtained complexes **85** and **86** (**Scheme 1.3**) [79], [90]. Compound **87** was synthesised by reacting gold(I) "polymer" (**84)** directly with a bridged phosphine. The same procedure can be used to obtain **85** and **86** by reaction with the appropriate phosphine [79].

The absorption and fluorescence spectra were measured for the gold(I) complexes that contain a phenyl spacer between the triple bond and the tpy unit. The fluorescence spectra offers proof of the luminescent properties of **85**, **86**, **87** [79].

A crystal structure was not obtained for **85** and **87**, but for **86** a crystal structure was solved. It shows a lack of intra- and intermolecular Au…Au interactions. Instead,

characteristic C-H..Au and C-H…π interactions are present and this influences the crystal packing (**Figure 1.37**) [79].

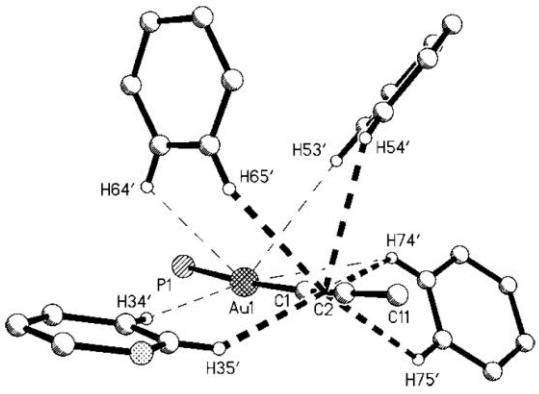


**Figure 1.37** Clustering of C-H…Au (thin dashed bonds) and C-H…π contacts (thick dashed bonds) at the P-Au-C≡C center of compound **86** [79].

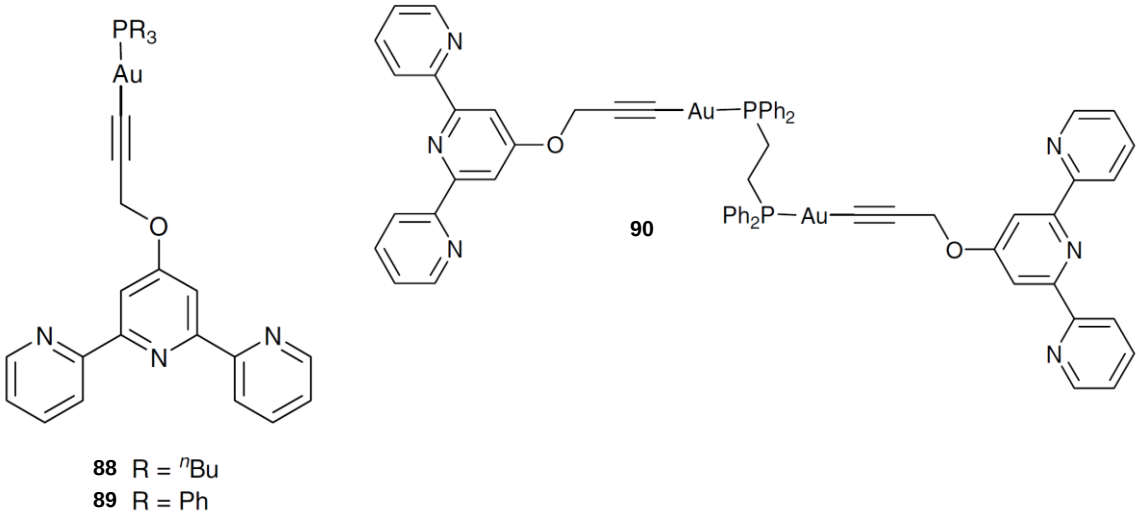


**Figure 1.38** Structures of **88**, **89**, **90** [91].

Compounds **88**, **89** and **90** were reported by Constable *et. al* and their molecular structures are shown in **Figure 1.38**. A -$CH_2O$- unit connects the tpy moiety with the alkylyl gold phosphine part of these molecules [91].

Absorption and fluorescence spectra are not shown and are not described in this article. The solved crystal structures do not reveal the presence of any intra- and inter molecular Au-Au interactions for these compounds. However, weak hydrogen bonds of C-H…O (for **90**) and C-H…N types (**88** and **90**) control the crystal packing of **88** and **90** (**Figures 1.39** and

**1.40**) [91]. C-H…N and C-H…π weak interactions are present in the crystal structure of **88** and they support an assembly with a dimeric motif. Dimers form a characteristic pattern, which is built along the a-axis (**Figure 1.39**) [91]. C-H…N and C-H…O weak hydrogen bond and C-H…π interactions in the crystal packing of **90** are responsible for the formation of chains arranged in layers which interlock with each other (**Figure 1.40**) [91].

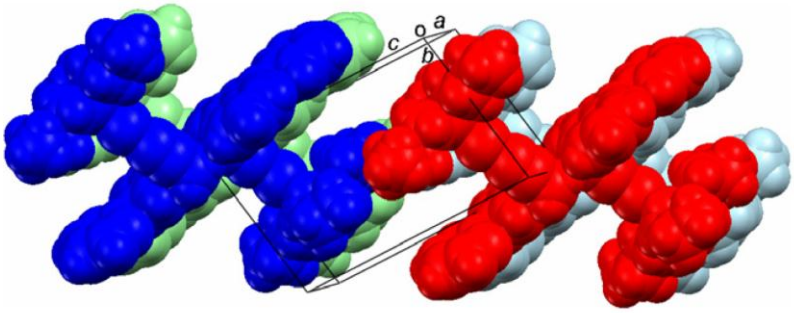


**Figure 1.39** Four dimers of **88** showing their assembly into rows along the a-axis, and the resulting domains of alkyl chains (centre of unit cell) and tpy groups [91].

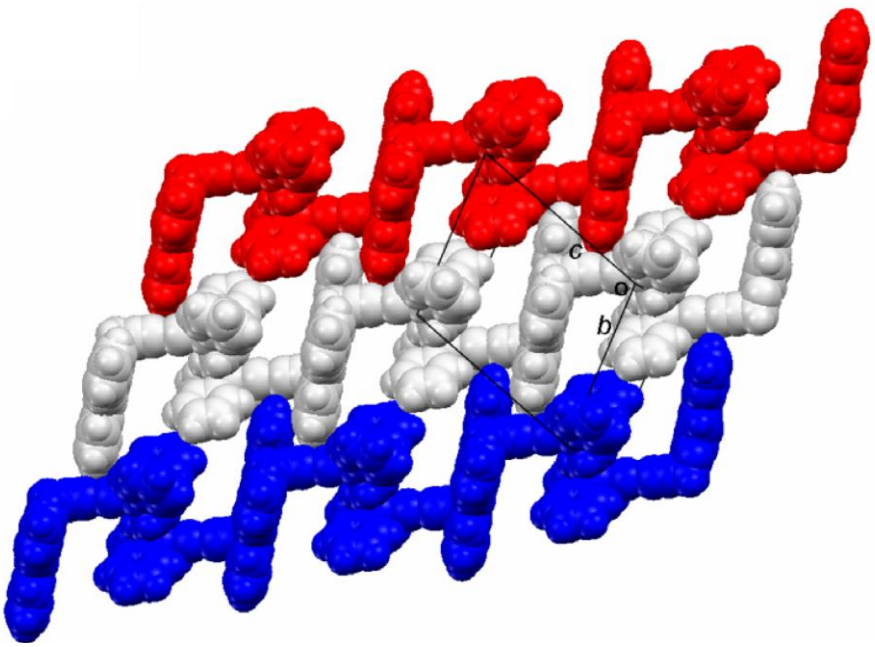


**Figure 1.40** Non-classical hydrogen bonding interactions between molecules of **90** form chains, which are marked in blue, silver and red [91].

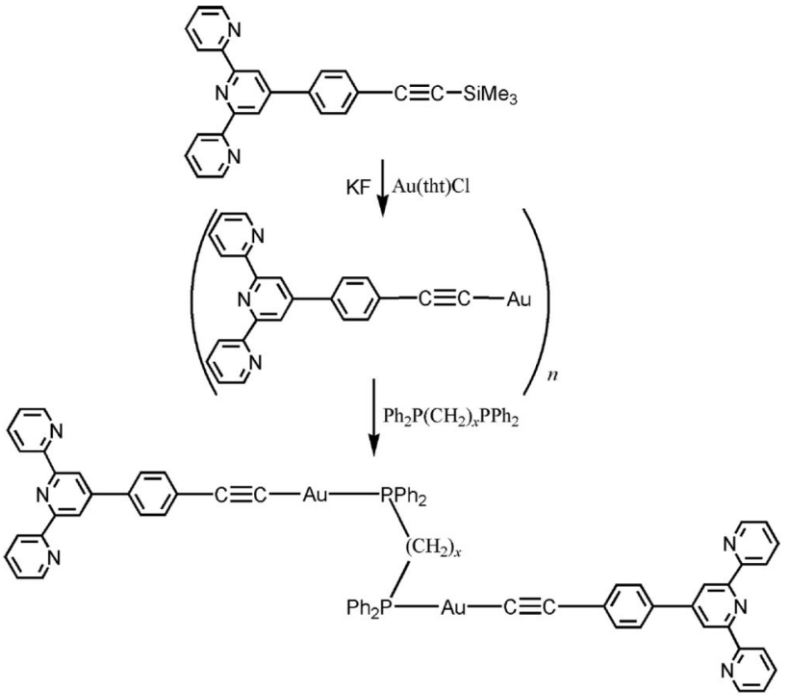


**Figure 1.41** Synthetic strategy for making **91-95** [92].

A family of dinuclear luminescent gold(I) complexes **91**-**95** is illustrated in **Figure 1.41** and was synthesised and characterised by Li *et. al.* The lack of Au-Au interactions in the crystal structure of **91** and **92** was observed. In the case of **92** no weak interactions were observed. π-π interactions between the pyridine rings and C-H…Au weak interactions dominate the crystal packing of **91** and they support the formation of the 3D framework. [92].

The absorption spectra for **91**-**95** have similar features. There are no noticeable differences observed from changing the bridging phosphine chain length [92].

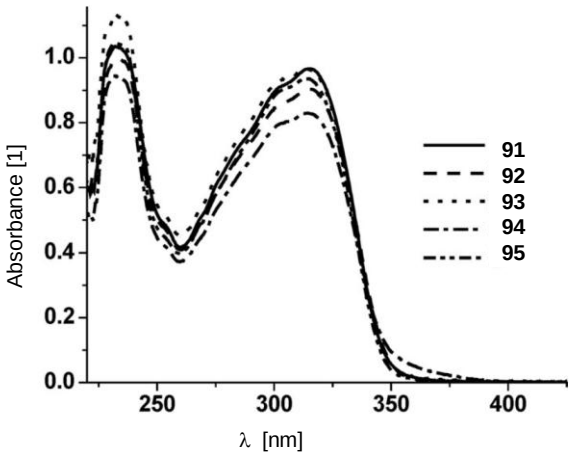


**Figure 1.42** UV/Vis absorption spectra of **91**–**95** in $CH_2Cl_2$ at 298 K [92].

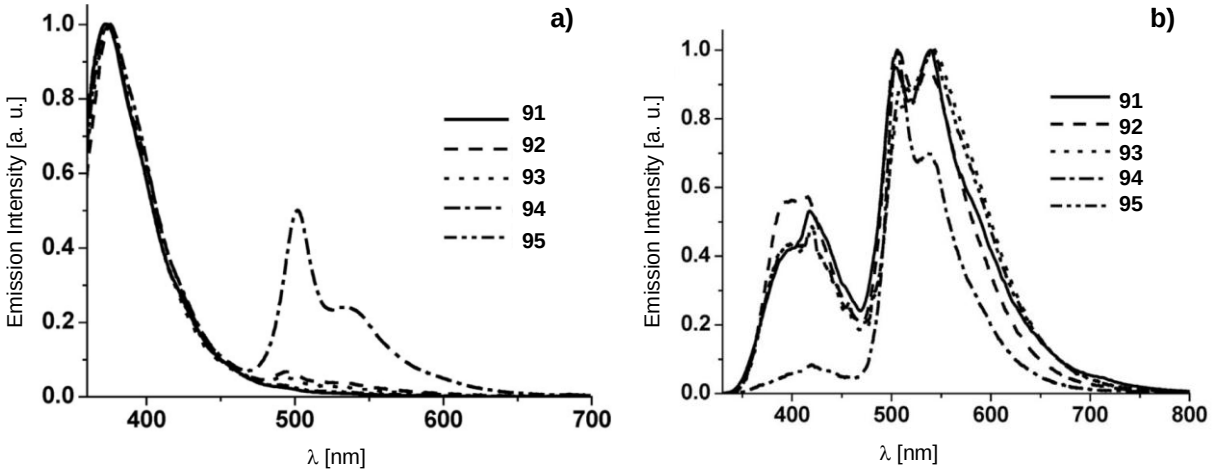


**Figure 1.43** Emission spectra of **91–95** in fluid $CH_2Cl_2$ solution (**a**) in the solid state (**b**) at room temperature [92].

Compounds **91-95** exhibit dual emission and the authors tentatively suggest the $^1(\pi\text{-}\pi^*)$ excited state of the alkynyl ligand transitions occur with high energy wavelengths and the $^3(\pi\text{-}\pi^*)$ excited state of the acetylide ligand, mixed probably with some Au orbital character, transitions occur with low energy wavelengths (**Figure 1.43**) [92].

# 2. Aim of this thesis

The aim of this thesis was to investigate gold(I) phosphine derivatives of 4,4'-di-ethynyl substituted 2,2'-bipyridine and 4'-ethynyl-2,2':6',2''-terpyridine, specifically with regard to their structural and photophysical properties. These studies included the characterisation of these compounds and the optimised synthesis of a new series of 4,4'-di-ethynyl substituted 2,2'-bipyridine and 4'-ethynyl-2,2':6',2''-terpyridine compounds decorated with gold(I)triarylphosphine units or with gold(I)trialkylphosphine units. The reaction of *catena*-[4'-(2-gold-1-ethynyl)-2,2':6',2''-terpyridine] with 1,2-bis(diphenyl-phosphino)ethane led to the formation of a novel bridged ligand, which exhibited interesting properties.

Further studies included the formation of Ru(II), Fe(II), Zn(II) containing complexes of the above mentioned series of gold(I) phosphine derivatives.

# 3. Synthesis and characterisation of $(R_3PAu{-}{\equiv})_2bpy$

## 3.1. Experimental for L1-L6

**4,4'-Bis[2-(trimethysilyl)-1-ethynyl]-2,2'-bipyridine (S1):**

Previously reported in reference: [93]

Formula: $C_{20}H_{24}N_2Si_2$

Formula weight: 348.59 [g/mol]

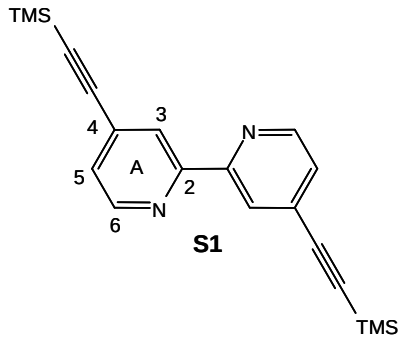


**S1**

4,4'-Dibromo-2,2'-bipyridine (500 mg, 1.6 mmol), bis(triphenylphosphine)palladium(II)-dichloride (38 mg, 68 μmol), CuI (38 mg, 200 μmol) and (trimethylsilyl)ethyne (380 mg, 0.54 ml, 3.8 mmol) were added to 15 ml dry THF. After addition of DIPA (predistilled with NaOH, 2.5 ml) the colour of the solution turned dark brown. The reaction was carried out under argon and the reaction mixture was placed in a microwave reactor (50 °C, 30 min), after which the reaction mixture was quenched with water (50 ml). 30 ml of $CH_2Cl_2$ was added to this mixture and the organic and aqueous phases were separated. The aqueous phase was extracted with $CH_2Cl_2$. The solvent from the organic phase was removed *in vacuo*. The dark brown crude material was dissolved in a mixture of hexane/$CH_2Cl_2$ (30/70) and was filtered through $Al_2O_3$ *in vacuo* to remove the black precipitate. Next, the filtrate was purified by column chromatography ($Al_2O_3$, hexane/$CH_2Cl_2$ - 30/70). Compound **S1** was isolated as a white crystalline solid (400 mg, 1.1 mmol, 71%).

**$^1$H NMR** (400 MHz, $CDCl_3$), δ [ppm]: 8.62 (d, $J$ = 5.0 Hz, 2H, $H^{A6}$), 8.43 (s, 2H, $H^{A3}$), 7.32 (dd, $J$ = 5.0, 1.5 Hz, 2H, $H^{A5}$), 0.26 (s, 18H, $H^{TMS}$).

**Preparation of the 4,4'-bis[2-($R_3P$)-gold-1-ethynyl]-2,2'-bipyridine:**

**General procedure 1.** $R_3PAuCl$ (R = Et, *i*-Pr, *t*-Bu, Ph, *m*-Tol, *p*-Tol), 4,4'-diethynyl-2,2'-bipyridine and CuI were dissolved in a mixture of $CH_2Cl_2$ (or THF) (6 ml) and toluene (2 ml). DIPA (predistilled with NaOH, 2 ml) or NaOAc was added to make the solution basic. The reaction mixture was stirred in the dark at room temperature for 12–16 h, after which the solution was filtered and the solvent removed from the filtrate *in vacuo*. The crude material was purified by preparative plate chromatography in the dark ($Al_2O_3$, $CH_2Cl_2$).

**General procedure 2.** $R_3PAuCl$ (R = Et, *i*-Pr, Ph, *p*-Tol), 4,4'-diethynyl-2,2'-bipyridine and CuI were added to THF (or $CH_2Cl_2$) (8 ml). DIPA (predistilled with NaOH, 2 ml) was added to make the solution basic. The reaction was carried out under argon and the reaction mixture was placed in a microwave reactor (50 °C, 30 min), after which the solution was filtered and the solvent removed from the filtrate. The crude material was purified by preparative plate chromatography in the dark ($Al_2O_3$, $CH_2Cl_2$).

**4,4'-Bis[2-{(triethylphosphino)gold}-1-ethynyl]-2,2'-bipyridine (L1):**

Formula: $C_{26}H_{36}Au_2N_2P_2$

Formula weight: 832.46 [g/mol]

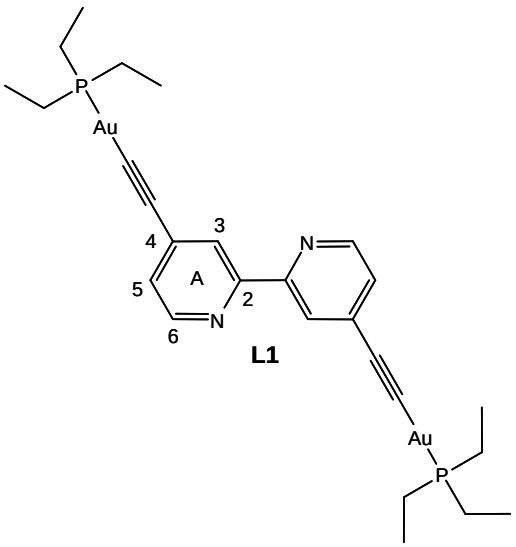


**L1**

$Et_3PAuCl$ (69 mg, 200 μmol), 4,4'-diethynyl-2,2'-bipyridine (20 mg, 98 μmol) and CuI (0.2 mg, 1 μmol). Compound **L1** was isolated as a white solid (26 mg, 31 μmol, 31 %).

**$^{1}$H NMR** (500 MHz, $CDCl_3$), δ [ppm]: 8.50 (dd, $J$ = 5.0, 0.8 Hz, 2H, $H^{A6}$), 8.33 (dd, $J$ = 1.4, 0.8 Hz, 2H, $H^{A3}$), 7.27 (dd, $J$ = 5.0, 1.6 Hz, 2H, $H^{A5}$), 1.81 (dq, $J_{PH}$ = 9.6, $J_{HH}$ = 7.7 Hz, 12H, $H^{Et\text{-}CH2}$), 1.20 (dt, $J_{PH}$ = 18.1, $J_{HH}$ = 7.6 Hz, 18H, $H^{Et\text{-}CH3}$).

**$^{13}$C NMR** (126 MHz,$CDCl_3$), δ [ppm]: 156.00 ($C^{A2}$), 149.02 ($C^{A6}$), 134.13 ($C^{A4}$), 126.37 ($C^{A5}$), 124.28 ($C^{A3}$), 17.79 (d, $J_{PC}$ = 33.3 Hz, $C^{Et\text{-}CH2}$), 9.04 ($C^{Et\text{-}CH3}$), C≡C signals not observed.

**$^{31}$P NMR** (162 MHz, $CDCl_3$), δ [ppm]: 39.06.

**UV-Vis** ($CH_2Cl_2$, $\lambda_{max}$ [nm], ($\varepsilon$ [$dm^3mol^{-1}cm^{-1}$])): 236 (50000), 267 (56000), 284 (61000), 302 (24000), 316 (18000).

**Emission** ($CH_2Cl_2$, $\lambda_{ex}$ = 284 nm), $\lambda_{em}$ [nm]: 350, 438, 466.

**ESI-MS** ($CH_2Cl_2$, [m/z]): 433.3 ($[(Et_3P)_2Au]^+$, calc. 433.2), 833.3 ($[L1 + H]^+$, calc. 833.2), 1147.1 ($[L1 + Et_3PAu]^+$, calc. 1147.2).

**EA** [%], $C_{26}H_{36}Au_2N_2P_2$, calc. C: 37.51, H: 4.36, N: 3.37; found C: 37.48, H: 4.19, N: 3.16.

**4,4'-Bis[2-{(triisopropylphosphino)gold}-1-ethynyl]-2,2'-bipyridine (L2):**

Formula: $C_{32}H_{48}Au_2N_2P_2$

Formula weight: 916.62 [g/mol]

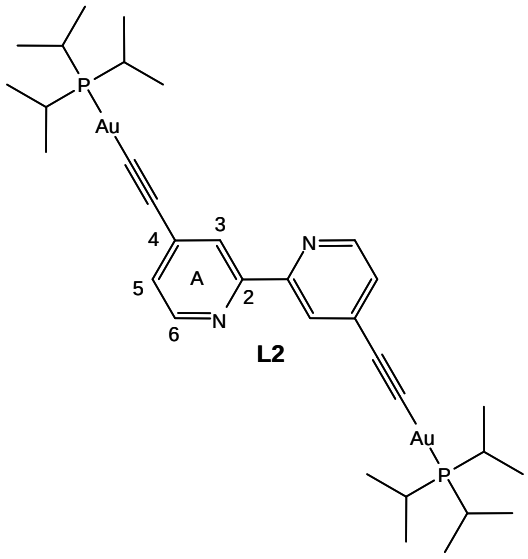


**L2**

*i*-$Pr_3PAuCl$ (77 mg, 200 μmol), 4,4'-diethynyl-2,2'-bipyridine (20 mg, 98 μmol) and CuI (0.2 mg, 1 μmol). Compound **L2** was isolated as a white solid (36 mg, 40 μmol, 40 %).

**$^{1}$H NMR** (500 MHz, $CDCl_3$), δ [ppm]: 8.49 (d, $J$ = 5.0 Hz, 2H, $H^{A6}$), 8.35 (s, 2H, $H^{A3}$), 7.27 (dd, $J$ = 5.0, 1.5 Hz, 2H, $H^{A5}$), 2.29 (m, 6H, $H^{i\text{Pr-}CH}$), 1.33 (dd, $J_{PH}$ = 15.5, $J_{HH}$ = 7.2 Hz, 36H, $H^{i\text{Pr-}CH3}$).

**$^{13}$C NMR** (126 MHz, $CDCl_3$), δ [ppm]: 155.97 ($C^{A2}$), 149.01 ($C^{A6}$), 134.22 ($C^{A4}$), 126.27 ($C^{A5}$), 124.34 ($C^{A3}$), 23.79 (d, $J_{PC}$ = 28.2 Hz, $C^{i\text{Pr-}CH}$), 20.45 ($C^{i\text{Pr-}CH3}$), C≡C signals not observed.

**$^{31}$P NMR** (162 MHz, $CDCl_3$), δ [ppm]: 67.62.

**UV-Vis** ($CH_2Cl_2$, $\lambda_{max}$ [nm], ($\varepsilon$ [$dm^3mol^{-1}cm^{-1}$])): 235 (59000), 267 (63000), 284 (70000), 302 (27000), 314 (21000).

**Emission** ($CH_2Cl_2$, $\lambda_{ex}$ = 284 nm), $\lambda_{em}$ [nm]: 348, 438, 464.

**ESI-MS** ($CH_2Cl_2$, [m/z]): 517.4 ($[(i\text{-}Pr_3P)_2Au]^+$, calc. 517.2), 917.4 ($[L2 + H]^+$, calc. 917.3), 1173.2 ($[L2 + (i\text{-}Pr_3PAu)]^+$, calc. 1173.4).

**EA** [%], $C_{32}H_{48}Au_2N_2P_2$, calc. C: 41.93, H: 5.28, N: 3.06; found C: 42.13, H: 5.21, N: 2.85.

**4,4'-Bis[2-{(tri-t-butylphosphino)gold}-1-ethynyl]-2,2'-bipyridine (L3):**

Formula: $C_{38}H_{60}Au_2N_2P_2$

Formula weight: 1000.78 [g/mol]

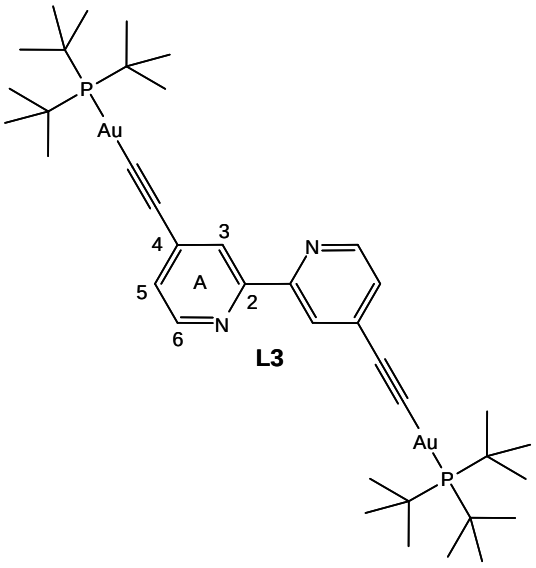


*t*-$Bu_3PAuCl$ (85 mg, 200 μmol), 4,4'-diethynyl-2,2'-bipyridine (20 mg, 98 μmol), NaOAc (24 mg, 290 μmol) and CuI (0.7 mg, 3.7 μmol). Compound **L3** was isolated as a white solid (54 mg, 54 μmol, 55 %).

**$^{1}$H NMR** (500 MHz, $CDCl_3$), δ [ppm]: 8.50 (d, $J$ = 5.0 Hz, 2H, $H^{A6}$), 8.37 (s, 2H, $H^{A3}$), 7.29 (d, $J$ = 5.0 Hz, 2H, $H^{A5}$), 1.53 (d, $J_{PH}$ = 13.3 Hz, 54H, $H^{t\text{-Bu}}$).

**$^{13}$C NMR** (126 MHz, $CDCl_3$), δ [ppm]: 155.93 ($C^{A2}$), 148.99 ($C^{A6}$), 134.38 ($C^{A4}$), 126.16 ($C^{A5}$), 124.44 ($C^{A3}$), 39.28 (d, $J_{PC}$ = 18.0, $C^{t\text{-Bu-CH}}$), 32.57 (d, $J_{PC}$ = 4.0 Hz, $C^{t\text{-Bu-CH3}}$), C≡C signals not observed.

**$^{31}$P NMR** (202 MHz, $CDCl_3$), δ [ppm]: 91.78.

**UV-Vis** ($CH_2Cl_2$, $\lambda_{max}$ [nm], ($\varepsilon$ [$dm^3mol^{-1}cm^{-1}$])): 235 (74000), 267 (81000), 284 (87000), 302 (35000), 314 (27000 ).

**Emission** ($CH_2Cl_2$, $\lambda_{ex}$ = 268 nm), $\lambda_{em}$ [nm]: 337, 439, 465.

**ESI-MS** ($CH_2Cl_2$, [m/z]): 1001.4 ($[L3 + H]^+$, calc. 1001.8).

**EA** [%], $C_{38}H_{60}Au_2N_2P_2$, calc. C: 45.61, H: 6.04, N: 2.80; found C: 45.25, H: 6.00, N: 2.91.

**4,4'-Bis[2-{(triphenylphosphino)gold}-1-ethynyl]-2,2'-bipyridine (L4):**

Formula: $C_{50}H_{36}Au_2N_2P_2$

Formula weight: 1120.71 [g/mol]

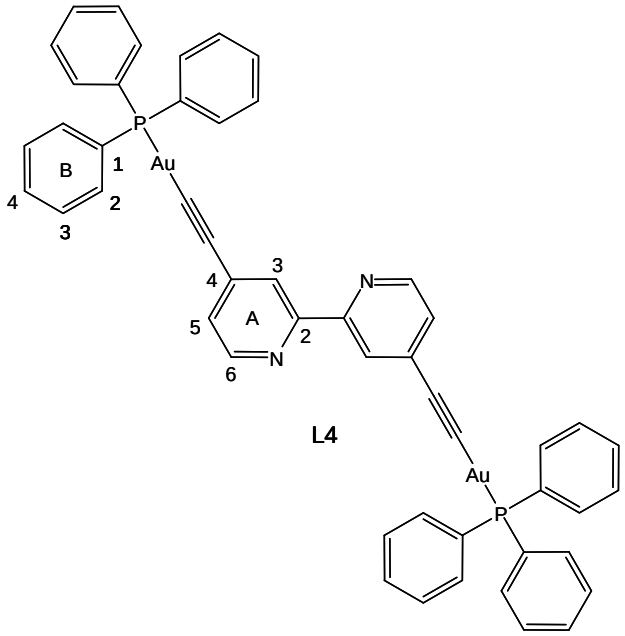


$Ph_3PAuCl$ (130 mg, 260 µmol), 4,4'-diethynyl-2,2'-bipyridine (26 mg, 130 µmol) and CuI (0.2 mg, 1 µmol). Compound **L4** was isolated as a white solid (97 mg, 87 µmol, 68 %).

**$^{1}$H NMR** (500 MHz, $CDCl_3$), δ [ppm]: 8.51 (d, $J$ = 5.0 Hz, 2H, $H^{A6}$), 8.38 (s, 2H, $H^{A3}$), 7.51 (m, 18H, $H^{B3/2+B4}$), 7.44 (m, 12H, $H^{B2/3}$), 7.30 (dd, $J$ = 5.0, 1.1 Hz, 2H, $H^{A5}$) ppm.

**$^{13}$C NMR** (126 MHz, $CDCl_3$), δ [ppm]: 156.00 ($C^{A2}$), 149.05 ($C^{A6}$), 134.44 (d, $J_{PC}$ = 13.8 Hz; $C^{B2/3}$), 134.00 ($C^{A4}$), 131.78 ($C^{B4}$), 129.68 (d, $J_{PC}$ = 56.3 Hz, $C^{B1}$), 129.34 (d, $J_{PC}$ = 11.3 Hz, $C^{B2/3}$), 126.37 ($C^{A5}$), 124.30 ($C^{A3}$), C≡C signals not observed.

**$^{31}$P NMR** (162 MHz, $CDCl_3$), δ [ppm]: 39.00.

**UV-Vis** ($CH_2Cl_2$, $\lambda_{max}$ [nm], ($\varepsilon$ [$dm^3mol^{-1}cm^{-1}$])): 239 (92000), 268 (67000), 285 (72000), 302 (28000), 315 (21000)

**Emission** ($CH_2Cl_2$, $\lambda_{ex}$ = 285 nm), $\lambda_{em}$ [nm]: 338, 438, 466.

**ESI-MS** ($CH_2Cl_2$, [m/z]): 1121.8 ($[L4 + H]^+$, calc. 1121.2).

**EA** [%], $C_{50}H_{36}Au_2N_2P_2$ *****$1.5H_2O$, calc. C: 52.32, H: 3.42, N: 2.44; found C: 52.26, H: 3.46, N: 2.49.

**4,4'-Bis[2-{(tri-*m*-tolylphosphino)gold}-1-ethynyl]-2,2'-bipyridine (L5):**

Formula: $C_{56}H_{48}Au_2N_2P_2$

Formula weight: 1204.87 [g/mol]

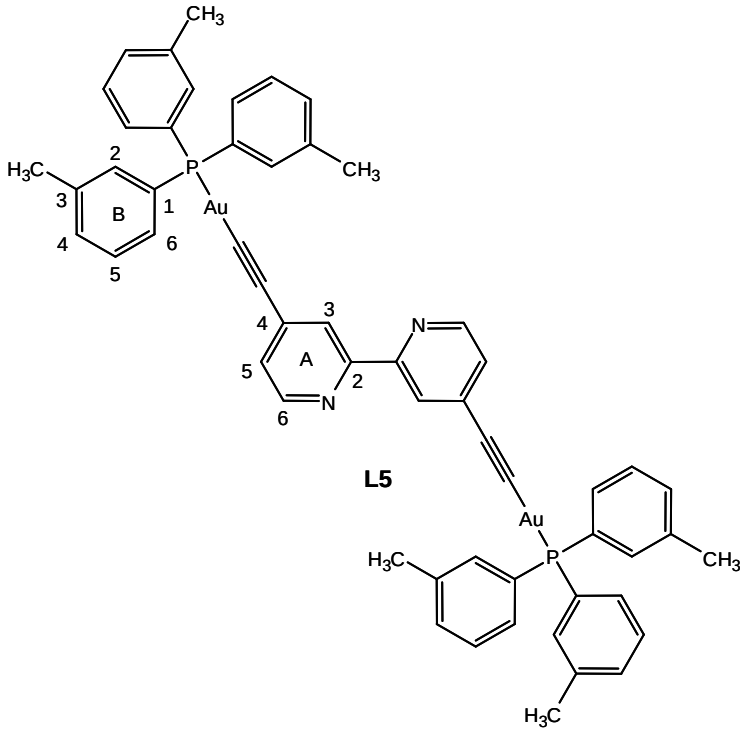


*m*-$Tol_3PAuCl$ (100 mg, 200 μmol), 4,4'-diethynyl-2,2'-bipyridine (20 mg, 98 μmol), NaOAc (24 mg, 290 μmol,) and CuI (0.7 mg, 3.7 μmol). Compound **L5** was isolated as a white solid (69 mg, 58 μmol, 59 %).

**$^{1}$H NMR** (600 MHz, $CDCl_3$), δ [ppm]: 8.57 (d, $J$ = 5.0 Hz, 2H, $H^{A6}$), 8.45 (s, 2H, $H^{A3}$), 7.47 (d, $J_{PH}$ = 13.7 Hz, 6H, $H^{B2}$), 7.39 – 7.32 (m, 14H, $H^{A5, B4, B5}$), 7.29 (dd, $J_{PH}$ = 11.5 Hz, $J_{HH}$ 3.8 Hz, 6H, $H^{B6}$), 2.39 (s, 18H, $H^{m\text{-Tol-CH3}}$).

**$^{13}$C NMR** (151 MHz, $CDCl_3$), δ [ppm]: 156.02 ($C^{A2}$), 149.06 ($C^{A6}$), 139.13 (d, $J_{PC}$ = 142.3 Hz, $C^{AuiC\equiv C}$), 139.21 (d, $J_{PC}$ = 11.8 Hz, $C^{B3}$), 135.12 (d, $J$ = 15.7 Hz, $C^{B2}$), 134.06 ($C^{A4}$), 132.51 (d, $J$ = 2.4 Hz, $C^{B4}$), 131.30 (d, $J_{PC}$ = 11.9 Hz, $C^{B6}$), 129.73 (d, $J_{PC}$ = 56.0 Hz , $C^{B1}$), 129.10 (d, $J_{PC}$ = 11.4 Hz, $C^{B5}$), 126.35 ($C^{A5}$), 124.34($C^{A3}$), 101.94 (d, $J_{PC}$ = 27.1 Hz, $C^{iC\equiv CAu}$), 21.61($C^{m\text{-Tol-CH3}}$).

**$^{31}$P NMR** (162 MHz, $CDCl_3$), δ [ppm]: 42.50.

**UV-Vis** ($CH_2Cl_2$, $\lambda_{max}$ [nm], ($\varepsilon$ [$dm^3mol^{-1}cm^{-1}$])): 237 (109000), 252 (85000), 269 (81000), 284 (88000), 302 (35000), 314 (26000).

**Emission** ($CH_2Cl_2$, $\lambda_{ex}$ = 284 nm), $\lambda_{em}$ [nm]: 338, 439, 468.

**ESI-MS** ($CH_2Cl_2$, [m/z]): 805.5 ([(*m*-$Tol_3P)_2Au]^+$, calc. 805.7), 1205.7 ([L5 + H]$^+$, calc. 1205.9), 1227.5 ([L5 + Na]$^+$, calc. 1227.9).

**EA** [%], $C_{56}H_{48}Au_2N_2P_2$, calc. C: 55.82, H: 4.02, N: 2.33; found C: 55.56, H: 4.06, N: 2.44.

**4,4'-Bis[2-{(tri-*p*-tolylphosphino)gold}-1-ethynyl]-2,2'-bipyridine (L6):**

Formula: $C_{56}H_{48}Au_2N_2P_2$

Formula weight: 1204.87 [g/mol]

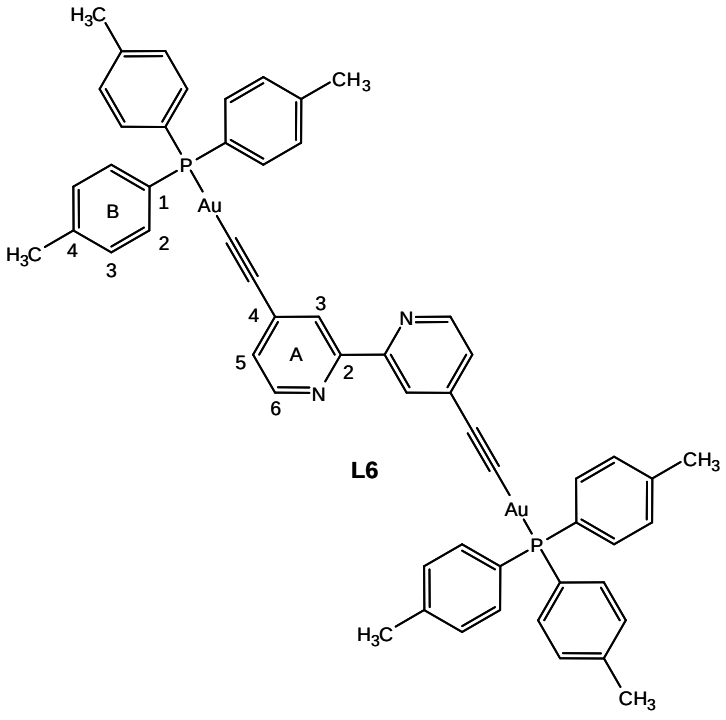

(*p*-Tol)$_3$PAuCl (105 mg, 200 µmol), 4,4'-diethynyl-2,2'-bipyridine (20 mg, 98 µmol) and CuI (0.2 mg, 1 µmol). Compound **L6** was isolated as a white solid (62 mg, 52 µmol, 53 %).

**$^1$H NMR** (500 MHz, $CDCl_3$), δ [ppm]: 8.51 (d, $J$ = 5.0 Hz, 2H, $H^{A6}$), 8.37 (s, 2H, $H^{A3}$), 7.41 (dd, $J_{PH}$ = 12.5, $J_{HH}$ = 8.0 Hz, 12H, $H^{B3}$), 7.30 (dd, $J$ = 5.0, 1.4 Hz, 2H, $H^{A5}$), 7.23 (d, $J_{PH}$ = 1.4, $J_{HH}$ = 8.0 Hz, 12 H, $H^{B2}$), 2.40 (s, 18 H, $H^{p\text{-Tol-CH3}}$).

**$^{13}$C NMR** (126 MHz, $CDCl_3$), δ [ppm]: 156.04 ($C^{A2}$), 149.06 ($C^{A6}$), 142.11 ($C^{B4}$), 134.34 (d, $J_{PC}$ = 14.1 Hz, $C^{B2/3}$), 134.09 ($C^{A4}$), 130.01 (d, $J_{PC}$ = 11.7 Hz, $C^{B2/3}$), 126.83 (d, $J_{PC}$ = 58.3 Hz, $C^{B1}$), 126.39 ($C^{A5}$), 124.33 ($C^{A3}$), 21.63 ($C^{p\text{-Tol-CH3}}$), C≡C signals not observed.

**$^{31}$P NMR** (162 MHz, $CDCl_3$), δ [ppm]: 40.59.

**UV-Vis** ($CH_2Cl_2$, $\lambda_{max}$ [nm], ($\varepsilon$ [$dm^3mol^{-1}cm^{-1}$])): 238 (112000), 253 (99000), 269 (78000), 285 (81000), 303 (32000), 315 (24000)

**Emission** ($CH_2Cl_2$, $\lambda_{ex}$ = 285 nm), $\lambda_{em}$ [nm]: 338, 438, 466.

**ESI-MS** ($CH_2Cl_2$, [m/z]): 805.2 ([(*p*-Tol$_3$P)$_2$Au]$^+$, calc. 805.2), 1205.1 ([L6 + H]$^+$, calc. 1205.3), 1705.0 ([L6 + *p*-Tol$_3$PAu]$^+$, calc. 1705.4).

**EA** [%], $C_{56}H_{48}Au_2N_2P_2$*****$Et_2O$*$H_2O$, calc. C: 55.56, H: 4.66, N: 2.16; found C: 55.67, H: 4.54, N: 2.12.

## 3.2. Ligand synthesis of L1-L6

A rise of interest in gold(I) phosphine derivatives results from the potential wide spectrum of applications of this group of complexes. Some have interesting luminescent and optical properties [94], [101], [102]. They can potentially also be used as drugs against cancer [99], [100] due to their cytotoxic properties and also against the HIV virus [7] and the presence of the gold metal enhances antiviral activity.

**Figure 3.1** shows six new gold(I) phosphine derivatives of 4,4'-dialkynyl substituted 2,2'-bipyridine.

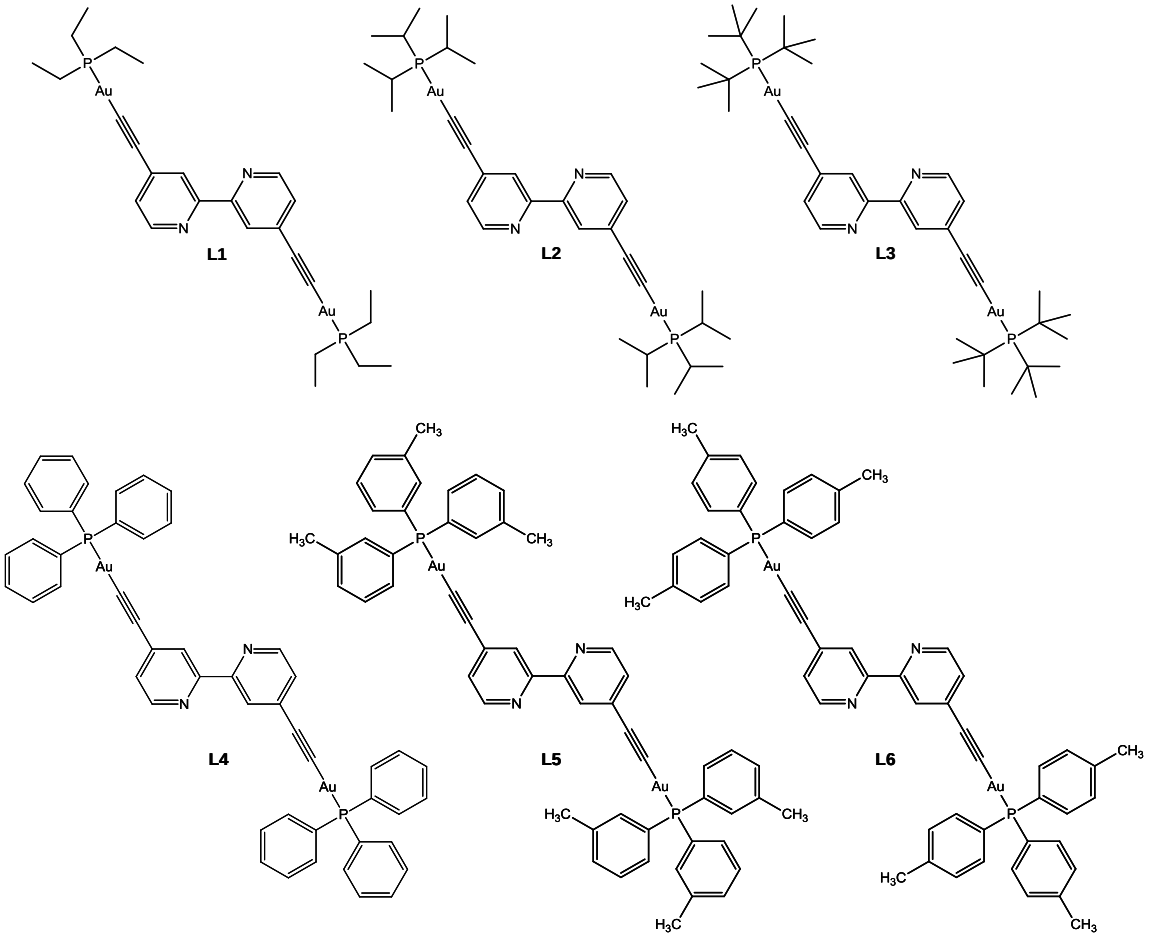


**Figure 3.1** Structures of **L1-L6**.

Compounds **L1-L6** were obtained by multi-step synthesis and the method of synthesis (**Scheme 3.1**) used was modified from that previously published.

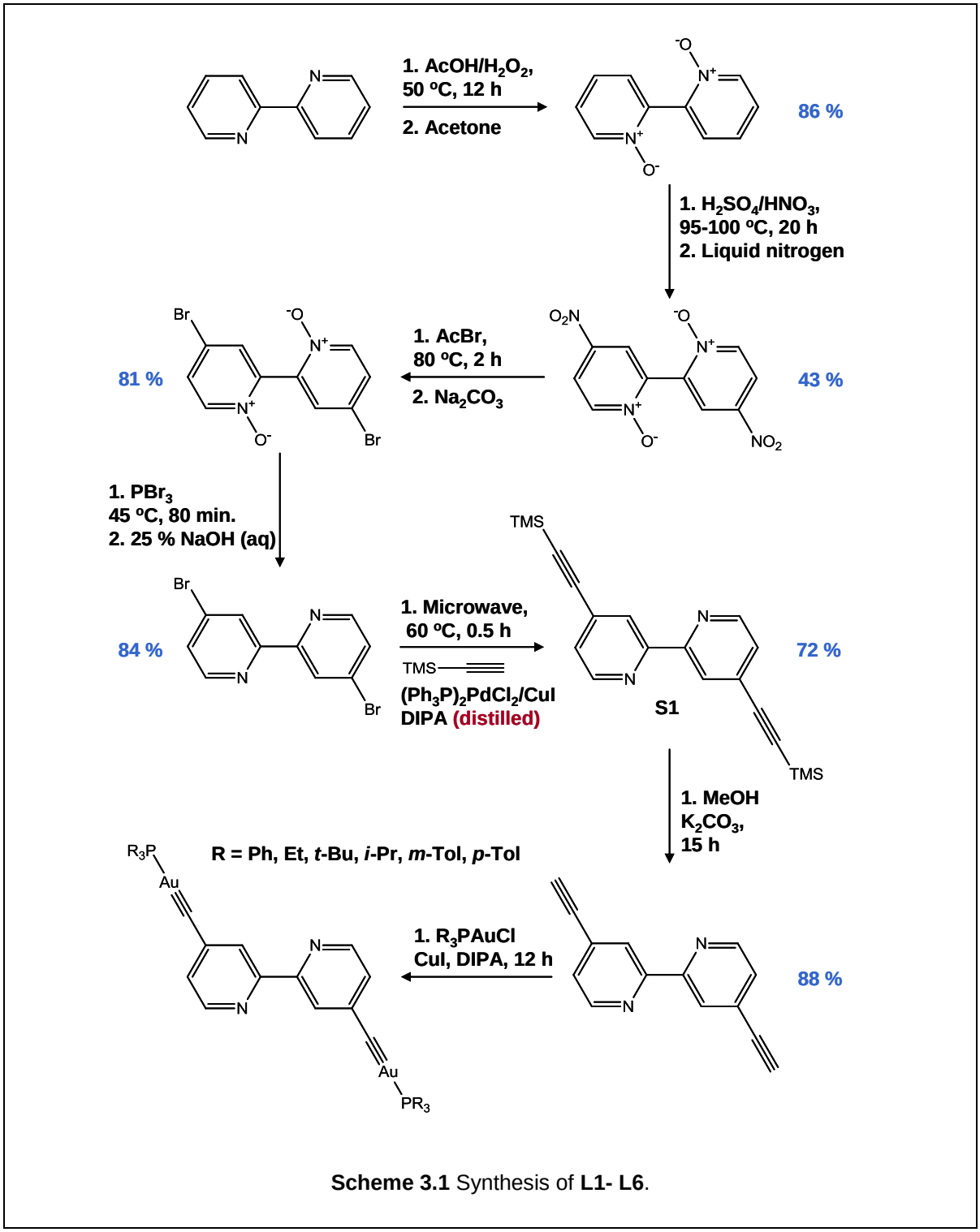


**Scheme 3.1** Synthesis of **L1- L6**.

In order to obtain the 4,4'-dialkynyl substituted 2,2'-bipyridine, in the first step 2,2'-bipyridine was oxidised to 2,2'-bipyridine-N,N'-dioxide using a combination of published methods [95] and [96]. Addition of a large volume of acetone in the final stage improved the yield (from 63 % to 86 %) and purity of the product.

Next, following the procedure described by Kavanagh and Leech [97], 4,4'-dinitro-2,2'-bipyridine-N,N'-dioxide was obtained as a result of nitration of the 4,4' positions of 2,2'-bipyridine-N,N'-dioxide but the final yield of the reaction in this case was much lower (43 %) than the authors claimed (86 %). In order to obtain dry product, which is crucial in the next step (bromination [98]), it is recommended to dry the product for one week in the desiccator, occasionally washing with cold $Et_2O$ and grinding, as this quickens the drying process.

The reduction of 4,4'-dibromo-2,2'-bipyridine-N,N'-dioxide was reported by Marker and Case [98], using an excess of $PBr_3$ as the reducing agent. If the substrates used in the bromination reaction are not dry, $PBr_3$ reacts violently with any water present in the reaction environment and that can decrease the yield of this reaction. The product was isolated mainly from the organic layer and washed with an aqueous solution of 25 % NaOH. The filtration through $Al_2O_3$ allows the isolation of pure 4,4'-dibromo-2,2'-bipyridine with good yield (84 %).

One common coupling reaction of terminal alkynes with aryl or vinyl halides is Sonogashira coupling, which was used in this case to obtain 4,4'-bis[2-(trimethysilyl)-1-ethynyl]-2,2'-bipyridine (**S1**). The published method [93] was modified. The reaction was carried out in a microwave reactor, which shortened the reaction time from 12 h to 30 min. Highly water and oxygen free conditions are required for efficient Sonogashira coupling, therefore the amine used in this reaction was freshly distilled. Also changing the purification method led to the product being obtained in good yield (~ 70 %). In order to isolate 4,4'-ethynyl-2,2'-bipyridine in the next step, the deprotection of trimethysilyl groups was carried out as described by Ziessel and co-workers [93].

Compounds **L1-L6** were obtained using similar procedures to the gold(I) phosphine-decorated 2,2':6',2''-terpyridine ligands [91]. The method was modified with the result that the products were obtained in reasonable yields (32-70 %).

Compounds **L1-L6** are light sensitive in solution, so they had to be protected from light during all the reaction and purification steps. The preparative plate chromatography was carried out in the dark and used as a purification method to avoid the decomposition of products and resulted in good separation of the impurities.

## 3.3. NMR spectroscopic studies of L1-L6

$^{1}$H NMR, $^{13}$C NMR and $^{31}$P NMR spectroscopies were used to characterise all $(R_3PAu{-}{\equiv})_2$bpy ligands. All spectra were measured in deuterated chloroform ($CDCl_3$). All the $^{1}$H and $^{13}$C peaks could be assigned using DEPT and 2-dimensional COSY, HMQC, HMBC and NOESY methods. The $^{1}$H NMR spectra show both $^{1}$H-$^{1}$H and $^{1}$H-$^{31}$P couplings. The $^{1}$H NMR spectrum with peak assignment of **L1** is illustrated in **Figure 3.2**.

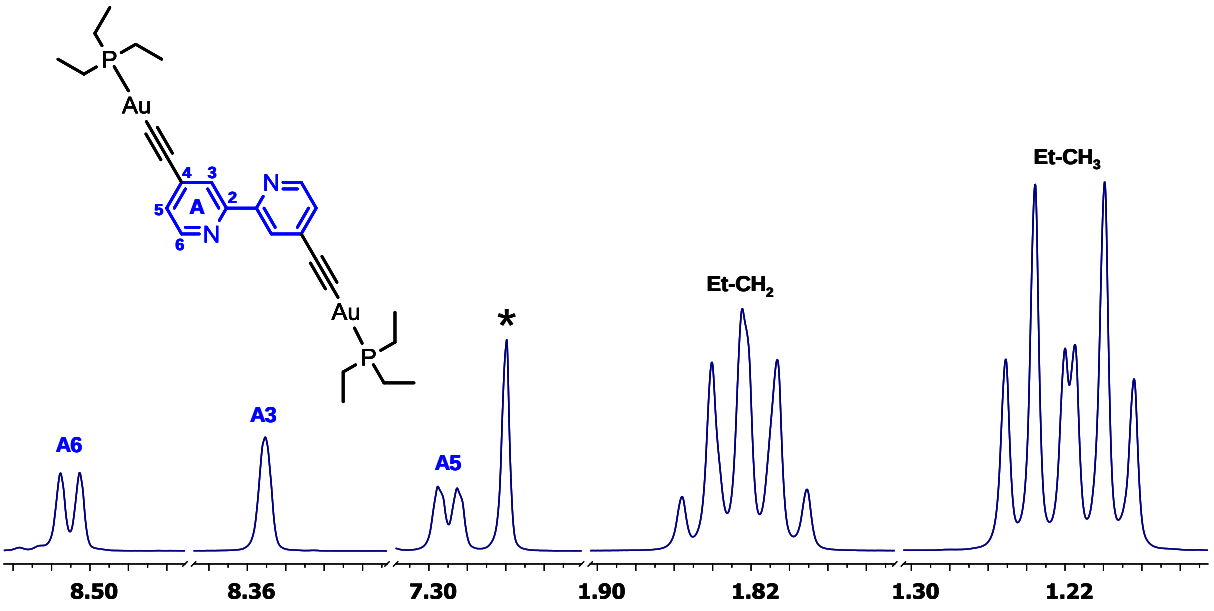


**Figure 3.2** 500 MHz $^{1}$H NMR spectrum of **L1**, δ [ppm]. The solvent peak (residual $CHCl_3$) is also visible (*).

The assignment of $^{13}$C NMR peaks was more difficult due to the lower sensitivity of $^{13}$C compared to that of $^{1}$H. In the standard experiment (NS = 1024, dτ = 2 sec), the quaternary carbons, due to shorter relaxation times, appear in the spectrum as very small peaks, which are hardly distinguished from the baseline. Additionally, the $^{13}$C NMR spectra show the $^{31}$P-$^{13}$C couplings, which make some of the peaks more difficult to resolve. For those reasons, the signals from the two carbons forming a triple bond in **L1** are not resolved in the $^{13}$C NMR spectra. The $^{13}$C NMR spectrum with peak assignment of **L1** is illustrated in **Figure 3.3**. The $C^{Et\text{-}CH2}$ peak is visible as a doublet due to a coupling with $^{31}$P. Coupling to $^{31}$P is not observed in the case of the $C^{Et\text{-}CH3}$ peak.

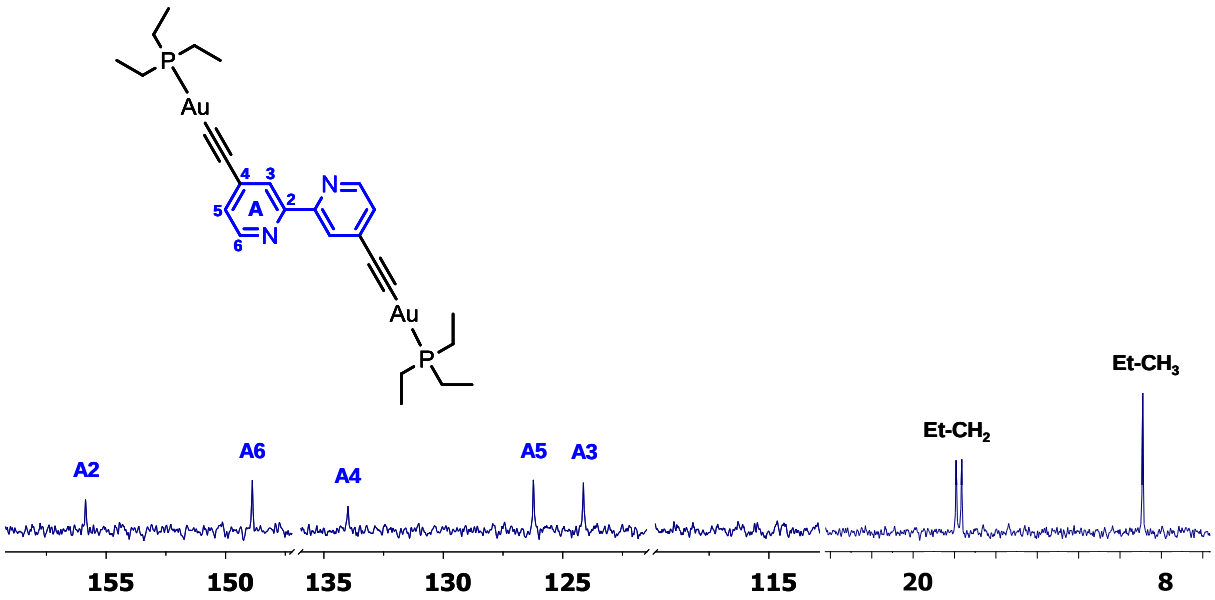


**Figure 3.3** 126 MHz $^{13}$C NMR spectrum of **L1**, δ [ppm].

Even though the signals due to the quaternary carbons forming a triple bond in **L1** are not observed in the $^{13}$C NMR spectrum, the strong cross peaks for $C^{iC\equiv CAu}$ and $H^{A6}$, $H^{A3}$ and $H^{5}$ appear in the 2-dimensional HMBC spectrum (**Figure 3.4**).

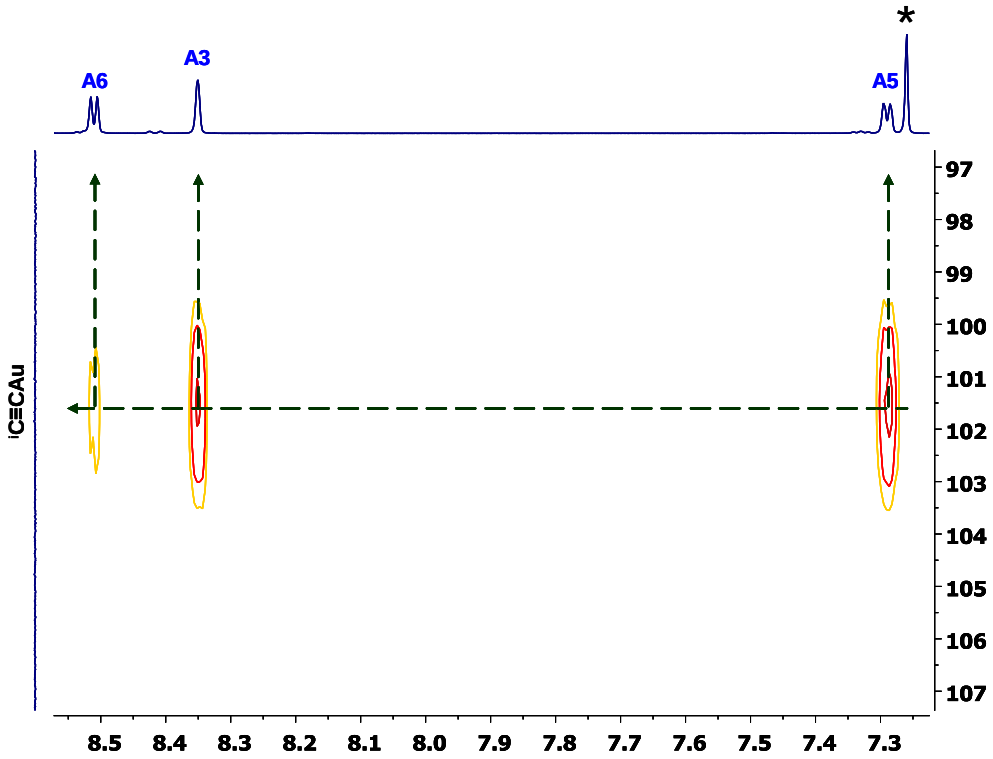


**Figure 3.4** HMBC spectrum (500MHz instrument) of **L1**, δ [ppm]. The solvent peak (residual $CHCl_3$) is also visible (*).

The $^{1}$H NMR spectrum with peak assignment of **L5** is illustrated in **Figure 3.5**.

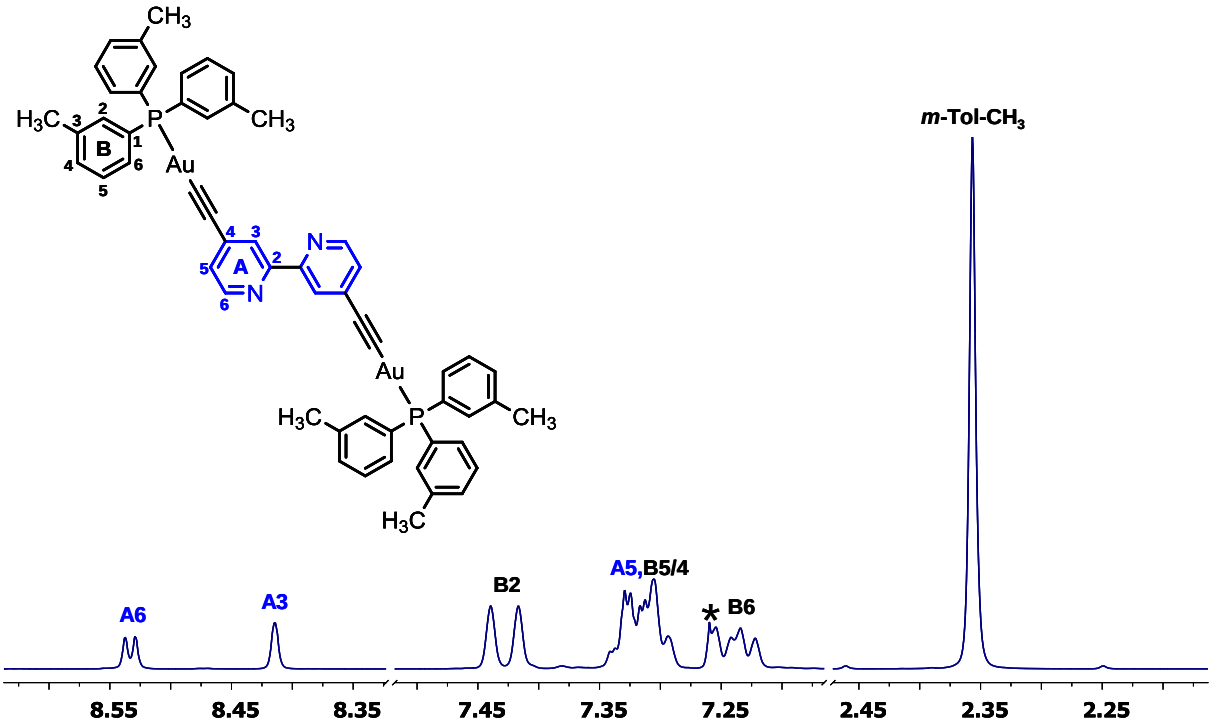


**Figure 3.5** 600 MHz $^{1}$H NMR spectrum of **L5**, δ [ppm]. The solvent peak (residual $CHCl_3$) is also visible (*).

The $^{13}$C NMR spectrum with peak assignment of **L5** is illustrated in **Figure 3.6**. The recording of the spectrum at 600 MHz enables the assignment of all carbon peaks, including the two carbons forming the triple bond in **L5**. In the spectrum they appear as two doublets with chemical shifts 139.13 and 101.94 ppm. The coupling constants are $J_{PC}$ = 142.3 Hz and $J_{PC}$ = 27.1 Hz respectively. The best solution to assign these peaks would have been to run a 2-dimensional experiment to look at the phosphorus-carbon correlation. In theory the weak cross peak from $C^{AuiC\equiv C}$ should be visible in the 2-dimensional HMBC spectrum as a coupling with $H^{A3}$ or $H^{A5}$ (four bonds). However, because there are other stronger cross peaks, which overlap in this area of the spectrum, the weaker cross peaks are very difficult to resolve. Therefore this peak was assigned by comparing the coupling constant and chemical shifts with similar compounds known from the literature [91]. This is not a problem with the second quaternary carbon ($C^{iC\equiv CAu}$), because the strong cross peaks with $C^{A6}$, $C^{A3}$ and $C^{A5}$ appear in the 2-dimensional HMBC spectrum (**Figure 3.7**).

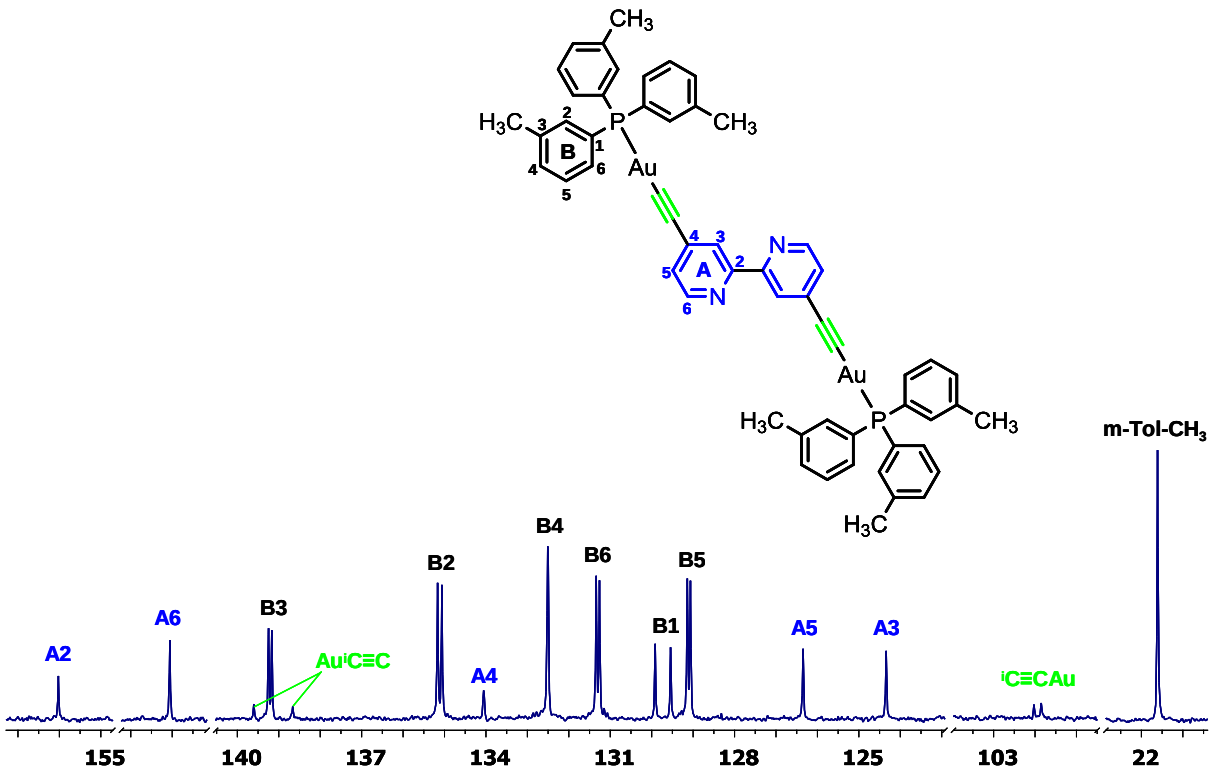


**Figure 3.6** 151 MHz $^{13}$C NMR spectrum of **L5**, δ [ppm].

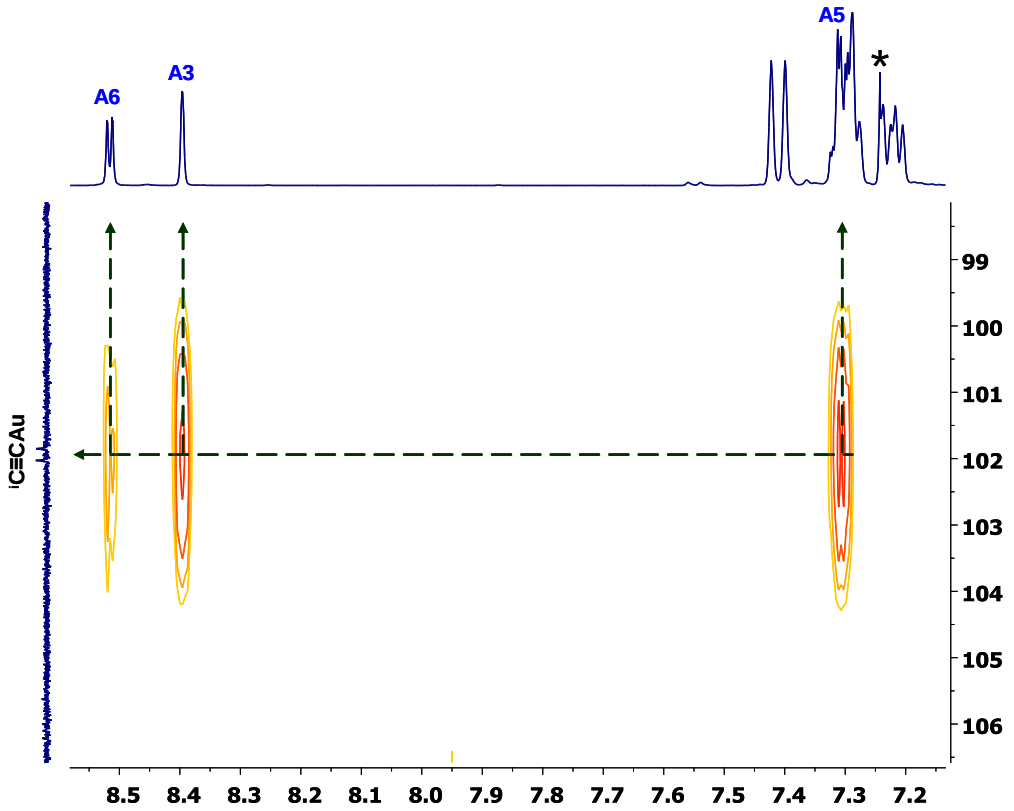


**Figure 3.7** HMBC spectrum (500 MHz instrument) of **L5**, δ [ppm]. The solvent peak (residual $CHCl_3$) is also visible (*).

$^{31}$P NMR spectroscopy is very helpful in characterisation of gold(I) phosphine derivatives and also allows to determine the purity of these complexes. **Table 3.1** lists $^{31}$P NMR spectroscopic data for **L1-L6.** $^{31}$P NMR resonances for all ligands are shifted towards higher frequencies compared with signals for $R_3PAuCl$. This trend is the same as in the case of $R_3P$ and $R_3PAuCl$. For that reason $^{31}$P NMR spectroscopy can be used to indicate the formation of **L1-L6**.

| | **$R_3P$** | **$R_3PAuCl$** | **$(R_3PAu{-}\equiv)_2bpy$** | **$\Delta\,\delta$** |
|---|---|---|---|---|
| **L1 (R= Et)** | -22.4 | 32.0 | 39.1 | 7.1 |
| **L2 (R= *i*-Pr)** | 17.4 | 65.0 | 67.6 | 2.6 |
| **L3 (R= *t*-Bu)** | 58.4 | 87.5 | 91.8 | 4.3 |
| **L4 (R= Ph)** | -5.4 | 30.2 | 39.0 | 8.8 |
| **L5 (R= *m*-Tol)** | -5.2 | 29.7 | 42.5 | 12.8 |
| **L6 (R= *p*-Tol)** | -7.3 | 28.2 | 40.6 | 12.4 |

**Table 3.1** $^{31}$P NMR spectroscopic data for **L1-L6**, 162 MHz, $CDCl_3$, $\delta$ [ppm].
$\Delta\,\delta = \delta\,^{31}P((R_3PAu{-}\equiv)_2bpy) - \delta\,^{31}P(R_3PAuCl)$.

## 3.4. UV-Vis spectroscopic studies of L1-L6

All absorption spectra for **L1-L6** were measured in $CH_2Cl_2$ solution and before the absorption measurements, were protected from the light to prevent the photodegadation of **L1-L6** in solution (see section 3.6). **Figure 3.8** shows the absorption spectra for **L1-L6** and **Table 3.2** lists the values of extinction coefficients calculated for $\lambda_{max}$.

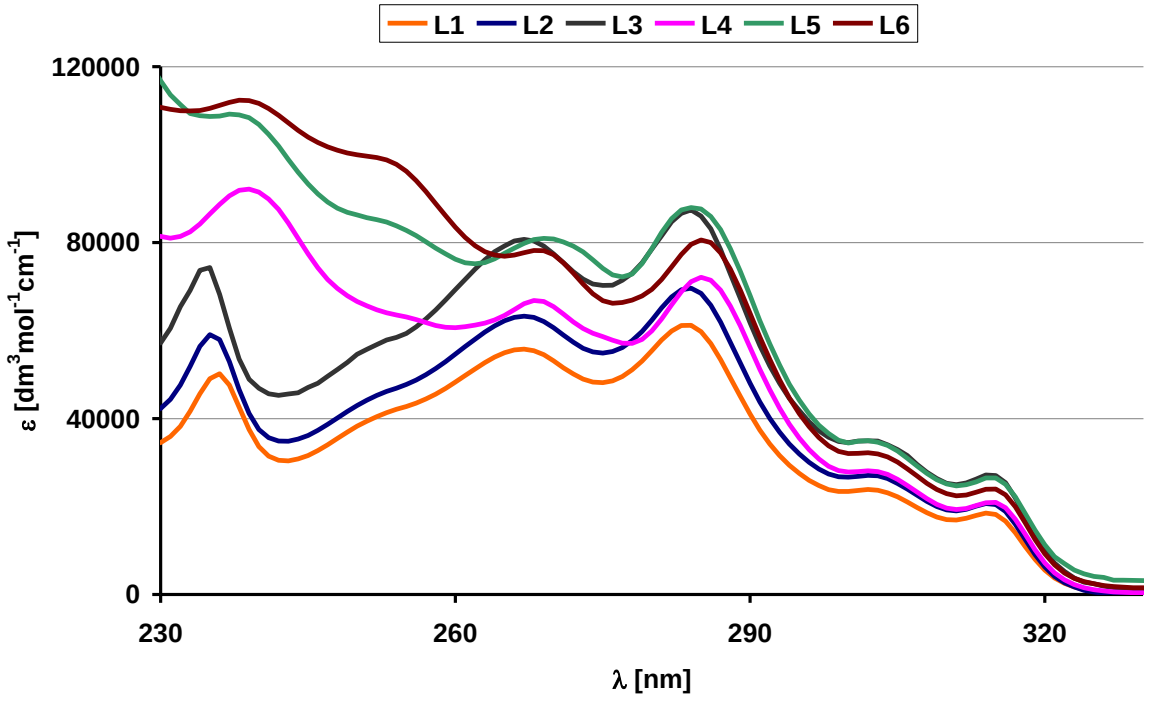


**Figure 3.8** Absorption spectra in for **L1-L6** in $CH_2Cl_2$ solution.

| Compound nr. | $\lambda_{max}$ [nm], ($\varepsilon$ / $10^4$ [$dm^3mol^{-1}cm^{-1}$]) |
|---|---|
| **L1 (R= Et)** | 236 (5.0), 267 (5.6), 284 (6.1), 302 (2.4), 314 (1.8) |
| **L2 (R= *i*-Pr)** | 235 (5.9), 267 (6.3), 284 (7.0), 302 (2.7), 314 (2.1) |
| **L3 (R= *t*-Bu)** | 235 (7.4), 267 (8.1), 284 (8.7), 302 (3.5), 314 (2.7) |
| **L4 (R= Ph)** | 239 (9.2), 268 (6.7), 285 (7.2), 302 (2.8), 315 (2.1) |
| **L5 (R= *m*-Tol)** | 237 (10.9), 252 (8.5), 269 (8.1), 284 (8.8), 302 (3.5), 314 (2.6) |
| **L6 (R= *p*-Tol)** | 238 (11.2), 253 (9.9), 269 (7.8), 285 (8.1), 303 (3.2), 315 (2.4) |

**Table 3.2** Electronic absorption spectroscopic data for **L1-L6** in $CH_2Cl_2$ solution.

The shape of the absorption curves and the $\lambda_{max}$ positions are similar for all ligands. However in the case of **L4-L6**, with triarylphosphine substituents, a more intense band at 239,

237 and 238 nm respectively, with respect to **L1-L3** was observed. This could be attributed to the additional π–π* transitions stemming from the aromatic substituents in **L4-L6**. The absorption spectra of **L5, L6** display the additional bands at 252 and 253 nm respectively, probably as a result of the influence of the electron donating methyl group.

Absorption band assignment for **L1-L6** is difficult without performing theoretical calculations. This is also the reason for unclear absorption band assignment in literature [79], [104], [105] for similar compounds displaying similar electron transitions.

In an attempt to overcome the above problem, the spectra shown in **Figure 3.9** were measured to simplify the process of absorption band assignment for **L1-L6**.

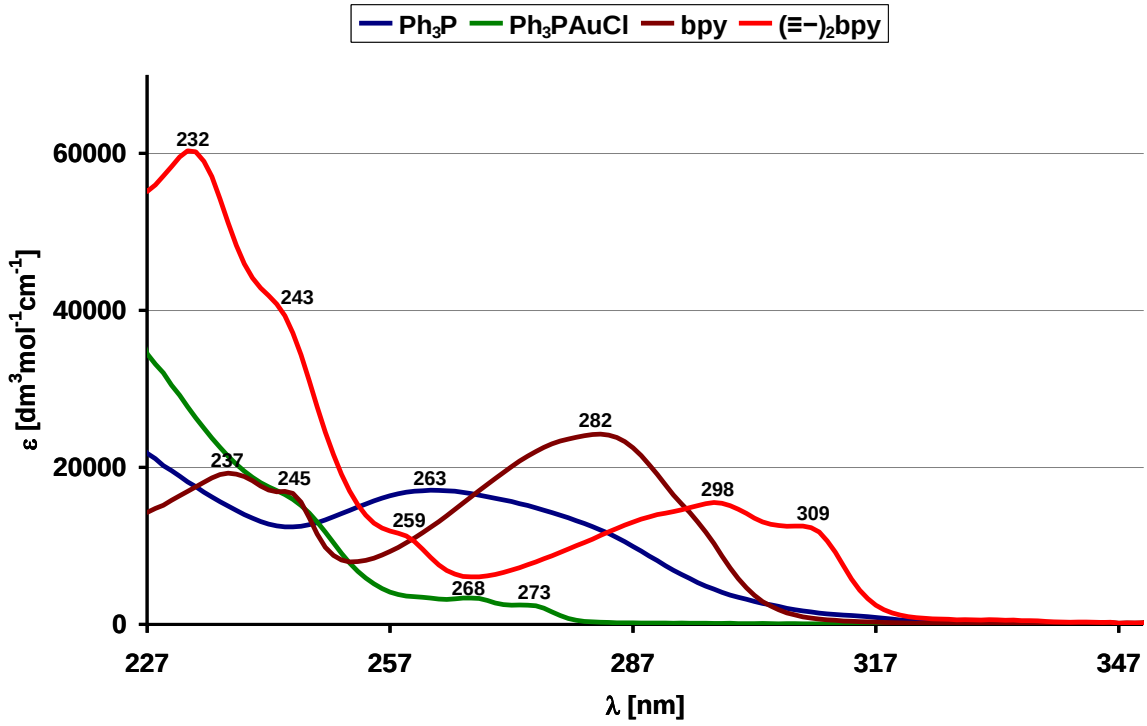


**Figure 3.9** Absorption spectra for **$Ph_3P$**, **$Ph_3PAuCl$**, **bpy**, **$(≡−)_2$bpy** in $CH_2Cl_2$ solution.

The absorption spectrum of 4,4'-diethynyl-2,2'-bipyridine shows bands at 232 nm with a shoulder at 243 nm and overlapping bands at 298 and 309 nm. These bands are respectively blue-shifted and red-shifted in comparison to bands in the spectrum of 2,2'-bipyridine, which occur at 237 and 245 nm and 262 nm respectively. The red-shift of the highest wavelength absorption band is caused by the increase in π-electron conjugation in bpy in 4,4'-diethynyl-2,2'-bipyridine.

The band at 237 with a shoulder at 245 nm in the spectrum of 2,2'-bipyridine can be assigned to π→σ* or n→π*/σ* (normally lower intensity) transitions, which are overlapping

in the spectrum. Similar transitions can be also seen for 4,4'-diethynyl-2,2'-bipyridine, but for this compound an increase in band intensity is observed. This may be due to the influence of the electron rich alkyne units, as similar effects were observed for the aromatic phosphine containing ligands **L4**-**L6**.

Bands for **L1**-**L6** at 302 (303) nm and 314 (315) nm are red-shifted with respect to the bands at 298 and 309 nm in 4,4'-diethynyl-2,2'-bipyridine, which suggest the influence of the electron density of the Au d-orbitals. The involvement of Au-orbitals is responsible for the development bands at 267 (268, 269) nm and 284 (285) nm for **L1**-**L6**. Also, the alkynyl groups, characterized by linear geometry, structural rigidity and the extended π-electron delocalization, enable interactions with metal centers through overlap of π-d orbitals [103]. Tentatively, by comparison with the results of other authors [101]-[103], bands at 267 (268, 269) nm and 284 (285) nm may be assigned to σ(Au-P)→π* (C≡C), π–π* (C≡C) from alkynyl group and metal-to-ligand charge-transfer (MLCT [d(Au)→π*(C≡C, alkynyl)]).

## 3.5. Fluorescence spectroscopic studies of L1-L6

All **L1-L6** are emissive as expected from molecules containing in the structure [-P-Au–≡–] –units [79], [101]-[103].

The photodegradation processes for **L1-L6** have been studied during the fluorescence measurements when these compounds were excited with $\lambda_{ex}$ = 235-239 nm. This is described in more detail in section 3.6.

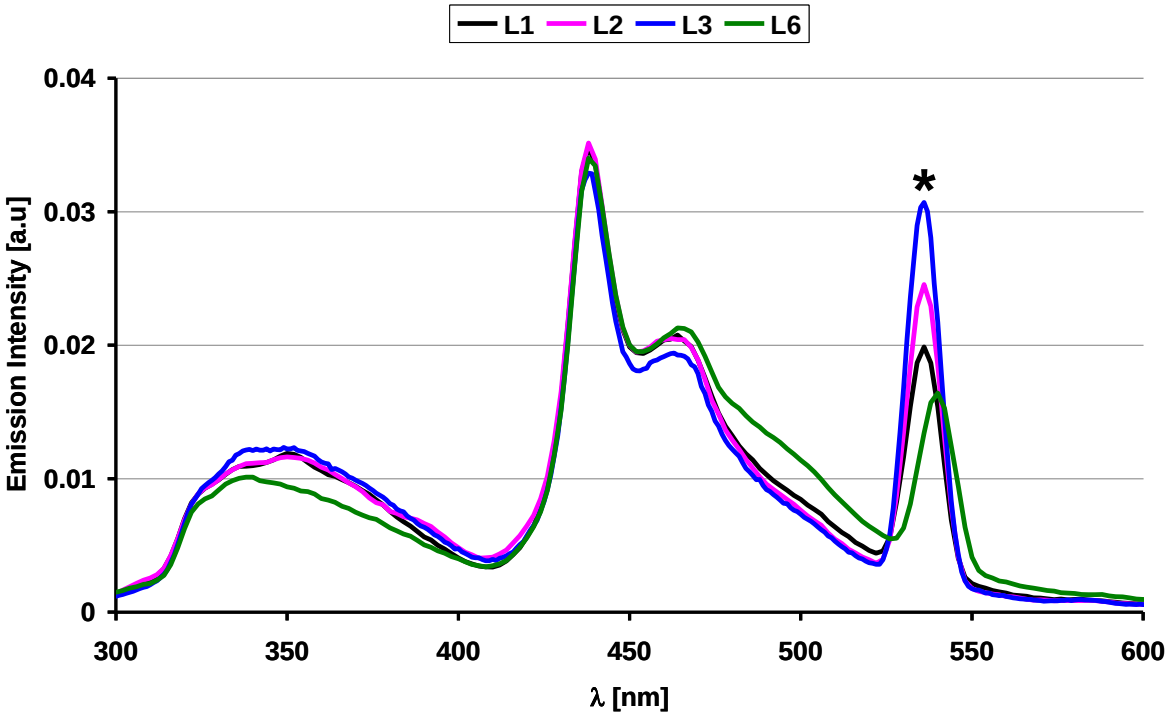


**Figure 3.10** Emission spectra of **L1, L2, L3, L6**. Excitation $\lambda_{ex}$ = 267 or 269 nm, slit 5/5, concentration of each $CH_2Cl_2$ solution is 1.2 * $10^{-5}$ mol/$dm^3$, * = first harmonic.

| Compound nr. | $\lambda_{ex}$ [nm] | $\lambda_{em}$ [nm] |
|---|---|---|
| **L1 (R= Et)** | 267 | 350, 438, 466 |
| **L2 (R= *i*-Pr)** | 267 | 348, 438, 464 |
| **L3 (R= *t*-Bu)** | 267 | 337, 439, 465 |
| **L4 (R= Ph)** | 268 | 338, 438, 466 |
| **L5 (R= *m*-Tol)** | 268 | 338, 439, 468 |
| **L6 (R= *p*-Tol)** | 269 | 338, 438, 466 |

**Table 3.3** Fluorescence spectroscopic data for **L1-L6** in $CH_2Cl_2$ solution.

**Figure 3.10** shows the emission spectra for **L1**, **L2**, **L3**, **L6**, which were measured for the same concentrations and slit opening. **Table 3.3** lists the values of $\lambda_{em}$ for **L1-L6** and their corresponding $\lambda_{ex}$.

The shapes of the fluorescence spectra are very similar for all **L1-L6** and are virtually independent of phosphine substituents. The excitation of **L1-L6** with $\lambda_{ex}$ = 284 (285) nm (**Table 3.3**) revealed three emission bands: 338 (337, 348, 350) nm and two overlapping bands at 438 (439) nm and 466 (465, 464, 468) nm. Tentatively, these emission bands could be assigned to mixed IL [$\pi\rightarrow\pi*$(C≡CR)] and MLCT [d(Au)$\rightarrow\pi^*$(C≡C)] transitions with predominantly IL transitions and [$\sigma$(Au–P)$\rightarrow\pi^*$(C≡C)] transitions [101], [102], [106].

## 3.6. Photodegradation of L1-L6

Many Ag- and Au-containing compounds are not stable in solution and decompose under the influence of light [107]-[109]. Usually, the higher the temperature, the faster this process is. All the $(R_3PAu{-}{\equiv})_2$bpy ligands prepared in this work are light sensitive in solution. The $^1$H NMR spectra in **Figure 3.11** illustrate the process of photodegradation with time.

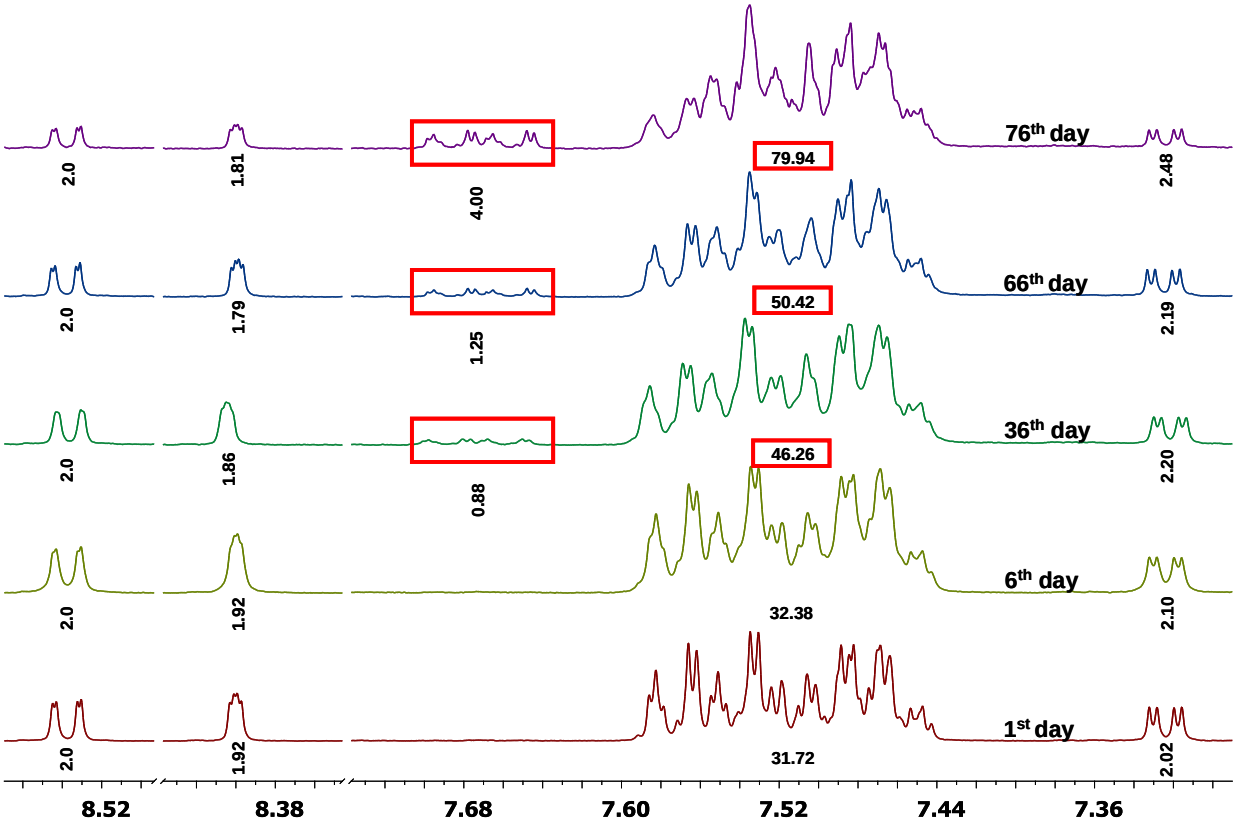


**Figure 3.11** 400 MHz $^1$H NMR spectra of **L4** showing photodegradation with time, δ [ppm]. The relative integrals of the signals are shown.

Probably, the bonds between the triple bonded carbon and gold, or gold and phosphorus, of **L4** are broken and result in new species in solution. They can be observed as peaks appearing in the range of 7.64 – 7.70 ppm.

The solubility of the material in the NMR sample decreases during the photodegradation process. Also, the shape of the multiplet assigned to the protons from the triphenylphosphine part of **L4** changes, which suggests regrouping in this part of the compound. The relative integral signal assigned to the triphenylphosphine part of **L4** increases and a slight amount of yellow precipitate is observed in the NMR-tube. Analysis of

the relative integral values suggest that bpy-containing spiecies are present in the precipitate. The characterisation of the precipitate was not possible due to the very small amount of it.

Additional peaks also appear in the $^{31}$P NMR spectrum (**Figure 3.12**). They are consistent with the formation of a new phosphorus-containing species in solution. The chemical shift of the first peak ($\delta$ = 29.84 ppm) is in the same range as that of $Ph_3PAuCl$ or $[Ph_3PAu]^+$ [110], but unambiguously assigning both additional signals in the $^{31}$P NMR spectrum is difficult.

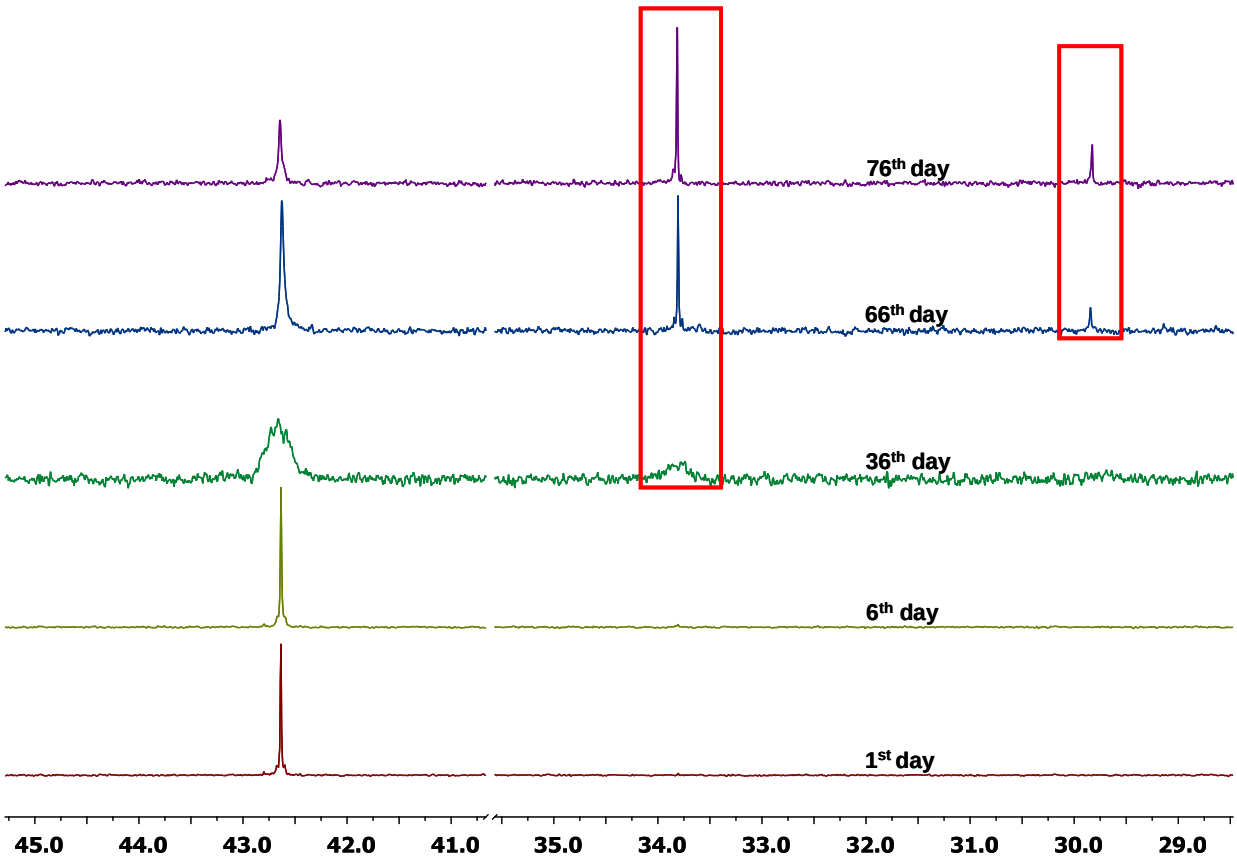


**Figure 3.12** 162 MHz $^{31}$P NMR spectra of **L4** showing photodegradation with time, $\delta$ [ppm]. Additional peaks, which appeared in the $^{31}$P NMR spectrum during this process, are marked by red boxes.

The photodegradation of **L1-L6** can be observed during fluorescence measurements (**Figure 3.13, 3.14**). The emission spectra were recorded over a period of about 10-30 min (approximately 10-30 spectra). The compounds were excited with $\lambda_{ex}$ = 235-239 nm and a decay of all the fluorescence bands for **L1-L6** was observed. On the excitation at higher wavelength, such changes either were not observed, were much slower or hardly discernible depending on the compound under observation.

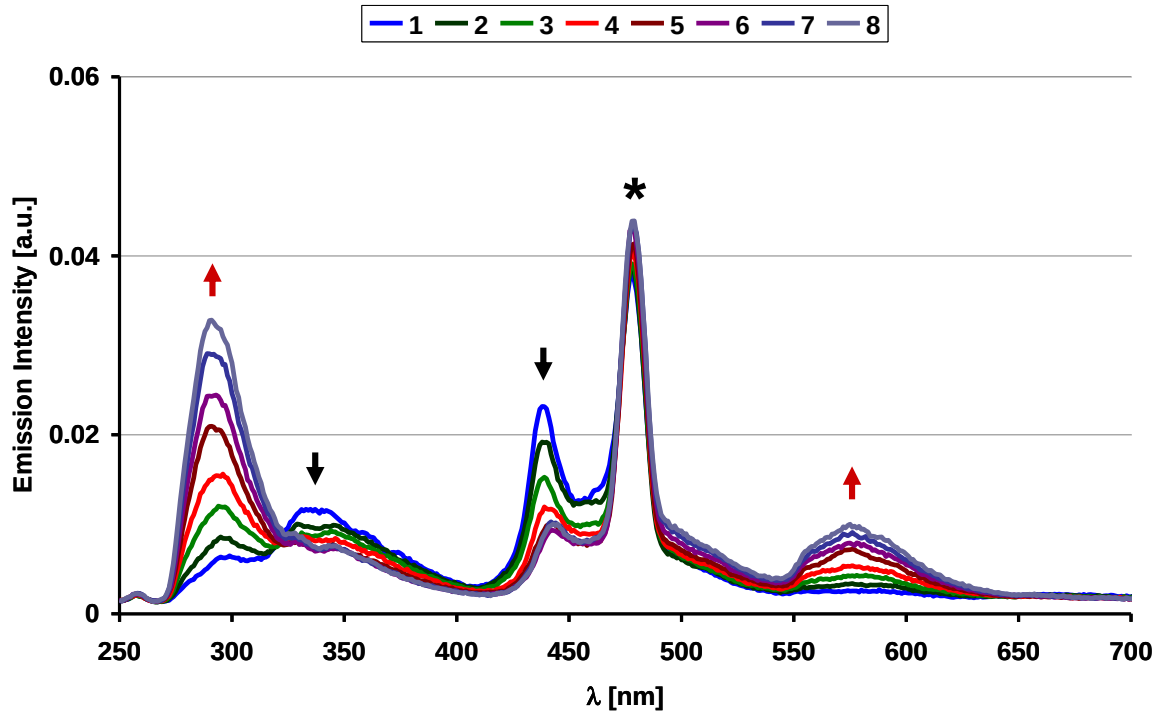


**Figure 3.13** Emission spectrum of a $CH_2Cl_2$ solution of **L6** as a function of time ($\lambda_{ex}$ = 238 nm, * = first harmonic). The measurement time was approximately 8 min.

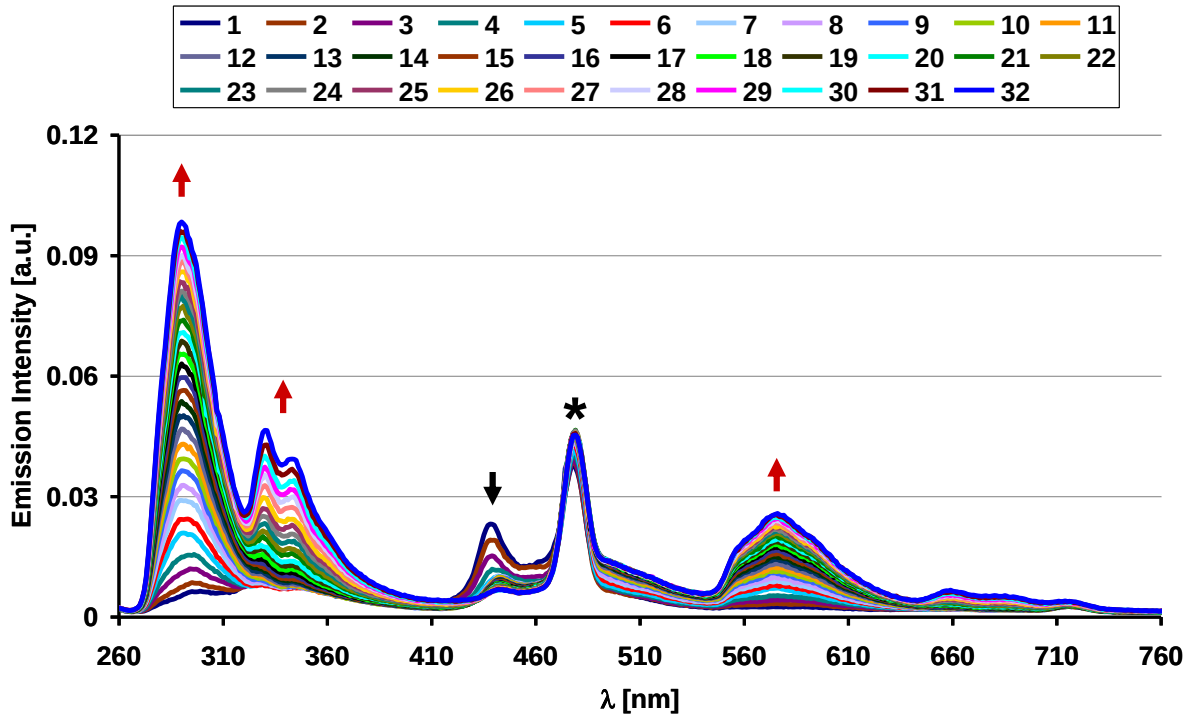


**Figure 3.14** Emission spectrum of a $CH_2Cl_2$ solution of **L6** as a function of time ($\lambda_{ex}$ = 238 nm, * = first harmonic). The measurement time was approximately 30 min.

The formation of emissive compounds was observed as a result of the photodegradation of **L4-L6**. Additional bands (**Table 3.4**) appeared in the fluorescence spectrum and their intensity increased at the expense of the bands already assigned to **L4-L6** (**Figure 3.13, 3.14**). The observed emission (about 580 nm) upon photodegradation is not inconsistent with the formation of small gold nanoclusters [111].

| Compound nr. | $\lambda_{ex}$ [nm] | $\lambda_{em}$ [nm] | $\lambda_{em}$ [nm] after photodegradation |
|---|---|---|---|
| **L4 (R= Ph)** | 239 | 338, 438, 466 | 292, 493 |
| **L5 (R= *m*-Tol)** | 237 | 338, 439, 468 | 294, 585 |
| **L6 (R= *p*-Tol)** | 238 | 338, 438, 466 | 291, 331, 344, 577 |

**Table 3.4** Fluorescence spectroscopy data for **L4-L6** in $CH_2Cl_2$ solution after photodegradation.

Absorption spectra were measured for **L4** and **L6** immediately after each series of emission spectra ($\lambda_{ex}$ = 238 or 239 nm) and revealed new absorption bands at 274, 321, 332 and 363 nm for **L4** (**Figure 3.15**) and 277, 321, 334, 363 nm for **L6** (**Figure 3.16**).

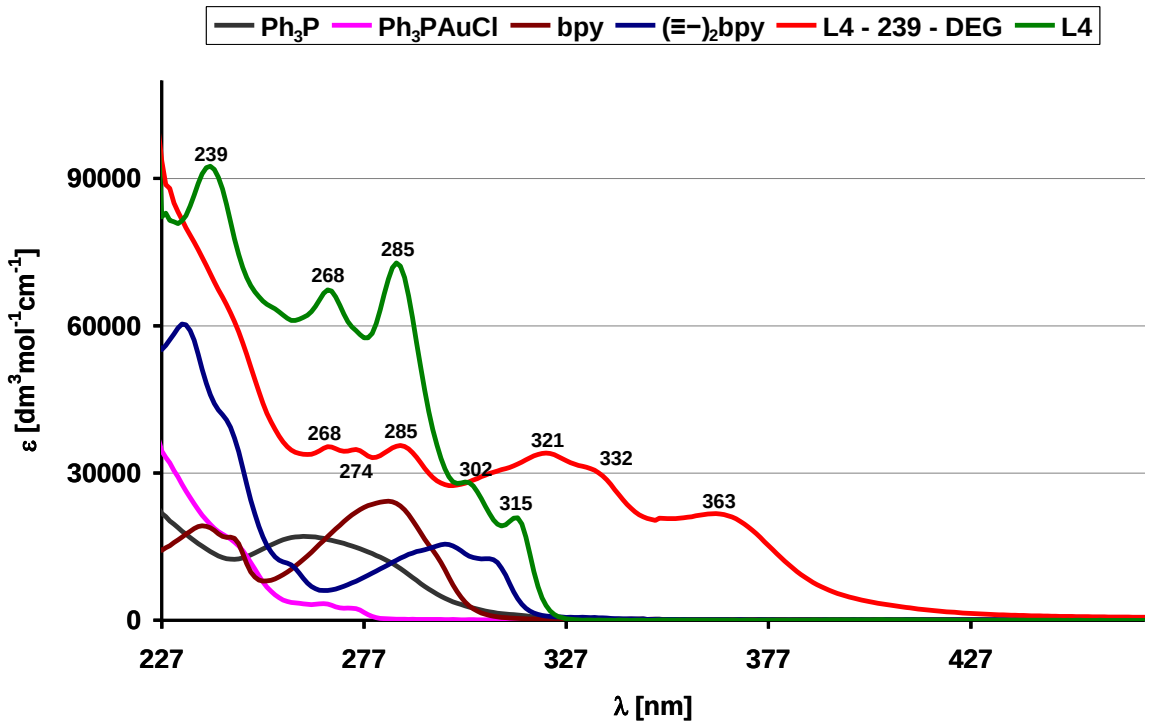


**Figure 3.15** Absorption spectrum for **L4** in $CH_2Cl_2$ solution before and after photodegradation. Absorption spectra for $Ph_3P$, $Ph_3PAuCl$, bpy, and $(\equiv\!-)_2$bpy are also shown.

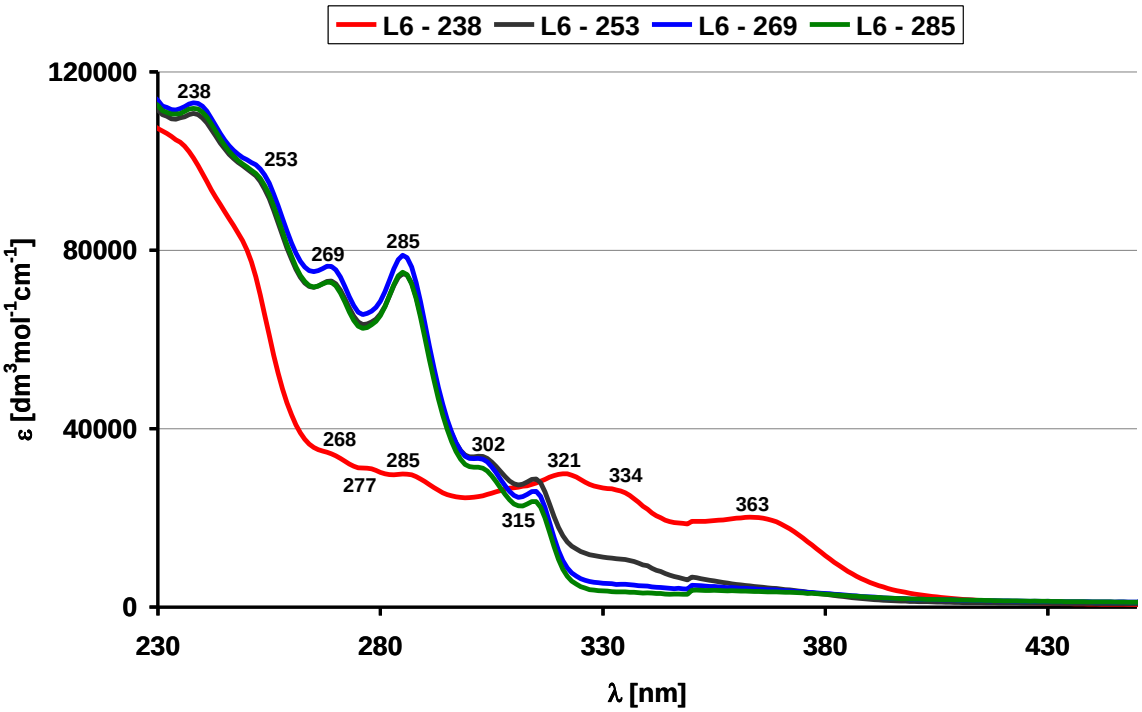


**Figure 3.16** Absorption spectra for **L6** in $CH_2Cl_2$ solution recorded after a series of fluorescence measurements for different $\lambda_{ex}$ (values stated at the top of figure).

The absorption spectra were measured immediately after each series of emission spectra for $\lambda_{ex}$ > 238 nm (e.g.: **L6**, $\lambda_{ex}$ = 253, 269, 285 nm). They either do not show photodegradation or the effect of the photodegradation was hardly discernible (**Figure 3.16**), as observed in the fluorescence spectra.

From the experiments carried out, it was not possible to determine the nature of the photodegradation products. They probably arise from cleavage of the alkynyl-gold bond, which is suggested by the decrease of the characteristic band intensities at 238, 269, 285 nm in the absorption spectrum (**Figure 3.16**). These bands may be assigned to alkyne-centered π→π* transitions and bpy/alkyne π→π* transitions with involvement of Au orbitals [101]-[103].

The photodegradation of **L1** and **L2** observed after a series of fluorescence measurements ($\lambda_{ex}$ = 235, 236 nm) either did not lead to the formation of emissive compounds or the bands are much less intense than degradation products of **L4**-**L6** (**Figure 3.17**). The quenching of the emissions of **L1** and **L2** is much faster (approximately 10 min) than in the case of **L4**-**L6**, which suggest lower stability of these first two compounds.

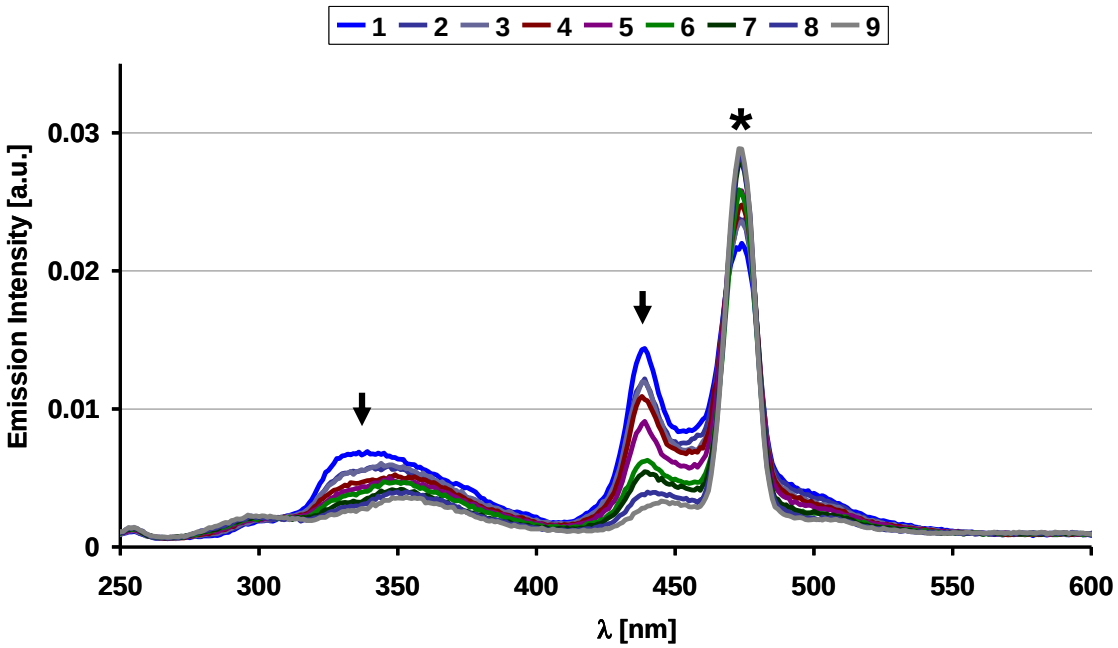


**Figure 3.17** Emission spectrum of a $CH_2Cl_2$ solution of **L2** as a function of time ($\lambda_{ex}$ = 235 nm, * = first harmonic). The measurement time was approximately 9 min.

The fragmentation of **L1**-**L6** can also be observed during ESI-MS measurements. The fragmentation patterns and m/z values (e.g.: for **L2**: 517.4 ($[(i\text{-}Pr_3P)_2Au]^+$, calc. 517.2), 917.4 ($[\mathbf{L2} + H]^+$, calc. 917.3), 1173.2 ($[\mathbf{L2} + (i\text{-}Pr_3PAu)]^+$, calc. 1173.4) enables the identification of $[R_3PAu]^+$ and $[(R_3P)_2Au]^+$ as two products of this process.

## 3.7. X-ray diffraction studies of L1-L6

A series of compounds **L1-L6** was obtained by changing the phosphine substituents (**L1** contains two $Et_3P$ units, and **L2** – *i*-$Pr_3P$, **L3** – *t*-$Bu_3P$, **L4** – $Ph_3P$, **L5** – *m*-$Tol_3P$, **L6** – *p*-$Tol_3P$), which influences the crystal packing. The bulk of a phosphine ligand can be measured by the Tolman cone angle (θ).

In the 1970's, the Tolman cone angle was measured by using physical models of molecules and Tolman defined the θ angle as follows:

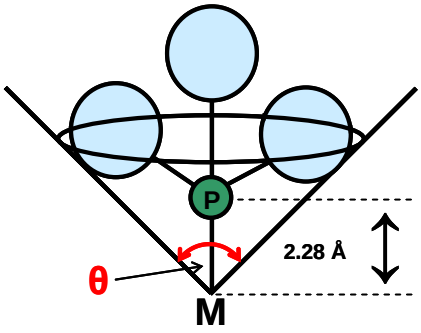


**Figure 3.18** The cone angle, θ.

"The steric parameter, θ, for symmetric ligands (all three substituents the same) is the apex angle of a cylindrical cone, centered 2.28 Å (2.57cm) from the center of the P atom, which just touches the van der Waals radii of the outermost atoms of the model"[112].

**Figure 3.18** illustrates the Tolman cone angle. The size of the ligand affects the reactivity of the attached metal centre, which is particularly important in the case of catalysts, but also influences molecular packing within a crystal structure. **Table 3.5** lists values of the ligand cone angle for a selection of phosphine substituents including those relevant to this thesis.

Molecular structures of **L1-L6** show that the 2,2'-bipyridine moiety adopts the expected *transoid* conformation. Au…Au interactions are observed for **L1** and **L2**, however for **L3-L6** the shortest distance between two gold atoms is longer (4.7631(5) Å to 6.996(1) Å), and there are no Au…Au interactions observed. If only the Tolman cone angle is considered, there should not be much difference in the Au…Au distance between ligands with triarylphosphine units and ligands with trialkylphosphine units. The value of the Tolman cone angle for (*p*-Tol)$_3$P and $PPh_3$ is 145 ° and for (i-Pr)$_3$P is 160°.

| $PR_3$ | θ [°] |
|---|---|
| $PH_3$ | 87 |
| $PEt_3$ | 132 |
| P(*i*-Pr)$_3$ | 160 |
| P(*t*-Bu)$_3$ | 182 |
| $P(Ph)_3$ | 145 |
| P(*m*-Tol)$_3$ | 165 |
| P(*p*-Tol)$_3$ | 145 |

**Table 3.5** Values of the ligand cone angle for the chosen phosphine substituents [112], [113].

However, the packing of molecules depends

not only on the size of the molecules but also on the intermolecular and intramolecular interactions occuring. While the Tolman cone angle defines the volume of a triphosphine ligand, it does not take into consideration the empty space inside the cone (which is not filled by phosphine substituents) or the height of the cone itself. The analysis of the crystal packing of **L4-L6** shows that the empty space inside the phosphine cone is serving to interlock the two phosphine substituents from two independent molecules of **L4-L6** and that weak intermolecular π–π interactions stabilise this arrangement. This may lead to the observed increase in the Au…Au distance. The lack of Au…Au interactions observed for **L2** can be attributed to the steric demands of tri(*t*-butyl)phosphine units which have a large Tolman cone angle of 182°.

## Crystal structure description of L1-L6.

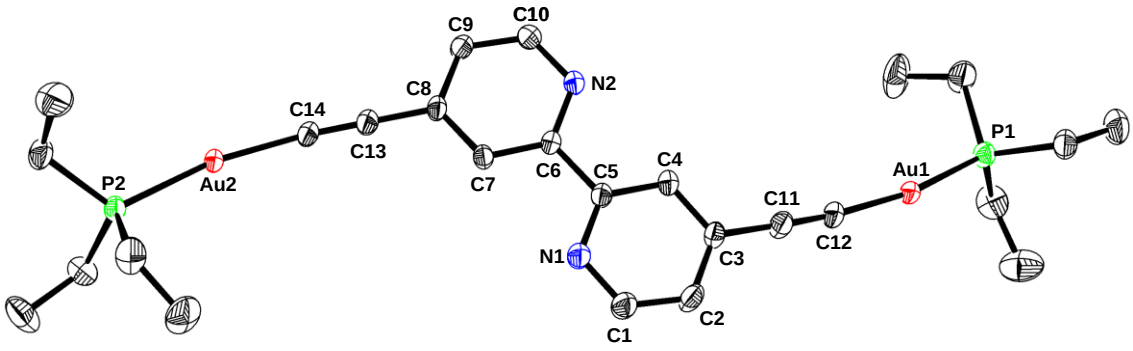


**Figure 3.19** Molecular structure of **L1** (ORTEP - probability ellipsoids - 70 %). All H atoms are omitted for clarity.

| Bond | Length [Å] | Bond angle | Value [°] |
|---|---|---|---|
| **Au1−P1** | 2.2808(6) | **Au2$^{i}$−Au1−P1** | 102.797(17) |
| **Au1− C12** | 2.004(2) | **Au2$^{i}$−Au1−C12** | 85.95(7) |
| **Au2− P2** | 2.2801(6) | **P1−Au1−C12** | 170.77(7) |
| **Au2−C14** | 1.999(2) | **Au1$^{ii}$−Au2−P2** | 99.261(16) |
| **C11−C12** | 1.213(3) | **Au1$^{ii}$−Au2−C14** | 90.50(7) |
| **C13−C14** | 1.216(3) | **P2−Au2−C14** | 167.52(7) |
| | | **C3−C11−C12** | 173.2(3) |
| **Bond angle** | **Value [°]** | **C11−C12−Au1** | 171.2(2) |
| **C8−C13−C14** | 176.6(3) | **C13−C14−Au2** | 166.7(2) |

**Table 3.6** Selected bond lengths and bond angles of **L1.**

X-ray quality single crystals of **L1** in the form of colourless needles were obtained by slow diffusion of $Et_2O$ into a $CH_2Cl_2$ solution of **L1**. The compound crystallized in the monoclinic system, space group $P2_1/c$. The unit cell comprises four molecules and the labelling of atoms is shown in **Figure 3.19**. The selected bond lengths and bond angles of **L1** are summarised in **Table 3.6**

The dominant aurophilic interactions in **L1** with Au2…Au1$^{ii}$ distance 3.1239(14) Å, (distance between the two nearest gold atoms from different molecules, symmetry code as in **Figure 3.20**), result in the assembly of polymeric chains as is shown in **Figure 3.20**. Angles Au2$^{i}$–Au1–C12 and Au1$^{ii}$–Au2–C14 are 85.95(7) and 90.50(7)° respectively, symmetry codes: i = 1+x, 3/2-y, 1/2+z, ii: -1+x, 3/2-y, -1/2+z.

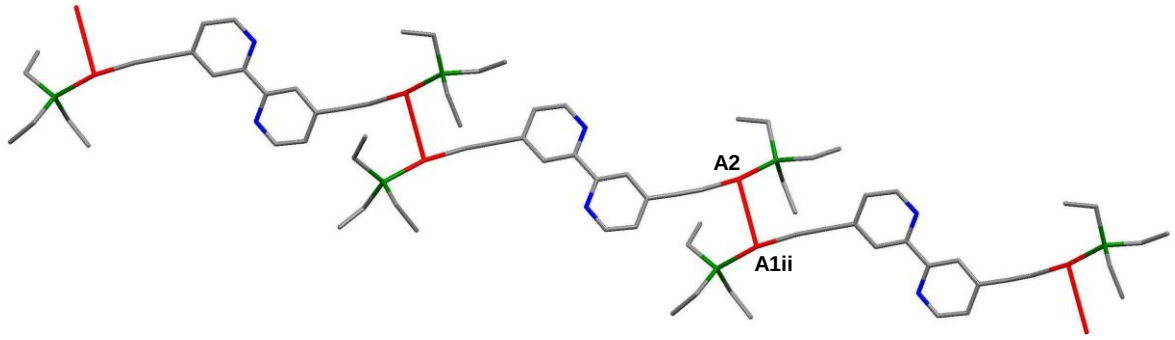


**Figure 3.20** Molecules of **L1** form a chain by virtue of short Au…Au contacts (symmetry code: ii: -1+x, 3/2-y, -1/2+z)

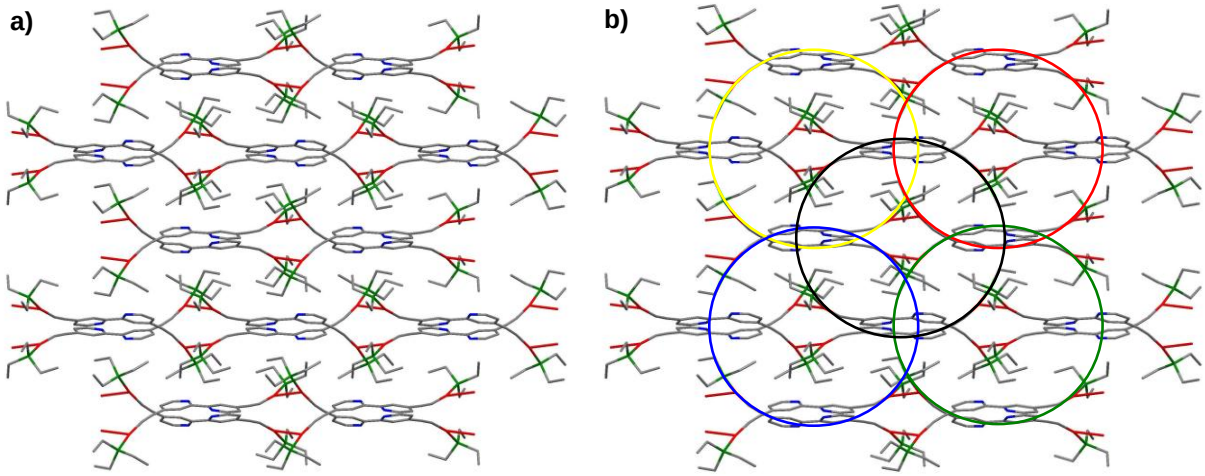


**Figure 3.21** The crystal packing of **L1**: a) view along the c-axis, b) view along the c-axis with marked characteristic motif.

Weak interactions between phosphine units and the triple C-C bond ($^{Et}$C−H…$C_{alkyne}$) and weak hydrogen bonding (C−H…N, **Figure 3.22**) influence the bond angles for Au2$^{i}$–Au1–P1 and Au1$^{ii}$–Au2–P2 (102.797(17) and 99.261(16)° respectively).

The Au…Au contacts, the weak interactions between $^{Et}$C–H and $C_{alkyne}$ and weak non-classical hydrogen bonds (C–H…N) for **L1** lead to twisting of the pyridine ring planes and bending of the atomic wires (C8-P2 or C3-P1) in two different directions and consequently, outstretched s-shapes are formed.

The projection along the c-axis shows that four units: two atomic wires (C3-P1) with two pyridine rings and two atomic wires (C8-P2) form circular-shapes as is marked in colour in **Figure 3.21, b)**. The four building blocks are parts of different molecules. Each circle connects with four others and the radius of those circles is approximately 7.3 Å.

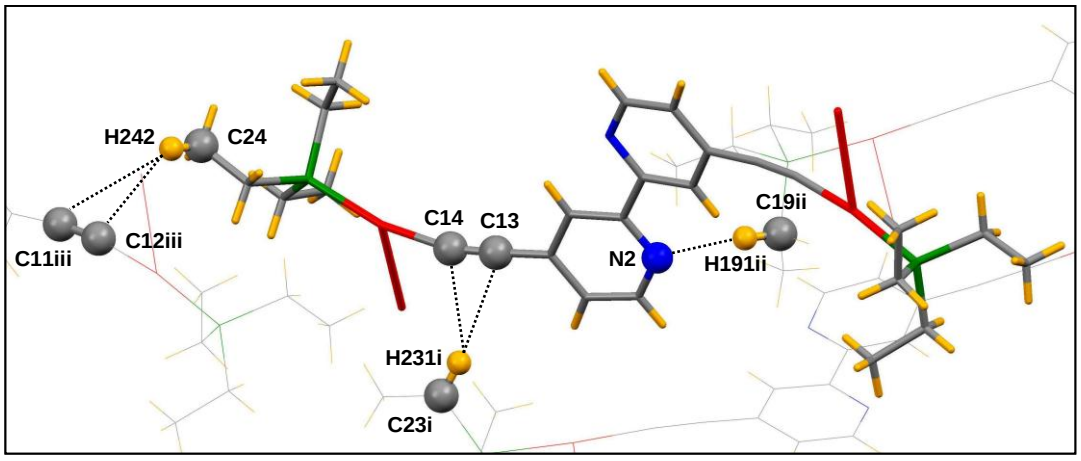


**Figure 3.22** Weak interactions: $^{Et}$C−H…$C_{alkyne}$ and non-classical hydrogen bond (C−H…N) for **L1**. Symmetry codes as listed in **Table 3.7**.

| D−H…A | H…A [Å] | D…A [Å] | D−H…A [°] | Symmetry code |
|---|---|---|---|---|
| **C23$^{i}$−H231$^{i}$…C13** | 2.94 | 3.899(4) | 168 | i: x, 3/2-y, 1/2+z |
| **C23$^{i}$−H231$^{i}$…C14** | 2.82 | 3.659(4) | 144 | i: x, 3/2-y, 1/2+z |
| **C19$^{ii}$−H191$^{ii}$…N2** | 2.66 | 3.617(4) | 171 | ii: 1-x, -1/2+y, 3/2-z |
| **C24−H241…C11$^{iii}$** | 3.32 | 3.967(5) | 127 | iii: 1-x, y, 1+z |
| **C24−H241…C12$^{iii}$** | 2.85 | 3.521(5) | 127 | iii: 1-x, y, 1+z |

**Table 3.7** Bond lengths and bond angles for $^{Et}$C−H…$C_{alkyne}$ and non-classical hydrogen bond (C−H…N) for **L1**.

The weak interactions between $^{Et}$C–H and $C_{alkyne}$ and non-classical hydrogen bonds (C–H…N) shown in **Figure 3.22** stabilise the assembly of polymeric chains of **L1.** The proton H231$^{i}$ is an acceptor in forming non-classical hydrogen bonds of C–H…N type for both C13 and C14 as donors, which causes a decrease of the angle for C23$^{i}$–H231$^{i}$…C14 to 144°. Angles for C24−H241…C11$^{iii}$ and C24−H241…C12$^{iii}$ amount to 127° and 126° showing the influence of sharing the acceptor (H241), Au…Au, and $^{Et}$C−H…$C_{alkyne}$ interactions [115], [116], [117].

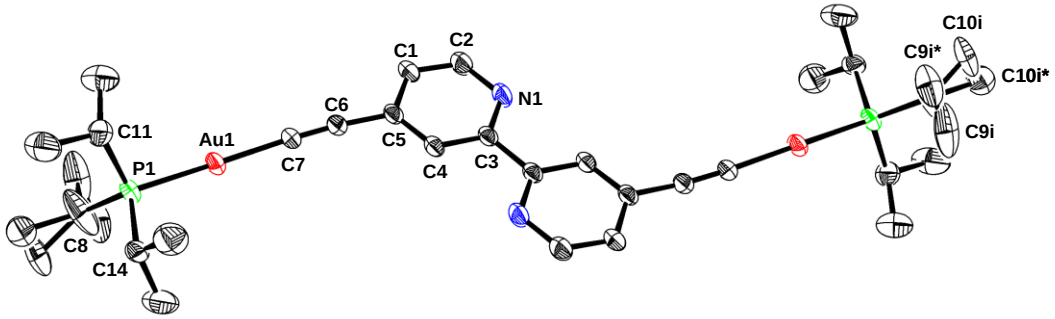


**Figure 3.23** Molecular structure of **L2** (ORTEP - probability ellipsoids - 30 %). The molecule is centrosymmetric. One half of the molecule is generated by the following symmetry operation: 1-x, 1-y, 1-z. All H atoms are omitted for clarity.

The crystal structure of **L2** was solved in the orthorhombic space group *Pbcn*. Crystals in the form of colourless plates were obtained by slow diffusion of $Et_2O$ into a $CH_2Cl_2$ solution of **L2**. The molecule **L2** is centrosymmetic and one of the isopropyl groups is disordered as is shown in **Figure 3.23** Four molecules fill the volume of the unit cell and the selected bond lengths and bond angles of **L2** are summarised in **Table 3.8**

| Bond | Lengths [Å] | Bond angle | Value [°] |
|---|---|---|---|
| **Au1−P1** | 2.282(2) | **P1−Au1−C7** | 172.8(3) |
| **Au1−C7** | 1.996(8) | **C6−C7−Au1** | 175.5(8) |
| **C6−C7** | 1.192(11) | **C3−C6−C7** | 175.0(9) |

**Table 3.8** Selected bond lengths and bond angles of **L2**.

Au-Au interactions, with the shortest Au1….Au1$^{ii}$ distance 3.3947(9) Å (symmetry code ii: 1-x, y, 1/2-z), result in chain assemblies shown in **Figure 3.24**. The differences between polymeric chains for **L1** and **L2** are caused by the differences in phosphine size (Tolman

cone angle for $Et_3P$ 132° and for *i*-$Pr_3P$ 160°) and in the case of **L2**, molecules adopt a zigzag form (**Figure 3.24**, **3.25 a**)). The polymeric chain of **L2** is stabilised similarly to **L1** by the weak interactions between $^{Et}C–H$ and $C_{alkyne}$ and non-classical hydrogen bonds of C–H...N type (**Figure 3.26**).

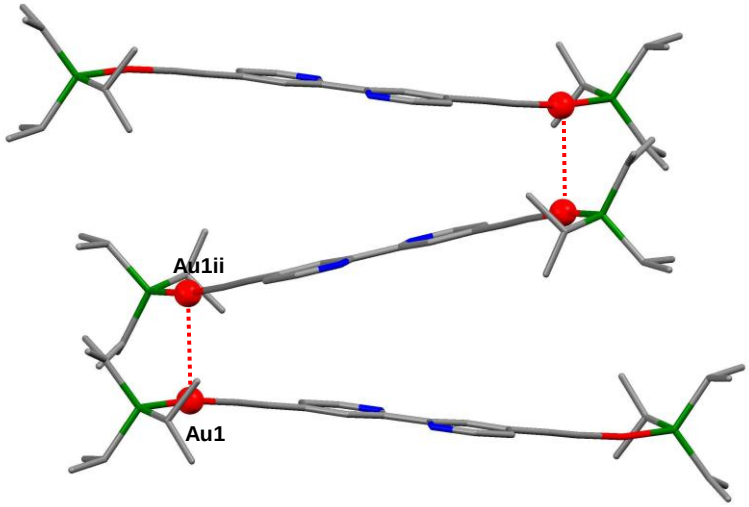


**Figure 3.24** The shortest Au…Au contacts for **L2**, symmetry code ii: 1-x, y, 1/2-z.

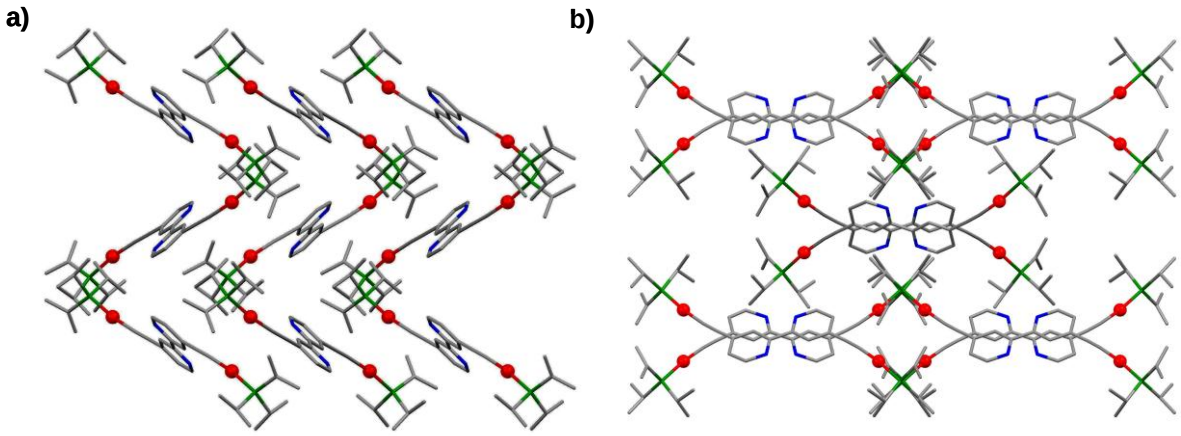


**Figure 3.25** The crystal packing of **L2**: a) view along the b-axis, b) view along the c-axis.

Au…Au interactions also influence the crystal packing of **L2** (**Figure 3.25**). The view along the c-axis shows a complicated arrangement, which in this projection seems to be connected chains with eye-shaped links (**Figure 3.25**, **b**).

The weak C–H…$C_{alkyne}$ interactions and non-classical hydrogen bond (C–H...N) for **L2** are shown in **Figure 3.26**, and the values of the relevant bond lengths and bond angles are listed in **Table 3.9**

Those interactions play a crucial part in the chain assemblies of **L2** [115]-[117].

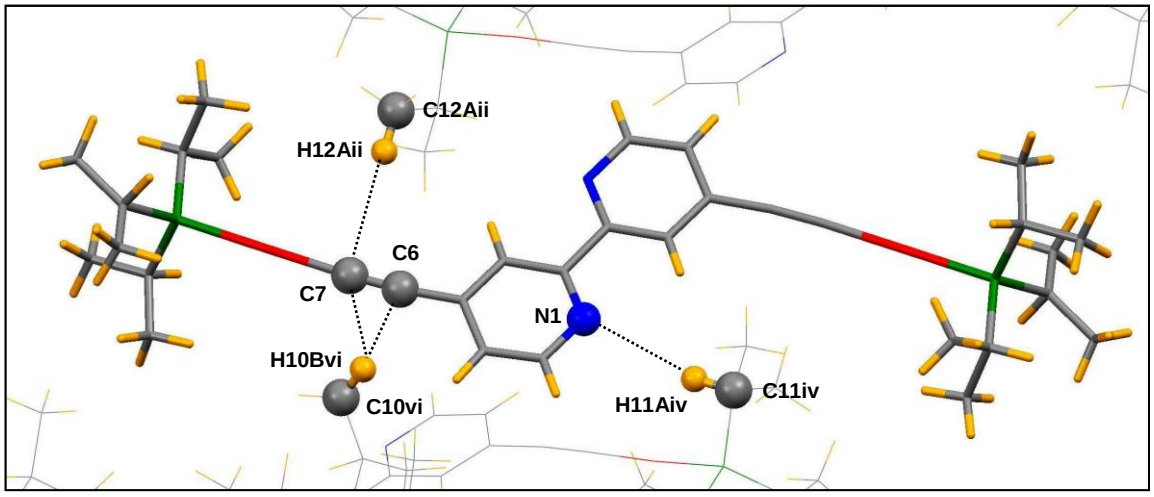


**Figure 3.26** Weak interactions: C−H…$C_{alkyne}$ and non-classical hydrogen bonds of C−H...N type for **L2**. Symmetry codes as listed in **Table 3.9**.

| D−H…A | H…A [Å] | D…A [Å] | D−H…A [°] | Symmetry code |
|---|---|---|---|---|
| **$C11^{iv}$−$11A^{iv}$…N1** | 2.88 | 3.84(1) | 161 | iv: -1/2+x, 1/2-y, 1-z |
| **$C10^{vi}$−$H10B^{vi}$…C6** | 2.95 | 3.89(3) | 164 | vi: x, -y, 1/2+z |
| **$C10^{vi}$−$H10B^{vi}$…C7** | 2.94 | 3.77(3) | 144 | vi: x, -y, 1/2+z |
| **$C12^{ii}$−$H12A^{ii}$…C7** | 2.96 | 3.94(2) | 180 | ii: 3/2-x, 1/2+y, z |

**Table 3.9** Bond lengths and angles for C−H…$C_{alkyne}$ interactions and non-classical hydrogen bonds of C−H...N type for **L2**.

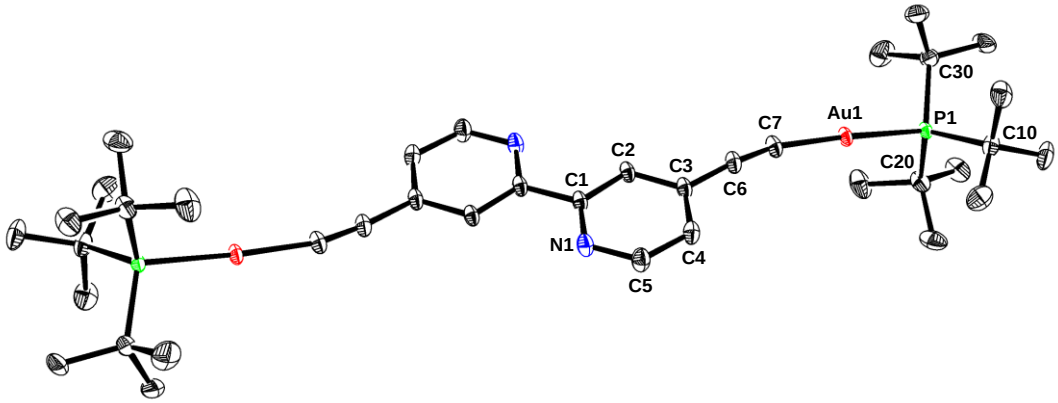


**Figure 3.27** Molecular structure of **L3** (ORTEP - probability ellipsoids - 30 %). The molecule is centrosymmetric. One half of the molecule is generated by the following symmetry operation: -x, 1-y, 2-z. All H atoms are omitted for clarity.

Crystals of **L3** in the form of colourless needles were obtained by slow diffusion of $Et_2O$ into a $CH_2Cl_2$/toluene solution of **L3** and proved to be suitable for X-ray measurements. The crystal structure was solved in monoclinic space group $P2_1/c$ (**Figure 3.27**) and selected bond lengths and angles of **L3** are listed in **Table 3.10** The molecule of **L3** is centrosymmetric (**Figure 3.27**).

| Bond | Length [Å] | Bond angle | Value [°] |
|---|---|---|---|
| **Au1−P1** | 2.3024(8) | **P1−Au1−C7** | 177.02(11) |
| **Au1−C7** | 2.010(3) | **C6−C7−Au1** | 168.7(3) |
| **C6−C7** | 1.199(4) | **C3−C6−C7** | 173.3(4) |

**Table 3.10** Selected bond lengths and bond angles of **L3.**

The large value of the Tolman cone angle (182°) for *t*-$Bu_3P$ prevents any Au…Au interactions and increases the shortest Au1…Au1$^{ii}$ distances to 6.290(1) Å (symmetry code ii: 1-x, 2-y, 2-z) and 6.901(1) Å (Au1$^{i}$…Au1$^{iv}$, symmetry code i: -x, 1-y, 2-z, iv: x, 3/2-y, 1/2+z) as is shown in **Figure 3.28**. The bulk of the *t*-$Bu_3P$ ligand causes an increase of the Au1…P1 distance to 2.3024(8) Å, which is the longest of all the gold(I) phosphine derivatives of 4,4'-dialkynyl substituted 2,2'-bipyridine presented here.

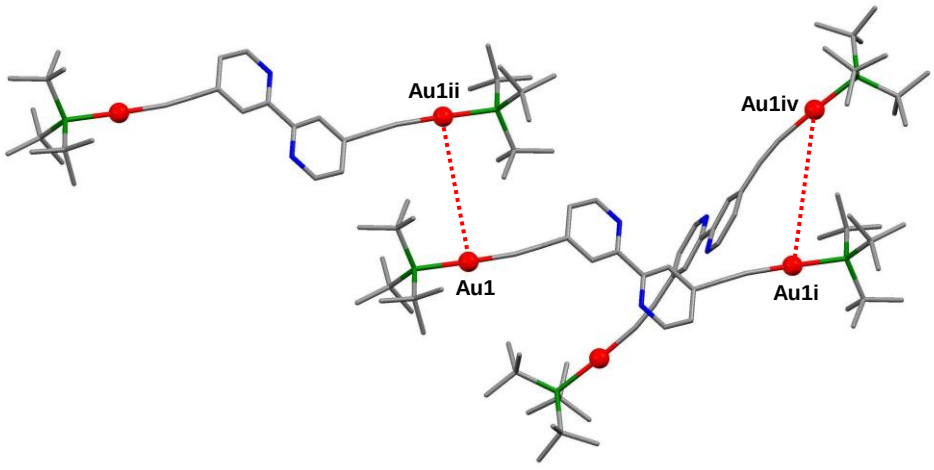


**Figure 3.28** The shortest Au…Au distances for **L3**. Symmetry codes are explained in the text.

The crystal packing of **L3** is shown in **Figure 3.29**. The horizontal wavy zigzag form with coplanar pyridine rings is illustrated in the view along the c-axis **Figure 3.29 b)**.

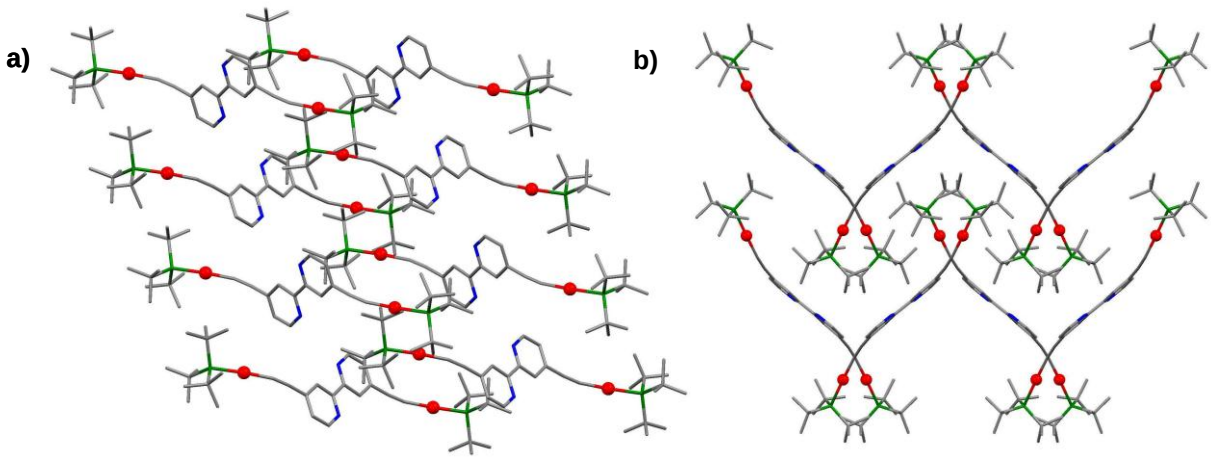


**Figure 3.20** The crystal packing of **L3**: a) view along the b-axis, b) view along the c-axis.

The unit cell contains two molecules of **L3** and there are no significant voids in the crystal structure. Molecules of **L3** form two kinds of layers marked by green and grey colours in the space-filling representation in **Figure 3.30** in which t-$Bu_3P$ units are involved in $CH_3 \ldots \pi$ contacts to pyridine rings.

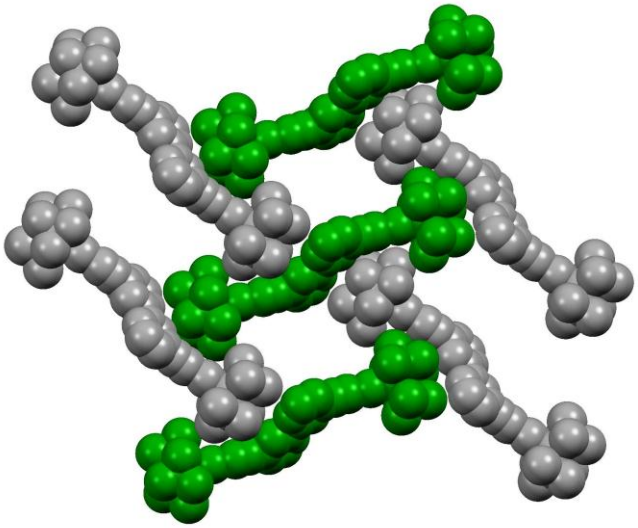

**Figure 3.30** The crystal packing of **L3** in space-filling representation showing phosphine units with $CH_3 \ldots \pi$ contacts to pyridine rings.

The crystal structure of **L4,** solved in triclinic space group Pī, and is illustrated in **Figure 3.31**. X-ray quality single crystals of **L4** in the form of colourless needles were obtained by slow diffusion of $Et_2O$ into a $CH_2Cl_2$/toluene solution of **L4**. The unit cell contains one molecule of **L4** with two independent gold atoms and one disordered solvent molecule ($Et_2O$).

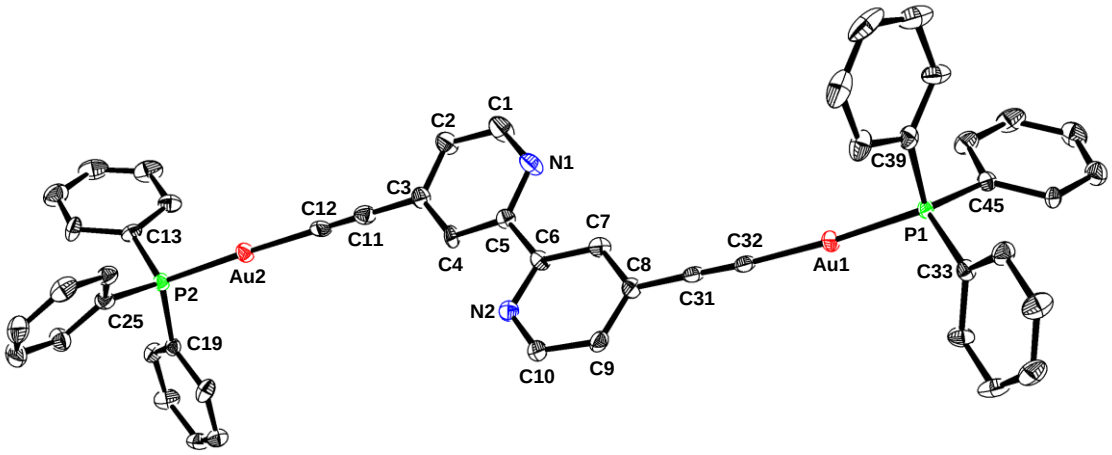


**Figure 3.31** Molecular structure of **L4** (ORTEP - probability ellipsoids - 40 %). Disordered solvent molecule and all H atoms are omitted for clarity.

Atoms C3, C11, C12, Au2 lie almost perfectly in a straight line with a deviation less than 1°, while for atoms C8, C31, C32, Au1 this deviation is 5.5°. The values of selected bond lengths and angles of **L4** are listed in **Table 3.11**.

| Bond | Length [Å] | Bond angle | Value [°] |
|---|---|---|---|
| **Au1−P1** | 2.2625(12) | **P1−Au1−C32** | 174.64(17) |
| **Au1−C32** | 2.000(6) | **C31−C32−Au1** | 175.7(5) |
| **Au2−P2** | 2.2710(14) | **P2−Au2−C12** | 177.68(16) |
| **Au2−C12** | 2.015(7) | **C11−C12−Au2** | 179.6(6) |
| **C11−C12** | 1.160(9) | **C8−C31−C32** | 176.4(6) |
| **C31−C34** | 1.184(8) | **C3−C11−C12** | 179.4(7) |

**Table 3.11** Selected bond lengths and bond angles of **L4.**

Steric hindrances of the phenyl rings and indirectly, the π–π interactions of the phenyl rings (**Figure 3.33**) observed in the crystal packing of **L4**, result in there being no Au...Au interactions. The shortest Au…Au distances for **L4** are Au2...Au2$^{i}$ 4.7631(5) Å

(symmetry code i: 2-x, -y, -z) and $Au1^{ii}\ldots Au^{iii}$ 5.9997(5) Å, (symmetry code ii: 1-x, -y, -z, iii: 1+x, -1+y, -1+z) are shown in **Figure 3.32**.

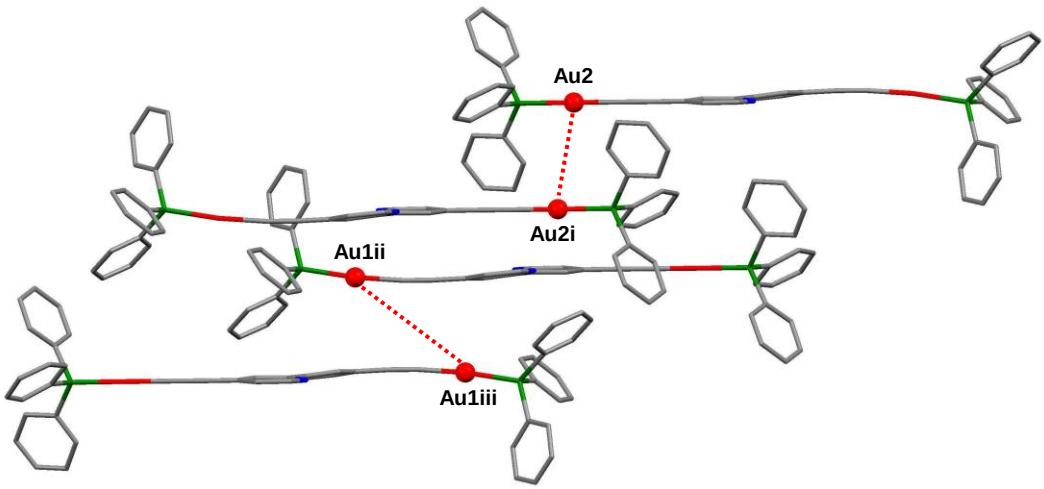


**Figure 3.32** The shortest Au…Au distances for **L4**. The layered arrangement of **L4** can be also observed**.** Symmetry codes are explained in the text.

The C–H…π interactions in **L4** between symmetry related molecules are shown as a grey, space-filling representation in **Figure 3.33** (H481–A1(centroid) = 2.54 Å, C48…A1(centroid) = 3.45 Å, the dihedral angle between the phenyl rings planes (denoted in grey) is 83° (symmetry code ii: 1-x, 1-y, 1-z). The π–π face-to-face interactions for **L4** are shown as a blue space-filling representation ($C16\ldots C16^{i}$ = 3.51(1) Å, $C15\ldots C15^{i}$ = 3.67(1) Å, C16…C15i (or C15…C16i) = 3.33(1) Å, and due to symmetry the planes of the phenyl rings in blue are perfectly parallel, symmetry code i: 3-x, -y, -z) [114].

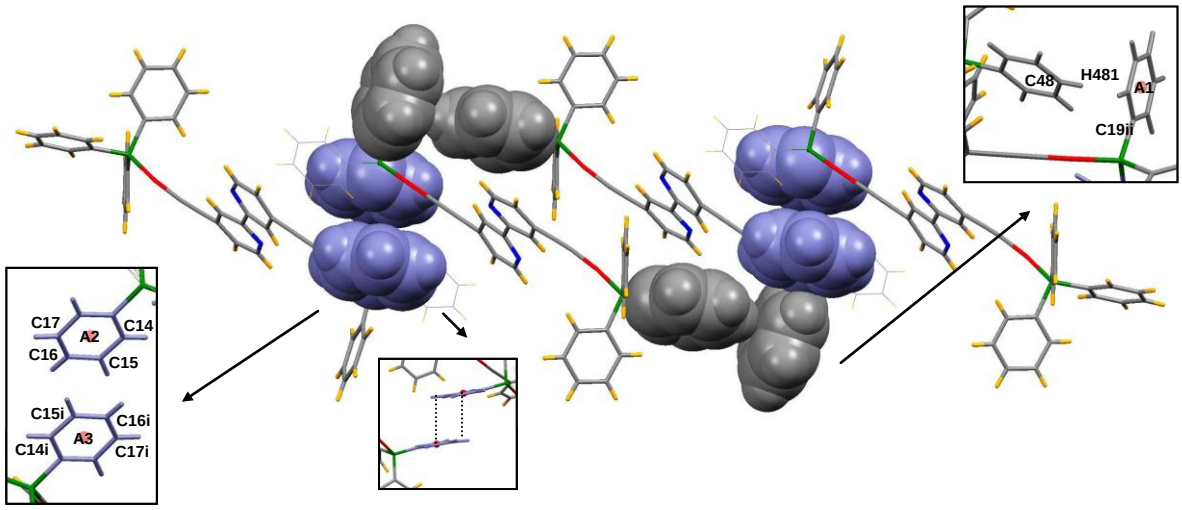


**Figure 3.33** C-H…π and face-to-face π–π interactions for **L4**. Symmetry codes are explained in the text.

These kinds of interactions (**Figure 3.33**) are dominant in the crystal packing of **L4** and they most likely influence the length of the shortest Au…Au distance.

Similarly to **L1** and **L2,** C–H…$C_{alkyne}$ interactions are observed in **L4** (**Figure 3.34**, C31...H221$^{i}$ = 2.72 Å, C31…C22$^{i}$ = 3.58(1) Å, C32...H221$^{i}$ = 2.78 Å, C32…C22$^{i}$ = 3.57(1) Å, symmetry code i: -1+x, 1+y, z) [117]. The decrease of angles C31–H221$^{i}$…C22$^{i}$ and

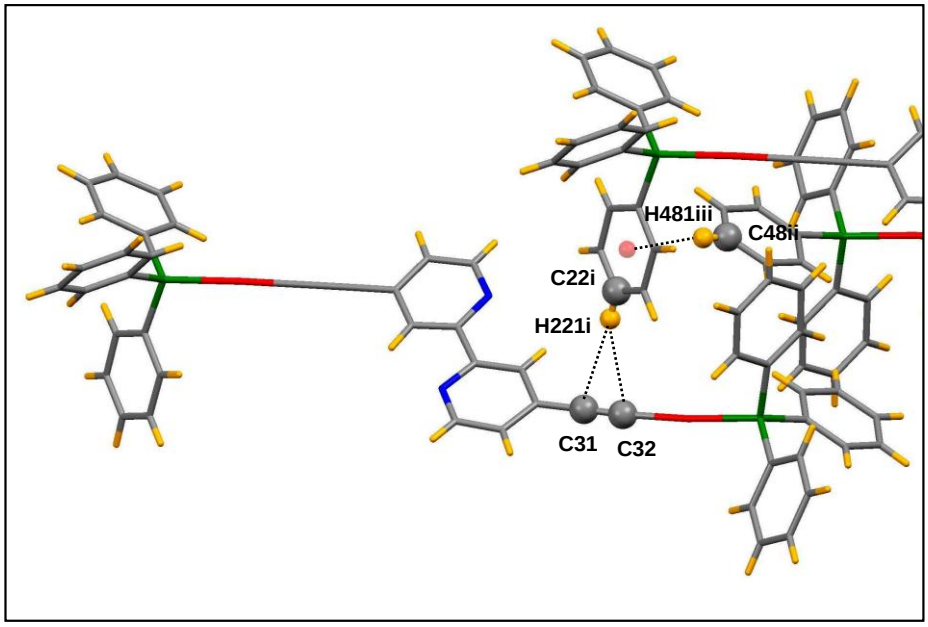


**Figure 3.34** C–H…$C_{alkyne}$ interactions for **L4**. Symmetry codes are explained in the text.

C32–H221$^{i}$…C22$^{i}$ to 154° and 142° respectively, is caused by competition with the stronger edge-to-face π–π interactions as is shown in **Figure 3.34**.

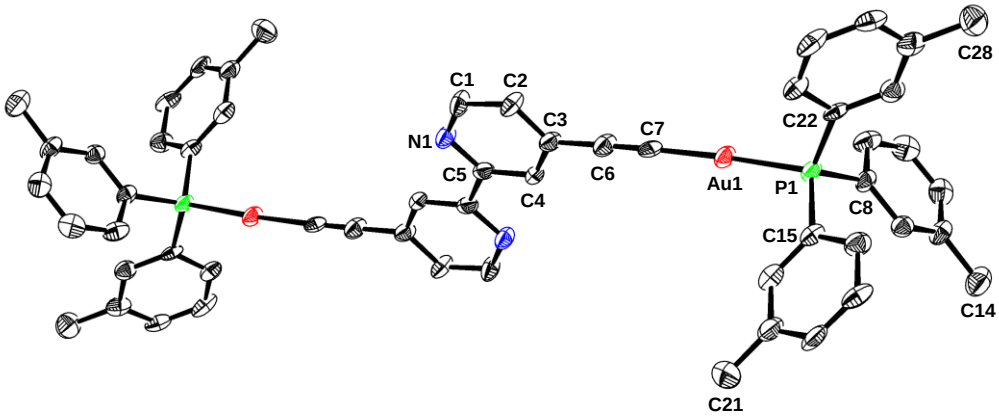


**Figure 3.35** Molecular structure of **L5** (ORTEP - probability ellipsoids - 50 %). The molecule is centrosymmetric. One half of the molecule is generated by symmetry code: 1-x, -y, -z. All H atoms are omitted for clarity.

An X-ray quality single crystal of **L5** in the form of a colourless block was obtained by slow diffusion of $Et_2O$ into a $CH_2Cl_2$/toluene solution of **L5**. The crystal structure was solved in monoclinic space group $P2_1/n$ and the molecule of **L5** is centrosymmetric (symmetry code: 1-x, -y, -z). The unit cell contains two molecules of **L5** and the labelling scheme is shown in **Figure 3.35** In **Table 3.12** selected bond lengths and angles of **L5** are listed.

| Bond | Lengths [Å] | Bond angle | Value [°] |
|---|---|---|---|
| **Au1−P1** | 2.275(3) | **P1−Au1−C7** | 177.2(3) |
| **Au1−C7** | 2.001(11) | **C6−C7−Au1** | 173.5(10) |
| **C6−C7** | 1.175(16) | **C3−C6−C7** | 178.9(12) |

**Table 3.12** Selected bond lengths and bond angles of **L5.**

Also in the case of **L5**, Au…Au interactions are not observed. The shortest Au…Au distances (Au1…Au1$^{ii}$ and Au1…Au1$^{iv}$) for **L5** are 6.996(1) Å (symmetry codes ii: 3/2 –x, 1/2 + y, 1/2 –z, iv: 3/2 –x, -1/2 + y, 1/2 –z). The characteristic motif where three Au1-atoms are vertices of an isosceles triangle (marked by the red dotted line in the **Figure 3.36**) with two equal sides of 6.996(1) Å and the triangle base Au1$^{iv}$…Au1$^{ii}$ = 9.379(2) Å, is present in the crystal packing of **L5** (**Figure 3.36**).

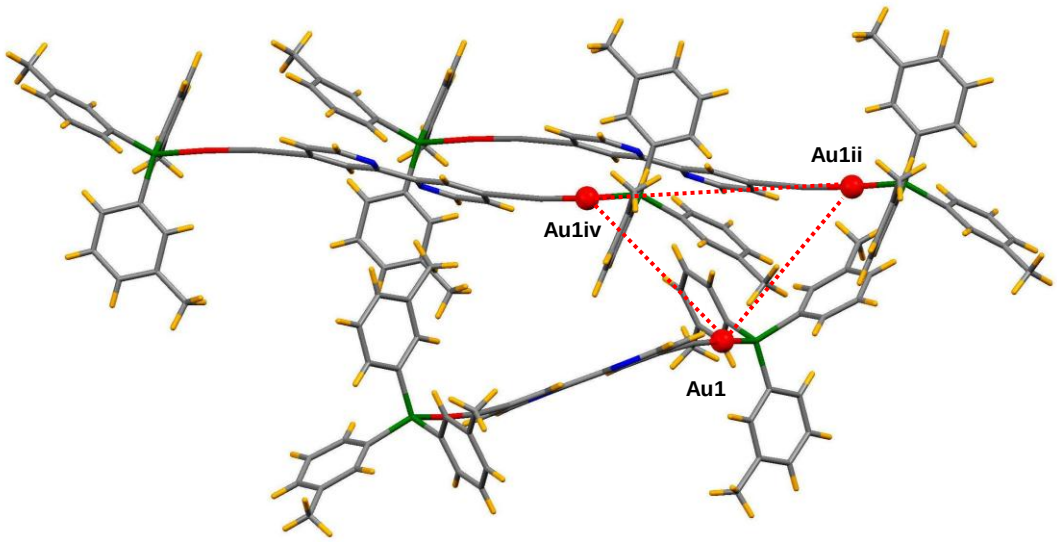


**Figure 3.36** The shortest Au…Au distances for **L5**. The Au1…Au1$^{iv}$ and Au1…Au1$^{ii}$ distances are equal. Symmetry codes are explained in the text.

The much longer Au…Au distance in **L5** than for **L1** and **L2** is caused by steric hindrance from the *m*-tolyl rings. The C-H…π and π–π interactions between the *m*-tolyl rings may also influence this distance (**Figure 3.37**). The parallel aromatic rings are displaced, which is necessary for efficient face-to-face π–π stacking ($C10^{i}$…A2(centroid) and $C10^{iv}$…A1(centroid) distance of 3.94 Å, $C10^{i}$…$C10^{iv}$ = 3.89(2) Å, symmetry codes, i: 1-x, -y, -z, iv: 1-x, 1-y, 1-z) [115].

For **L5** C–H…$C_{alkyne,}$ interactions can also be observed and they are shown in **Figure 3.37** ($C6^{i}$…$H26A^{iii}$ distance of 2.75 Å, $C6^{i}$…$C26^{iii}$ = 3.58(2) Å, angle $C6^{i}$…$H26A^{iii}$–$C26^{iii}$ = 146°, symmetry codes i: 1-x, -y, -z, iii: 1-x, 1-y, -z) in a similar way to **L1**, **L2** and **L4** [117].

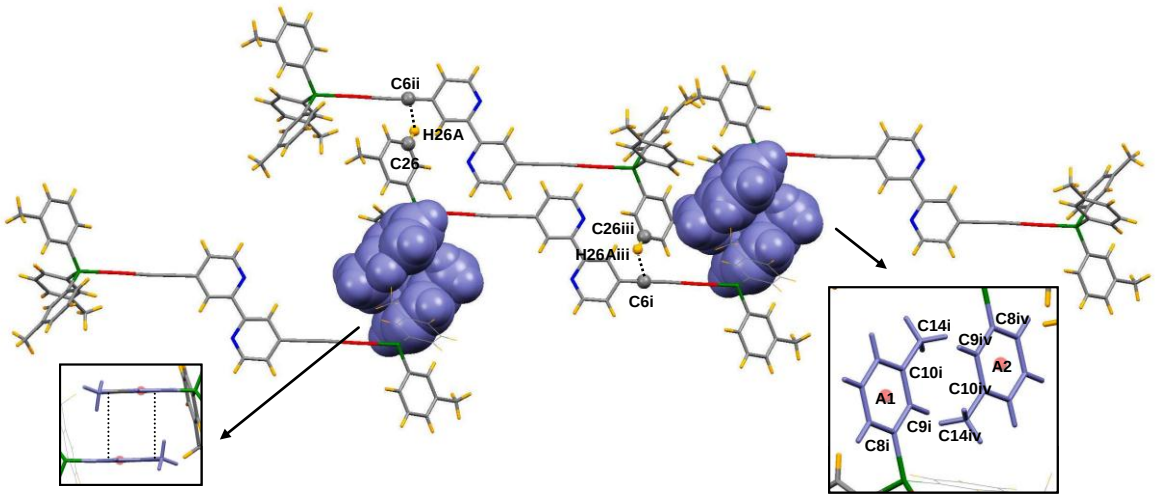


**Figure 3.37** π–π interactions between parallel, displaced *m*-tolyl rings and C–H…$C_{alkyne}$ interactions for **L5**. Symmetry codes are explained in the text.

Non-classical hydrogen bonds of C-H…N type present in the crystal packing of **L5** are shown in **Figure 3.48** ($N1…H12A^{ii}$ = 2.71 Å, $N1…C12^{ii}$ = 3.44(2) Å, angle $N1…H12A^{ii}$–$C12^{ii}$ = 134°, symmetry code ii: 3/2-x, -1/2+y, 1/2-z) [115], [116]. Proton $H12A^{ii}$ also takes part in weak C-H..π interactions between one of the *m*-tolyl rings and pyridine ring ($C5…H12A^{ii}$ = 2.74 Å, $C5…C12^{ii}$ = 3.58(2) Å, angle $C5…H12A^{ii}$–$C12^{ii}$ = 148°, symmetry code ii: 3/2-x, -1/2+y, 1/2-z). The sharing of proton H12A in these two interactions influences the value of the following angles: $N1…H12A^{ii}$–$C12^{ii}$ and $C5…H12A^{ii}$–$C12^{ii}$, and is also the reason why the angle between the planes of the *m*-tolyl and pyridine rings is 43°.

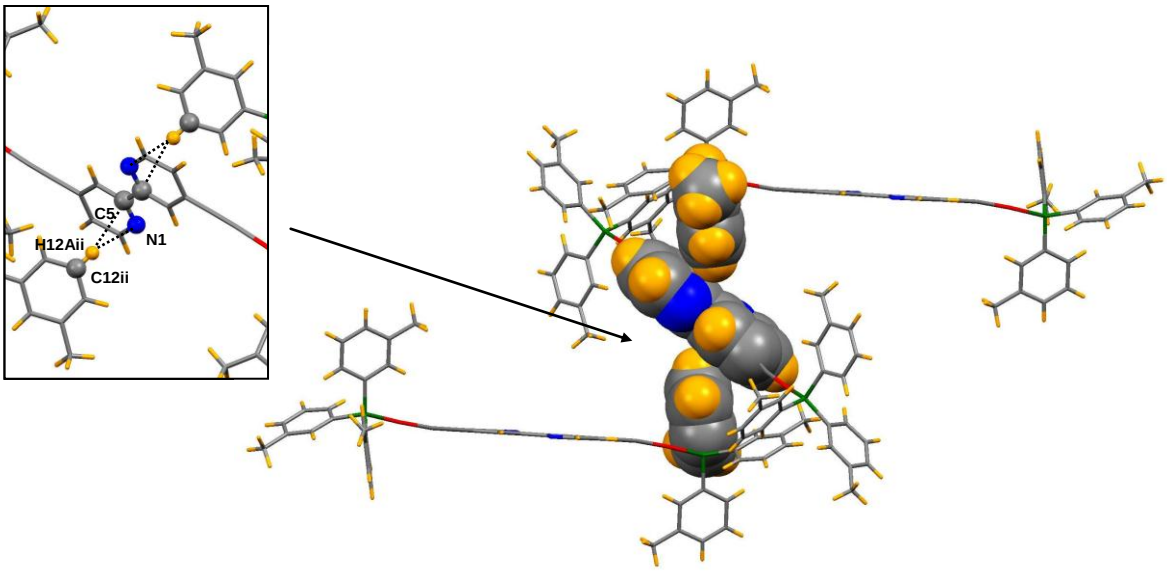


**Figure 3.38.** Weak interactions between *m*-tolyl rings and pyridine rings in **L4**. Symmetry codes are explained in the text.

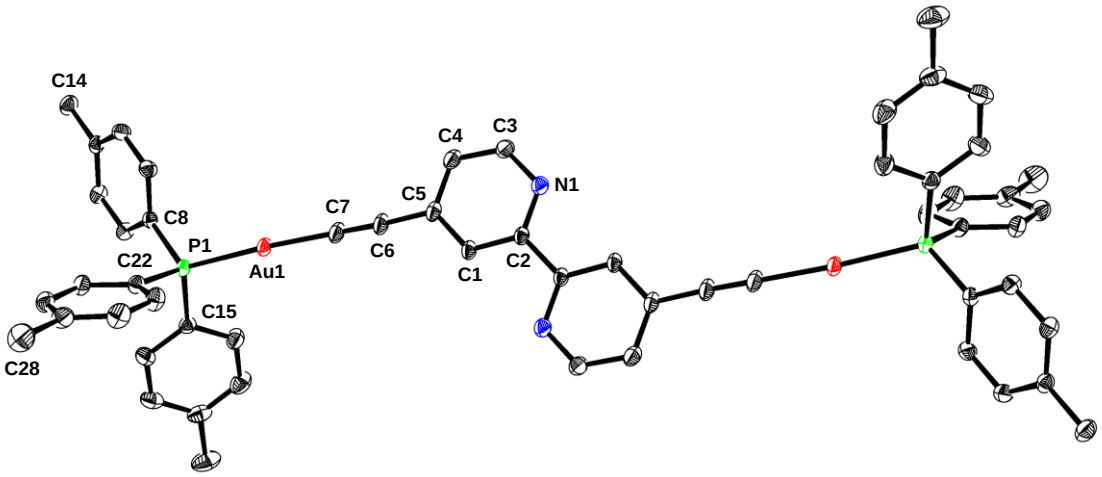


**Figure 3.39** Molecular structure of **L6** (ORTEP - probability ellipsoids - 50 %). The molecule is centrosymmetric. One half of the molecule is generated by symmetry operation: -x, 2-y, -z. Disordered solvent molecule and all H atoms are omitted for clarity.

As a result of slow diffusion of $Et_2O$ into a $CH_2Cl_2$/toluene solution of **L6**, crystals in the form of colourless prisms were obtained. The molecular structure of **L6** (**Figure 3.39**) was solved in triclinic space group Pī and the unit cell contains one molecule of **L6** and one disordered molecule of solvent ($Et_2O$). Molecule **L6** is centrosymmetric (symmetry code: -x, 2-y, -z). Selected bond lengths and bond angles of **L6** are summarised in **Table 3.13**.

| Bond | Lengths [Å] | Bond angle | Value [°] |
|---|---|---|---|
| **Au1−P1** | 2.2802(3) | **P1−Au1−C7** | 176.83(5) |
| **Au1−C7** | 1.9974(13) | **C6−C7−Au1** | 178.94(15) |
| **C6−C7** | 1.2125(18) | **C5−C6−C7** | 177.06(17) |

**Table 3.13** Selected bond lengths and bond angles of **L6.**

Au...Au interactions were not observed for **L6**, as for all the ligands containing the triarylphosphine units. The shortest Au…Au distance for **L6** is 5.3031(4) Å (symmetry code ii: 1-x, 1-y, -z) and is shown in **Figure 3.40**. The crystal packing in **Figure 3.40** shows horizontal layers of pyridine rings, which are separated by *p*-tolyl$_3$P units. Pairs of *p*-tolyl rings are coplanar, the same as atomic wires C5-Au1, and both of these motifs form a pattern in the form of a zigzag strip marked by the green lines in **Figure 3.40**.

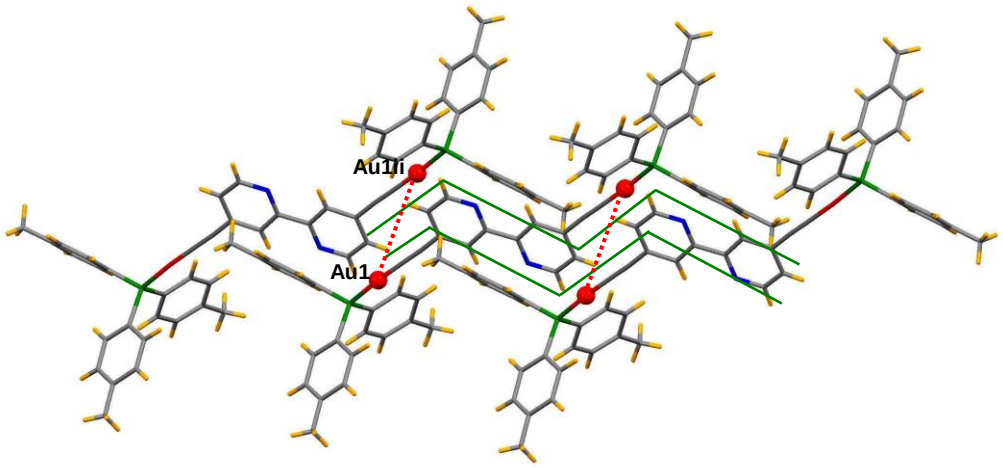


**Figure 3.40** The shortest Au…Au distances for **L6**. Symmetry codes are explained in the text.

π–π interactions between parallel, displaced *p*-tolyl rings (**Figure 3.41**) shown as a blue space-filling representation (A1(centroid)…C12$^{v}$ = C11…C13$^{v}$ = 3.704(2) Å, C12…C11$^{v}$ = 3.601(2) Å, C12…C12$^{v}$ = 3.339(2) Å, symmetry code v: 1-x, -y, -z) increases the shortest distance between Au-Au atoms [114].

Weak C–H…C$_{alkyne}$ interactions (C6…H12$^{ii}$ = 3.23 Å, C6…C12$^{ii}$ = 4.035(3) Å, angle C6…H12$^{ii}$-C12$^{ii}$ = 142°, C7...H12$^{ii}$ = 2.8 Å, C7…C12$^{ii}$ = 3.764(3) Å, angle C7…H12$^{ii}$–C12$^{ii}$ = 158°, symmetry code ii: -1+x, y, z) are also observed in the crystal packing of **L6** (**Figure 3.41**) [117].

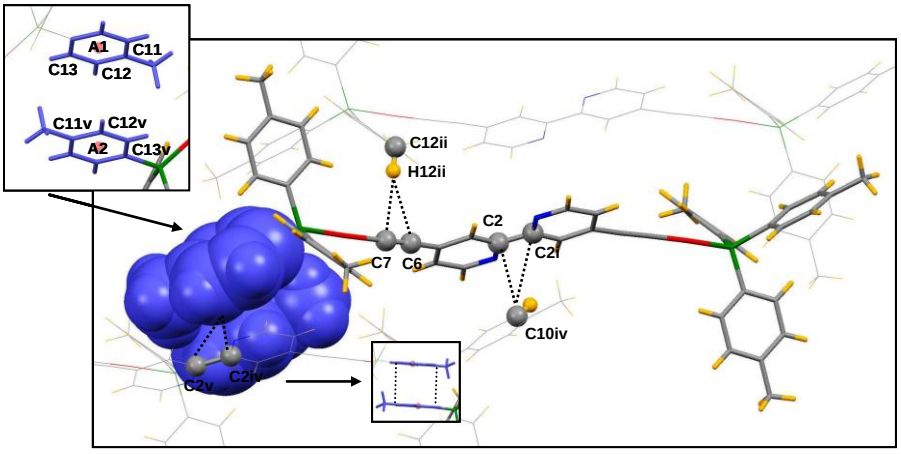


**Figure 3.41** π–π interactions between parallel, displaced *p*-tolyl rings and C−H…$C_{alkyne}$ interactions for **L6**. Symmetry codes are explained in the text.

One of the *p*-tolyl rings, which takes a part in the mentioned displaced π–π interactions, also interacts with pyridine rings (C2…$C10^{iv}$ = 3.292(2) Å, $C2^{i}$…$C10^{iv}$ = 3.493(2) Å, symmetry code i: -x, 2-y, -z, iv: 1-x, 1-y, -z). The latter interaction is also marked in **Figure 3.41**.

# 4. Synthesis and characterisation of $PR_3Au{-}{\equiv}{-}tpy$

## 4.1. Experimental for L7-L11

### 4'-[2-Trimethylsilanyl-1-ethynyl]-2,2':6',2''-terpyridine (S2)

Previously reported in reference: [118]

Formula: $C_{20}H_{19}N_3Si$

Formula weight: 329.47 [g/mol]

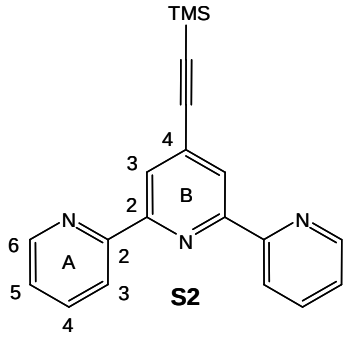


4'-[((Trifluoromethyl)sulfonyl)oxy]-2,2':6',2''-terpyridine (500 mg, 1.3 mmol), bis-(triphenylphosphine)palladium(II)dichloride (58 mg, 100 μmol), CuI (58 mg, 300 μmol) and (trimethylsilyl)ethyne (260 mg, 0.37 ml, 2.6 mmol) were added to 15 ml dry THF. After addition of DIPA (predistilled with NaOH, 2.5 ml) the colour of solution turned black. The reaction was carried out under argon and the reaction mixture was placed in a microwave reactor (50 °C, 30 min), after which the reaction mixture was quenched with water (50 ml). 30 ml of $CH_2Cl_2$ was added to this mixture and the organic and aqueous phases were separated. The aqueous phase was extracted with $CH_2Cl_2$. The solvent from the organic phase was removed *in vacuo*. The dark brown crude material was dissolved in a mixture of hexane/$CH_2Cl_2$ (30/70) and was filtered through $Al_2O_3$ *in vacuo* to remove the black precipitate. Next, the filtrate was purified by column chromatography ($Al_2O_3$, hexane/$CH_2Cl_2$ - 30/70). Compound **S2** was isolated as a white solid (340 mg, 1.0 mmol, 79 %).

**$^1$H NMR** (400 MHz, $CDCl_3$), δ [ppm]: 8.70 (d, $J$ = 4.0 Hz, 2H, $H^{A6}$), 8.59 (d, $J$ = 7.9 Hz, 2H, $H^{A3}$), 8.50 (s, 2H, $H^{B3}$), 7.85 (td, $J$ = 7.8, 1.6 Hz, 2H, $H^{A4}$), 7.33 (dd, $J$ = 6.8, 5.3 Hz, 2H, $H^{A5}$), 0.27 (s, 9H, $H^{TMS}$).

***catena*-[4'-(2-Gold-1-ethynyl)-2,2':6',2''-terpyridine] (S3)**

Formula: $(C_{17}H_{10}AuN_3)$*n

Formula weight: (453.25)*n [g/mol]

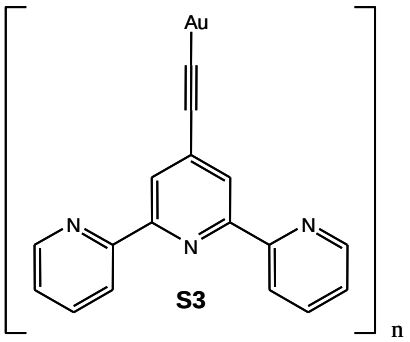


4'-Ethynyl-2,2':6',2''-terpyridine (50 mg, 190 μmol), Au(tht)Cl (64 mg, 190 μmol) and NaOAc (78 mg, 950 μmol) were added to a mixture of 5 ml THF and 5 ml MeOH. The reaction was carried out under argon. Although the presence of oxygen inhibits this reaction, a catalytic amount of water (present in the solvents) in the reaction is necessary to improve the solubility of the inorganic base. After 6-12 h of stirring, a pale yellow precipitate was obtained, which was filtered *in vacuo* and washed with MeOH. During all the manipulations, the solution was protected from the light in order to avoid gold deposition. Compound **S3** was isolated as yellow solid (72 mg, 159 μmol, 82 %).

**Preparation of the 4'-[2-$R_3$P-gold(I)-1- ethynyl]-2,2':6',2''-terpyridine:**

**General procedure.** $R_3PAuCl$, 4'-ethynyl-2,2':6',2''-terpyridine**,** CuI (catalyst) were dissolved in $CH_2Cl_2$ (8 ml) and MeOH (2 ml). After this, NaOAc ware added to make the solution basic. The reaction mixture was stirred at room temperature in the dark for 12–16 h, after which the solution was filtered and the solvent removed from the filtrate *in vacuo*. The crude material was purified by preparative plate chromatography in the dark ($Al_2O_3$, $CH_2Cl_2$).

**4'-[2-{(Triphenylphosphino)gold}-1- ethynyl]-2,2':6',2''-terpyridine (L7):**

Formula: $C_{35}H_{25}AuN_3P$

Formula weight: 715.53 [g/mol]

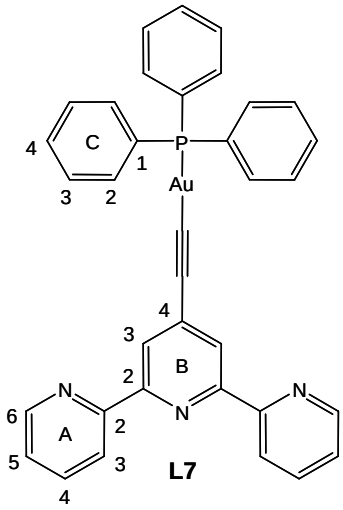


$Ph_3PAuCl$ (38 mg, 78 μmol), 4'-ethynyl-2,2':6',2''-terpyridine (20 mg, 78 μmol), NaOAc (13 mg, 160 μmol) and CuI (0.7 mg, 3.6 μmol). Compound **L7** was isolated as a white solid (39 mg, 55 μmol, 71 %).

**$^1$H NMR** (500 MHz, $CDCl_3$), δ [ppm]: 8.68 (d, $J$ = 4.0 Hz, 2H, $H^{A6}$), 8.56 (d, $J$ = 8.2 Hz, 2H, $H^{A3}$), 8.54 (s, 2H, $H^{B3}$), 7.81 (t, $J$ = 7.7 Hz, 2H, $H^{A4}$), 7.56 (m, 6H, $H^{C2/C3}$), 7.51 (m, 3H, $H^{C4}$), 7.47 (m, 6H, $H^{C2/C3}$), 7.29 (m, 2H, $H^{A5}$).

**$^{13}$C NMR** (126 MHz, $CDCl_3$), δ [ppm]: 156.42($C^{A2}$), 155.36($C^{B2}$), 149.31($C^{A6}$), 136.75($C^{A4}$), 135.22($C^{B4}$), 134.47 (d, $J_{PC}$ = 13.9 Hz, $C^{C2/3}$), 131.75 (d, $J_{PC}$ = 2.3 Hz, $C^{C4}$), 129.81 (d, $J_{PC}$ = 55.9 Hz, $C^{C1}$), 129.34 (d, $J_{PC}$ = 11.3 Hz, $C^{C2/3}$),124.19($C^{B3}$), 123.68($C^{A5}$), 121.25 ($C^{A3}$ ), 102.32 (poorly resolved, $C^{iC\equiv CAu}$), signal for $C^{AuiC\equiv C}$ not observed.

**$^{31}$P NMR** (162 MHz, $CDCl_3$), δ [ppm]: 42.42.

**UV-Vis** ($CH_2Cl_2$, $\lambda_{max}$ [nm], ($\varepsilon$ [$dm^3mol^{-1}cm^{-1}$])): 229 (53000), 244 (50000), 277 (54000), 289 (62000), 319 (9000), 331 (6000).

**Emission** ($CH_2Cl_2$, $\lambda_{ex}$ = 244 nm), $\lambda_{em}$ [nm]: 339, 355.

**ESI-MS** ($CH_2Cl_2$, [m/z]): 716.3 ($[L7 + H]^+$, calc. 716.5), 721.1 ($[(Ph_3P)_2Au]^+$, calc. 721.5).

**EA** [%], $C_{35}H_{25}AuN_3P$, calc. C: 58.75, H: 3.52, N: 5.87; found C: 58.55, H: 3.72, N: 5.92.

**[μ-[1,1'(1,2-Ethanediyl)bis[1,1-diphenylphosphine]]]bis[2-(4'(2,2':6',2''-terpyridinyl)-ethynyl)]digold (L8)**
or
**1,2-Bis[(4'-(2-gold-1-ethynyl)-2,2':6',2''-terpyridinyl)diphenylphosphino]ethane (L8):**

Formula: $C_{60}H_{44}Au_2N_6P_2$

Formula weight: 1304.91 [g/mol]

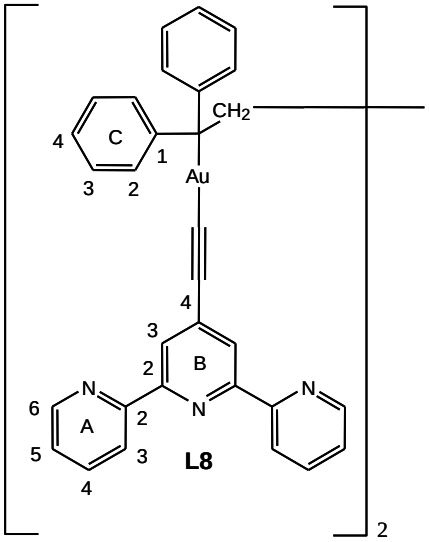


Under nitrogen, a mixture of dppe (22 mg, 55 μmol) and **S3** (4'-[2-gold-1-ethynyl]-2,2':6',2''-terpyridine (50 mg, 110 μmol)) in $CH_2Cl_2$ (10 ml) was stirred for 30 - 60 min. The solvent from the reaction mixture was evaporated. The crude material was purified by preparative plate chromatography in the dark ($Al_2O_3$, $CH_2Cl_2$). Compound **L8** was isolated as a white solid (31 mg, 24 μmol, 43 %).

**$^1$H NMR** (500 MHz, $CDCl_3$), δ [ppm]: 8.70 (d, $J$ = 4.6 Hz, 4H, $H^{A6}$), 8.58 (d, $J$ = 8.0 Hz, 4H, $H^{A3}$), 8.57 (s, 4H, $H^{B3}$), 7.84 (td, $J$ = 7.8, 1.5 Hz, 4H, $H^{A4}$), 7.72 (br, 8H, $H^{C2}$), 7.52 (br, 12H, $H^{C3/4}$), 7.32 (dd, $J$ = 7.2, 4.9 Hz, 4H, $H^{A5}$), 2.71 (br, 4H, $H^{dppe\text{-}CH2}$).
**$^{13}$C NMR** (126 MHz, $CDCl_3$), δ [ppm]: 156.31($C^{A2}$), 155.39($C^{B2}$), 149.29($C^{A6}$), 136.82($C^{A4}$), 135.05($C^{B4}$), 133.61($C^{C2}$), 132.42($C^{C4}$), 129.80($C^{C3}$), 124.08($C^{B3}$), 123.78($C^{A5}$), 121.27($C^{A3}$), 102.03 (poorly resolved, $C^{iC\equiv CAu}$), 24.01 (d, $J_{PC}$ = 12.3 Hz $C^{dppe\text{-}CH2}$), signals for $C^{C1}$ and $C^{AuiC\equiv C}$ not observed.
**$^{31}$P NMR** (162 MHz, $CDCl_3$), δ [ppm]: 40.63.
**UV-Vis** ($CH_2Cl_2$, $\lambda_{max}$ [nm], ($\varepsilon$ [$dm^3mol^{-1}cm^{-1}$])): 230 (122000), 239 (116000), 254 (100000), 277 (136000), 289 (156000), 319 (26000), 332 (19000).
**Emission** ($CH_2Cl_2$, $\lambda_{ex}$ = 241 nm), $\lambda_{em}$ [nm]: 341, 355.

**ESI-MS** ($CH_2Cl_2$, [m/z]): 993.7 ($[(dppe)_2Au]^+$, calc. 993.8), 1048.6 ($[AudppeAu{-}{\equiv}tpy]^+$, calc. 1048.6), 1305.8 ($[L8 + H]^+$, calc. 1305.9).

**EA** [%], $C_{60}H_{44}Au_2N_6P_2*2H_2O$, calc. C: 53.74, H: 3.61, N: 6.27; found C: 53.76, H: 3.41, N: 6.00.

**4'-[2-{(Tri-*o*-tolylphosphino)gold}-1-ethynyl]-2,2':6',2''-terpyridine (L9):**

Formula: $C_{38}H_{31}AuN_3P$

Formula weight: 757.61 [g/mol]

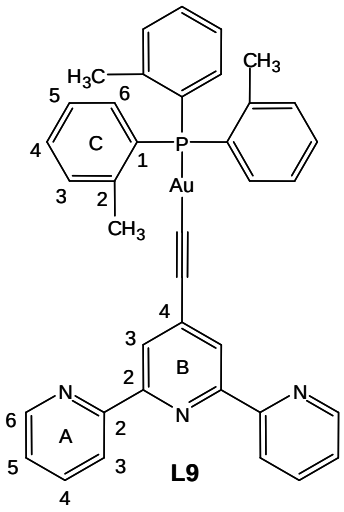


**L9**

*o*-$Tol_3PAuCl$ (42 mg, 78 μmol), 4'-ethynyl-2,2':6',2''-terpyridine (20 mg, 78 μmol), NaOAc (13 mg, 160 μmol) and CuI (0.7 mg, 3.6 μmol). Compound **L9** was isolated as a white solid (36 mg, 48 μmol, 62 %).

**$^1$H NMR** (500 MHz, $CDCl_3$), δ [ppm]: 8.67 (dd, $J$ = 4.7, 0.8, 2H, $H^{A6}$), 8.55 (d, $J$ = 7.9, 2H, $H^{A3}$), 8.50 (s, 2H, $H^{B3}$), 7.81 (td, $J$ = 7.7, 1.8, 2H, $H^{A4}$), 7.46 (t, $J$ = 7.5, 3H, $H^{C4}$), 7.40 – 7.35 (m, 3H, $H^{C3}$), 7.28 (ddd, $J$ = 7.4, 4.8, 1.0, 2H, $H^{A5}$), 7.19 (t, $J$ = 7.6, 3H, $H^{C5}$), 6.93 (dd, $J_{PH}$ = 12.2, $J_{PH}$ = 7.7, 3H, $H^{C6}$), 2.75 (s, 9H, $H^{o\text{-Tol-CH3}}$).

**$^{13}$C NMR** (126 MHz, $CDCl_3$), δ [ppm]: 156.43($C^{A2}$), 155.26($C^{B2}$), 149.28($C^{A6}$), 143.29 (d, $J_{PC}$ = 13.0 Hz, $C^{C2}$), 136.75($C^{A4}$), 135.40 ($C^{B4}$), 133.74 (d, $J_{PC}$ = 8.5 Hz, $C^{C6}$), 132.32 (d, $J_{PC}$= 8.5 Hz, $C^{C3}$), 131.76 ($C^{C4}$), 126.79 (d, $J_{PC}$ = 9.5 Hz, $C^{C5}$), 126.31 (d, $J_{PC}$ = 54.6 Hz, $C^{C1}$), 124.15($C^{B3}$), 123.66($C^{A5}$), 121.23($C^{A3}$), 102.34 (d, $J_{PC}$ = 26.6 Hz, $C^{iC{\equiv}CAu}$ ), 23.83 (d, $J_{PC}$ = 11.0 Hz, $C^{o\text{-Tol-CH3}}$), $C^{AuiC{\equiv}C}$ signal not observed.

**$^{31}$P NMR** (162 MHz, $CDCl_3$), δ [ppm]: 24.29.

**UV-Vis** ($CH_2Cl_2$, $\lambda_{max}$ [nm], ($\varepsilon$[$dm^3mol^{-1}cm^{-1}$])): 251 (53000), 280 (59000), 288 (64000), 318 (9000), 332 (6000).

**Emission** ($CH_2Cl_2$, $\lambda_{ex}$ = 252 nm), $\lambda_{em}$ [nm]: 341, 354.

**ESI-MS** ($CH_2Cl_2$, [m/z]): 758.4 ($[L9 + H]^+$, calc. 758.6), 805.3 ($[(o\text{-}Tol_3P)_2Au]^+$, calc. 805.7).

**EA** [%], $C_{38}H_{31}AuN_3P$*0.8 $H_2O$, calcd C: 59.12, H: 4.26, N: 5.44; found C: 59.14, H: 4.11, N: 5.38.

**4'-[2-{(Triethylphosphino)gold}-1-ethynyl]-2,2':6',2''-terpyridine (L10):**

Formula: $C_{23}H_{25}AuN_3P$

Formula weight: 571.41 [g/mol]

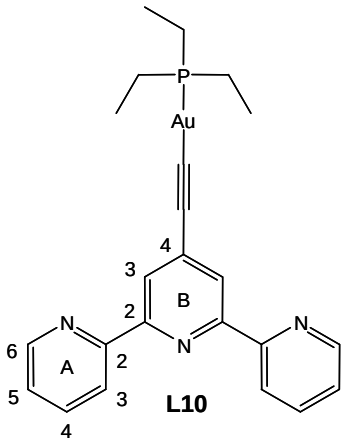


$Et_3PAuCl$ (27 mg, 78 μmol), 4'-ethynyl-2,2':6',2''-terpyridine (20 mg, 78 μmol), NaOAc (13 mg, 160 μmol) and CuI (0.7 mg, 3.6 μmol). Compound **L10** was isolated as a white solid (33 mg, 58 μmol, 74 %).

**$^1$H NMR** (500 MHz, $CDCl_3$), δ [ppm]: 8.68 (d, $J$ = 4.1 Hz, 2H, $H^{A6}$), 8.55 (d, $J$ = 7.9 Hz, 2 H, $H^{A3}$), 8.51 (s, 2H, $H^{B3}$), 7.82 (td, $J$ = 7.8, 1.4 Hz, 2H, $H^{A4}$), 7.30 (dd, $J$ = 7.0, 5.1 Hz, 2H, $H^{A5}$), 1.84 (dq, $J_{PH}$ = 15.4 Hz, $J_{HH}$ = 7.7 Hz, 6H, $^{Et\text{-}CH2}$), 1.28 – 1.19 (m, 9H, $^{Et\text{-}CH3}$).

**$^{13}$C NMR** (126 MHz, $CDCl_3$), δ [ppm]: 156.44 ($C^{A2}$), 155.31 ($C^{B2}$), 149.30 ($C^{A6}$), 136.75 ($C^{A4}$), 135.36 ($C^{B4}$), 124.17 ($C^{B3}$), 123.67 ($C^{A5}$), 121.25 ($C^{A3}$), 17.94 (d, $J_{PC}$ = 33.3 Hz, $C^{Et\text{-}CH2}$), 9.06 ($C^{Et\text{-}CH3}$), C≡C signals not observed.

**$^{31}$P NMR** (162 MHz, $CDCl_3$), δ [ppm]: 38.46.

**ESI-MS** ($CH_2Cl_2$, [m/z]): 433.2 ($[Et_3P)_2Au]^+$, calc. 433.3), 572.2 ($[L10 + H]^+$, calc. 572.4), 594.1, ($[L10 + Na]^+$, calc. 594.4).

Compound obtained, not enough pure for UV-Vis and fluorescence measurements.

**4'-[2-{(Triisopropylphosphino)gold}-1-ethynyl]-2,2':6',2''-terpyridine (L11):**

Formula: $C_{26}H_{31}AuN_3P$

Formula weight: 613.48 [g/mol]

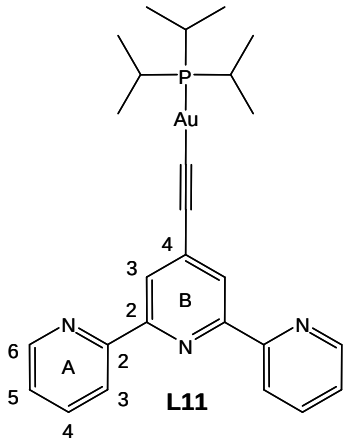


*i*-$Pr_3$PAuCl (30 mg, 78 μmol), 4'-ethynyl-2,2':6',2''-terpyridine (20 mg, 78 μmol), NaOAc (13 mg, 160 μmol) and CuI (0.7 mg, 3.6 μmol). Compound **L11** was isolated as a white solid (29 mg, 48 μmol, 61 %).

**$^1$H NMR** (400 MHz, $CDCl_3$), δ [ppm]: 8.67 (ddd, $J$ = 4.8, 1.8, 0.9 Hz, 2H, $H^{A6}$), 8.54 (dt, $J$ = 8.0, 1.0 Hz, 2H, $H^{A3}$), 8.52 (s, 2H, $H^{B3}$), 7.81 (td, $J$ = 7.8, 1.0 Hz, 2H, $H^{A4}$), 7.28 (ddd, $J$ = 7.5, 4.8, 1.2 Hz, 2H, $H^{A5}$), 2.31 (ddt, $J_{PH}$= 14.3 Hz, $J_{HH}$= 9.0 Hz, $J_{HH}$= 7.2 Hz, 3H, $H^{i\text{-Pr-CH2}}$), 1.33 (dd, $J$ = 15.5, 7.2 Hz, 18H, $H^{i\text{-Pr-CH3}}$).

**$^{13}$C NMR** (126 MHz, $CDCl_3$), δ [ppm]: 156.43 ($C^{A2}$), 155.27 ($C^{B2}$), 149.29 ($C^{A6}$), 136.73 ($C^{A4}$), 135.45 ($C^{B4}$), 124.16 ($C^{B3}$), 123.64 ($C^{A5}$), 121.21 ($C^{A3}$), 23.80 (d, $J_{PC}$ = 28.4 Hz, $C^{i\text{-Pr-CH2}}$), 20.43 (d, $J_{PC}$ = 5.1 Hz, $C^{i\text{-Pr-CH3}}$), C≡C signals not observed.

**$^{31}$P NMR** (162 MHz, $CDCl_3$), δ [ppm]: 67.65.

**ESI-MS** ($CH_2Cl_2$, [m/z]): 517.4 ($[(i\text{-}Pr_3P)_2Au]^+$, calc. 517.2), 614.3 ($[L11 + H]^+$, calc. 614.5), 970.6 ($[L11 + i\text{-}Pr_3PAu]^+$, calc. 970.7).

Compound obtained, not enough pure for UV-Vis and fluorescence measurements.

## 4.2. Ligand synthesis of L7-L11

Gold(I) phosphine-decorated 2,2':6',2"-terpyridine ligands were previously investigated [91], [92] with regard to their luminescent properties, which can potentially find applications in advanced materials.

**Figure 4.1** shows five new gold(I) phosphine derivatives of 4'-alkynyl substituted 2,2':6',2"-terpyridine, in which the alkyne is directly attached to tpy. Previously [91], an $O(CH_2)_n$ spacer had been used as a connection between tpy and alkyne units.

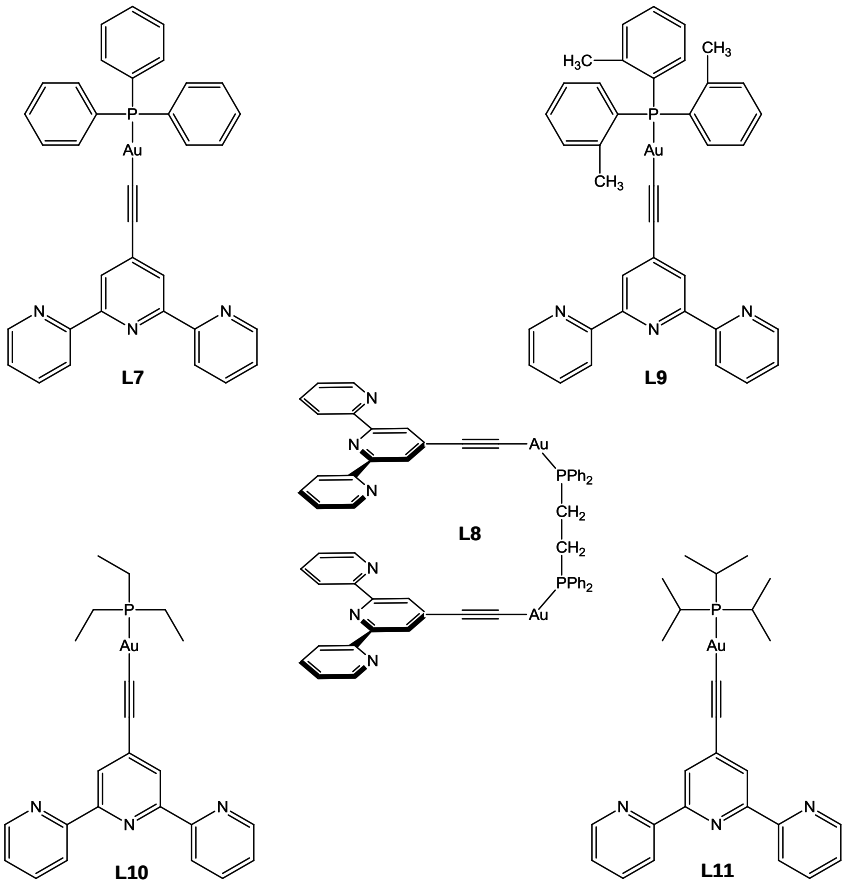


**Figure 4.1** Structures of **L7–L11**.

Compounds **L7, L9-L11** were obtained by multi-step synthesis and the way of synthesis used (**Scheme 4.1**) was modified from that previously published.

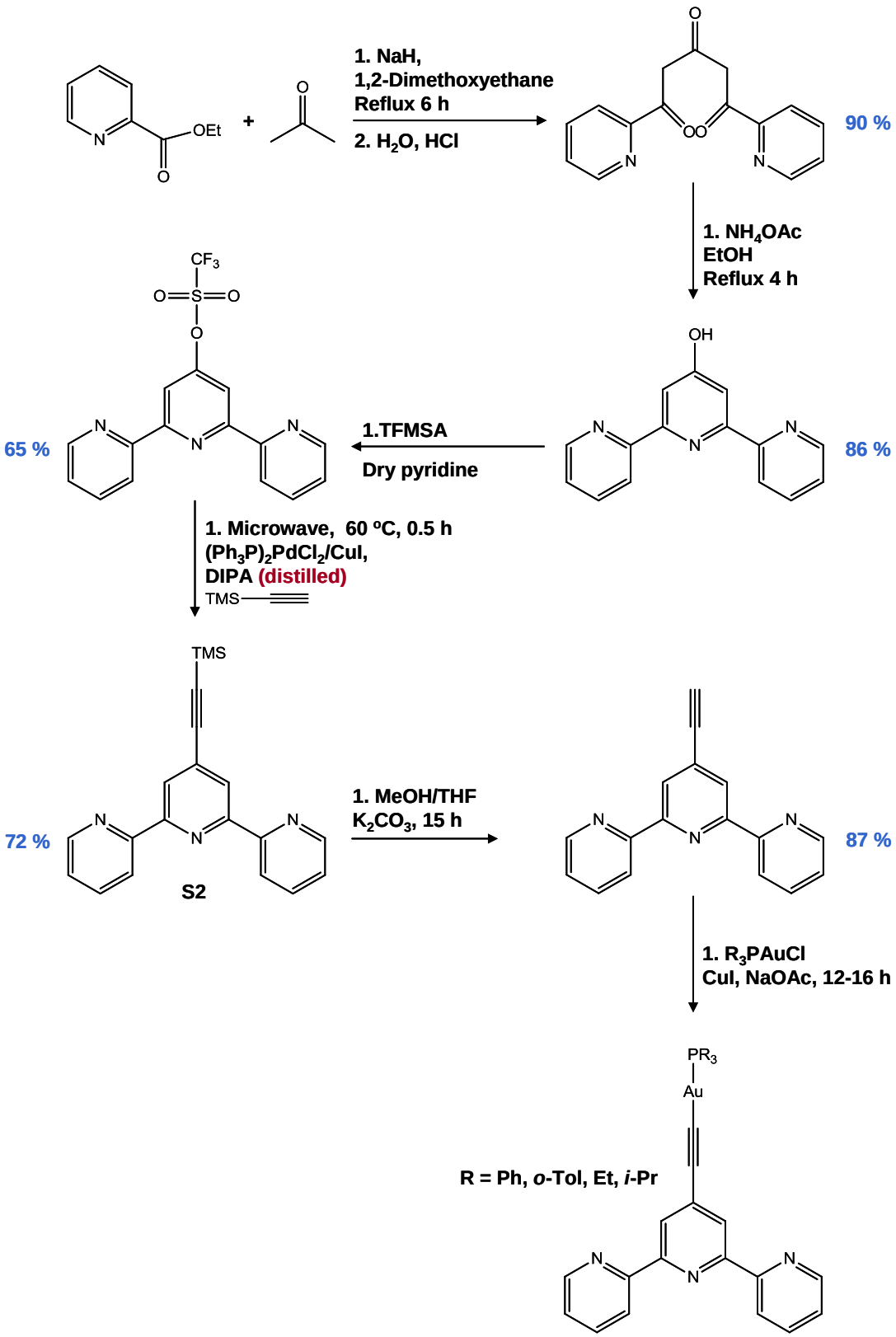


**Scheme 4.1** Synthesis of **L7, L9-L11**.

The condensation of acetone and ethyl 2-pyridinecarboxylate leads to l,5-bis(2'-pyridyl)-pentane-1,3,5-trione as reported by Constable and Ward [118], and Potts and Knowar [119]. In order to close the central pyridine ring in the next step, the yellow product obtained was reacted with ammonium acetate [118]. The purification of the brownish crude material (4'-hydroxy-2,2':6',2''-terpyridine) is not necessary (there is no noticeable loss in yield) and after drying it can be reacted with trifluoromethanesulfonic anhydride to obtain 4'-[(trifluoromethyl)sulfonyl]oxy]-2,2':6',2''-terpyridine [119].

The (trimethylsilyl)-1-ethynyl substitution in the 4'-position of 2,2':6',2''-terpyridine to give compound **S2** was reached by Sonogashira coupling, using the same modified synthesis and purification method as **L1-L6**. The deprotection of trimethysilyl groups was carried out as described by Grosshenny and co-workers [120] but $K_2CO_3$ was used as the base instead of KF.

Similar procedures to **L1-L6** were used to obtain **L7** and **L9-L11.** The method was modified by using an inorganic base (**Scheme 4.1**) instead of DIPA and led to the products in reasonable yields (60-70 %).

Compounds **L7** and **L9-L11** were purified using preparative plate chromatography, which was carried out in the dark to avoid decomposition of products, which were light sensitive in solution. This purification method achieves good separation of products (**L7** and **L9-L11**) from impurities.

Compound **L8** can be obtained using the some strategy as **L7** and **L9-L11** but there were problems with the complete separation of one side product. This was the main reason for finding another method, which is illustrated in **Scheme 4.2**. The synthesis strategy of **L8** was designed by analogy with the methods reported by Ferrer *et al.* [108] and Vicente *et al.* [79], which have been used to synthesise similar types of compounds.

The straightforward and efficient synthesis described by Uson *et al.* [121] involves reducing Au(III) to Au(I) and isolating the white powder, Au(tht)Cl. This compound is reacted with 4'-ethynyl-2,2':6',2''-terpyridine in the presence of a base and leads to *catena*-[4'-(2-gold-1-ethynyl)-2,2':6',2''-terpyridine] (**S3**). Finally, **L8** was obtained by reacting *catena*-[4'-(2-gold-1-ethynyl)-2,2':6',2''-terpyridine] with dppe.

Compound **L8** is light sensitive in solution, so it had to be protected from light during all the reaction and purification steps. As in the case of **L7, L9-L11**, the preparative plate chromatography was used as a purification method for this compound. This synthetic strategy led to the isolation of pure **L8.**

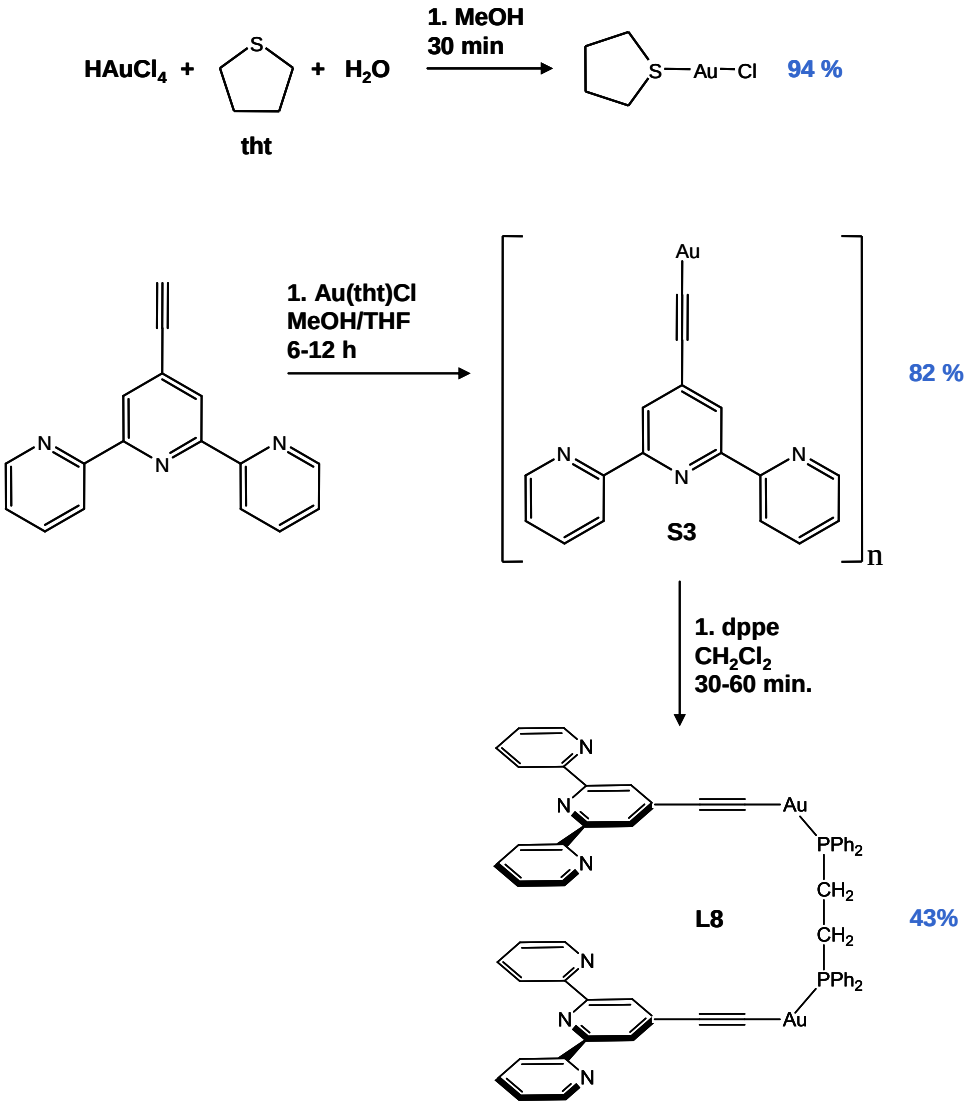


**Scheme 4.2** Synthesis of **L8**.

## 4.3. NMR spectroscopic studies of L7-L11

Compounds **L7-L11** were characterised using $^{1}H$ NMR, $^{13}C$ NMR and $^{31}P$ NMR spectroscopies. DEPT and 2-dimensional COSY, HMQC, HMBC and NOESY NMR techniques helped to assign all $^{1}H$ and $^{13}C$ NMR peaks. All spectra were measured in $CDCl_3$. Both $^{1}H$ - $^{1}H$ and $^{1}H$ - $^{31}P$ couplings appear in the $^{1}H$ NMR spectra. The $^{1}H$ NMR spectrum with peak assignment of **L9** is illustrated in **Figure 4.2**.

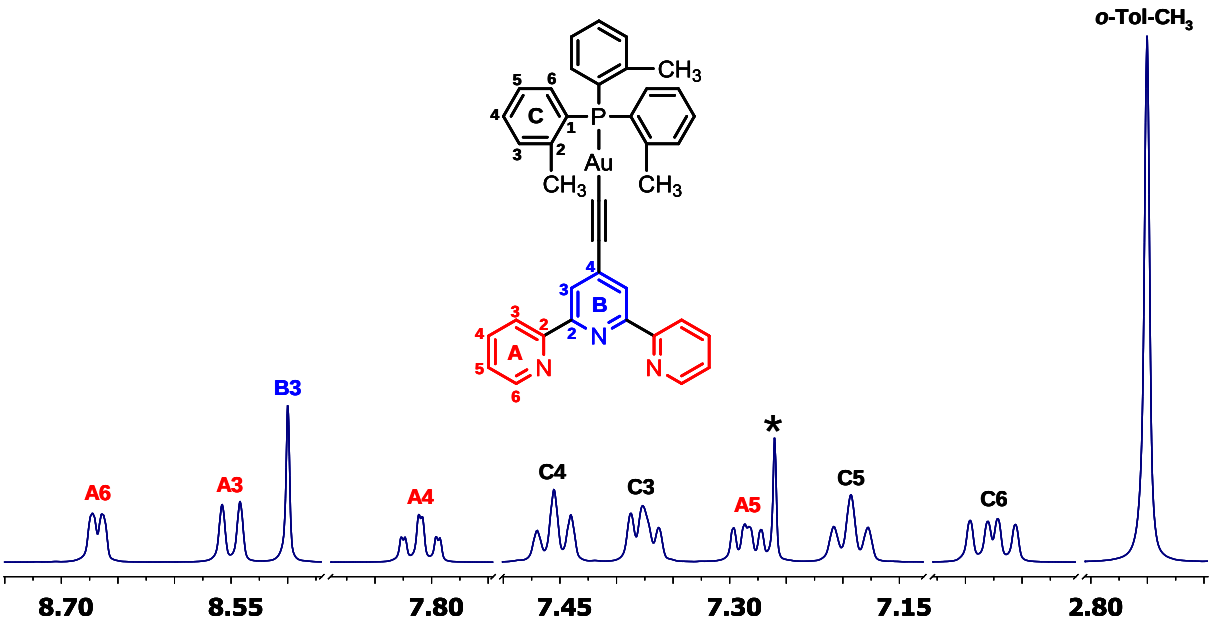


**Figure 4.2** 500 MHz $^{1}H$ NMR spectrum of **L9**, δ [ppm]. The solvent peak (residual $CHCl_3$) is also visible (*).

The assignment of $^{13}C$ NMR peaks was more difficult due to the lower sensitivity of $^{13}C$ compared to that of $^{1}H$. As in the case of the $(PR_3Au{-}{\equiv})_2$bpy ligands, in the standard experiment (NS = 1024, dτ = 2 sec), there were some difficulties with the resolution of quaternary carbons caused by their shorter relaxation times and additionally the $^{13}C$ – $^{31}P$ couplings, which decreased the intensity of peaks arising from $C^{C1}$, $C^{iC{\equiv}CAu}$ and $C^{AuiC{\equiv}C}$. For these reasons, the signals from the two carbons forming the triple bond are not observed in the $^{13}C$ NMR spectra in most cases. The $^{13}C$ NMR spectrum with peak assignment of **L9** is illustrated in **Figure 4.3**. For this ligand, a doublet for $C^{iC{\equiv}CAu}$ is discernible from the background noise due to coupling with $H^{B3}$ and is also observable in the 2-dimensional HMBC spectrum (**Figure 4.4**).

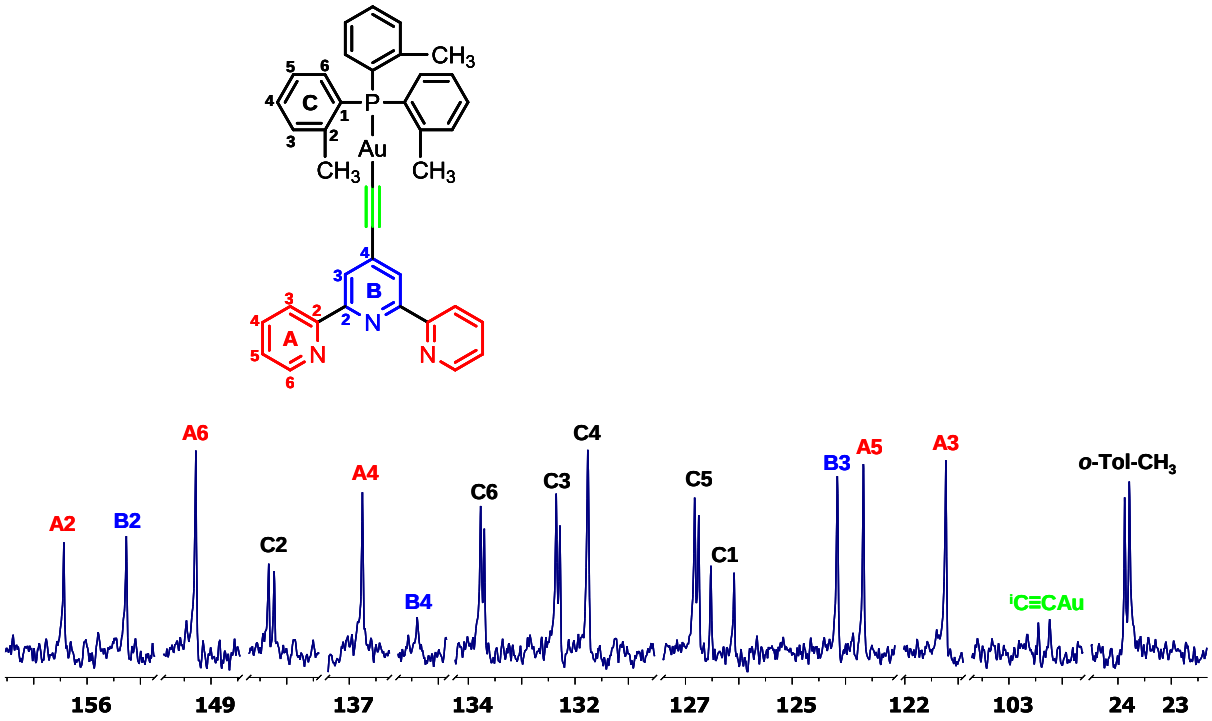


**Figure 4.3** 126 MHz $^{13}$C NMR spectrum of **L9**, δ [ppm].

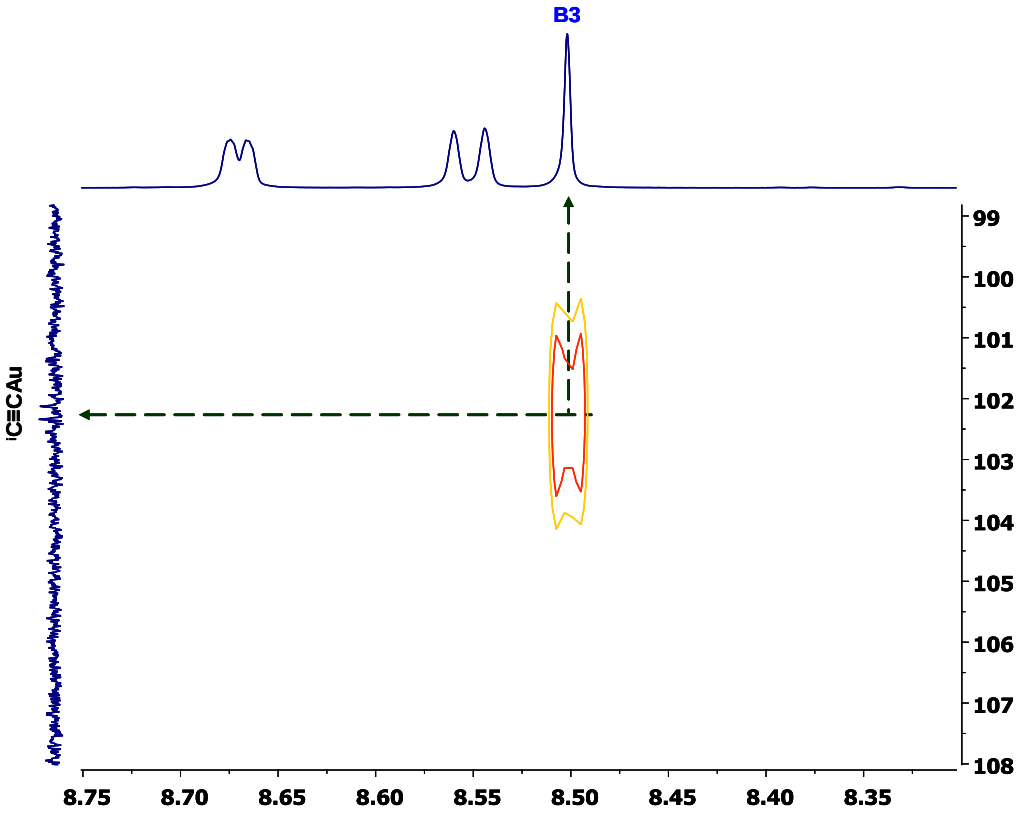


**Figure 4.4** HMBC spectrum (500 MHz instrument) of **L9**, δ [ppm].

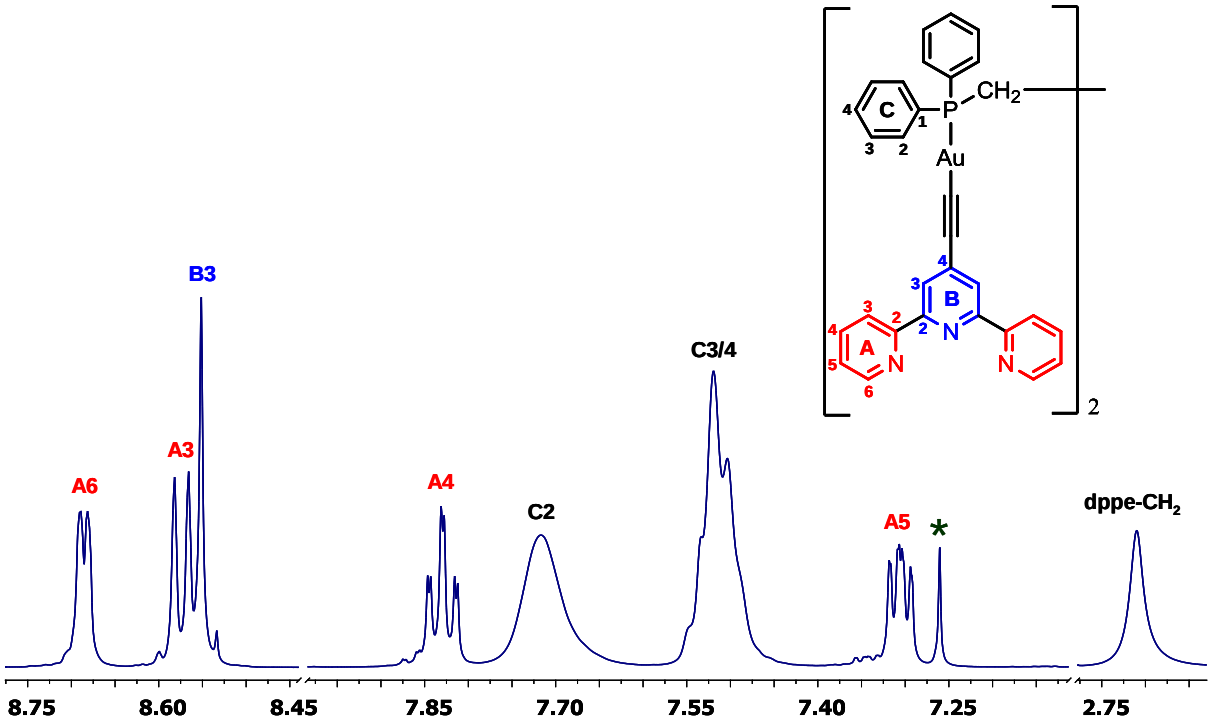


**Figure 4.5** 500 MHz $^{1}$H NMR spectrum of **L8**, δ [ppm]. The solvent peak (residual $CHCl_3$) is also visible (*).

Of the ligands studied, **L8** has the most interesting chemical structure. The bridged phosphine is connected to the alkynyl substituted tpy's through Au-atoms. The $^{1}$H NMR spectrum of **L8** with peak assignment is illustrated in **Figure 4.5** Peaks due to protons in the phenyl rings and $CH_2$ groups are broadened, and the couplings with $^{31}$P or other $^{1}$H are poorly discernible.

For **L8**, the peaks from the quaternary carbons forming the triple bonds of ligand are not observed in the $^{13}$C NMR spectrum in the standard experiment (NS = 1024, dτ = 2 sec), but the cross peak for $C^{iC\equiv CAu}$ and $H^{B3}$ appears in the 2-dimensional HMBC spectrum (**Figure 4.6**). Because of coupling with $^{31}$P the $C^{C1}$ peak becomes so insensitive to the NMR experiment and is very difficult to resolve it from the baseline noise.

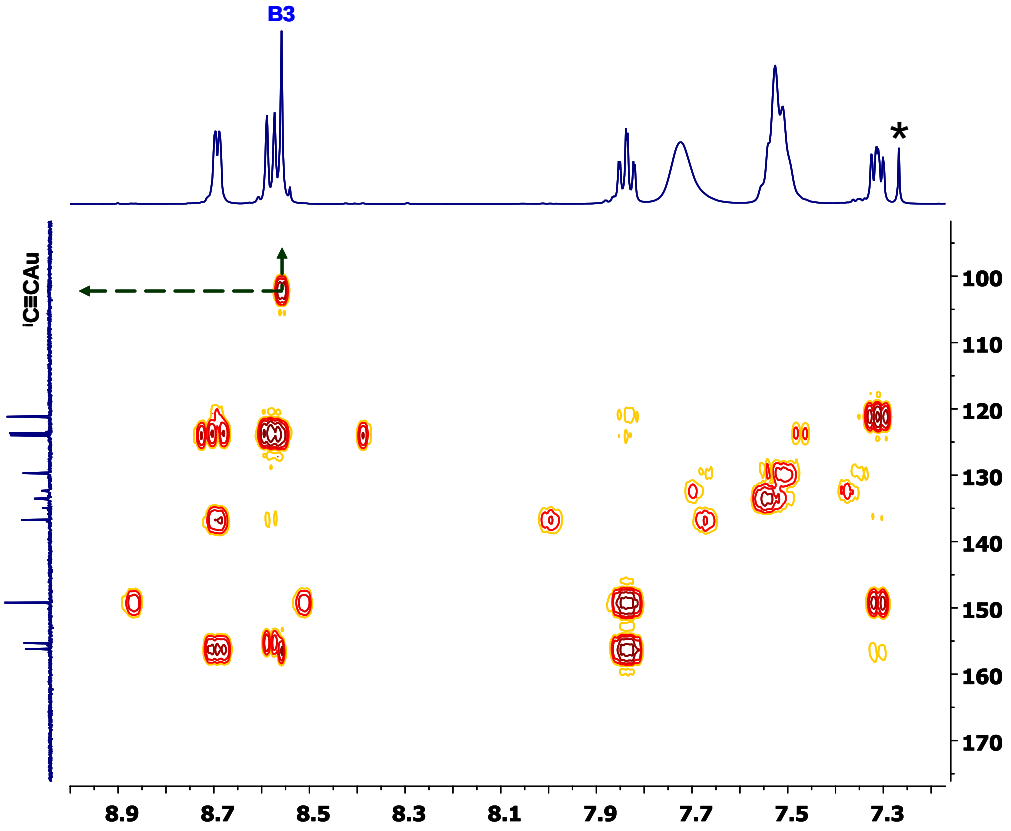


**Figure 4.6.** HMBC spectrum (500 MHz instrument) of **L8**, δ [ppm]. The solvent peak (residual $CHCl_3$) is also visible (*).

$^{31}P$ NMR spectroscopic data for **L7-L11** are summarised in **Table 4.1**. The $^{31}P$ peaks for all ligands are shifted towards higher frequencies compared with peaks arising from $R_3PAuCl$. This trend is also the same in the case $R_3P$, $R_3PAuCl$ and **L1-L6**.

| | $R_3P$ | $R_3PAuCl$ or $(dppe)(AuCl)_2$ | $R_3PAu{-}{\equiv}tpy$ or L8 | Δ δ |
|---|---|---|---|---|
| **L7 (R= Ph)** | -5.4 | 30.2 | 42.4 | 12.2 |
| **L8 (dppe)** | -12.6 | 33.5 | 40.6 | 7.1 |
| **L9 (R= *o*-Tol)** | -29.6 | 5.2 | 24.3 | 19.1 |
| **L10 (R= Et)** | -22.4 | 32.0 | 38.5 | 6.5 |
| **L11 (R= *i*-Pr)** | 17.4 | 65.0 | 67.7 | 2.7 |

**Table 4.1** $^{31}P$ NMR spectroscopic data for **L7-L11**, 162 MHz, $CDCl_3$, δ [ppm].
Δ δ = δ $^{31}P(R_3PAu{-}{\equiv}{-}tpy$ or **L8**) - δ $^{31}P(R_3PAuCl$ or dppe).

The peak shifts in the $^{31}P$ NMR spectra can be used to indicate the formation of **L7-L11** and also assess the purity of these complexes.

## 4.4. UV-Vis spectroscopic studies of L7-L9

Compounds **L7-L9** are light sensitive in solution (see section 4.6), so $CH_2Cl_2$ solutions of **L7-L9** were protected from the light before absorption measurements. **Figure 4.7** shows the absorption spectra for **L7-L9**, **≡−tpy** and **Table 4.2** lists the values of extinction coefficients calculated for $\lambda_{max}$.

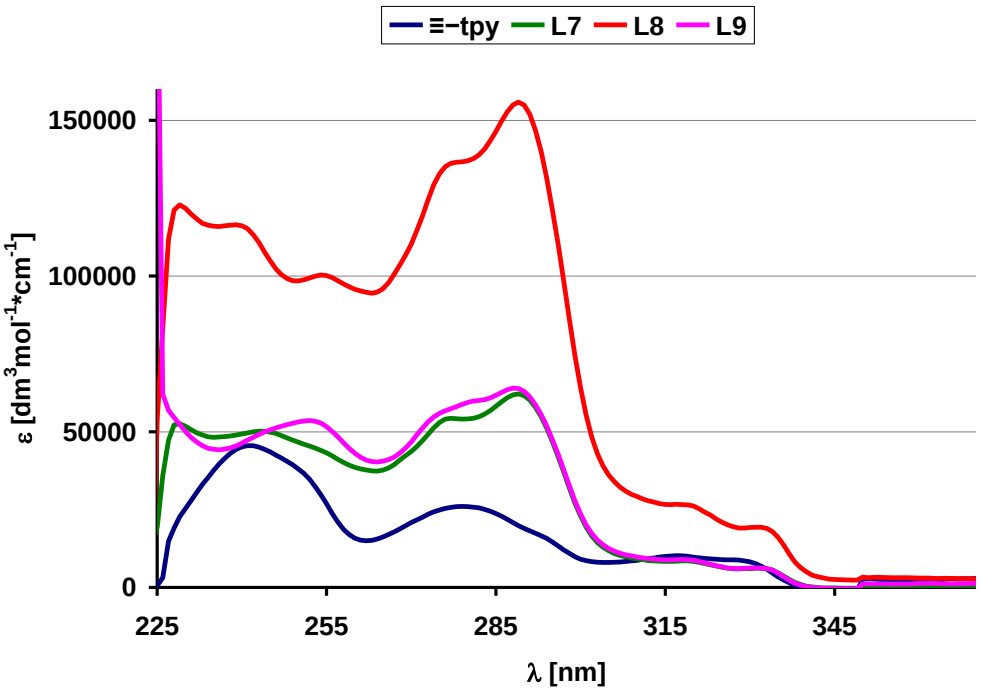


**Figure 4.7** Absorption spectra in for **≡−tpy** and **L7-L9** in $CH_2Cl_2$ solution.

| Compound nr. | $\lambda_{max}$ [nm], ($\varepsilon$ / $10^4$ [$dm^3mol^{-1}cm^{-1}$]) |
|---|---|
| **L7 (R= Ph)** | 229 (5.3), 244 (5.0), 277 (5.4), 289 (6.2), 319 (0.9), 331 (0.6) |
| **L8 (dppe)** | 230 (12.2), 239 (11.6), 254 (10.0), 277 (13.6), 289 (15.6), 319 (2.6), 332 (1.9) |
| **L9 (R= *o*-Tol)** | 251 (5.3), 280 (5.9), 288 (6.4), 318 (0.9), 332 (0.6) |

**Table 4.2** Electronic absorption spectroscopic data for **L7-L9** in $CH_2Cl_2$ solution.

Similarly to **L1-L6**, band assignment for **L7-L9** is difficult and without theoretical calculations the results are uncertain. Tentatively, by comparison with the results of other authors [101]-[103], peaks at $\lambda$ <275 nm may be attributed to n→π*/σ* (non-bonding electrons from N-atom), or π→π* transitions from the aromatic phosphine substituents. The

lower energy absorption peaks at 319 and 332 nm could be assigned to n→π* and the π→π* transitions of the conjugated chain respectively. Peaks at 254, 277 (280), 289 (288) nm may be assigned as σ→π* (σ refers to the bonding orbital of Au-P and π* denotes the antibonding molecular orbital of aryl rings from **L7**-**L9**), the σ(Au-P)→π* (C≡C), π→π* (C≡C) from alkynyl group and metal-to-ligand charge-transfer (MLCT [d(Au)→π*(C≡C, alkynyl)]). For **L8** the presence of Au-Au bonds makes possible metal–metal-to-ligand charge-transfer MMLCT [d(Au-Au)→π*(C≡C, alkynyl)]) transition [101]-[103].

## 4.5. Fluorescence spectroscopic studies of L7-L9

The presence of [-P-Au−≡−]–units in **L7-L9** strongly influences the luminescent properties of these compounds. Fluorescence measurements demonstrated both the light emitting properties of **L7-L9** and also the light sensitivity of these ligands; the latter is described in section 4.6. **Figure 4.8** shows the emission spectrum for **L8** and **Table 4.3** lists the values of $\lambda_{em}$ and their corresponding $\lambda_{ex}$ for all three compounds.

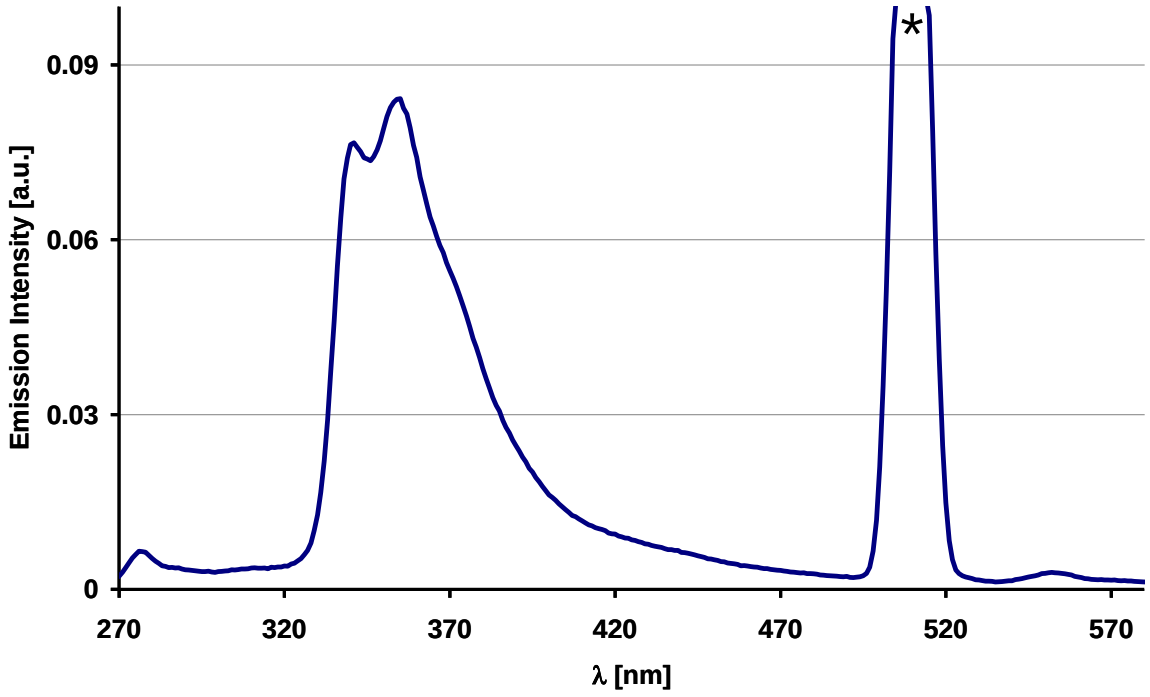


**Figure 4.8** Emission spectrum of **L8**. Excitation $\lambda_{ex}$ = 254 nm, slit 5/5 , concentration of $CH_2Cl_2$ solution is 1.2 * $10^{-5}$ mol/$dm^3$, * = first harmonic.

| Compound nr. | $\lambda_{ex}$ [nm] | $\lambda_{em}$ [nm] |
|---|---|---|
| **L7 (R= Ph)** | 244 | 339, 355 |
| **L8 (dppe)** | 254 | 341, 355 |
| **L9 (R= *o*-Tol)** | 252 | 341, 354 |

**Table 4.3** Fluorescence spectroscopic data for **L7-L9** in $CH_2Cl_2$ solution.

The compounds **L7-L9** were excited with $\lambda_{ex}$ = 241-252 (**Table 4.3**) and two overlapping emission bands at 339 (341) nm and 355 (354) nm were observed. The range of band width and the shapes of the fluorescence curves were very similar for all **L7-L9**, which suggest similar electron transfers during the emission process.

Similarly for analogous compounds found in literature, these emission bands may be associated with mixed IL [π→π∗(C≡CR)] and MLCT [d(Au)→π*(C≡C)] transitions with predominantly IL transitions and [σ(Au–P)→π*(C≡C)] transitions. The Au-Au bond in **L8** allows postulate possibility of metal–metal-to-ligand charge-transfer MMLCT [d(Au-Au)→π*(C≡C, alkynyl)]) emission [101], [102], [106].

## 4.6. Photodegradation of L7-L9

Compounds **L7-L9** are light sensitive in solution and therefore behave similarly to **L1-L6.** A decay of all fluorescence bands was observed during a series of fluorescence spectra measurements ($\lambda_{ex}$ = 230 nm) and new fluorescence bands (**Figure 4.9**, **Table 4.4**) were observed in the fluorescence spectrum**.**

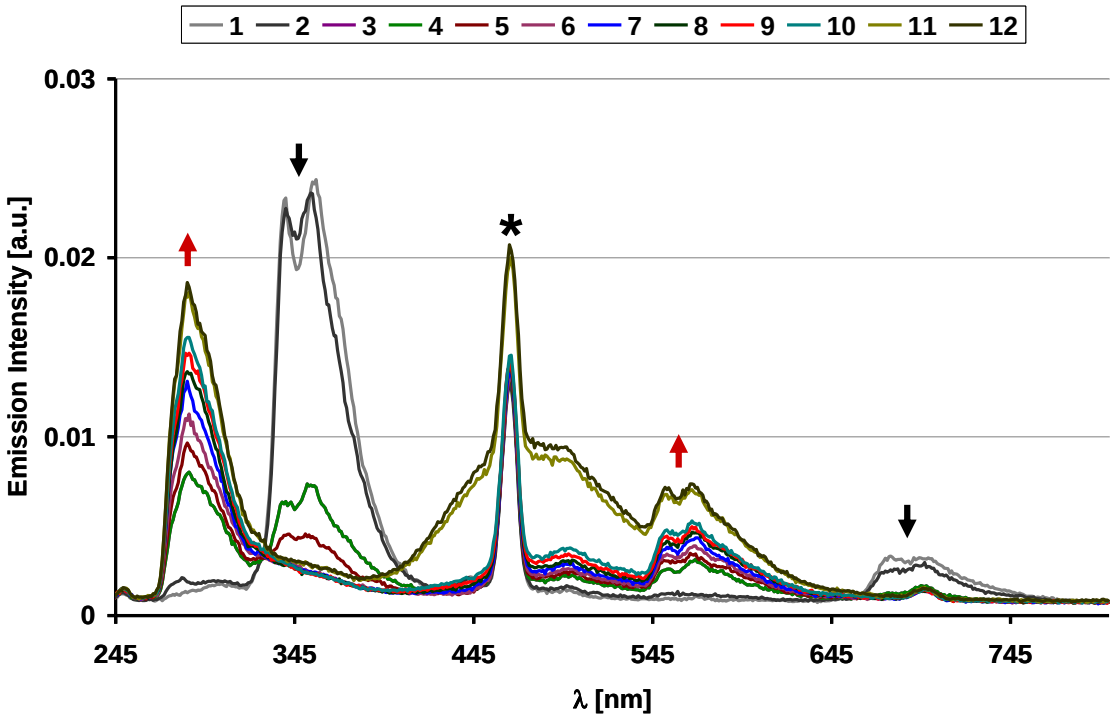


**Figure 4.9** Emission spectrum of a $CH_2Cl_2$ solution of **L7** as a function of time ($\lambda_{ex}$ = 230 nm, * = first harmonic). The measurement time was approximately 12 min.

| Compound nr. | $\lambda_{ex}$ [nm] | $\lambda_{em}$ [nm] | $\lambda_{em}$ [nm] after photodegradation |
|---|---|---|---|
| **L7 (R= Ph)** | 230 | 339, 355 | 286, 486, 555, 568 |
| **L8 (dppe)** | 230 | 341, 355 | 286, 520 |
| **L9 (R= *o*-Tol)** | 230 | 341, 354 | 295, 584 |

**Table 4.4** Fluorescence spectroscopic data for **L7-L9** in $CH_2Cl_2$ solution after photodegradation.

Compound **L8** behaves similarly to the trialkynylphosphanegold(I) derivatives of bpy and the photodegradation products appear with much smaller emission bands in the spectrum (**Figure 4.10**).

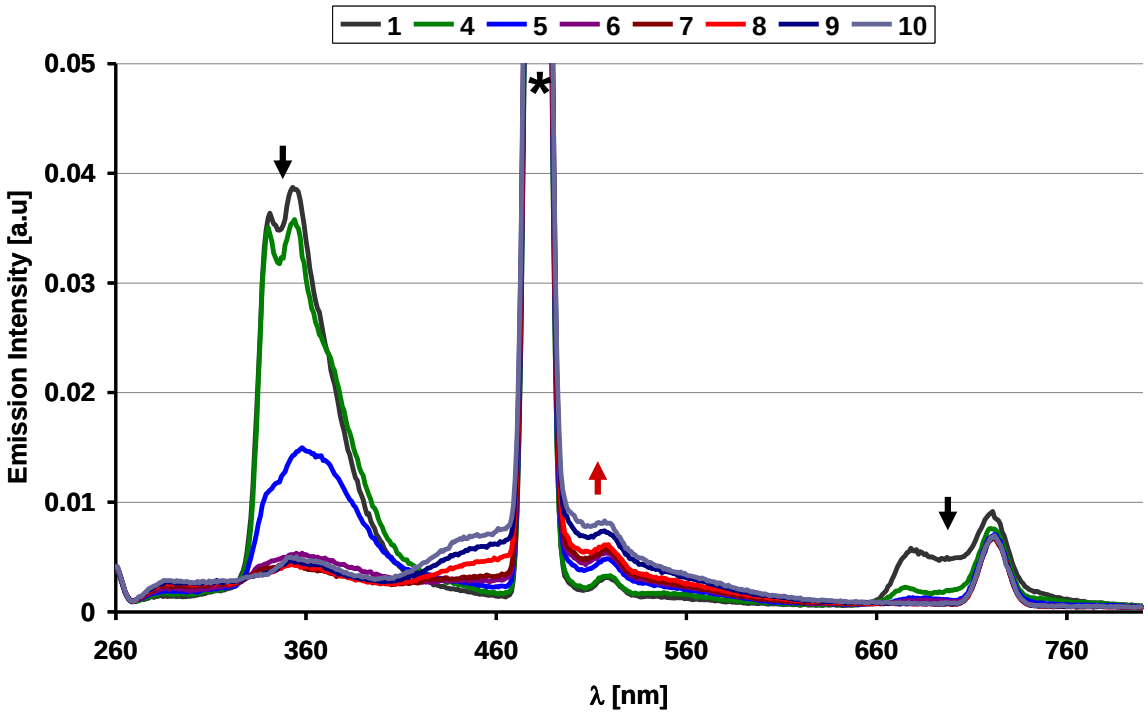


**Figure 4.10** Emission spectrum of a $CH_2Cl_2$ solution of **L8** as a function of time ($\lambda_{ex}$ = 230 nm, * = first harmonic). The measurement time was approximately 10 min.

A series of fluorescence measurements for $\lambda_{ex}$ > 230 nm (e.g.: **L7**, $\lambda_{ex}$ = 244, 277, 289, 319, 331 nm) do not elicit the photodegradation or the effect is slower or hardly discernible in the fluorescence spectra.

The nature of the photodegradation products was not determined but this process, by analogy with observed photodegradation process for **L4** (see section 3.6), could be proposed to proceed as follows: cleavage of the alkynyl-gold bond and the formation of the unidentified products.

## 4.7. X-ray diffraction studies of L7-L9

A family of four ligands (**L7, L9-L11**) were obtained *via* a multistep synthesis, featuring the reaction of 4'-ethynyl-2,2':6',2''-terpyridine with triarylphosphinegold(I) chlorides and trialkylphosphinegold(I) chlorides. The novel bridged ligand (**L8**) was obtained by reacting catena-[4'-(2-gold-1-ethynyl)-2,2':6',2''-terpyridine] with dppe.

X-ray quality single crystals of three of these ligands (**L7-L9**) were isolated and structures were determined by X-ray diffraction. Molecular structures of **L7-L9** show the expected transoid conformation of the terpyridine rings and a lack of Au…Au interactions was observed in the case of **L7** and **L8**.

The different phosphine substituents in **L7-L9** influence not only the properties of these compounds, but also their crystal packing. The parameter measuring the steric properties of the phosphine ligand was defined in section 3.7 as the Tolman cone angle (see **Figure 3.18**, section 3.7).

**Table 4.5** summarises values of the ligand cone angle for the phosphine substituents which were used to synthesise **L7-L9**. Initially, the Tolman cone angle was measured only for a phosphine ligand with three identical substituents, but subsequently it was extended to asymmetrical phosphines (like dppe) as the symmetrically substituted bulky phosphine may adopt an unsymmetrical conformation [112], [122].

| $PR_3$ | θ [°] |
|---|---|
| $PH_3$ | 87 |
| $PPh_3$ | 145 |
| **dppe** | 125 |
| $P(o\text{-Tol})_3$ | 194 |

**Table 4.5** Values of the ligand cone for the chosen phosphine substituents [112], [113].

The Tolman cone angle defines only the size of the phosphine, therefore other factors must be used to predict the presence of Au…Au interactions in the case of **L7-L9.** In these ligands, π–π interactions between the phenyl rings or *o*-tolyl rings play a crucial role in the crystal packing.

**Crystal structure description of L7-L9.**

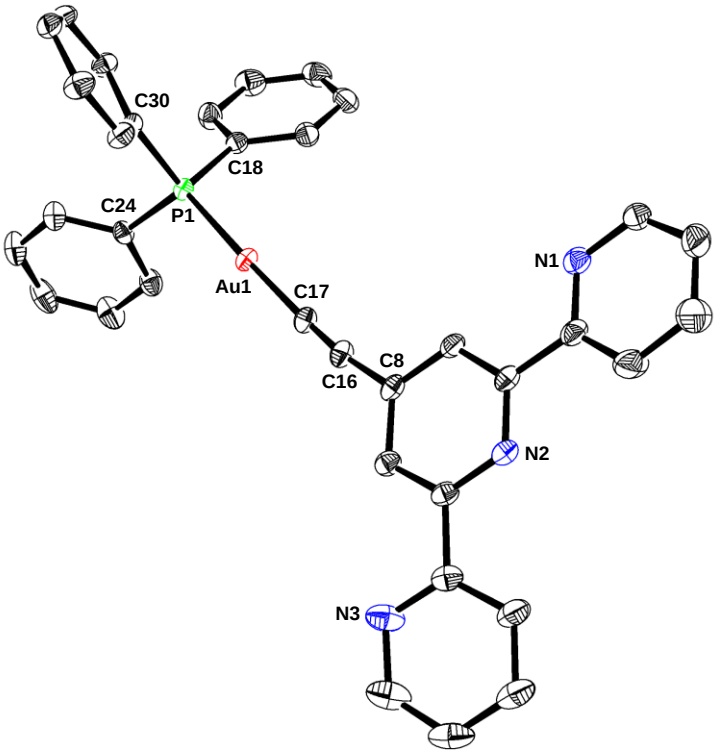


**Figure 4.11** Molecular structure of **L7** (ORTEP - probability ellipsoids – 40 %). All H atoms are omitted for clarity.

X-ray quality single crystals in the form of colourless plates were obtained by slow diffusion of $Et_2O$ into $CH_2Cl_2$/toluene solution of **L7**. The crystal structure of **L7** was solved in the monoclinic space group $P2_1/c$. The unit cell comprises four molecules and the labelling of the atoms is shown in **Figure 4.11**. Selected bond lengths and bond angles of **L7** are listed in **Table 4.6**.

| Bond | Lengths [Å] | Bond angle | Value [°] |
|---|---|---|---|
| **Au1–P1** | 2.2742(10) | **P1–Au1–C17** | 176.93(11) |
| **Au1–C17** | 2.003(4) | **C16–C17–Au1** | 176.1(4) |
| **C16–C17** | 1.195(6) | **C8–C16–C17** | 172.8(4) |

**Table 4.6** Selected bond lengths and bond angles of **L7.**

As shown in **Figure 4.12** Au…Au interactions for **L7** are not observed and the shortest Au…Au distance ($Au1...Au1^{i}$ = $Au1...Au1^{ii}$) is 8.373(2) Å. The lack of Au…Au contacts is due to steric hindrance from the phenyl rings and to the π–π interactions between the phenyl rings (**Figure 4.14**), which increase the Au…Au distance.

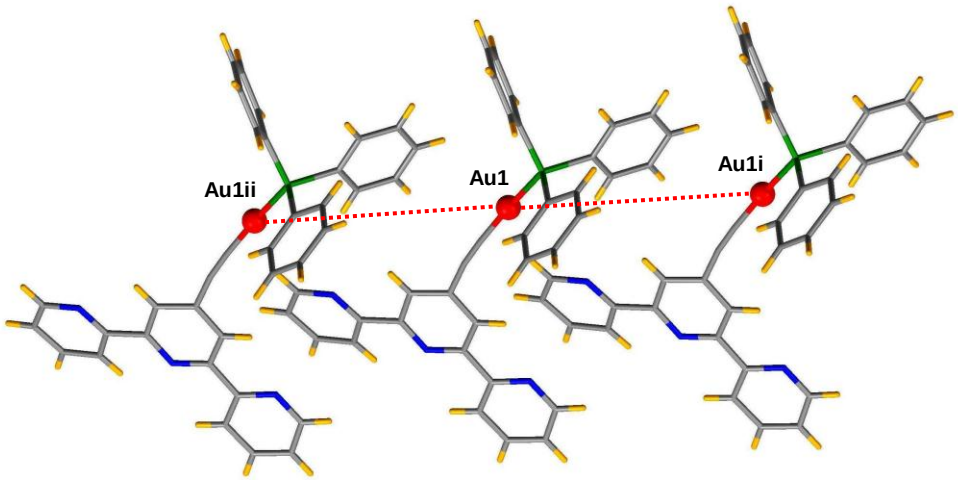


**Figure 4.12** The shortest Au…Au distance for **L7**. Symmetry codes i: x, 1+y, z, ii: x, -1+y, z. Au1...Au1$^{i}$ = Au1...Au1$^{ii}$ = 8.373(2) Å

A view of the crystal packing along the c-axis shows the characteristic layer separation of the tpy and phosphine moieties of **L7** (**Figure 4.13**), marked by blue and grey colours. The Au atoms are marked in red and the distance between them is 9.086(2) Å which is longer than the shortest Au…Au contacts for **L7** is 8.373(2) Å.

The $Ph_3P$ domains interlock and π–π interactions are clearly present between the phenyl groups, which is shown in **Figure 4.13** In contrast, adjacent tpy domains do not participate in this kind of interaction.

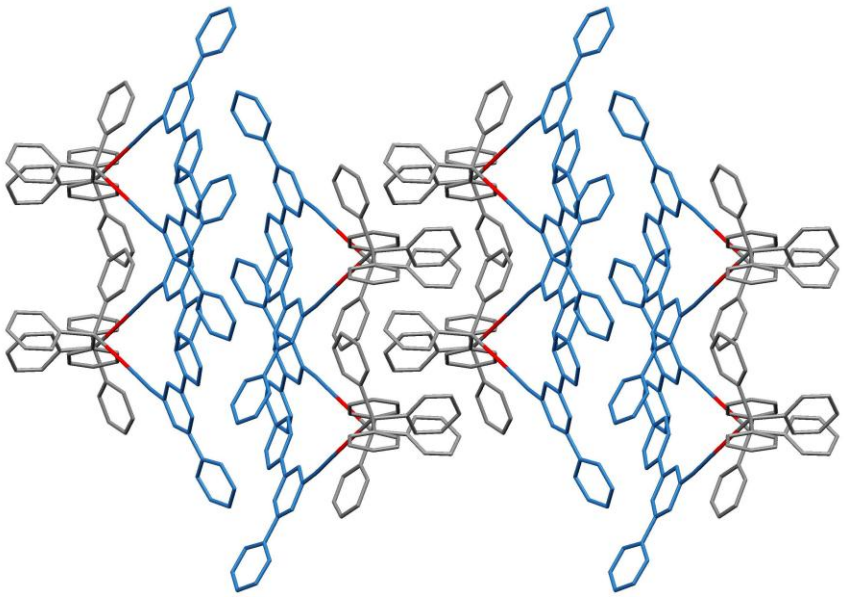

**Figure 4.13** The crystal packing of **L7**: view along the c-axis.

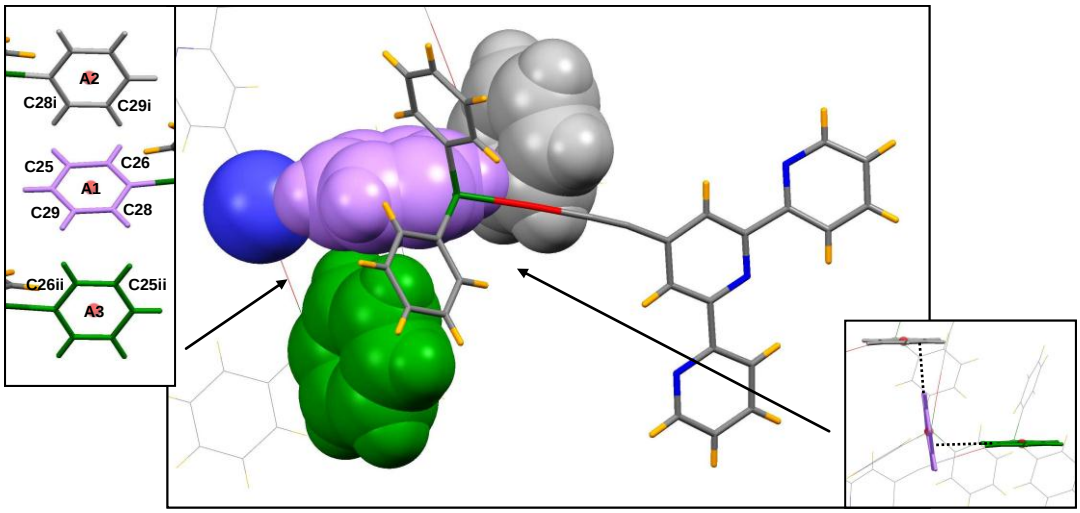


**Figure 4.14** Edge-to-face π–π interactions between phenyl rings and C−H…$C_{alkyne}$ interactions for **L7**. Symmetry codes are explained in the text.

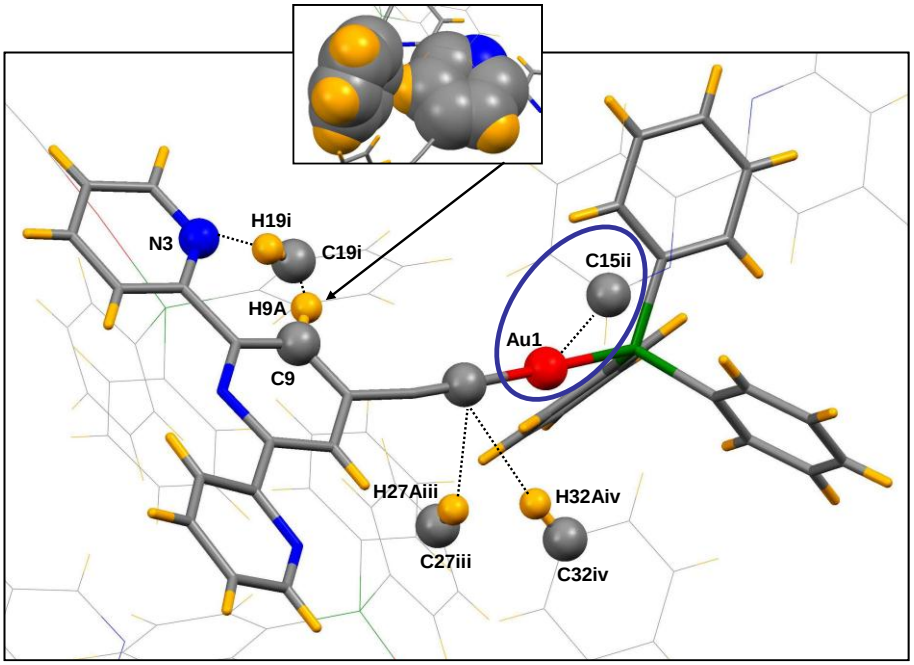


**Figure 4.15** Weak interactions: C−H…$C_{alkyne}$, non-classical hydrogen bond of C−H...N type, π–π interactions between the phenyl ring and one of the pyridine rings and Au1…$C15^{ii}$ contact (in blue) for **L7**. Symmetry codes are explained in the text.

The edge-to-face π–π interactions between phenyl rings have a dominant influence on the crystal packing, which is illustrated in **Figure 4.14** (C25...$C28^{i}$ = 3.624(6) Å,

C26…C29$^{i}$ = 3.681(6) Å, C25$^{ii}$…A1(centroid) = 3.85 Å, C26$^{ii}$…A1(centroid) = 3.96 Å symmetry codes i: -x, 1/2+y, 1/2-z, ii: -x, -1/2+y, 1/2-z, interplanar angles for the phenyl rings with A2(centroid)/A1(centroid) = 83°, due to symmetry rings with A2(centroid) and A3(centroid) are perfectly parallel) [114].

The phenyl ring marked in violet in **Figure 4.14** takes part in two kinds of interactions, the previously mentioned π–π stacking of phenyl rings, and also in the weak interactions: C−H…$C_{alkyne}$ (**Figure 4.14**, C17…H27A$^{iii}$ = 2.67 Å, C17…C27$^{iii}$ = 3.417(6) Å, angle C17…H27A$^{iii}$–C27$^{iii}$ = 136°, symmetry code iii: -x, 1/2+y, 1/2-z), which explains the decreased angle value for the second interaction [114]- [116].

Other kinds of π–π interactions involve one phenyl ring and one of the pyridine rings with an interplanar angle of 78° between them (C19$^{i}$…H9A = 2.90 Å, C19$^{i}$…C9 = 3.737(6) Å, symmetry code i: x, 1/2-y, -1/2+z) and is shown in **Figure 4.15** [114].

π–π interactions for **L7** may impact on the Au…Au distance and even with the Tolman cone angle of 145° for $Ph_3P$, which is smaller than 160° for i-$Pr_3P$, interactions between Au-Au atoms for **L7** are not possible.

Weak interactions: C−H…$C_{alkyne}$ (for **L7**: C17…H27A$^{iii}$ = 2.67 Å, C17…C27$^{iii}$ = 3.417(6) Å, angle C17…H27A$^{iii}$–C27$^{iii}$ = 136°, symmetry code iii: -x, 1/2+y, 1/2-z, C17…H32A$^{iv}$ = 2.90 Å, C17…C32$^{iv}$ = 3.605(7) Å, angle C17…H32A$^{iv}$–C32$^{iv}$ = 132°, symmetry code iv: x, 1+y, z) and non-classical hydrogen bonds of C–H...N type (for **L7**: N3…H19A$^{i}$ = 2.59 Å, N3…C19$^{i}$ = 3.527(6) Å, angle N3…H19A$^{i}$–C19$^{i}$ = 170°, symmetry code i: x, 1/2-y, -1/2+z, **Figure 4.15**) are present in the crystal packing for all compounds **L7-L9** [115]- [117].

A short contact involving the gold atom and the carbon in the pyridine ring can be found (Au1…C15$^{ii}$ = 3.264(4) Å, symmetry code i: x, 1/2-y, 1/2+z), which is marked by the blue circle in **Figure 4.15**. This contact can be observed only in the crystal packing of **L7**. For the other ligands from the bpy and tpy series any contacts with Au-atoms (excluding Au...Au) are not observed. Vincente *et al* reported specific C-H…Au short contacts in a compounds: [{Au(C≡Cbpyl)}$_2$($\mu$-dppd)] and [{Au(C≡Cbpyl)}$_2$($\mu$-dppe)] which are analogous to **L8** [79].

Compound **L8**, the molecular structure of which is illustrated in **Figures 4.16** and **4.17** crystallised in the form of colourless needles as a result of slow diffusion of $Et_2O$ into $CH_2Cl_2$/$CHCl_3$/toluene solution of **L8**. The crystal structure of **L8** was solved in the

monoclinic space group *Pc*. The unit cell contains only one molecule of **L8** and a half of solvent molecule ($CHCl_3$).

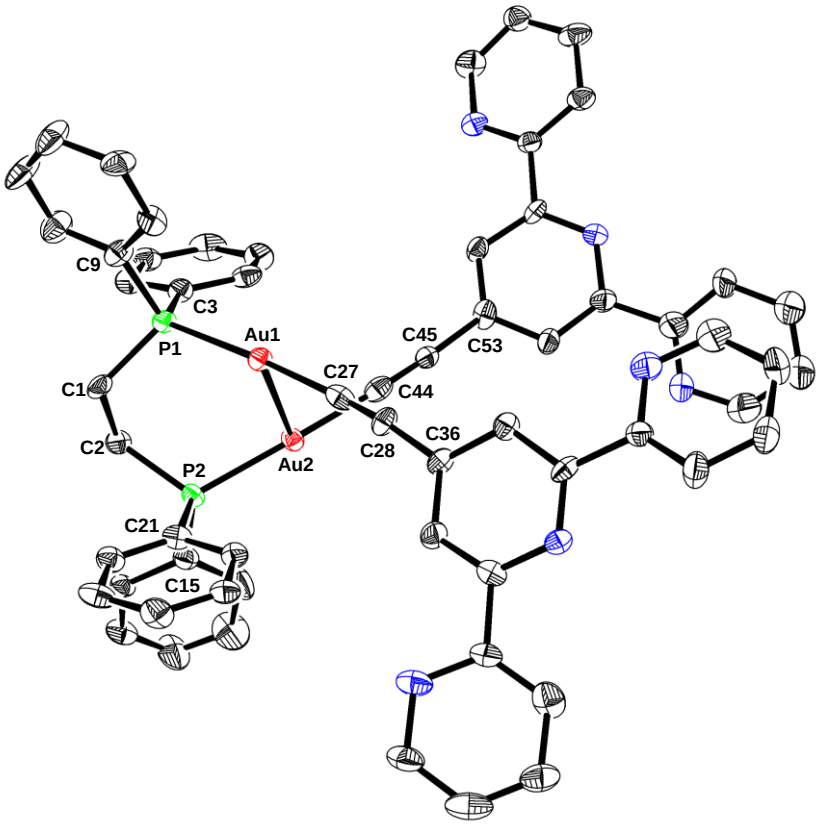


**Figure 4.16** Molecular structure of **L8** (ORTEP - probability ellipsoids- 30 %). Solvent molecules and all H atoms are omitted for clarity.

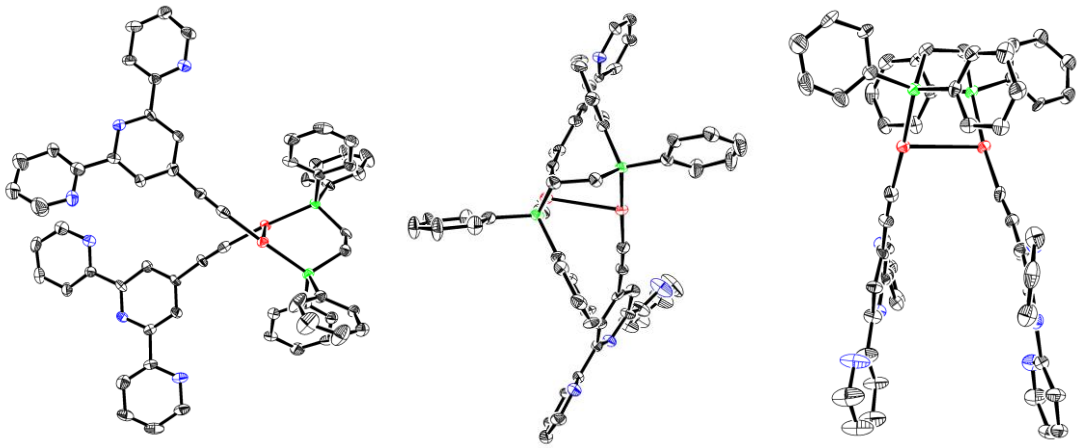

**Figure 4.17** Molecular structure of **L8 –** different views (ORTEP - probability ellipsoids - 30 %). Solvent molecules and all H atoms are omitted for clarity.

Values of important bond angles: P1−Au1−Au2, P2−Au2−Au1, C27−Au1−Au2, C44−Au2−Au1 are close to 90° with the maximal deviation 6°. Selected bond lengths and bond angles of **L8** are summarised in **Table 4.7** .

| Bond | Length [Å] | Bond angle | Value [°] |
|---|---|---|---|
| **Au1−Au2** | 2.9470(8) | **P1−Au1−Au2** | 87.54(9) |
| **Au1−P1** | 2.287(3) | **P2−Au2−Au1** | 88.37(10) |
| **Au1−C27** | 2.015(16) | **C27−Au1−Au2** | 96.0(4) |
| **C27−C28** | 1.18(2) | **C44−Au2−Au1** | 93.5(5) |
| **Au2−P2** | 2.272(4) | **C1−P1−Au1** | 113.6(4) |
| **Au2−C44** | 2.019(19) | **C2−P2−Au2** | 114.0(5) |
| **C44−C45** | 1.18(2) | **P1−Au1−C27** | 173.8(4) |
| **Bond angle** | **[°]** | **C27−C28−Au1** | 113.6(4) |
| **P2−Au2−C44** | 176.8(4) | **C27−C28−C36** | 171.0(17) |
| **C44−C45−Au2** | 176.4(15) | **C44−C45−C53** | 175.9(17) |

**Table 4.7** Selected bond lengths and bond angles of **L8**.

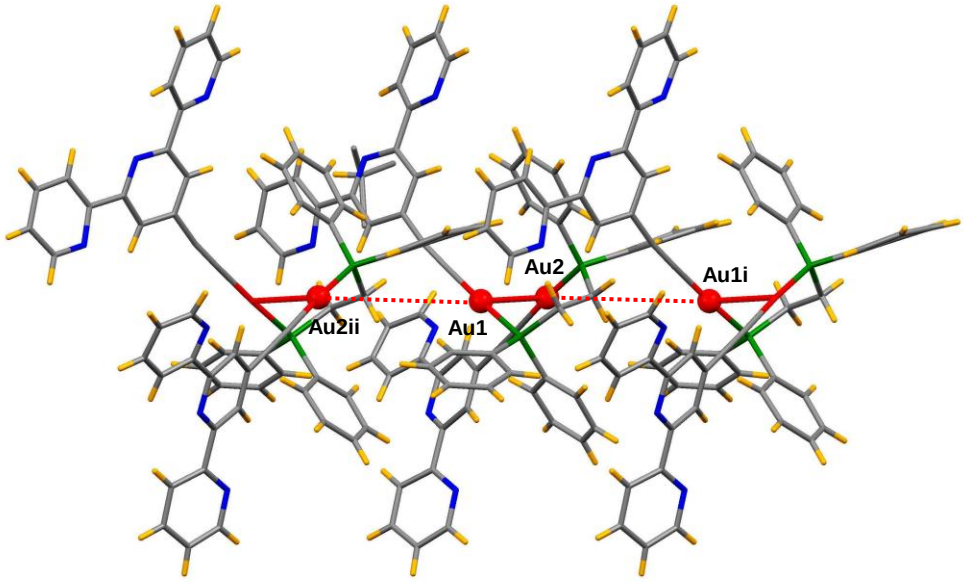


**Figure 4.18** The shortest Au…Au distances for **L8**. Au1−Au2 = 2.9470(8) Å, Au1...Au2$^{ii}$ = Au2...Au1$^{i}$ = 6.965(1) Å. Symmetry codes i: x, 1-y, 1/2+z, ii: x, 1-y, -1/2+z.

The intramolecular aurophilic interactions with an Au-Au separation of 2.9470(8) Å dominate the crystal packing of **L8** (**Figure 4.18**).

Any intermolecular Au-Au interactions are not observed, which is caused by steric demands but also the presence of π–π interactions similar to other ligands with aromatic substituents on the phosphine moiety probably influence on Au-Au distance (**Figure 4.18**).

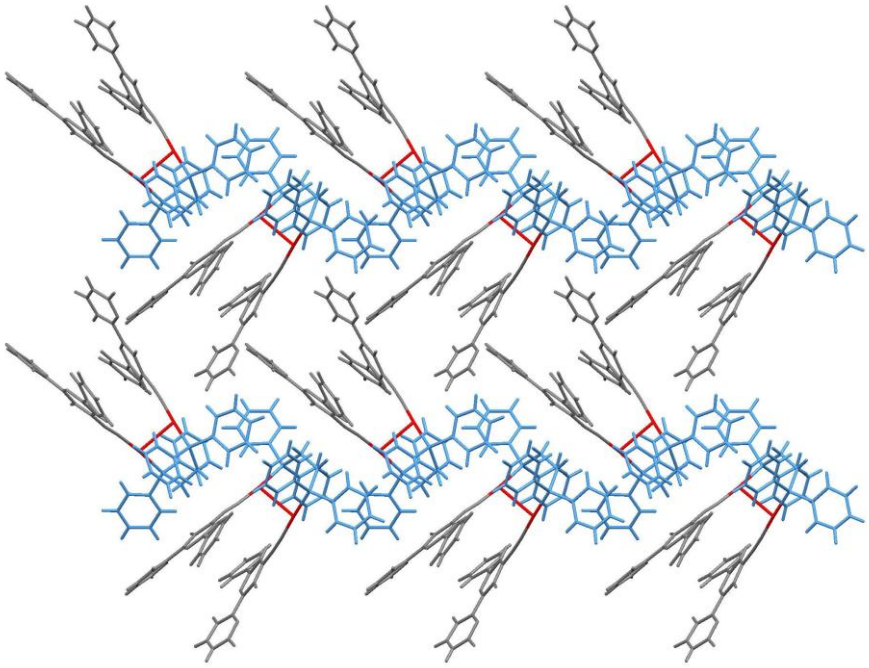

**Figure 4.19** The crystal packing of **L8**: view along the a-axis.

The crystal packing of **L8** (**Figure 4.19**, **Figure 4.20**) illustrates the separation of tpy and phosphine moieties marked in blue and grey in the figures, respectively. The view along the a-axis shows a characteristic herringbone pattern, whose assembly is supported by C–H…$C_{alkyne}$ interactions (C28…H22A$^{ii}$ = 2.88 Å, C28…C22$^{ii}$ = 3.82(2) Å, angle C28... H22A$^{ii}$–C22$^{ii}$ = 170°, symmetry code ii: x, 1-y, -1/2+z, C28…H2B$^{ii}$ = 2.86 Å, C28…C2$^{ii}$ = 3.82(2)Å, angle C28... H2B$^{ii}$–C2$^{ii}$ = 163°, symmetry code ii: x, 1-y, -1/2+z, C27…H2B$^{ii}$ = 2.71 Å, C27…C2$^{ii}$ = 3.67(2) Å, angle C27... H2B$^{ii}$–C2$^{ii}$ = 162°, symmetry code ii: x, 1-y, -1/2+z, C27…H16A$^{ii}$ = 2.65 Å, C27…C16$^{ii}$ = 3.53(2) Å, angle C27... H16A$^{ii}$–C16$^{ii}$ = 154°, symmetry code ii: x, 1-y, -1/2+z, marked in grey and in orange in **Figure 4.23**) [117] and weak non-classical hydrogen bonds of C–H...N type (N5…H31A$^{i}$ = 2.74 Å, N5…C31$^{i}$ = 3.58(2) Å, angle N5... H31A$^{i}$–C31$^{i}$ = 145°, symmetry code i: 1+x, 2-y, 1/2+z, **Figure 4.22**) [115], [116], as shown in **Figure 4.19**. Additionally, tpy moieties adopt a zigzag form marked in blue in **Figure 4.19.**

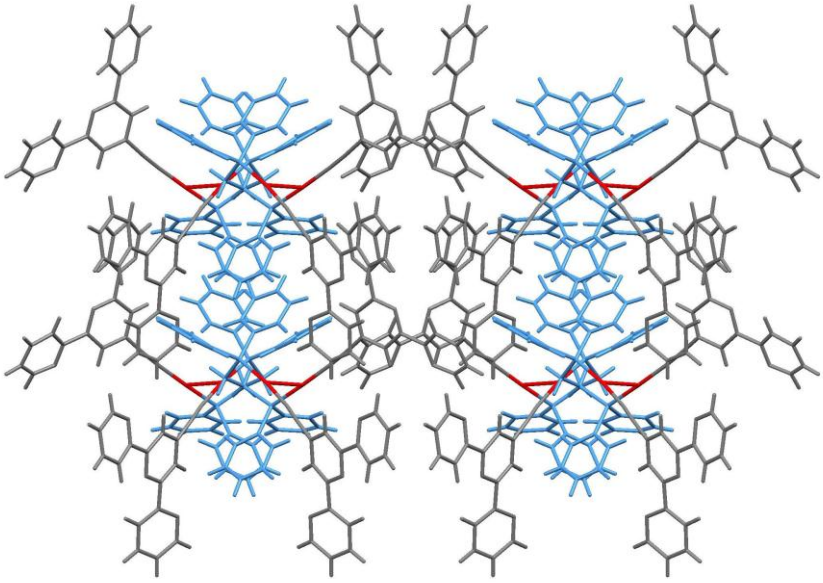

**Figure 4.20** The crystal packing of **L8** : view along the c-axis.

The assembly motif marked in blue is illustrated in a view along the c-axis of the crystal packing of **L8** (**Figure 4.20**).

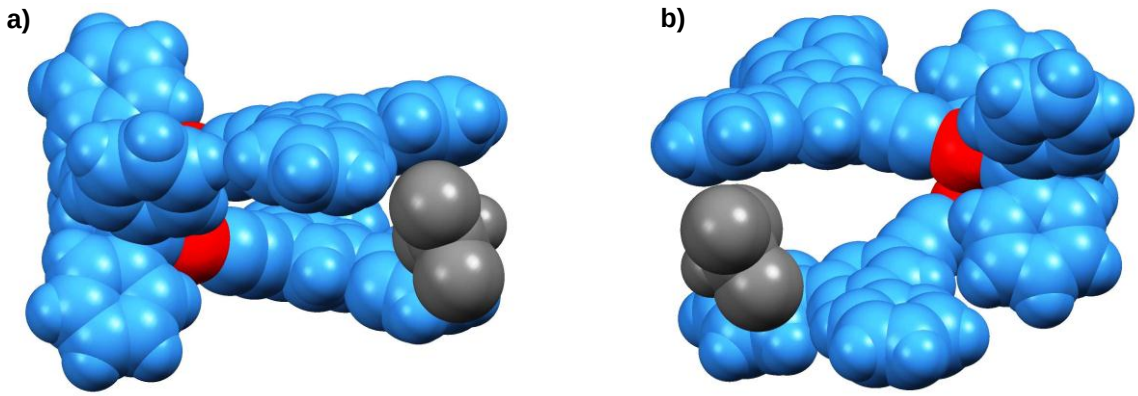


**Figure 4.21** Space-filling representation of **L8** showing the scissor effect (b) of two tpy-domains around a $CHCl_3$ solvent molecule (in grey).

The Au-Au bond is a torsional point of molecule **L8** and the two tpy domains do not adopt the expected "parallel sandwich position", in which they could interact by π–π stacking and the solvent molecule seems to block this kind of interactions. Instead "a scissor-like" arrangement can be observed in **Figure 4.21**, **b)**.

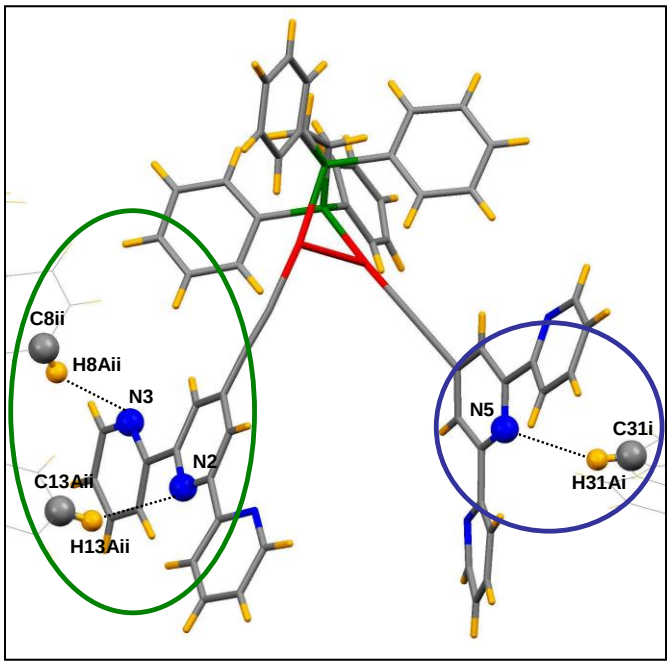


**Figure 4.22** Non-classical hydrogen bonds of C−H...N type for **L8**. Symmetry codes are explained in the text.

As opposed to **L7**, two types of non-classical hydrogen bonds are observed in the crystal packing of **L8**. One of them involves phenyl ring C atom as a donor and pyridine N atom as acceptor (marked by the green circle, N2…H13A$^{ii}$ = 2.67 Å, N2…C13$^{ii}$ = 3.47(2) Å, angle N2... H13A$^{ii}$–C13$^{ii}$ = 142°, N3…H8A$^{ii}$ = 2.73 Å, N2…C8$^{ii}$ = 3.61(2) Å, angle N3… H8A$^{ii}$–C8$^{ii}$ = 154°, symmetry code ii: -1+x, 1-y, -1/2+z), and the second involves the interaction between two pyridine rings (marked by the blue circle, N5…H31A$^{i}$ = 2.74 Å, N5…C31$^{i}$ = 3.58(2) Å, angle N5... H31A$^{i}$–C31$^{i}$ = 145°, symmetry code i: 1+x, 2-y, 1/2+z) as is shown in **Figure 4.22** [115], [116]. The tpy moieties do not interact by π–π stacking *via* the pyridine rings, but only by the afore-mentioned weak C–H...N interactions.

Molecules of **L8** exhibit edge-to-face π–π interactions between the phenyl rings, and the phenyl ring and the pyridine ring (C36…H22A$^{ii}$ = 2.89 Å, C36…C22$^{ii}$ = 3.68(2) Å, angle 73.09°, symmetry code ii: x, 1-y, -1/2+z, C24…H17A$^{ii}$ = 2.84 Å, C24…C17$^{ii}$ = 3.612 Å, C23…H17A$^{ii}$ = 2.86 Å, C23…C17$^{ii}$ = 3.64(3) Å, angle 72°, symmetry code ii: x, 1-y, -1/2+z, **Figure 4.23**) and C–H…$C_{alkyne}$ interactions (C45…H58A$^{i}$ = 2.86 Å, C45…C58$^{i}$ = 3.65(3) Å, angle C45... H58A$^{i}$–C58$^{i}$ = 142°, symmetry code i: x, 2-y, 1/2+z). Steric demands within **L8** influence the distance between the gold atoms from two independent molecules of **L8** and also increase the shortest distance between them to 6.965(1) Å (**Figure 4.18**) [114],

[117]. The π–π stacking between the phenyl rings, and the phenyl ring and the pyridine ring may also have an effect on this.

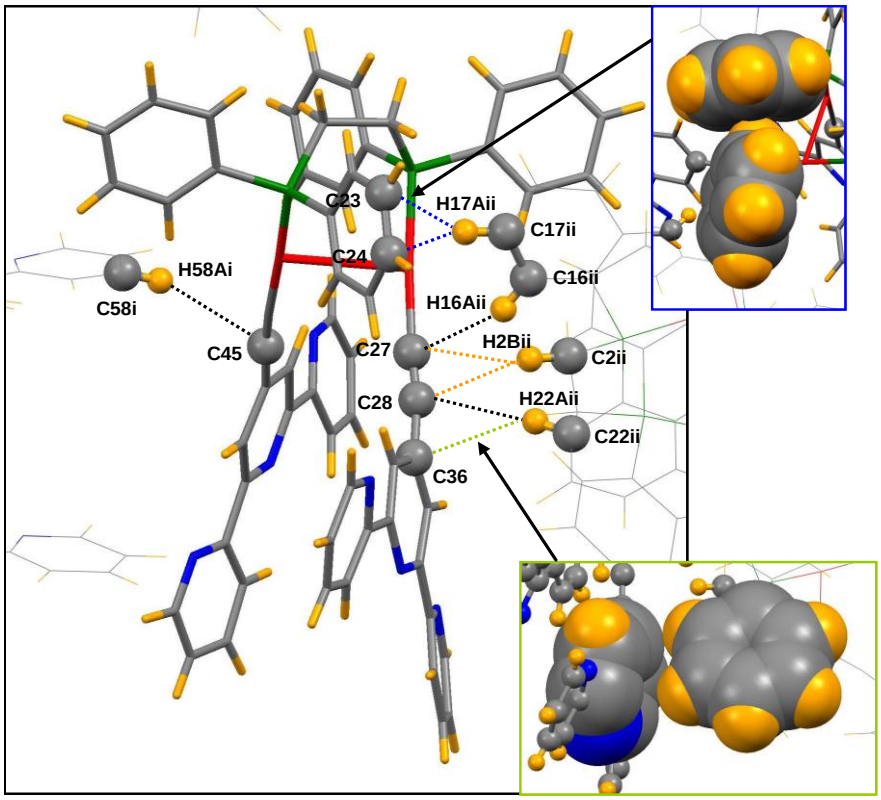


**Figure 4.23** Edge-to-face π–π interactions for **L8** between phenyl rings; and phenyl ring and pyridine ring respectively. C−H…$C_{alkyne}$ interactions for **L8**. Symmetry codes are explained in the text.

X-ray quality single crystals in the form of colourless plates were obtained by slow diffusion of $Et_2O$ into a $CH_2Cl_2$/toluene solution of **L9**. The crystal structure was solved in the triclinic space group Pī, (**Figure 4.24**). The asymmetric unit contains two independent molecules (**Figure 4.27**) and the unit cell comprises four molecules of **L9**. The molecular structure of **L9** is illustrated in **Figure 4.24**. Selected bond lengths and bond angles of **L9** are listed in **Table 4.8**.

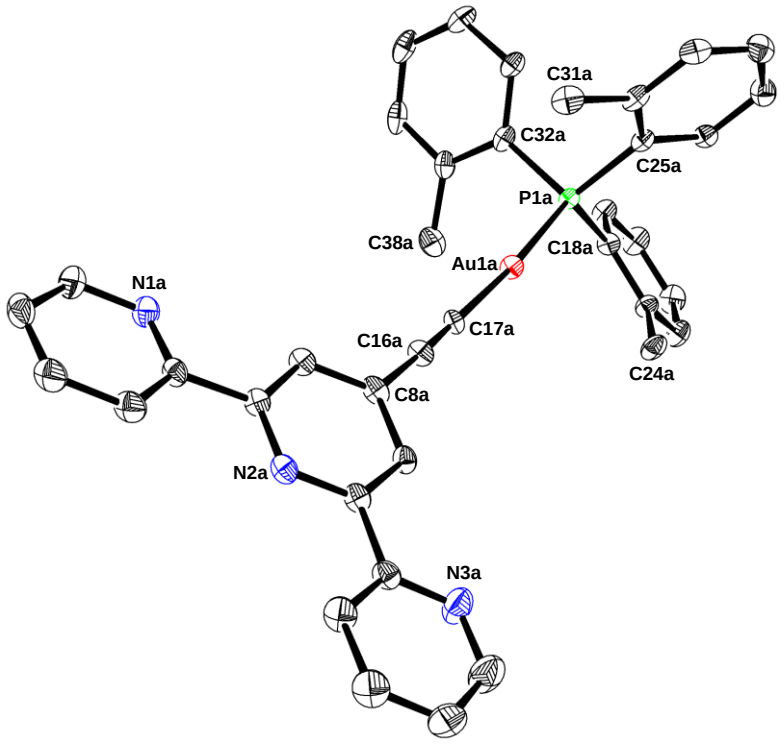


**Figure 4.24** Molecular structure of **L9** (ORTEP - probability ellipsoids – 40 %). All H atoms are omitted for clarity.

| Bond | Length [Å] | Bond angle | Value [°] |
|---|---|---|---|
| **Au1a–P1a** | 2.2859(14) | **P1a–Au1a–C17a** | 172.31(19) |
| **Au1a–C17a** | 1.996(6) | **C16a–C17a–Au1a** | 175.7(6) |
| **C16a–C17a** | 1.187(8) | **C8a–C16a–C17a** | 178.8(8) |
| **Au1b–P1b** | 2.2925(14) | **P1b–Au1b–C17b** | 174.98(17) |
| **Au1b–C17b** | 2.000(6) | **C16b–C17b–Au1b** | 175.5(5) |
| **C16b–C17b** | 1.195(8) | **C8b–C16b–C17b** | 177.4(7) |

**Table 4.8** Selected bond lengths and bond angles of **L9**.

The o-$Tol_3P$ substituents are very bulky (with a large Tolman cone angle of 194°) and as a result no aurophilic interactions are observed. The shortest Au…Au distance 7.9436(9) Å for **L9** (**Figure 4.25**) is shorter than for **L7** (8.373(2) Å), which is the longest intermolecular Au...Au distance of the ligands **L3-L8**.

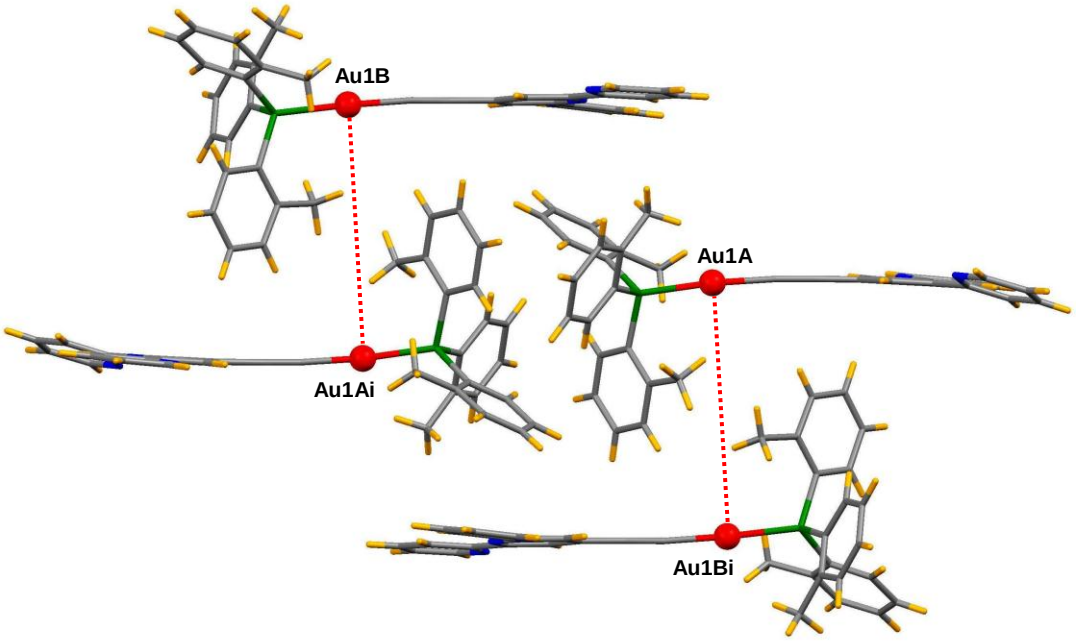


**Figure 4.25** The shortest Au…Au distance for **L9**, Au1A...Au1B$^{i}$ = Au1B...Au1A$^{i}$ = 7.9436(9) Å. Symmetry code i: 1-x, 1-y, 1-z.

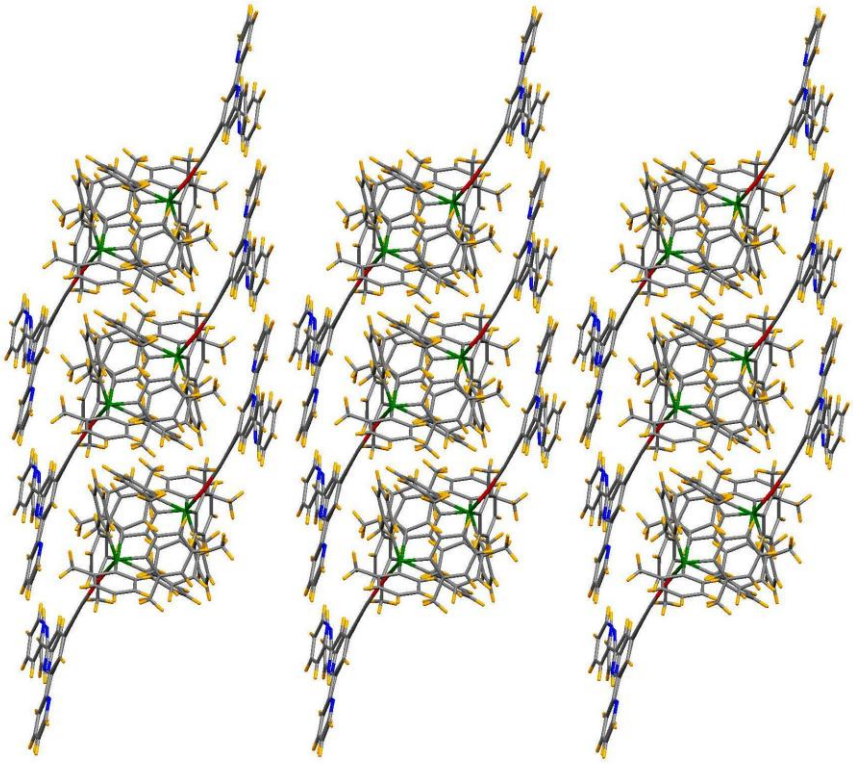

**Figure 4.26** The crystal packing of **L9**: view along the c-axis.

The crystal packing when viewed along the c-axis (**Figure 4.26**) exhibits the characteristic assembly motif of cubes with separated tpy and phospine domains, which are stabilised by the parallel, displaced face-to-face π–π interactions of pyridine rings (C2A$^{i}$…C10A = C10A$^{i}$…C2A = 3.358(9) Å, the distance between A3(centroid)…A5(centroid) = 3.77 Å, symmetry code: 3-x, 2-y, 2-z, **Figure 4.28**) and the weak non-classical hydrogen bond of C−H...N type, in which the pyridine N atoms also act as acceptors (N1B…H13B$^{iii}$ = 2.70 Å, N1B…C13A$^{iii}$ = 3.59(1) Å, angle N1B…H13B$^{iii}$–C13A$^{iii}$ = 155° symmetry code iii: -1+x, y, 1+z, **Figure 4.27**) and shown in **Figure 4.26** [114]-[116]. The face-to-face π–π stacking of the pyridine rings was not observed in the case of ligands **L1-L8**.

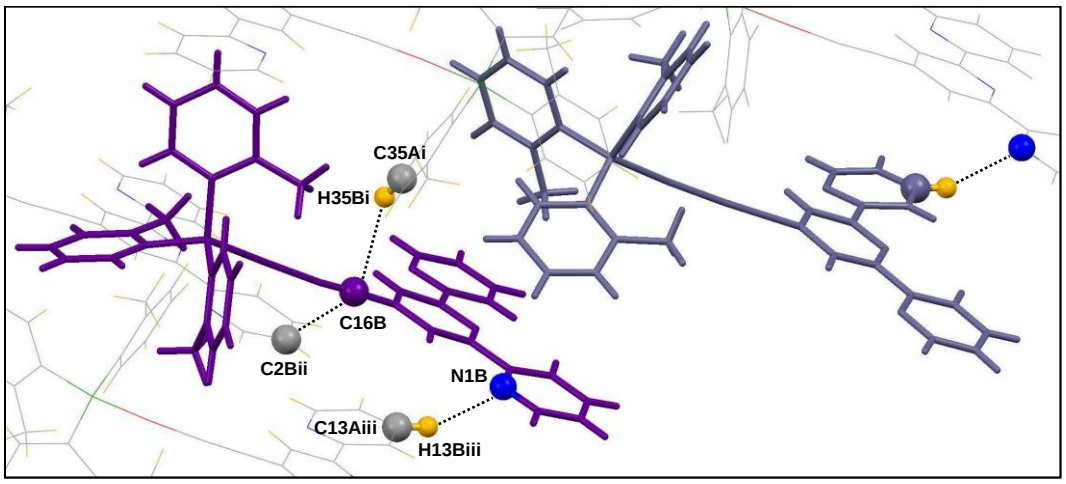


**Figure 4.27** Weak interactions: C−H…$C_{alkyne}$, non-classical hydrogen bonds of C−H...N type for **L9**. Symmetry codes are explained in the text. Two independent molecules of **L8** from the asymmetric unit are marked in violet and grey.

C–H…$C_{alkyne}$ interactions (C16B…H35B$^{i}$ = 2.83 Å, C16B…C35A$^{i}$ = 3.510(8) Å, angle C16B…H35B$^{i}$–C35A$^{i}$ = 129° symmetry code i: 1-x, 1-y, 1-z, C16B…C2B$^{ii}$ = 3.371(8) Å, symmetry code ii: -1+x, y, z) and non-classical hydrogen bond are presented in **Figure 4.27**.

The crystal packing is dominated by π–π interactions which may also enlarge the Au…Au distance to 7.9436(9) Å. At this distance, Au…Au interactions are not significant. The face-to-face π–π stacking of pyridine rings (marked in blue and grey in **Figure 4.28**), the edge-to face and edge-to-face π–π stacking between the *o*-tolyl rings and one of the pyridine rings ((C7A…H28A$^{ii}$ = 2.77 Å, C7A…C28B$^{ii}$ = 3.619(9) Å, the interplanar angle of the rings with A3(centroid)/A8(centroid) = 87° symmetry code ii: 1-x, 1-y, 1-z, C36B$^{iii}$…H9AA = 2.81

Å, C9A… C36B$^{iii}$ = 3.663(9) Å, the interplanar angle of the rings with A3(centroid)/A7(centroid) = 76° symmetry code ii: 1+x, y, 1+z, marked in dark and light grey in **Figure 4.28** and C5B…H28B = 3.04 Å, C5B…C28A = 3.314(9) Å, and distances between H28B…A2(centroid) = 3.19 Å, C28A…A2(centroid) = 3.57 Å, the interplanar angle between the rings with A1(centroid)/A2(centroid) = 30° symmetry code: x, y, z, marked in green in **Figure 4.28**), the edge-to-face π–π or C-H..π interactions between *o*-tolyl rings (C22A…C29B$^{ii}$ = 3.352(9) Å, the interplanar angle between rings with A4(centroid)/A5(centroid) = 30°, symmetry code: -x, 1-y, 1-z, marked in green in **Figure 4.29**, and C27B$^{i}$…H19A = 2.89 Å, C27B$^{i}$…C19B = 3.761(8) Å, the interplanar angle of rings with A2(centroid)/A3(centroid) = 89°, symmetry code: -1-x, 1-y, -z, C35B…H27A$^{i}$ = 2.67 Å, C35B…C27B$^{i}$ = 3.547(8) Å, the interplanar angle of rings with A1(centroid)/A3(centroid) = 71°, symmetry code: -1-x, 1-y, -z, C36B…H27A$^{i}$ = 2.81 Å, C36B…C27B$^{i}$ = 3.681(8) Å, symmetry code: -1-x, 1-y, -z, marked in blue in **Figure 4.29**) indicate a variety of π–π and C-H..π interactions for **L9** [114].

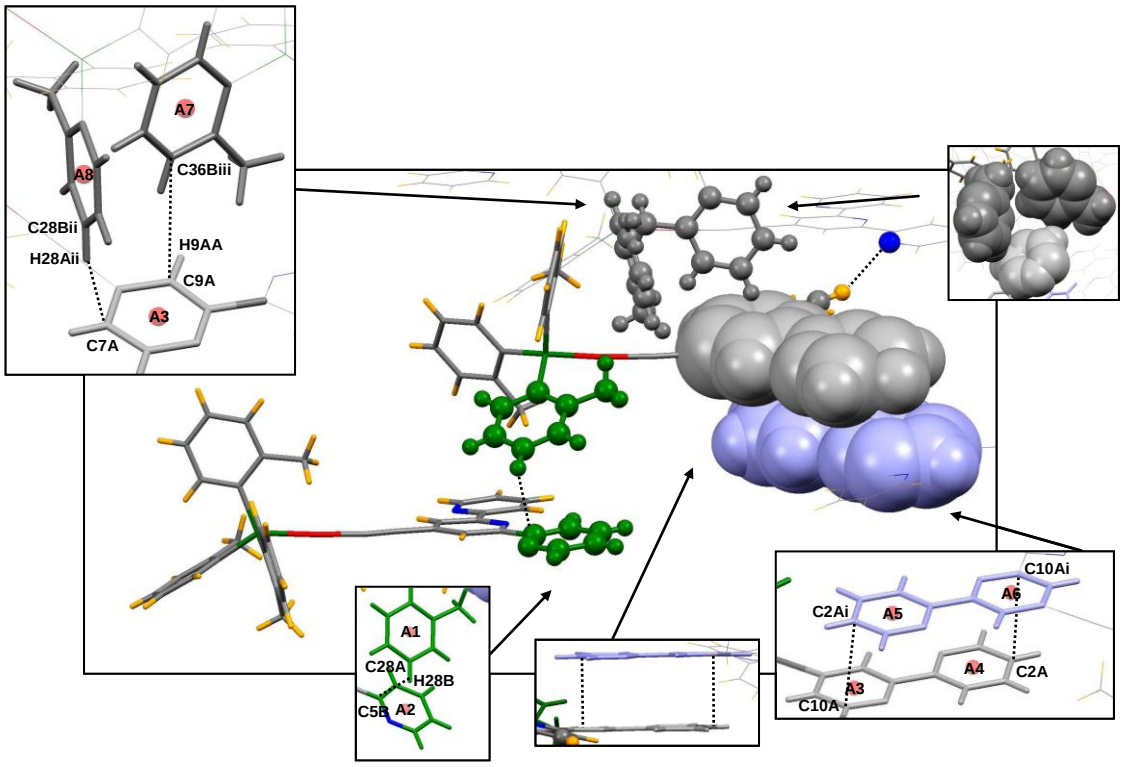


**Figure 4.28** Edge-to-face π–π interactions between *o*-tolyl rings and pyridine ring and parallel, displaced π–π interactions between pyridine rings for **L9**. Symmetry codes are explained in the text.

The asymmetric unit for **L9** contains two independent molecules, which was mentioned previously, and these molecules labelled as A and B interact *via* π–π interactions between *o*-tolyl rings and pyridine rings (marked in green in **Figure 4.28**).

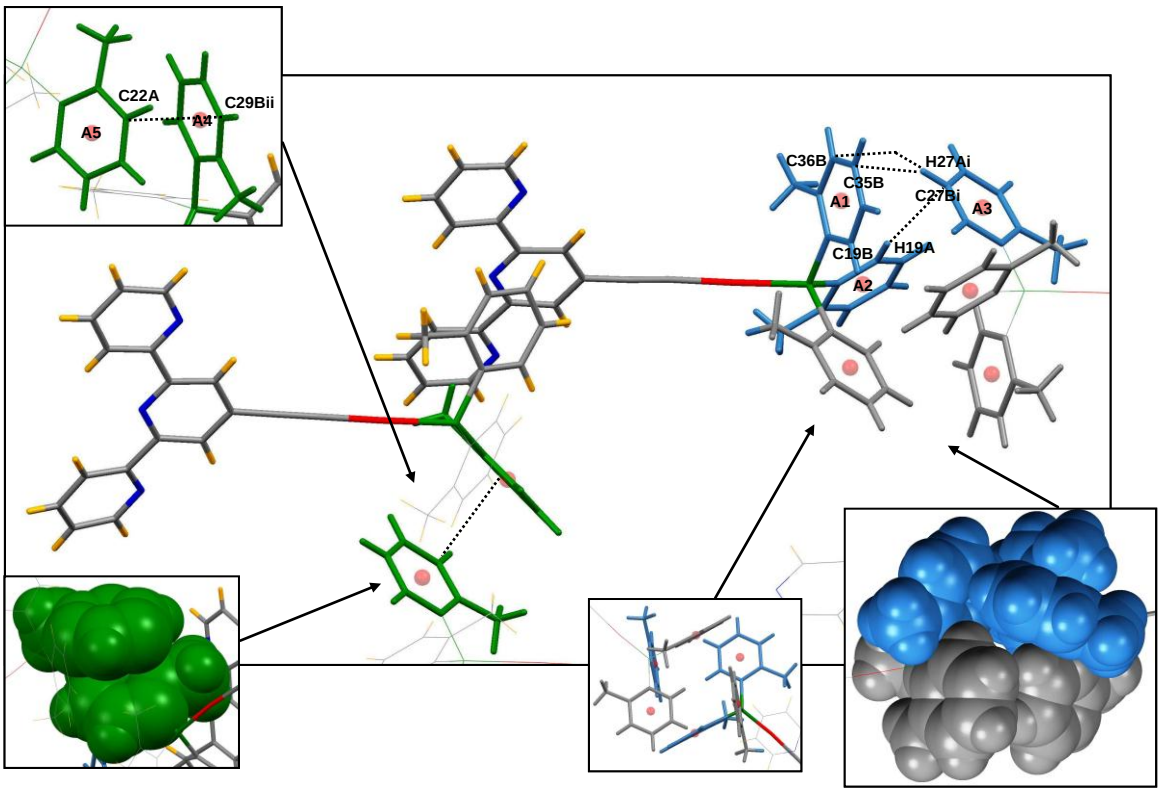


**Figure 4.29** Edge-to-face and face-to-face π–π interactions between *o*-tolyl rings for **L9**. Symmetry codes are explained in the text.

# 5. Strategies for the formation of metal complexes with gold-decorated ligands

Complexes of transition metals with 2,2'-bipyridine and 2,2':6',2"-terpyridine and with their derivatives are widely investigated due to their high complex stability constants and unique structural and luminescent properties. The complexes have found a wide range of the applications [68]-[77], [81]-[89].

With regard to structural properties two types of metal complexes can be obtained: homoleptic and heteroleptic. Homoleptic complexes are complexes that consist of a metal-ion and structurally identical ligands, while heteroleptic complexes consist of metal-ion and structurally diverse ligands.

As the isolation of pure Zn(II) complexes of **L4**, **L7**, **L8** and also Fe(II) complexes of **L4**, **L7**, **L8** was not achieved, the yield of the reaction in the experimental section was calculated as follows: n % (e.g. : 91 % for **C2**) is a yield calculated from the mass of the crude product. Because there were purification problems, the calculated yield was always the upper limit.

## 5.1. Experimental for C1-C8

**[Ru((≡–)$_2$bpy)(bpy)$_2$](PF$_6$)$_2$ (C1)**

Formula: $C_{34}H_{24}F_{12}N_6P_2Ru$

Formula weight: 907.59 [g/mol]

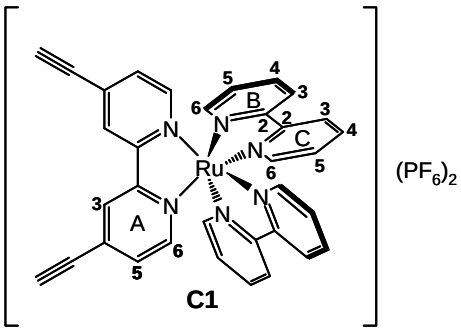


C1

$Ru(bpy)_2Cl_2$ (47 mg, 98 μmol) and 4,4'-diethynyl-2,2'-bipyridine (20 mg, 98 μmol) were suspended in 20 ml ethylene glycol and sealed in a microwave vial. The reaction was heated in a microwave reactor (160 °C, 10 min), after which the reaction mixture was added to 70 ml

of an aqueous solution of $NH_4PF_6$ (4 mmol, 65 mg). A red precipitate formed and was filtered over celite *in vacuo* and washed with water (50 ml) and ether (50 ml). The material was removed from the celite by dissolving with $CH_3CN$. Compound **C1** was isolated as a red solid (83 mg, 91 µmol, 93 %).

**$^1$H NMR** (500 MHz, $CD_3CN$), δ [ppm]: 8.59 (s, 2H, $H^{A3}$), 8.49 (d, *J* = 8.1 Hz, 4H, $H^{B3/C3}$), 8.09 – 8.04 (m, 4H, $H^{B4/C4}$), 7.71 (d, *J* = 5.8 Hz, 4H, $H^{B6/C6}$), 7.68 (d, *J* = 5.7 Hz, 2H, $H^{A6}$), 7.40 (dd, *J* = 12.8, 6.4 Hz, 6H, $H^{A5/B5/C5}$), 4.01 (s, 2H, $H^{C\equiv CH}$).
**$^{13}$C NMR** (126 MHz,$CD_3CN$), δ [ppm]: $^{13}$C NMR (126 MHz, $CD_3CN$) δ 157.76 ($C^{A2/B2/C2}$), 157.72 ($C^{A2/B2/C2}$), 157.68 ($C^{A2/B2/C2}$), 152.76 ($C^{B6/C6}$), 152.74 ($C^{B6/C6}$), 152.52($C^{A6}$), 139.01($C^{B4/C4}$), 138.99($C^{B4/C4}$), 132.25($C^{A5}$), 130.53($C^{A4}$), 128.60 ($C^{B5/C5}$), 128.59 ($C^{B5/C5}$), 127.81 ($C^{A3}$), 125.24 ($C^{B3/C3}$), 87.73 ($C^{HiC\equiv C}$), 80.11($C^{iC\equiv CH}$).
**UV-Vis** ($CH_3CN$, $\lambda_{max}$ [nm], ($\varepsilon$ [$dm^3mol^{-1}cm^{-1}$])): 245 (53000), 290 (87000), 351 (8000), 458 (16000).
**Emission** ($CH_3CN$, $\lambda_{ex}$ = 245 nm), $\lambda_{em}$ [nm]: 640.
**ESI-MS** ($CH_3CN$, [m/z]): 309.0 ($[(\equiv\!-)_2bpyRubpy_2]^{2+}$, calc. 309.06),
**EA** [%], $C_{34}H_{24}F_{12}N_6P_2Ru$ *3/2$H_2O$, calc. C: 43.69, H: 2.91, N: 8.99; found C: 43.75, H: 2.86, N: 8.73.

**$[Ru(L4)(bpy)_2](PF_6)_2$ (C2)**

Formula: $C_{70}H_{52}F_{12}N_6P_2Ru$

Formula weight: 1824.08 [g/mol]

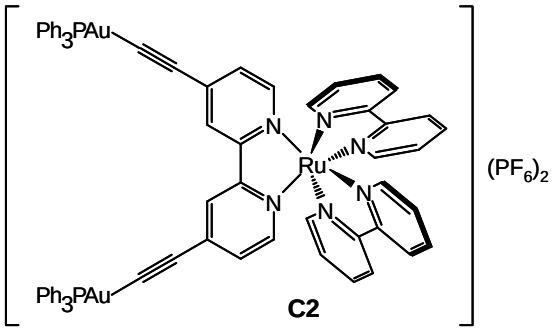

**C2**

$Ph_3PAuCl$ (44 mg, 88 µmol), and $[Ru((\equiv\!-)_2bpy)(bpy)_2](PF_6)_2$ (40 mg, 44 µmol) were dissolved in a mixture of $CH_2Cl_2$ (6 ml). DIPA (predistilled with NaOH, 2 ml) was added to

make the solution basic. The reaction mixture was stirred in the dark at room temperature for 12–16 h, after which the red solution was filtered and the solvent removed from the filtrate *in vacuo.* The red crude material, containing **C2**, was isolated, (73 mg, yield < 91 %, explained in text).

**$Zn(L4)_3(PF_6)_2$ (C3)**

Formula: $C_{151}H_{111}Au_6F_{12}N_6P_8Zn$

Formula weight: 3732.50 [g/mol]

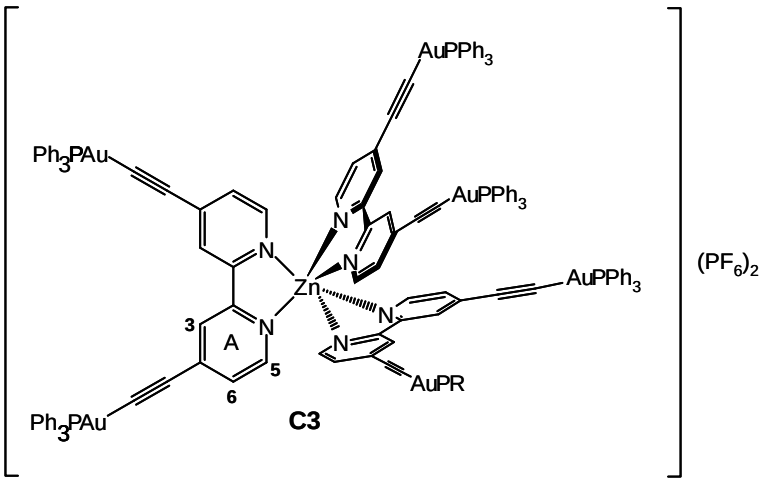


**L4 (**30 mg, 27 μmol) and $[Zn(H_2O)_6](PF_6)_2$ (5.5 mg, 12 μmol) were added to a mixture of 5 ml $CH_2Cl_2$ and 5 ml MeOH. The reaction mixture was stirred at room temperature in the dark for 12–16 h, after which the solution was filtered and the solvent removed from the filtrate *in vacuo*. A yellow-white crude solid, containing **C3,** was isolated (29 mg, yield < 85 %, explained in text).

**$^1$H NMR** (400 MHz, $CDCl_3$) δ [ppm]: 8.17 (s, 2H, $H^{A3}$), 7.77 (d, $J$ = 5.5 Hz, 2H, $H^{A6}$), 7.65 – 7.43 (m, 60H, $H^{Ph3P}$, $H^{A5}$).

**$^{31}$P NMR** (162 MHz, $CDCl_3$), δ [ppm]: 42.07.

**ESI-MS** ($CH_2Cl_2$, [m/z]): 720.4 ($[(Ph_3P)_2Au]^+$, calc. 721.15).

**$[Zn(L7)_2](PF_6)_2$ (C4)**

Formula: $C_{70}H_{50}Au_2F_{12}N_6P_4Zn$

Formula weight: 1786.39 [g/mol]

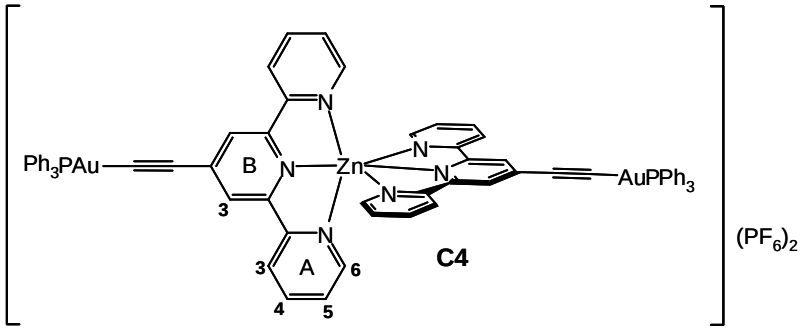


C4

The compound was obtained by using the same procedure as for **C3. L7** (40 mg, 56 μmol) and $[Zn(H_2O)_6](PF_6)_2$ (8.8 mg, 19 μmol). A yellow-white crude solid, containing **C4,** was isolated (45 mg, yield < 90 %, explained in text).

**$^1$H NMR** (400 MHz, $CD_3CN$), δ [ppm]:δ 8.65 (s, 2H, $H^{B3}$), 8.52 (d, *J* = 8.0 Hz, 2H, $H^{A3}$), 8.10 (t, *J* = 7.7 Hz, 2H, $H^{A4}$), 7.78 (d, *J* = 4.8 Hz, 2H, $H^{A6}$), 7.62 (m, 15H, $H^{Ph3P}$), 7.43 – 7.31 (m, 2H, $H^{A5}$).

**$^{31}$P NMR** (162 MHz, $CD_3CN$), δ [ppm]: 42.47.

**$[Zn_2(L8)_2](PF_6)_4$ (C5)**

Formula: $C_{120}H_{88}Au_2F_{24}N_{12}P_8Zn_2$

Formula weight: 3320.44 [g/mol]

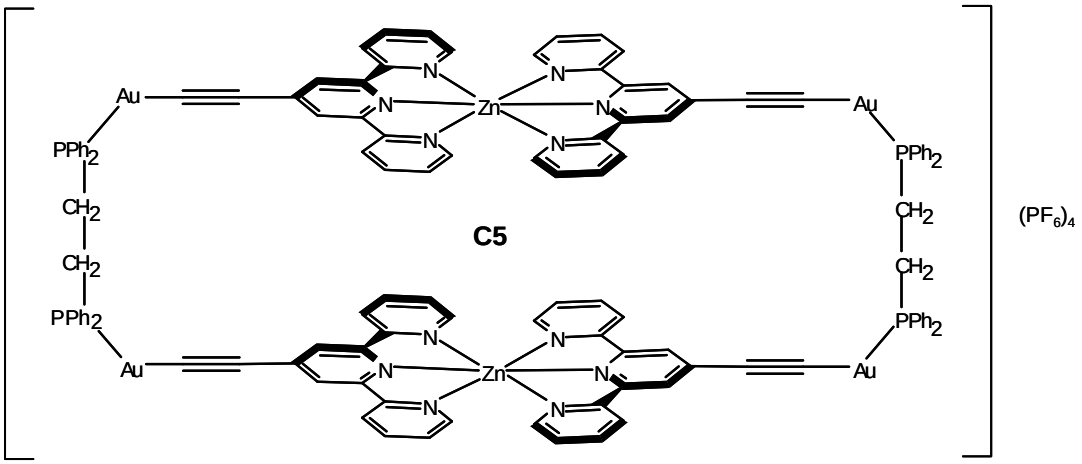


The compound was obtained by using the same procedure as for **C3. L8** (20 mg, 15 μmol) and $[Zn(H_2O)_6](PF_6)_2$ (10 mg, 22 μmol). A yellow-white crude solid, containing **C5,** was isolated (22 mg, yield < 88 % , explained in text).

**$[Fe(L4)]_3(BF_4)_2$ (C6)**

Formula: $C_{151}H_{111}Au_6B_2F_8FeN_6P_6$

Formula weight: 3606.63 [g/mol]

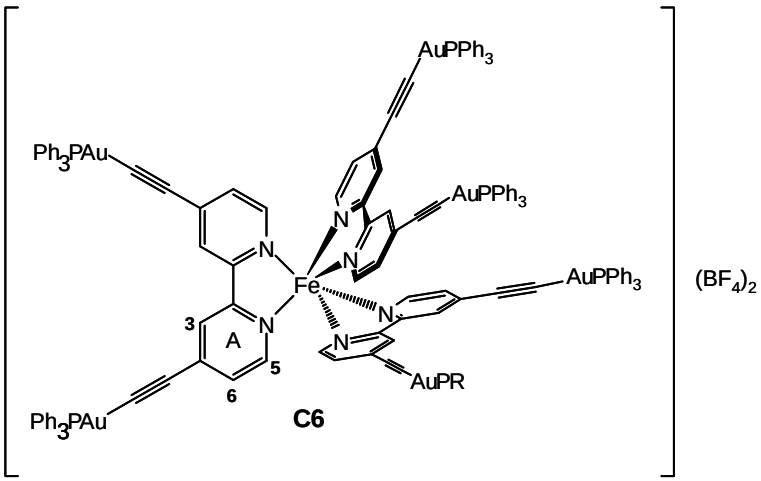

**L4 (**30 mg, 27 μmol) and $[Fe(H_2O)_6](BF_4)_2$ (4.0 mg, 12 μmol) were added to a mixture of 5 ml $CH_2Cl_2$ and 5 ml MeOH. The reaction mixture was stirred at room temperature in the dark for 12–16 h, after which the solution was filtered and the solvent removed from the filtrate *in vacuo.* A violet crude solid, containing **C6,** was isolated (30 mg, yield < 92 %, explained in text).

**$^1$H NMR** (400 MHz, $CDCl_3$), δ [ppm]: 8.16 (s, 2H, $H^{A3}$), 7.61 – 7.42 (m, 30 H, $H^{Ph3P}$), 7.37 (dd, *J* = 5.9, 1.4 Hz, 2H, $H^{A5}$), 7.20 (d, *J* = 6.0 Hz, 2H, $H^{A6}$).
**$^{31}$P NMR** (162 MHz, $CDCl_3$), δ [ppm]: 42.57.
**ESI-MS** ($CH_2Cl_2$, [m/z]): 720.4 ($[(Ph_3P)_2Au]^+$, calc. 721.15), 1121.8 ($[L4 + H]^+$, calc. 1121.2), 1479.1 (plus one charged, unassigned)

**$[Fe(L7)_2](BF_4)_2$ (C7)**

Formula: $C_{70}H_{50}Au_2B_2F_8FeN_6P_2$

Formula weight: 1660.52 [g/mol]

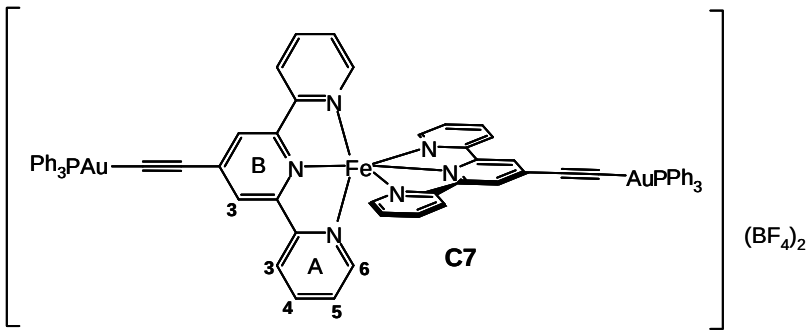


The compound was obtained by using the same procedure as for **C6. L7** (30 mg, 42 μmol) and $[Fe(H_2O)_6](BF_4)_2$ (8.1 mg, 24 μmol). A violet crude solid, containing **C7,** was isolated (28 mg, yield < 80 %, explained in text).

**$^1$H NMR** (400 MHz, $CD_3CN$), δ [ppm]: 8.88 (br, d, *J* = 52.0 Hz, 2H), 8.41 (br, 2H), 7.82 (br, 2H), 7.55 (br, d, *J* = 15.0 Hz, 28H, $H^{Ph3P}$), 7.38 (br, 2H), 7.04 (br, 4H).
**$^{31}$P NMR** (162 MHz, $CD_3CN$), δ [ppm]: 45.31.
**ESI-MS** ($CH_2Cl_2$, [m/z]): 720.4 ($[(Ph_3P)_2Au]^+$, calc. 721.15)

**$[Fe_2(L8)_2](BF_4)_4$ (C8)**

Formula: $C_{120}H_{88}Au_4B_4F_{16}Fe_2N_{12}P_4$

Formula weight: 3068.73 [g/mol]

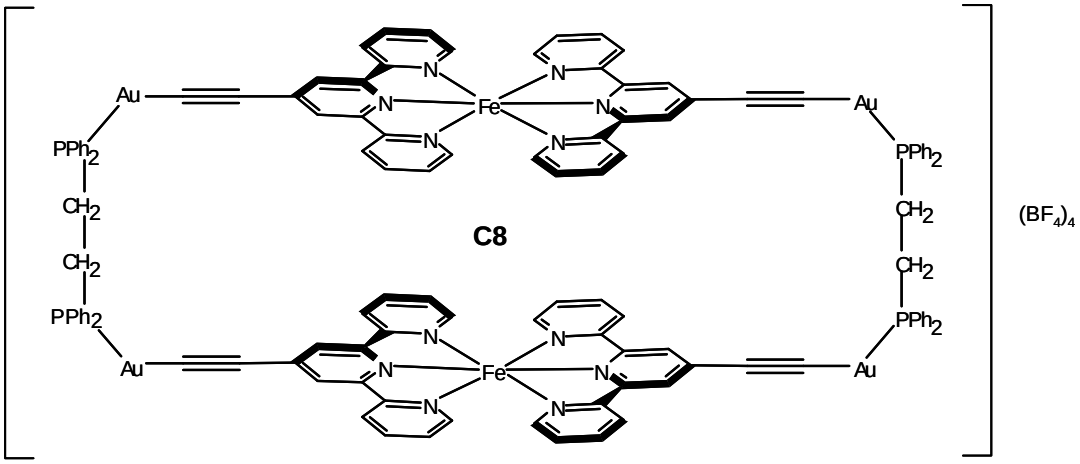


The compound was obtained by using the same procedure as for **C6. L8** (20 mg, 15 μmol) and $[Fe(H_2O)_6](BF_4)_2$ (7 mg, 20 μmol). A violet crude solid, containing **C8,** was isolated (23 mg, yield < 100 %, explained in text).

## 5.2. Ru(II) heteroleptic complexes with (≡–)$_2$bpy

Attempts to obtain a homoleptic Ru(II) complex in an overnight reflux reaction of $Ru(DMSO)_4Cl_2$ with **L4** did not produce $[Ru(\mathbf{L4})_3](PF_6)_2$, which was one of the aims of this thesis. An exchange of the labile DMSO by **L4** was not complete, which was indicated by the black-brown solution of the reaction mixture and confirmed by $^1$H NMR spectroscopy.

The reaction of **L4** with *cis*-$Ru(bpy)_2Cl_2$ followed by anion exchange to synthesise a heteroleptic complex $[Ru(\mathbf{L4})(bpy)_2](PF_6)_2$ at 160 °C in a microwave reactor led to the decomposition of **L4**, and metallic gold was observed on the walls of the microwave vial.

Reactions carried out in the microwave reactor and melting point measurements (where black particles appeared in the measurement capillary) led to the conclusion that compounds **L4** and **L7** exhibit low stability at temperatures higher than 100 °C and this conclusion can be extended also to the remaining $(R_3PAu{-}\equiv)_2$bpy and $R_3PAu{-}\equiv{-}$tpy ligands.

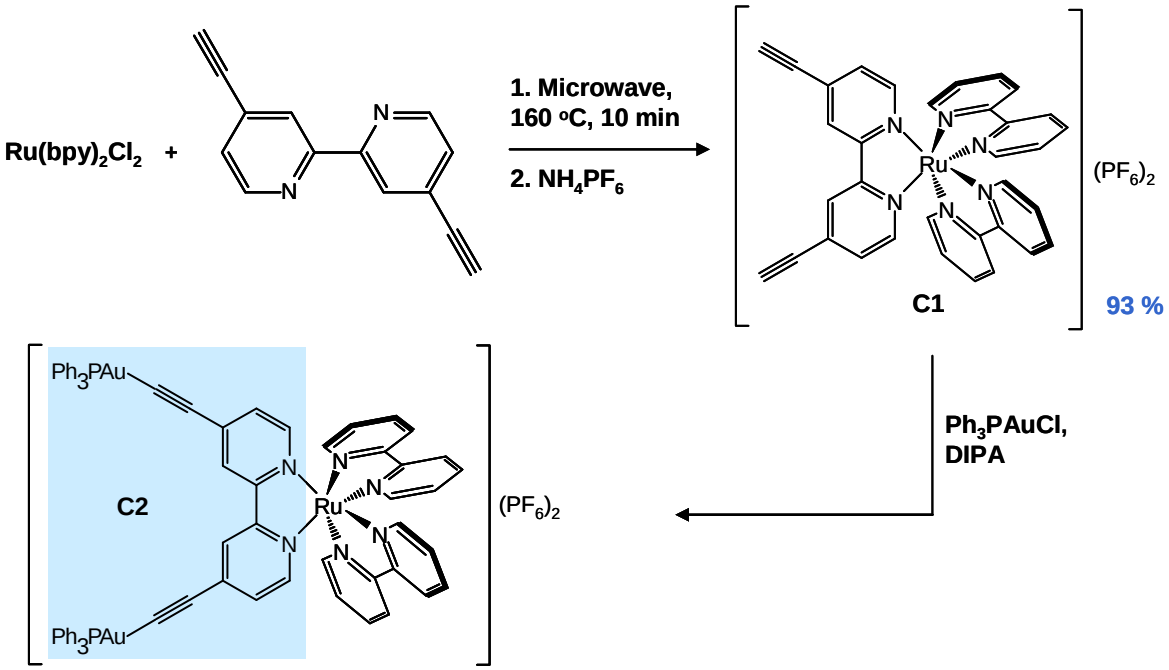


**Scheme 5.1** Synthetic strategy to prepare $[Ru(\mathbf{L4})(bpy)_2](PF_6)_2$.

With these results, finding a new strategy to obtain the Ru(II) complexes (**C2**, **Scheme 5.1**), in which the first step involves the reaction $Ru(bpy)_2Cl_2$ with (≡–)$_2$bpy and leads to **C1** and in the next, two alkynyl positions are decorated by phosphinegold(I) units, was necessary. An improvement of the yield to 93 % (from 84 %) in first step can be achieved by changing the solvent from MeOH to ethylene glycol and increasing the temperature to 160 °C.

Unfortunately, the second step did not lead to a pure product, but a characteristic red emission of the reaction mixture was observed after reaction. By studying the $^{1}H$ NMR spectrum, it was found that the reaction mixture still contained $Ph_3PAuCl$, $Et_3N$ and mono-phosphinegold(I)-substituted $[Ru((\equiv-)_2bpy)(bpy)_2]Cl2$. The separation of these remaining impurities from this mixture was not possible due to lower stability of the desired product in aqueous solution. Attempts to recrystallise the gold(I) decorated complex were not successful.

Carrying out this reaction with an inorganic base as $CH_3COONH_4$ instead of $Et_3N$, increasing the reaction time or direct reaction with $[Ru((\equiv-)_2bpy)(bpy)_2]Cl_2$ instead of $[Ru((\equiv-)_2bpy)(bpy)_2](PF_6)_2$ could possibly lead to a less impure final product.

Even though pure $[Ru(\mathbf{L4})(bpy)_2](PF_6)_2$ was not isolated, the characterisation of **C1** was completed, as **C1** is a new unreported Ru(II) complex and this is described is this section.

### 5.2.1 Characterisation of C1

Complex **C1** was obtained in a straightforward, synthetic route using a microwave reactor (section 5.1) and was fully characterised by NMR, UV-VIS, fluorescence spectroscopies, MS, EA and X-ray diffraction. These studies are presented below. Literature data [123], DEPT and 2-dimensional COSY, HMQC, HMBC and NOESY spectra were used to assign the peaks of the $^{1}H$ and $^{13}C$ NMR spectra.

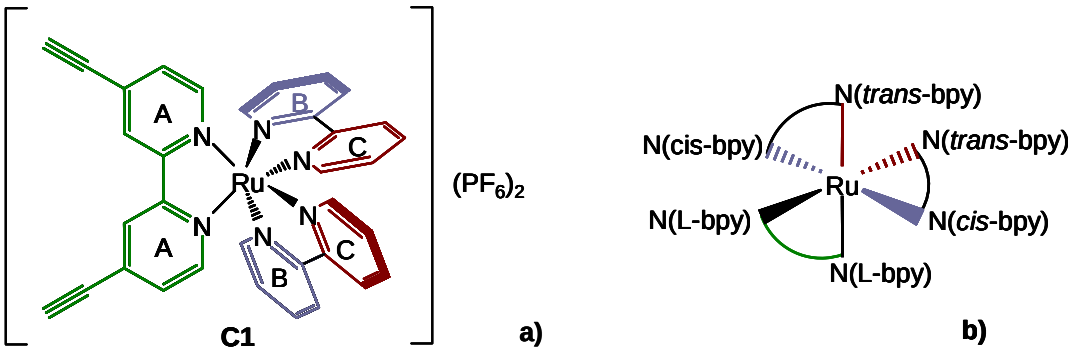


**Figure 5.2.** Diagram to show inequivalence of the two rings in each bpy ligand of $[Ru((\equiv-)_2bpy)(bpy)_2]^{2+}$: the light violet rings are *cis* to a ligand ring A and the dark red rings are *trans* to a ligand ring A.

Ru(II) complex cations $[Ru(L)(bpy)_2]^{2+}$, were L is a symmetrically disubstituted 2,2'-bipyridine ligand, exhibit symmetry $C_2$, differently than for $[Ru(bpy_3)]^{2+}$ complex ($D_3$). Decrease of symmetry for $[Ru(L)(bpy)_2]^{2+}$ causes that two pyridine ring of bpy-ligand to

become inequivalent, where for $[Ru(bpy)_3]^{2+}$ all pyridine rings are equivalent. In $[Ru(L)(bpy)_2]^{2+}$, two pyridine rings adopt the *cis*- (N(from L)-Ru-N(from bpy) bond angle about 90°, in light violet) and two other *trans*-position (N(from L)-Ru-N(from bpy) bond angle about 180°, in dark red) with regard to plane of L as shown in **Figure 5.2**. These symmetry changes are observed in the $^{1}H$ and $^{13}C$ NMR spectra of **C1**.

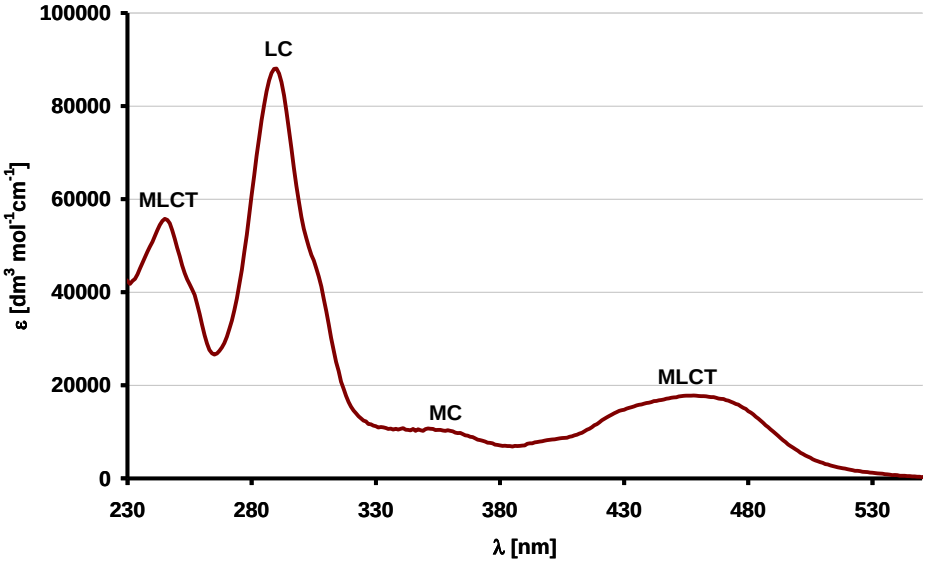


**Figure 5.1** Absorption spectrum of **C1** in $CH_3CN$ solution.

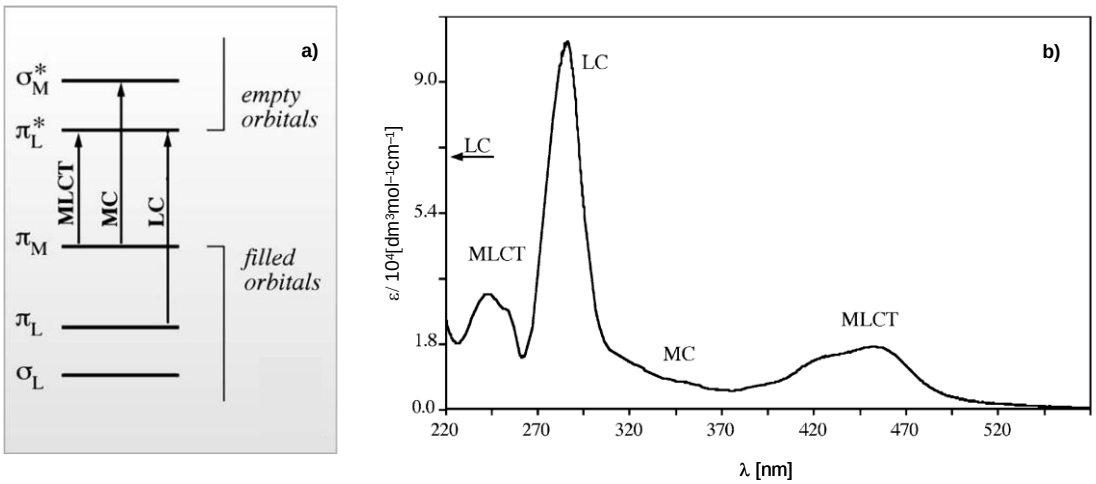


**Figure 5.2 a)**. Simplified molecular orbital diagram for Ru(II) polypyridine complexes in octahedral symmetry showing the three types of electronic transitions occurring at low energies, **b)** Electronic absorption spectrum of $[Ru(bpy)_3]^{2+}$ in alcoholic solution [124].

The electronic absorption spectroscopy studies of **C1** showed that bands 245, 290, 351 and 458 nm in the absorption spectrum (**Figure 5.1**) arise from MLCT (metal-to-ligand charge transfer, $\pi_M \rightarrow \pi_L^*$), LC (ligand-centered, $\pi_L \rightarrow \pi_L^*$), MC (metal-centered, $\pi_M \rightarrow \sigma_M^*$) and MLCT excited state transitions similar to $[Ru(bpy)_3]^{2+}$ (**Figure 5.2**).

The slight red-shift of all the absorption bands may be caused by the increase in π-electron conjugation (alkyl substituents) in **C1** compared to $[Ru(bpy)_3]^{2+}$ (240, 285, 322, 344, 450 nm in the case of $[Ru(bpy)_3]^{2+}$). However, the spectra were measured in different solvents and the solvent influence was not taken into the consideration [124].

**C1** exhibits an orange-red emission and the emission spectrum is shown in **Figure 5.3**. It reveals one intense band centred at 640 nm, which arises from the MLCT (metal-to-ligand charge transfer) transitions similar to that of $[Ru(bpy)_3]^{2+}$ [124].

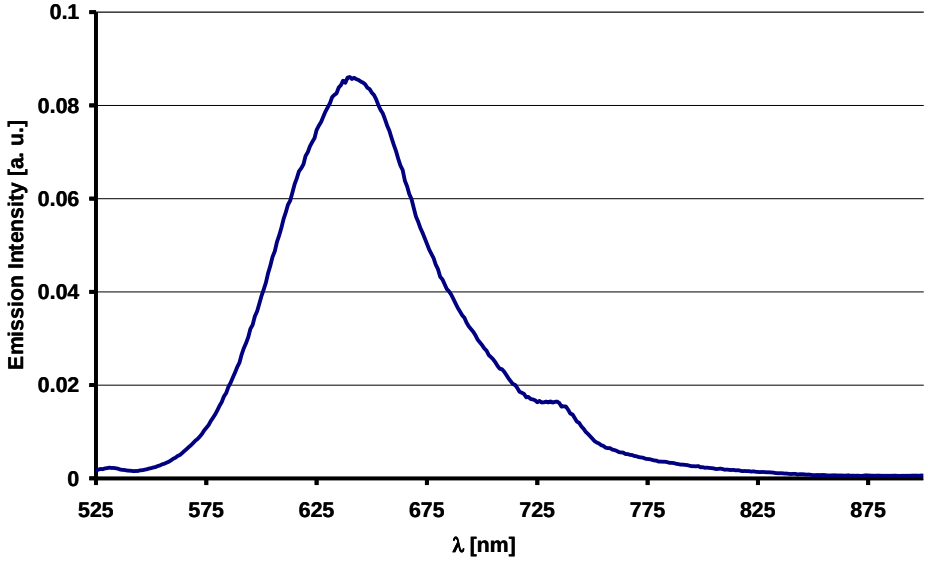


**Figure 5.3** Emission spectrum of **C1**. Excitation $\lambda_{ex}$ = 245 nm, slit 5/5, concentration of $CH_3CN$ solution is 2.2 * $10^{-6}$ mol/$dm^3$.

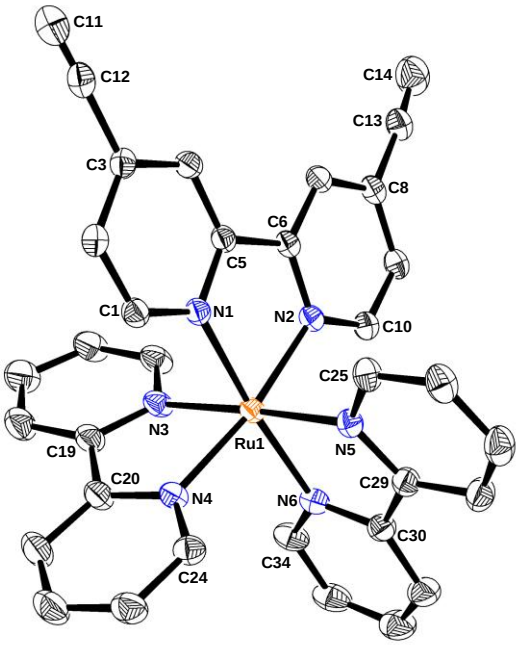


**Figure 5.4** Molecular structure of **C1** (ORTEP - probability ellipsoids – 20 %). All H atoms, counter-ions and solvent molecule were omitted for clarity.

X-ray diffraction studies determined the molecular structure of **C1** (**Figure 5.4**). It was solved in monoclinic space group $P2_1/c$ and the unit cell contains four molecules of **C1**. Half a molecule of solvent ($CH_3CN$) and two counter-ions of $PF_6^-$ (one disordered) are also present in the asymmetric unit. An X-ray quality single crystal of **C1** in the form of a red block was obtained by slow diffusion of $Et_2O$ into an $CH_3CN$ solution of **C1**. Selected bond lengths and bond angles of C1 are summarised in **Table 5.1**.

| Bond | Length [Å] | Bond angle | [°] |
|---|---|---|---|
| **Ru1–N1** | 2.054(3) | **N1–Ru1–N6** | 174.46(11) |
| **Ru1–N2** | 2.058(3) | **N2–Ru1–N4** | 170.92(12) |
| **Ru1–N3** | 2.057(3) | **N3–Ru1–N5** | 177.03(12) |
| **Ru1–N4** | 2.061(3) | **N1–Ru1–N4** | 94.52(11) |
| **Ru1–N5** | 2.060(3) | **N1–Ru1–N5** | 96.80(11) |
| **Ru1–N6** | 2.059(3) | **N2–Ru1–N3** | 94.36(12) |
| **C11–C12** | 0.971(7) | **N2–Ru1–N6** | 97.95(11) |
| **C13–C14** | 1.084(8) | **C3–C11–C12** | 177.1(5) |
| | | **C8–C13–C14** | 174.7(6) |

**Table 5.1** Selected bond lengths and bond angles of **C1**.

The crystal packing of **C1** is dominated by face to face π–π interactions (C2...C2$^{i}$ = 3.370(6) Å, C2…A2(centroid) distance of 3.95 Å, symmetry code, i: 1-x, 1-y, 1-z, and due to symmetry, the planes of the pyridine rings (in grey) are perfectly parallel, and C26...C32$^{ii}$ = 3.399(7) Å, C26…A4(centroid) distance of 3.92 Å, interplanar angles for the pyridine rings with A4(centroid)/A5(centroid) = 8°, symmetry code, i: x, 1/2-y, -1/2+z, marked in blue) and CH-π interactions (H33A$^{iii}$...C10 = 2.89 Å, C10...C33$^{iii}$ = 3.811(7) Å, H33A$^{iii}$…A3(centroid) distance of 3.25 Å, interplanar angles for the pyridine rings with A3(centroid)/A4(centroid) = 88°, symmetry code, i: x, 1/2-y, -1/2+z, marked in blue). These interactions are illustrated in **Figure 5.5**.

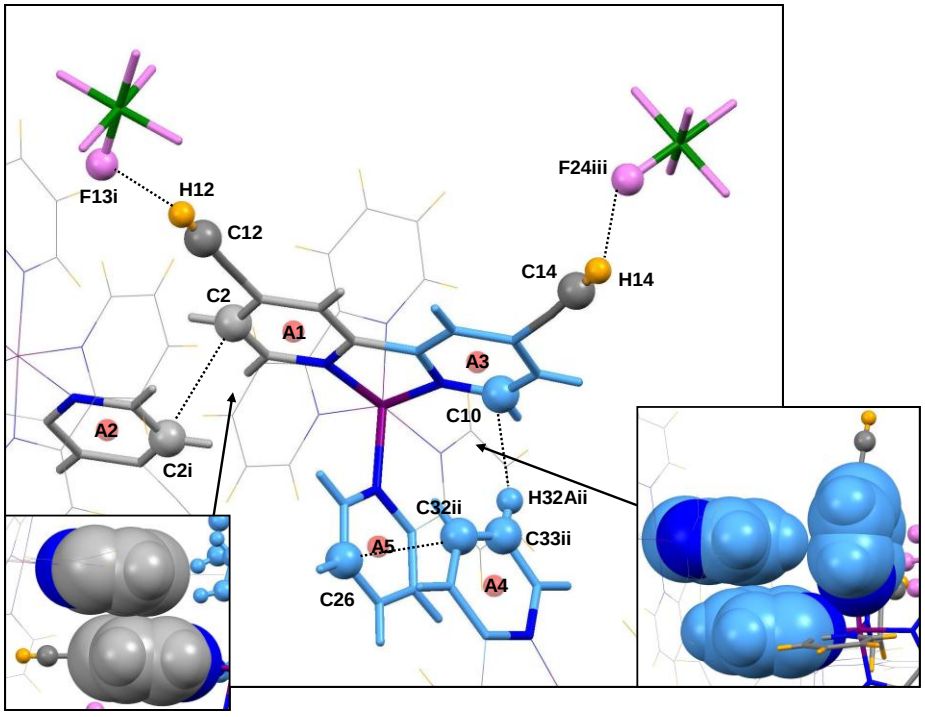


**Figure 5.5** C-H…π and face-to-face π–π interactions for **C1**. Weak C-H…F interactions with counter-ions are also marked. The symmetry codes are explained in the text.

Characteristic C-H…F weak interactions between two alkynyl units and $PF_6^-$ counter-ions (H12…F13$^{i}$ distance of 2.35 Å, C12…F13$^{i}$ = 3.25(1) Å, angle C12-H12…F13$^{i}$ = 166° and H14…F24$^{iii}$ distance of 2.48 Å, C14… F24$^{iii}$ = 3.339(8) Å, angle C14-H14… F24$^{iv}$ = 160°, symmetry codes i: 1-x, 1-y, 1-z, iii: -1+x, y, z) are also observed in the crystal packing of **C1** and they are marked in **Figure 5.5**.

## 5.3. Homoleptic complexes of $(R_3PAu{-}{\equiv})_2$bpy with Fe(II) and Zn(II)

The synthetic strategy illustrated in **Scheme 5.2** generates the homoleptic $[Zn(\mathbf{L4})_3](PF_6)_2$ (**C3**) as a white, luminescent crude product. Problems with solubility, purification and stability in solution of **C3** precluded the full characterisation of it.

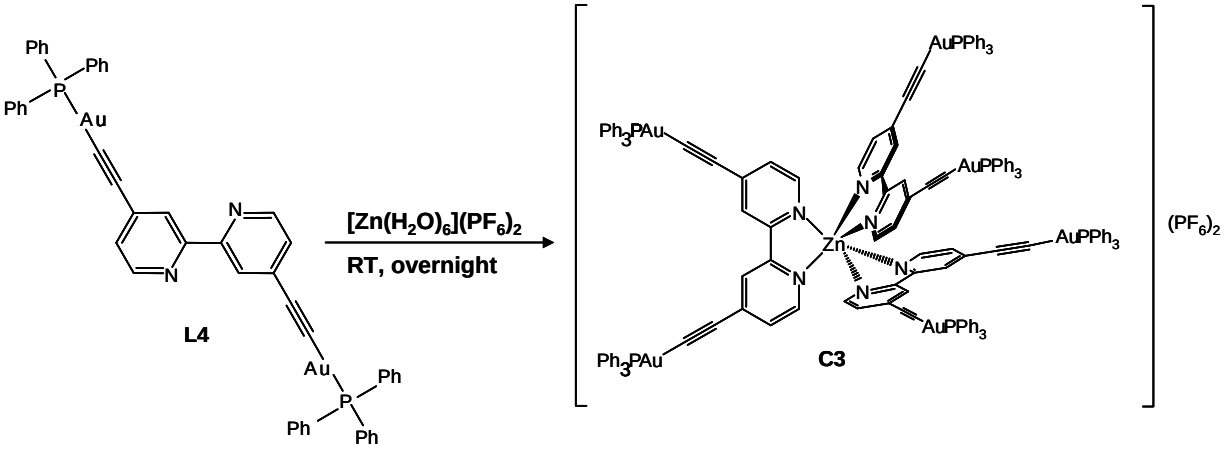


**Scheme 5.2.** Synthesis of $[Zn(\mathbf{L4})_3](PF_6)_2$.

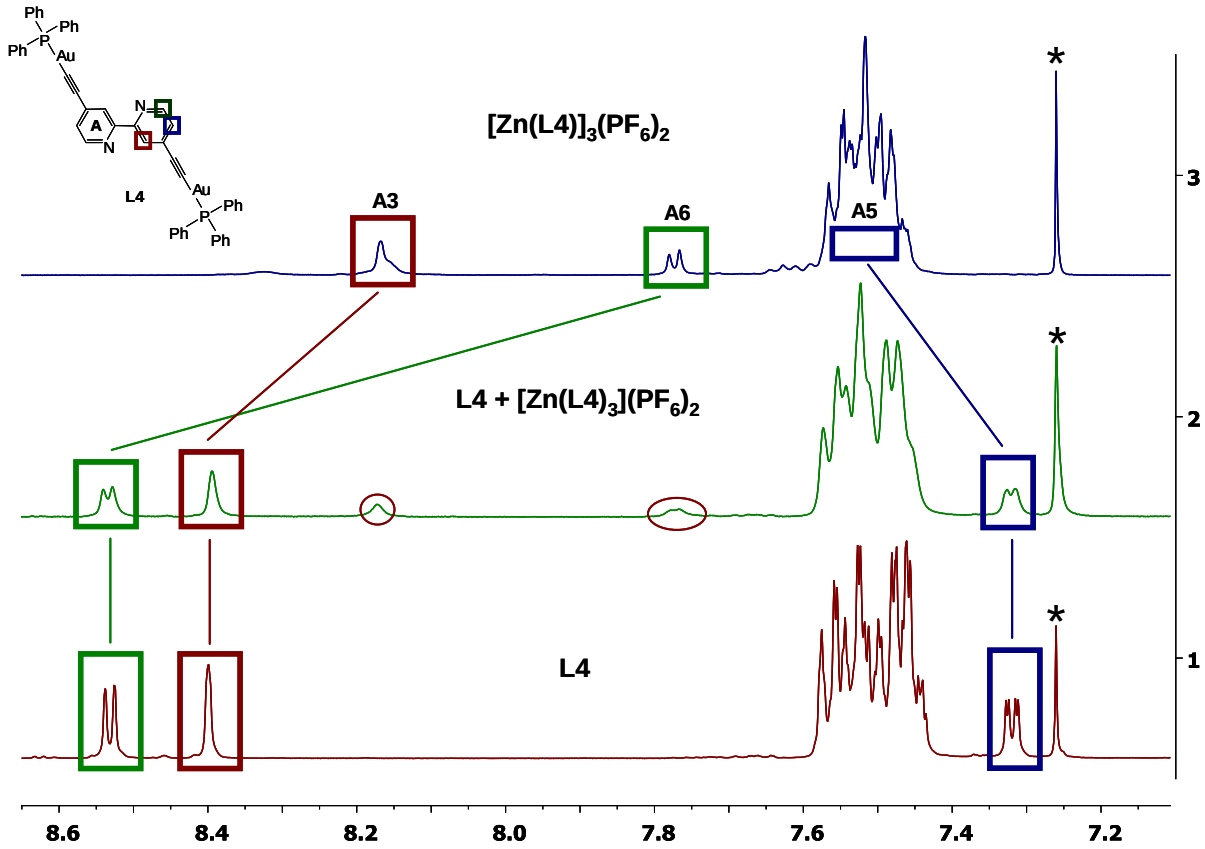


**Figure 5.6** $^1$H NMR spectra of **L4**, **L4** + $[Zn(\mathbf{L4})_3](PF_6)_2$ and $[Zn(\mathbf{L4})_3](PF_6)_2$ with peak assignment, δ [ppm]. The solvent peak (residual $CHCl_3$) is also visible (*).

The $^{1}$H NMR spectra presented in **Figure 5.6** indicate the formation of a metal complex with **L4**, observed *via* the shifting of peaks marked by green, red and dark blue boxes. A change in the conformation from *trans* to *cis* of **L4** in the case of the complex causes a large change in chemical shift for the signal $H^{A6}$ (marked in green), and smaller change in chemical shifts for the signals for $H^{A3}$ and $H^{A5}$.

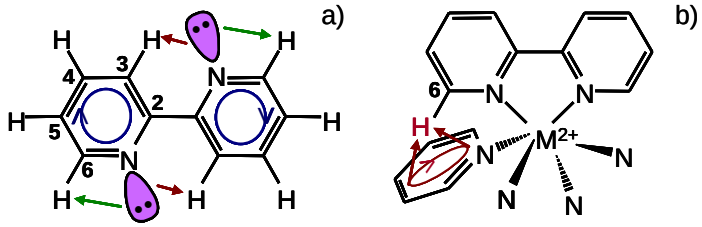


**Figure 5.7** The influence of the electron density for H atoms in free bpy ligand (a) and interactions of the π-electron current of a pyridine ring on $H^{A6}$ in the octahedral M(II)-complex (schematic diagram, b).

This characteristic change of chemical shifts in the $^{1}$H NMR spectra for free bpy-ligands and their transition metal(II) complexes for $H^{A6}$ peak are caused by the influence of electron density from the pyridine ring (complex) instead of the lone pair of electrons from the N-atom (ligand). **Figure 5.7** shows the influence of the lone pair of electrons for $H^{A3}$ and $H^{A6}$ in free 2,2'-bipyridine and shielding of $H^{A6}$ by π-elections from the pyridine ring of the adjacent in its metal complex, which explains the observed chemical shift changes of peaks $H^{A3}$ and $H^{A6}$ in the case of the free bpy-ligand and its complexes.

Complexation also narrowed the range of the $Ph_3P$-moiety multiplet in the $^{1}$H NMR spectrum (multiplet centred at 7.44 ppm).

The MALDI mass spectrum showed a dominant peak at m/z 720.4, which was assigned to $[(Ph_3P)_2Au]^+$. No other intense peaks were observed and no conclusion could be drawn about the formation of complex **C3**.

A colour change of the reaction mixture from colourless to violet (as in **Scheme 5.3)** occurred and this indicates complexation of Fe(II) to three bpy-moieties. Complex $[Fe(\mathbf{L4})_3](BF_4)_2$ (**C6**) was obtained in the way illustrated in **Scheme 5.3**. The signals in the $^{1}$H NMR spectrum were broadened, and this suggests the presence of Fe(III). Even a small amount of paramagnetic Fe(III) ($d^5$) in solution causes a broadening of the signals in the NMR spectrum. In addition, possible photodegradation of **L4** in solution and problems with purification **C6** limited the characterisation of this complex.

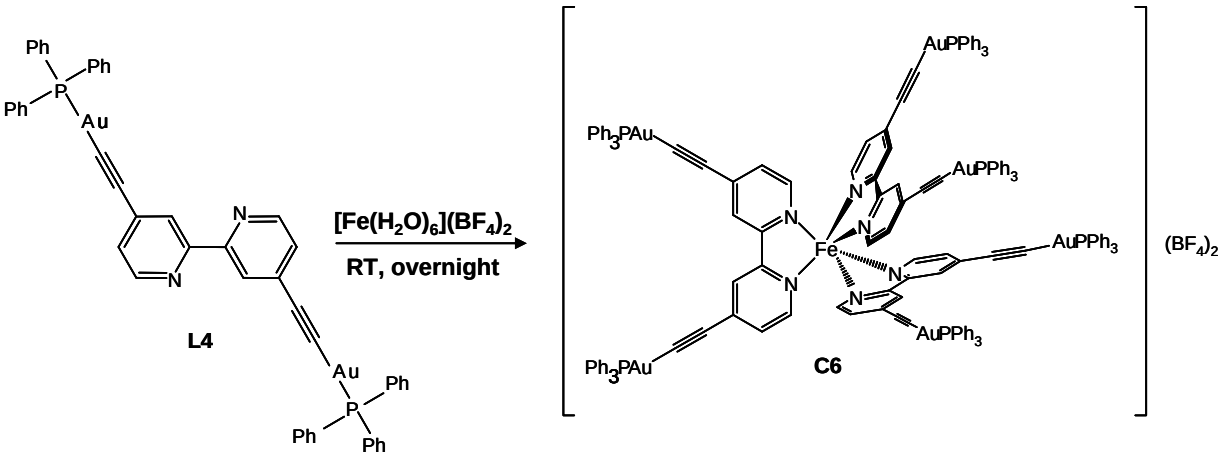


**Scheme 5.3** Synthesis of [Fe(**L4**)$_3$](BF$_4$)$_2$.

**Figure 5.8** illustrates the spectra of free ligand **L4** and its homoleptic Fe(II) complex. A chemical shift change of the $H^{A6}$, $H^{A3}$ and $H^{A5}$ signals marked in green, red, blue boxes, respectively, are indirect proof of the existence of **C6**.

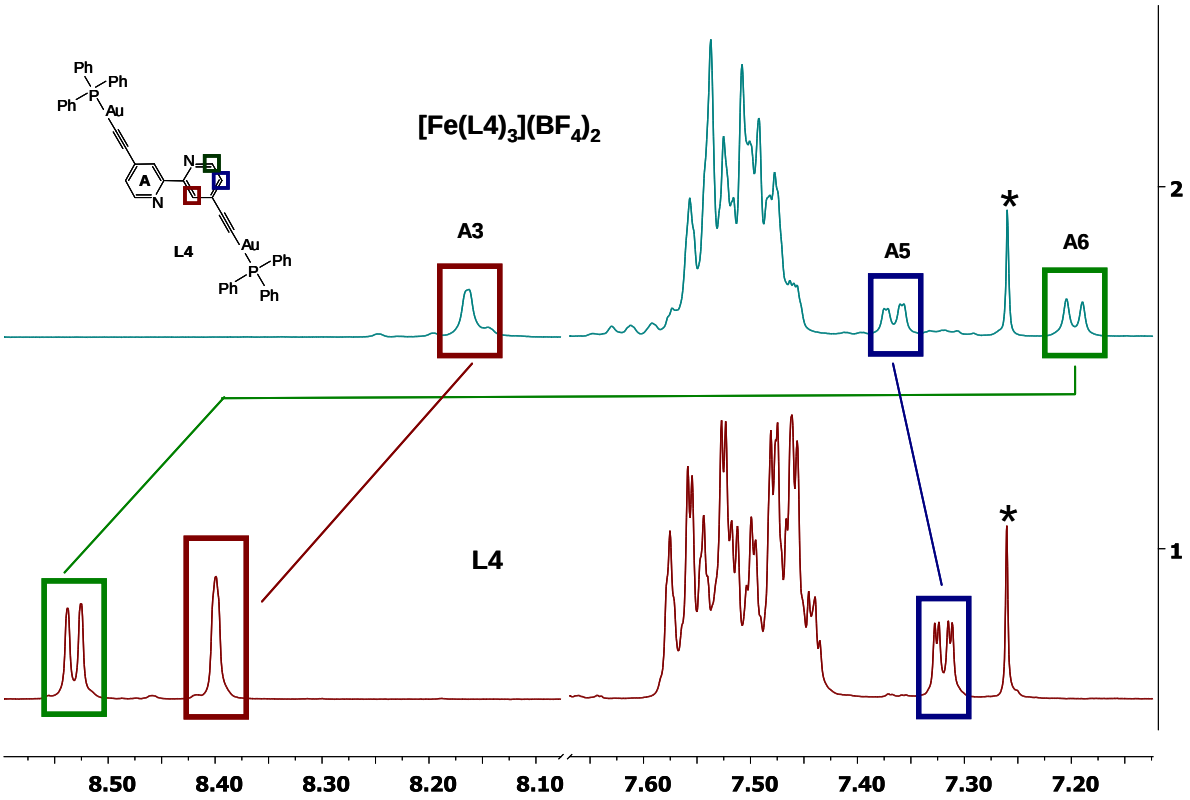


**Figure 5.8** $^1$H NMR spectra of **L4** and [Fe(**L4**)$_3$](BF$_4$)$_2$ with peak assignment, δ [ppm]. The solvent peak (residual $CHCl_3$) is also visible (*).

The dramatic change in the chemical shift of the $H^{A6}$ peaks in the direction of lower frequencies is caused by the interaction of this proton with π-electrons from the adjacent pyridine ring of another ligand and a decrease of the influence of a lone pair of electrons from N-atom. The lack of influence of lone pair electrons from the N-atom on $H^{A3}$ is also observed as shifting of the $H^{A3}$ signal in the direction of lower frequencies.

As in the case of the Zn-complex (**C6**), ESI mass spectra of the Fe(II)-complex showed a dominant peak at m/z 720.4 (assigned to $[(Ph_3P)_2Au]^+$) and also peaks at 1121.1 (assigned to [**L4** + H]$^+$) and 1479.1 (plus one charged, unassigned) but no conclusion could be drawn about the formation of complex (**C6**).

## 5.4 Homoleptic complexes of $R_3PAu{-}{\equiv}{-}$tpy Fe(II) and Zn(II)

Complexation of tpy-moieties to transition metals such as Zn(II) and Fe(II) causes a change in conformation of the ligand to the *cis*, *cis* positions, in which three N-atoms can coordinate to the metal-ion. These conformal changes can be followed by $^1$H NMR spectroscopy.

**Picture 5.1 C9** in UV light.

Reaction of **L7** with $[Zn(H_2O)_6](PF_6)_2$ (**Scheme 5.4**) leads to the formation of $[Zn(\mathbf{L7})_2](PF_6)_2$ (**C4**). The characteristic orange-yellow emission in the solid state and in solution of **C4** can be observed by excitation using a UV lamp light (see **picture 5.1**). With regards to the difficulties of purification of the reaction mixture of **C4** no quantitative fluorescence measurements were carried out.

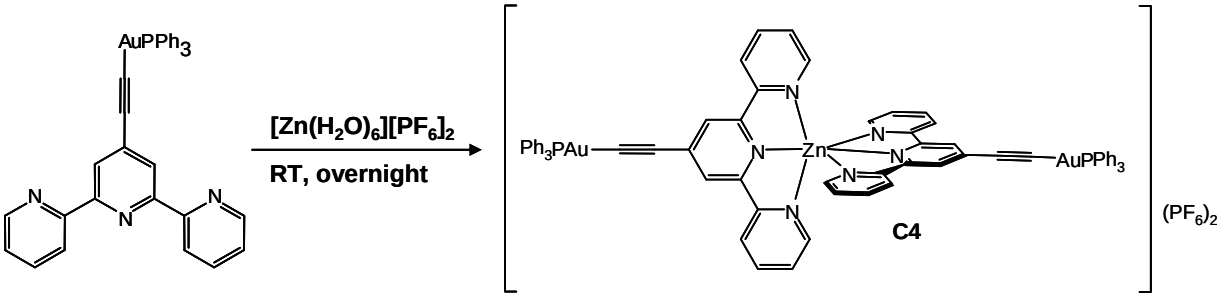


**Scheme 5.4.** Synthesis of $[Zn(\mathbf{L7})_2](PF_6)_2$ .

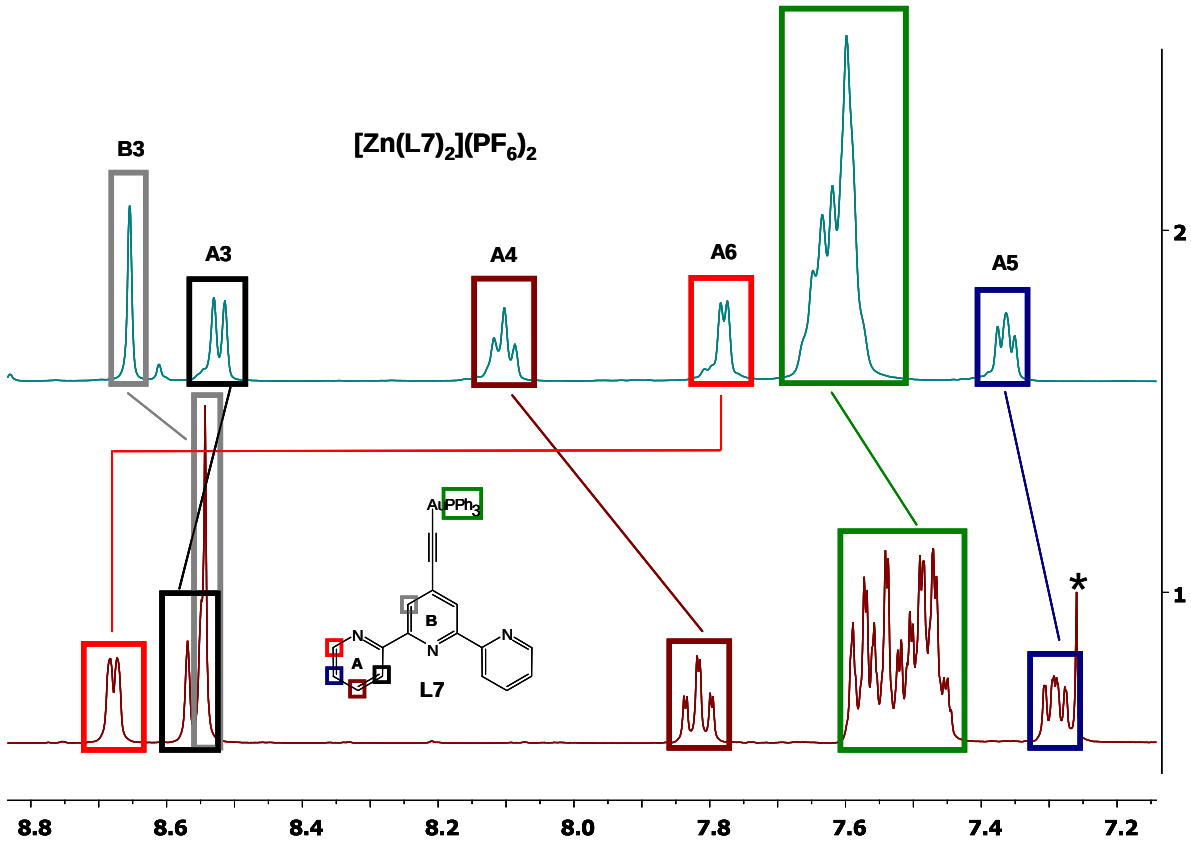


**Figure 5.9** $^{1}$H NMR spectra of **L7** and [Zn(**L7**)$_2$](PF$_6$)$_2$ with peak assignment, δ [ppm]. The solvent peak (residual $CHCl_3$) is also visible (*).

The $^{1}$H NMR spectra in **Figure 5.9** show the changes in chemical shift of the proton signals of **L7** after complexation with Zn(II), which are marked by coloured boxes and lines. Complexation influenced the positions of all protons in the spectrum. The signal for proton $H^{A6}$ (marked in red), which is located next to an N-atom, demonstrates the biggest change in chemical shift when comparing signals from free ligand and **C4**. This chemical shift in the direction of low frequencies is caused by, similar to bpy complexes, the location of $H^{A6}$ over the π-electrons of a pyridine ring from the second tpy ligand. The influence on the internal π-electrons in pyridine rings by change of conformation to the *cis*, *cis* tpy moieties and by coordination with metal-ion (drawing of π-electrons by metal-ion) shifts $H^{A4}$, $H^{A5}$ and $H^{A3}$ signals in direction of the high frequencies. A smaller influence of the lone pair electrons from N-atom for $H^{A3}$ upon coordination shifts the $H^{A3}$ signal in the direction lower frequencies. Also, the signals assigned to the $Ph_3P$-unit are significantly narrower in the Zn-complex **C4** and this is marked in green in **Figure 5.9**. The solvent effect, $CDCl_3$ for free ligand and $CD_3CN$ for complexes, was not considered in this analysis.

The crystallisation and further characterisation by MALDI-MS of **C4** was not successful due to low stability and the presence of impurities in solutions of this complex.

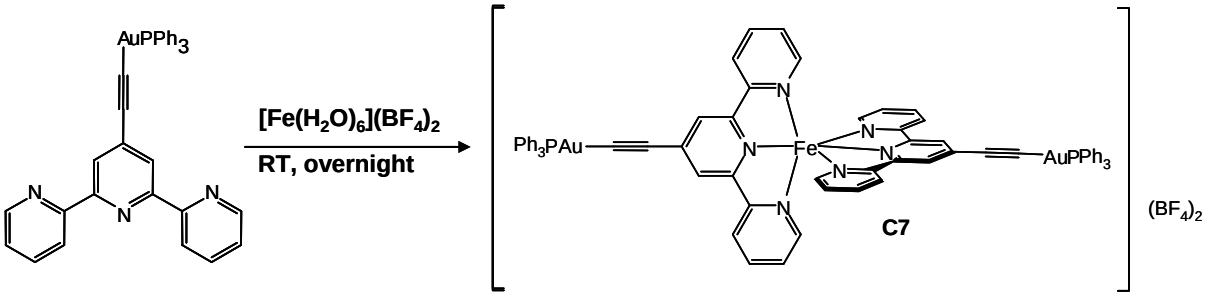


**Scheme 5.5** Synthesis of [Fe(**L7**)$_2$](BF$_4$)$_2$.

[Fe(**L7**)$_2$](BF$_4$)$_2$ (**C7**) was obtained as a crude, violet product and the procedure used is illustrated in **Scheme 5.5**.

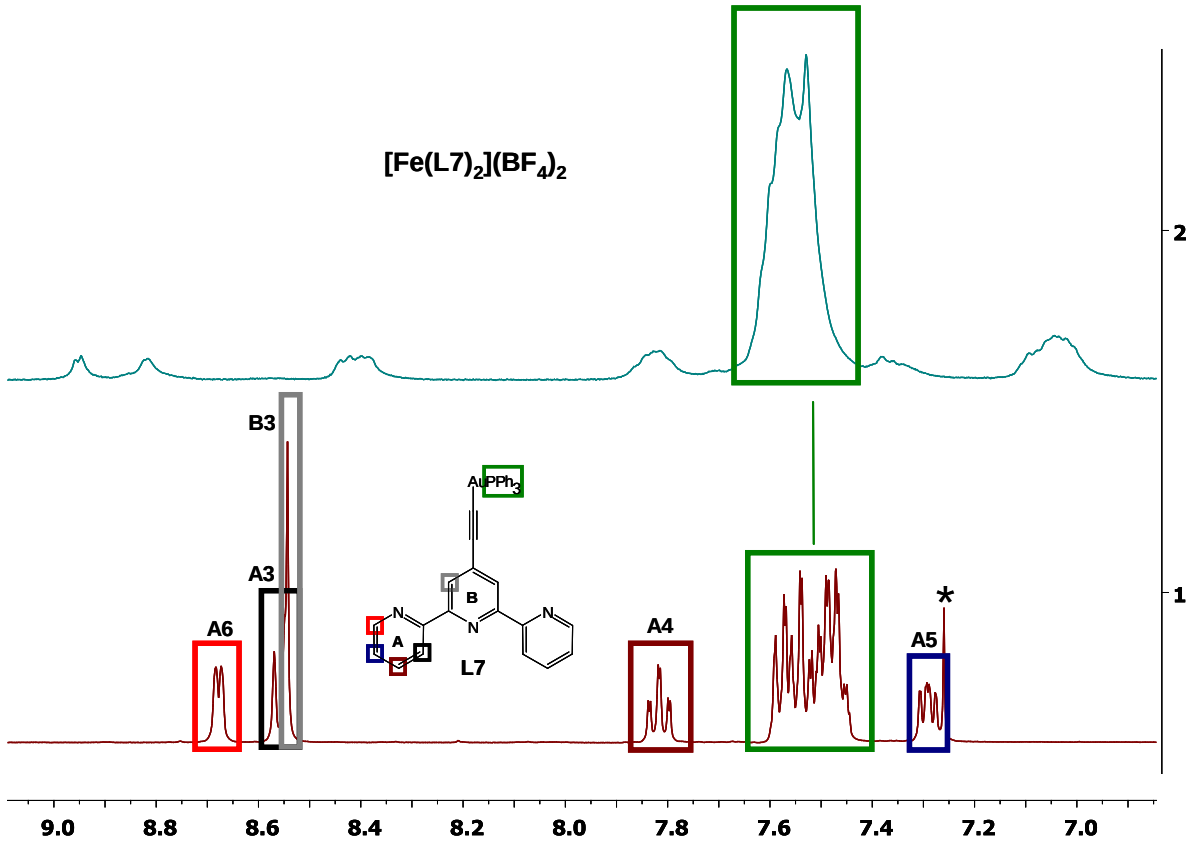


**Figure 5.10** $^1$H NMR spectra of **L7** with peak assignment and [Fe(**L7**)$_2$](BF$_4$)$_2$, δ [ppm]. The solvent peak (residual CHCl$_3$) is also visible (*).

The $^1$H NMR spectrum of **C7** with broadened signals suggests the presence of Fe(III) in solution (**Figure 5.10**). Changes in the chemical shifts of the signals after the complexation can be observed in the spectrum but they have not been assigned due to the poor resolution of the $^1$H NMR spectrum. The luminescent properties of ligand **L7** are quenched by the presence of the Fe-atom in the structure of complex **C7**.

The MALDI mass spectrum showed a dominant m/z peak at 720.4 (assigned to $[(Ph_3P)_2Au]^+$) which did not prove the formation of the complex (**C7**). Further characterisation of **C7** was not possible due to the low stability of this complex in solution.

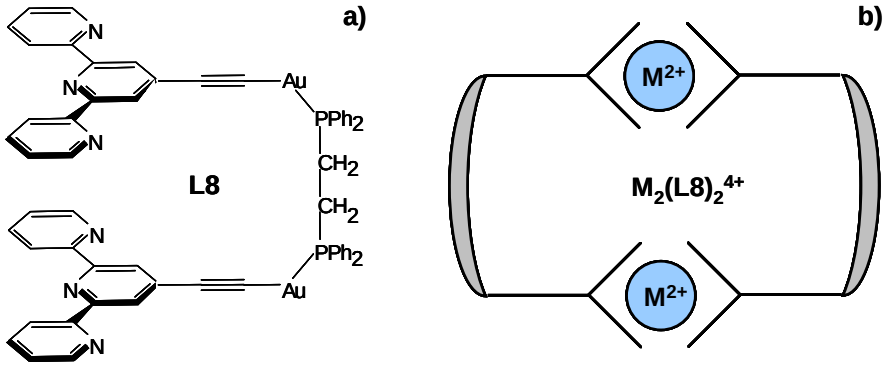


**Figure 5.11** Structure of **L8** (a) and schematic structure of possible Zn(II) and Fe(II) complexes with **L8** (b).

The molecular structure of **L8** (**Figure 5.12**) with a *cis*-conformation of tpy moieties forced by intramolecular aurophilic interactions is perfectly suitable to the formation of a macrocycle consisting of two **L8** and two metal-ions (**Figure 5.11**).

Preliminary experiments to obtain Fe(II) and Zn(II) complexes of **L8**, in the shape of structurally interesting metallo-macrocycle, illustrated in **Figure 5.11,** were carried out but were not completely successful. The conversion of the ligands to corresponding complexes was not complete, which was indicated by $^1$H NMR spectroscopy and the attempts of their purification led to the decomposition of the obtained complexes. Time constraints prevented this work from being extended.

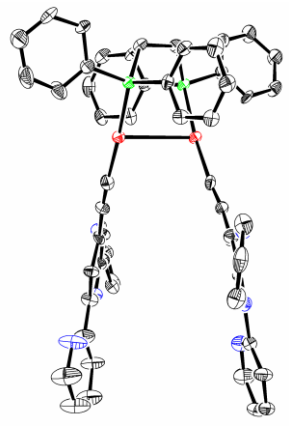

**Figure 5.12** Molecular structure of **L8**.

# 6. Conclusions and outlook

A family of luminescent bidentate and terdentate polypyridyl ligands, decorated with phosphinegold(I) units was obtained via a multi-step synthesis and was fully characterised by NMR, UV-Vis, fluorescence spectroscopies, MS, X-Ray and EA.

Six ligands **L1**-**L6** of $(R_3PAu{-}{\equiv})_2$bpy type were synthesized. Gold atoms in their molecular structures act as links between the π-conjugated aromatic system consisting of two aromatic connected pyridine (bpy) and alkynyl substituents in the 4,4' positions (triple bonds) and two trialkyl- or triarylphosphine units (**L1** contains two $Et_3P$ units, **L2** – *i*-$Pr_3P$, **L3** – *t*-$Bu_3P$, **L4** – $Ph_3P$, **L5** – *m*-$Tol_3P$, and **L6** – *p*-$Tol_3P$).

Four ligands **L7**, **L9**-**L11** of $PR_3Au{-}{\equiv}{-}$tpy type (**L7** contains a $Ph_3P$ unit, **L9**- *o*-$Tol_3P$, **L10**- $Et_3P$ and **L11** – *i*-$Pr_3P$) and **L8**, structurally the most interesting with a bridged phosphine unit, show similar gold linking. However, in this case the π-conjugated system consists of tpy which is substituted in the 4'-position by the alkynyl unit.

The presence of two Au-atoms in the molecular structures of **L1**-**L6** suggest the possibility of intra- and intermolecular aurophilic interactions in the solid state as well as in solution. It is worth mentioning that in general, aurophilic bonds (interactions) are classified as weak forces with a range of distances 2.8-3.5 Å (in section 1.2) [15].

X-ray diffraction studies of **L1**-**L9** revealed a high dependence between the steric requirements of the phosphine moiety as a steric hindrance and the existence of aurophilic interactions. For ligands with three aryl phosphine substituents (**L4**, **L5**, **L6**, **L7**, **L9**) no intra- (possible in compounds with at least two gold atoms in the molecule) and intermolecular Au-Au interactions were observed. The crystal packing in these compounds is dominated by π-π, C-H…π interactions, which may also influence the Au-Au distances.

Compounds **L1** and **L2** in the solid state, assemble in polymeric chains in which the links are connected by intermolecular aurophilic bonds of length 3.1239(14) Å and 3.3947(9) Å, respectively. Whereas, intramolecular Au-Au interactions (2.9470(8) Å) were found in the crystal structure of **L8**. In these compounds Au-Au interactions appear to control the overall crystal packing. **L8** does not exhibit intermolecular aurophilic interactions due to the steric hindrances of the phenyl rings from the phosphine units as for other ligands (**L4**, **L5**, **L6**, **L7**, **L9**) with aryl substituents on the phosphine moieties.

Electronic spectroscopic data for **L1**-**L6** show a change in the features of the spectra of these compounds with different phosphine substituents. The increase in band intensities in

the wavelength range of 230-260 nm for **L4**-**L6** with aryl substituents in the phosphine unit compared to **L1**-**L3** with alkyl substituents in the phosphine unit was observed. This may be caused by the additional π–π* transitions originating from the aromatic substituents in the case of **L4**-**L6**.

Additional bands in the absorption spectrum and much higher extinction coefficients for **L8** than for **L7** and **L9** can be explained studying the molecular structure of **L8**, as it consists of double the number of absorbing centres per molecule and also by the influence of intermolecular aurophilic interactions.

Fluorescence spectroscopic studies illustrated the luminescent properties of **L1**-**L9**. Changes in phosphine substituents from trialkyl to triaryl in the case of **L1**-**L6** do not influence the luminescent properties of solutions of these compounds. The fluorescence spectra of **L1**-**L6** exhibit very similar features and intensities of the observed bands. These emission bands may be assigned to mixed IL [π→π*(C≡CR)] and MLCT [d(Au)→π*(C≡C)] transitions with predominantly IL transitions and [σ(Au–P)→π*(C≡C)] transitions [101], [102], [106].

The fluorescence spectra of **L7**-**L9** exhibit very similar features but the emission intensity for **L8** is higher than for **L7**, **L8** due to double the number of the light emitting units in its molecular structure. The emission bands **L7**-**L9** may arise from the following transitions: mixed IL [π→π*(C≡CR)] and MLCT [d(Au)→π*(C≡C)] transitions with predominantly IL transitions, [σ(Au–P)→π*(C≡C)] transitions. In the case of **L8**, there may be a contribution from aurophilic interactions due to MMLCT [d(Au-Au)→π*(C≡C, alkynyl)]) transition [2], [3], [5].

A series of fluorescence measurements confirmed the decomposition of **L1**-**L9** and their light sensitive properties, which limits the use of these compounds as luminescent materials.

Zn(II)-complexes of **L4**, **L7** and **L8** were also synthesised. Difficulties with their purification and potential low stability suggest that further studies are needed to characterise these complexes and study their luminescent properties in detail. Similar conclusions can be drawn from the Fe(II)-complexes of **L4**, **L7** and **L8**. They do not exhibit luminescent properties and problems with oxidation of Fe(II) to Fe(III) occurred.

Specifically, finding a purification method for the Zn(II)- and Fe(II)-complexes with **L8** will lead to metallosupramolecular macrocycles with an interesting crystal structure, and luminescent properties in the case of Zn(II)-complex.

Potentially, gold(I) complexes of **L1**-**L9** (see chapter 1) can be used in antiviral and antitumor therapy with regards to their photoactive properties and their photodegradation. Studies to confirm these hypotheses are fully recommended.

# References


[1] M. Heindel, *Freemasonry and Catholicism*, Rosicrucian Fellowship, Oceanside , **1996**.

[2] A. M. Helmenstine, *Turning Lead into Gold: Is Alchemy Real?,* http://chemistry.about.com/cs/generalchemistry/a/aa050601a.htm, retrieved June 2011

[3] G. J. Higby, *Gold Bull.*, **1982**, *15*, 130.

[4] R. Bhattacharya, P. Mukherjee, *Adv. Drug Deliv. Rev.*, **2008**, *60*, 1289.

[5] L. C. Kennedy, L. R. Bickford, N. A. Lewinski, A. J. Coughlin, Y. Hu, E. S. Day, J. L. West, R. A. Drezek, *Small*, **2011**, *7*, 169.

[6] E. R. T. Tiekink, *Crit. Rev. Oncol. Hematol.*, **2002**, *42*, 225.

[7] P. Fonteh, D. Meyer, *Metallomics*, **2009**, *1*, 427.

[8] R. G. Pearson, *Science*, **1966**, *151*, 172.

[9] M. P. Melancon, W. Lu, Z. Yang, R. Zhang, Z. Cheng, A. M. Elliot, J. Stafford, T. Olson, J. Z. Zhang, C. Li, *Mol. Cancer Ther.*, **2008**, *7*, 1730.

[10] A. M. Gobin, M. H. Lee, N. J. Halas, W. D. James, R. A. Drezek, J. L. West, *Nano Lett.*, **2007**, *7*, 1929.

[11] S. Zhang, L. Yan, M. Altman, M. Laessle, H. Nugent, F. Frankel, D. A. Lauffenburger, G. M. Whitesides, A. Rich, *Biomaterials*, **1999**, *20*, 1213.

[12] M. Ozkan, *DDT*, **2004**, *9*, 1065.

[13] K. Y. Lee, Y. W. Lee, K. Kwon, J. Heo, J. Kim, S. W. Han, *Chem. Phys. Lett.*, **2008**, *453*, 77.

[14] A. Becue, A. Scoundrianos, C. Champod, P. Margot, *Forensic Science International*, **2008**, *179*, 39.

[15] H. Schmidbaur, A. Schier, *Chem. Soc. Rev.*, **2008**, *37*, 1931.

[16] S. Akerstrom, *Ark. Kemi*, **1959**, *14*, 387.

[17] H. Schmidbaur, *Acc. Chem. Res*., **1975**, *8*, 62.

[18] S. L. Lawton, W. J. Rohrbaugh, G. T. Kokotailo, *Inorg. Chem.*, **1972**, *11*, 2227.

[19] H. Schmidbaur, A. Wohlleben, F. E. Wagner, O. Orama, G. Huttner, *Chem. Ber*., **1977**, 1748.

[20] J. J. Guy, P. G. Jones, M. J. Mays, G. M. Sheldrick, *J. Chem. Soc., Dalton Trans.*, **1977**, 8.

[21] S. Esperas, *Acta Chem. Scand*., *Ser. A*, **1976**, *30*, 527.

[22] H. Schmidbaur, J. R. Mandl, A. Frank, G. Huttner, *Chem.Ber*., **1976**, *109*, 466.

[23] H. Schmidbaur, T. Pollok, R. Herr, F. E. Wagner, R. Bau, J. Riede, G. Muller, *Organometallics*, **1986**, *5*, 566.

[24] H. Schmidbaur, R. Herr, J. Riede, *Chem. Ber*., **1984**, *117*, 2322.

[25] H. Schmidbaur, W. Graf, G. Muller, *Angew. Chem. Int. Ed.*, **1988**, *27*, 417.

[26] R. Uson, A. Laguna, M. Laguna, M. C. Gimeno, *J. Chem. Soc., Dalton Trans*., **1989**, 1883.

[27] J. Vicente, M.-T. Chicote, I. Saura-Llamas, P. G. Jones, K. Meyer-Base, C. F. Erdbrugger, *Organometallics*, **1988**, *7*, 997.

[28] P. Lange, A. Schier, H. Schmidbaur, *Z. Naturforsch., B: Chem. Sci.*, **1997**, *52*, 769.

[29] C. Ganesamoorthy, M. S. Balakrishna, P. P. George. J. T. Mague, *Inorg. Chem*., **2007**, *46*, 848.

[30] N. V. Skorodumova, S. I. Simak, *Comput*. *Mater*. *Sci*., **2000**, *17*, 178.

[31] H. Schmidbaur, K. Dziwok, A. Grohmann, G. Muller, *Chem. Ber.*, **1989**, *122*, 893.

[32] K. Dziwok, H. Lachmann, G. Müller, H. Schmidbaur, *Chem. Ber.*, **1990**, *123*, 423.

[33] D. S. Eggleston, J. V. McArdle, G. E. Zuber, *J. Chem. Soc.,Dalton Trans*., **1987**, 677.

[34] A. Deak, T. Megyes, G. Tarkanyi, P. Kiraly, L. Biczok, G. Palinkas, P. J. Stang, *J. Am. Chem. Soc.*, **2006**, *128*, 12668.

[35] S. Gambarotta, C. Floriani, A. Chiesi-Villa, C. F. Guastini, *J. Chem. Soc., Chem. Commun.*, **1983**, 1304.

[36] E. M. Lane, T. W. Chapp, R. P. Hughes, D. S. Glueck, B. C. Feland, G. M. Bernard, R. E. Wasylishen, A. L. Rheingold, *Inorg. Chem*., **2010**, *49*, 3950.

[37] R. Narayanswamy, M. A. Young, E. Parkhurst, M. Ouellette, M. E. Kerr, D. M. Ho, R. C. Elder, A. E. Bruce, M. R. M. Bruce, *Inorg. Chem.*, **1993**, *32*, 2506.

[38] K. Angermaier, E. Zeller, H. Schmidbaur, *J. Organomet. Chem.*, **1994**, *472*, 371.

[39] T. Mathieson, A. Schier, H. Schmidbaur, *J. Chem. Soc., Dalton Trans.*, **2001**, 1196.

[40] Z. Assefa, M. A. Omary, B. G. McBurnett, A. A. Mohamed, H. H. Patterson, R. J. Staples and J. P. Fackler, *Inorg. Chem.*, **2002**, 41, 6274.

[41] U. Siemeling, D. Rother, C. Bruhn, H. Fink, T. Weidner, F. Trager, A. Rothenberger, D. Fenske, A. Priebe, J. Maurer, R. Winter, *J. Am. Chem. Soc*., **2005**, *127*, 1102.

[42] A. Kishimura, T. Yamashita, T. Aida, *J. Am. Chem. Soc.*, **2005**, *127*, 179.

[43] V. W.-W. Yam, T.-F. Lai, C-M. Che, *J. Chem.Soc., Dalton Trans.*, **1990**, 3747.

[44] V. W.-W. Yam, E. C.-C. Cheng, *Top. Curr. Chem.*, **2007**, *281*, 269.

[45] V. W.-W. Yam, K. K.-W. Lo, *Chem. Soc. Rev.*, **1999**, *28*, 323.

[46] V. W.-W. Yam, C.-K. Li, C.-L. Chan, *Angew. Chem. Int. Ed.*, **1998**, *37*, 2857.

[47] H. Scheffler, Y. You, I. Ott, *Polyhedron*, **2010**, *29*, 66.

[48] M.G. Lewis, S. DaFonseca, N. Chomont, A.T. Palamara, M. Tardugno, A. Mai, M. Collins, W.L. Wagner, J. Yalley-Ogunro, J. Greenhouse, B. Chirullo, S. Norelli, E. Garaci, A. Savarino, *AIDS*, **2011**, *25*, 1347.

[49] I. Ott, *Coord. Chem. Rev*., **2009**, *253*, 1670.

[50] J. C. Lima, L. Rodriguez, *Chem. Soc. Rev.*, **2011**, DOI: 10.1039/c1cs15123a.

[51] U.E. I. Horvath, J. M. McKenzie, S. Cronje, H. G. Raubenheimer, L. J. Barbour, *Chem. Commun.*, **2009**, *43*, 6598.

[52] S.–K. Yip, E. C.-C. Cheng, L.-H. Yuan, N. Zhu, V. W.-W. Yam, *Angew. Chem. Int. Ed.*, **2004**, *43*, 4954.

[53] J. Vicente, M.-T. Chicote, M. M. Alvarez-Falcon, D. Bautista, *Organometallics*, **2004,** *23*, 5707.

[54] W. Lu, N. Zhu, C.-M. Che, *J. Organomet. Chem.*, **2003**, *670*, 11.

[55] M. Ferrer, A. Gutierrez, L. Rodriguez, O. Rossell, J. C. Lima, M. Font-Bardia, X. Solans, *Eur. J. Inorg. Chem.*, **2008**, 2899.

[56] L. A. Summers in A. R. Katritzky "*Advances in Heterocyclic Chemistry*", Academic Academic Press, New York, **1984**, *35*, 281.

[57] A. Almenningen, O. Bastiansen, S. Gundersen, S. Samdal, *Acta Chem. Scand*. **1989**, *43*, 932 Press, New York, **1984**, *35*, 281.

[58] C. Qi, X. Sun, C. Lu, J. Yang, Y. Du, H. Wu, X.-M. Zhang, *J. Organomet. Chem*., **2009**, *694*, 2912.

[59] L. Shaoa, Y. Dub, M. Zenga, X. Lia,W. Shena, S. Zuoa, Y. Lua, X.-M. Zhanga, C. Qia, *Appl. Organometal. Chem.*, **2010**, *24*, 421.

[60] E. C. Constable, *Adv. Inorg. Chem. Radiochem*., **1989**, *34*, 1.

[61] G. Atkinson, J. E. Bauman, *Inorg. Chem*., **1962**, *1*, 900.

[61] K. Yamasaki and M. Yasuda, *J. Am. Chem. Soc*., **1956**, *78*, 1324.

[63] F. Gao, H. Chao, F. Zhou, L.-C. Xu, K.-C. Zheng, L.-N. Ji, *Helv. Chim. Acta*, **2007**, *90*, 37.

[64] H. Xu, Q.-Q. Zhu, J. Lu, X.-J. Chen, J. Xiao, Z.-G. Liu, S-P. Chen, M.-L. Tong, L.-N. Ji , Y. Liang, *Inorg. Chem. Comm*., **2010**, *13*, 711.

[65] A. Guale *"Tuning Fluorescence Properties of 2,2'-Bipyridine Using Metal Cations"* M.S. Thesis, Addis Ababa University, **2010**.

[66] F. Trecourt, B. Gervais, M. Mallet, G. Queguiner, *J. Org. Chem.*, **1996**, *61*, 1673.

[67] F. Trecourt, B. Gervais, O. Mongin, C. Le Gal, F. Mongin, G. Queguiner, *J. Org. Chem.*, **1998**, *63*, 2892.

[68] H.-X. Ju, Y.-K. Ye, J.-H. Zhao,Y.-L. Zhu, *Anal. Biochem*., **2003**, *313*, 255.

[69] V. Vo, Z. G. Kabuloglu-Karayusuf, S. W. Carper, B. L. Bennett, C. Evilia, *Bioorg. Med. Chem*., **2010**, *18*, 1163.

[70] K. E. Elwell, "*Novel cisplating analogs: Synthesis, characterization and cytotoxicity in breast cells"*, M.S. Thesis, University of Nevada, Las Vegas, **2005**.

[71] M. A. Soldatov, I. Ascone, A. Congiu-Castellano, L. Messori, M. A. Cinellu, A. Balerna, A V Soldatov, G. E. Yalovega, *J. Phys.: Conf. Ser.* 190, **2009**, 1.

[72] J.-M. Lehn, A. Rigault, J. Siegel, J. Harrowfield, B. Chevriert, D. Moras, *Proc. Natl. Acad. Sci. USA*, **1987**, *84*, 2565.

[73] W. Zarges, J. Hall, J.-M. Lehn, C. Bolm, *Helv. Chim. Acta*, **1991**, *74*, 1843.

[74] D. P. Funeriu, J.-M. Lehn, K. M. Fromm, D. Fenske, *Chem. Eur. J.*, **2002**, *6*, 2103.

[75] A. Hagfeldtt, M. Gratzel, *Chem, Rev.*, **1995**, *95*, 49.

[76] E. C. Constable, A. Hernandez-Redondo, C. E. Housecroft, M. Neuburger, S. Schaffner, *Dalton Trans.*, **2009**, 6634.

[77] B. O'Regan, M. Gratzel, *Nature*, **1991**, *353*, 737.

[78] H.-B. Xu, L.-Y. Zhang, J. Ni, H.-Y. Chao, Z.-N. Chen, *Inorg. Chem.*, **2008**, *47*, 10744.

[79] J. Vicente, J. Gil-Rubio, N. Barquero, P. G. Jones, D. Bautista, *Organometallics*, **2008**, *27*, 646.

[80] E. C. Constable, *Adv. Inorg. Chem. Radiochem*., **1986**, *30*, 69.

[81] M. Kimura, T. Shiba, T. Muto, K. Hanabusa and H. Shirai, *Chem. Commun.*, **2000**, 11.

[82] G. R. Newkome, K. S. Yoo, S.-H. Hwang, C. N. Moorefield, *Tetrahedron*, **2003**, *59* 3955.

[83] M. Chiper, A.Winter, R. Hoogenboom, D. A. M. Egbe, D. Wouters, S.Hoeppener, C.-A. Fustin, J.-F. Gohy, U. S. Schubert, *Macromolecules*, **2008**, *41*, 8823.

[84] M. Kimura, M. Sano, T. Muto, K. Hanabusa, H. Shirai, N. Kobayashi, *Macromolecules* **1999**, *32*, 7951.

[85] M. Chiper, M. A. R. Meier, D. Wouters, S. Hoeppener, C.-A. Fustin, J.-F. Gohy, U. S. Schubert, *Macromolecules*, **2008**, *41*, 2771.

[86] P. J. Carter, C.-C. Cheng, H. H. Thorp, *J. Am. Chem. Soc.*, **1998,** *120*, 632.

[87] H. Inoue, T. Furukawa, M. Shimizu, T. Tamura, M. Matsui, E. Ohtsuka, *Chem. Commun.*, **1999**, 45.

[88] S. Ito, S. M. Zakeeruddin, R. Humphry-Baker, P. Liska, R. Charvet, P. Comte, M. K. Nazeeruddin, P. Pechy, M. Takata, H. Miura, S. Uchida, M. Gratzel, *Adv. Mater.*, **2006**, *18*, 1202.

[89] P. Bonhote, J. E. Moser, N. Vlachopoulos, L. Walder, S. M. Zakeeruddin, R. Humphry-Baker, P. Pechy, M. Gratzel, *Chem. Commun.*, **1996,** 1163.

[90] J. Vicente, M. T. Chicote, *Coord. Chem. Rev,*. **1999**, *195*, 1143.

[91] E. C. Constable , C. E. Housecroft , M. Neuburger, S. Schaffner, E. J. Shardlow, *Polyhedron*, **2008**, 27, 65.

[92] X.-L. Li, K.-J. Zhang, J.-J. Li, X.-X. Cheng, Z.-N. Chen, *Eur. J. Inorg. Chem.*, **2010**, 3449.

[93] R. Ziessel, J. Suffert, M. T. Youinou, *J. Org. Chem.*, **1996**, *61*, 6535.

[94] M. Bardaji, A. Laguna, J. Vicente, P. G. Jones, *Inorg. Chem.*, **2001**, *40*, 2675.

[95] R. A. Jones, B. D. Roney, W. H. F. Sasse, K. O. Wade, *J. Chem. Soc. (B),* **1967**, 106.

[96] H. Arzoumanian, R. Bakhtchadjian, G. Agrifoglio, R. Atencio, A. Briceno, *Trans. Met. Chem.*, **2006**, *31*, 681.

[97] P. Kavanagh, D. Leech, *Tetrahedon Lett.*, **2004**, *45*, 121.

[98] G. Marker, F. H. Case *J. Am. Chem. Soc.*, **1958**, *80*, 2745.

[99] C.-H. Chui, R. S.-M. Wong, R. Gambari, G. Y.-M. Cheng, M. C.-W. Yuen, K.-W. Chan, S.-W. Tong, F.-Y. Lau, P. B.-S. Lai, K.-H. Lam, C.-L. Ho, C.-W. Kan, K. S.-Y. Leung, W.-Y. Wong, *Bioorg. Med. Chem.*, **2009**, *17*, 7872.

[100] J. J. Liu, P. Galettis, A. Farr, L. Maharaj, H. Samarasinha, A. C. McGechan, B. C. Baguley, R. J. Bowen, S. J. Berners-Price, M. J. McKeage, *J. Inorg. Biochem.*, **2008**, *102*, 303.

[101] K.-L. Cheung, S.-K. Yip, V. W.-W. Yam, *J. Organomet. Chem.*, **2004**, *689*, 4451.

[102] V. W.-W. Yam, K.-L. Cheung, S.-K. Yip, K.-K. Cheung, *J. Organomet. Chem.*, **2003**, *681*, 196.

[103] V. W-W. Yam, *Acc. Chem. Res.*, **2002,** *35*, 555.

[104] Y. Yamamoto, M. Shiotsuka, S. Onaka, *J. Organomet. Chem.*, **2004**, *689*, 2905.

[105] W.-Y. Wong, L. Liu, S.-Y. Poon, K.-H. Choi, K.-W. Cheah, J.-X. Shi, *Macromolecules*, **2004**, *37*, 4496.

[106] X.-X. Lu, C.-K. Li, E. C.-C. Cheng, N. Zhu, V. W.-W. Yam, *Inorg. Chem.*, **2004**, 43, 2225.

[107] L. Lettko, J. S. Wood, M. D. Rausch, *Inorg. Chim. Acta*, **2000**, *308*, 37.

[108] M. Ferrer, M. Mounir, L. Rodriguez, O. Rossell, S. Coco, P. Gomez-Sal, A. Martin,

*J. Organomet. Chem.*, **2005**, *690*, 2200.

[109] C. P. McArdle, M. C. Jennings, J. J. Vittal, R. J. Puddephatt, *Chem. Eur. J.*, **2001**, *7*, 3572.

[110] A. Kolb, P. Bissiier, H.Schmidbaur, *Inorg. Chem.*, **1993**, *32*, 5132.

[111] Y. Bao, C. Zhong, D. M. Vu, J. P. Temirov, R. B. Dyer, J. S. Martinez**,** *J. Phys. Chem. C,* **2007,** *111*, 12194.

[112] C. A. Tolman, *Chem. Rev.*, **1977**, *77*, 313.

[113] R. Meijboom, A. Muller, A. Roodt, *Acta Cryst. E*, **2006**, *62*, 1603.

[114] C. Janiak, *Dalton Trans*., **2000**, *21*, 3885.

[115] G. Desiraju, T. Steiner, *The Weak Hydrogen Bond*, Oxford University Press, Oxford, **1999**.

[116] G. A. Jeffrey, *An Introduction to Hydrogen Bonding*, Oxford University Press, Oxford, **1997**.

[117] G. Desiraju, *Acc. Chem. Res.*, **2002**, *35*, 565.

[118] E. C. Constable, M. D. Ward, *J. Chem. Soc., Dalton Trans.*, **1990**, 1405.

[119] K. T. Potts, D. Konwar, *J. Org. Chem.*, **1991**, *56*, 4815.

[120] V. Grosshenny, F. M. Romero, R. Ziessel, *J. Org. Chem.*, **1997**, *62*, 1491.

[121] R. Uson, A. Laguna, M. Laguna, *Inorg. Synth.*, **1989**, *26*, 85.

[122] A. Immirzi, A. Musco, *Inorg. Chim. Acta*, **1977**, *25*, L41.

[123] E. C. Constable, C. E. Housecroft, M. Neuburger, P. J. Rosel, S. Schaffner, J. A. Zampese, *Chem. Eur. J.*, **2009**, *15*, 11746.

[124] S. Campagna, F. Puntoriero, F. Nastasi, G. Bergamini, V. Balzani, *Top Curr. Chem.*, **2007**, *280*, 117.

# **Appendix A** - Crystal data and structure refinement of **L1**- **L9** and **C1**.

| **Compound** | **L1** |
|---|---|
| **Empirical Formula** | $C_{26}H_{36}Au_2N_2P_2$ |
| **Formula Weight [g/mol]** | 832.47 |
| **Temperature [K]** | 123 |
| **Crystal System** | monoclinic |
| **Space Group** | $P2_1/c$ |
| **Unit cell dimensions:** | |
| **a [Å]** | 14.5466(4) |
| **b [Å]** | 14.5575(4) |
| **c [Å]** | 12.9700(4) |
| **α [°]** | 90.00 |
| **β [°]** | 96.508(2) |
| **γ [°]** | 90.00 |
| **Volume [Å$^3$]** | 2728.86(14) |
| **Z** | 4 |
| **Crystal Description** | colourless needle |
| **Crystal Size [mm]** | 0.08 x 0.09 x 0.27 |
| **Density [g*cm$^{-3}$]** | 2.026 |
| **Absorption Coefficient [mm$^{-1}$]** | 10.874 |
| **θ range for data collection [°]** | 1.986 to 39.091 |
| **Reflections collected** | 119769 |
| **Independent reflections** | 15011 |
| **R(int)** | 0.047 |
| **Completeness to θ [° (%)]** | 36.745 (99.8 ) |
| **Parameters** | 289 |
| **Goodness of fit** | 1.0559 |
| **wR2** | 0.0198 |
| **Final R1 [I>3σ(I)]** | 0.0187 |

**Table 1** Crystal data and structure refinement for **L1**.

| Compound | L2 |
|---|---|
| **Empirical Formula** | $C_{32}H_{48}Au_2N_2P_2$ |
| **Formula Weight [g/mol]** | 916.6 |
| **Temperature [K]** | 173 |
| **Crystal System** | orthorhombic |
| **Space Group** | *P*bc*n* |
| **Unit cell dimensions:** | |
| **a [Å]** | 13.571(3) |
| **b [Å]** | 15.069(3) |
| **c [Å]** | 16.309(3) |
| **α [°]** | 90.00 |
| **β [°]** | 90.00 |
| **γ [°]** | 90.00 |
| **Volume [Å$^3$]** | 3335.3(12) |
| **Z** | 4 |
| **Crystal Description** | colourless plate |
| **Crystal Size [mm]** | 0.01 x 0.12 x 0.40 |
| **Density [g*cm$^{-3}$]** | 1.825 |
| **Absorption Coefficient [mm$^{-1}$]** | 8.906 |
| **θ range for data collection [°]** | 2.37 to 25.50 |
| **Reflections collected** | 102936 |
| **Independent reflections** | 3104 |
| **R(int)** | 0.2171 |
| **Completeness to θ [° (%)]** | 25.50 (99.5) |
| **Parameters** | 199 |
| **Goodness of fit** | 1.243 |
| **wR2** | 0.179 |
| **Final R1 [I>2σ(I)]** | 0.0677 |

**Table 2** Crystal data and structure refinement for **L2**.

| Compound | L3 |
|---|---|
| **Empirical Formula** | $C_{38}H_{60}Au_2N_2P_2$ |
| **Formula Weight [g/mol]** | 1000.76 |
| **Temperature [K]** | 223 |
| **Crystal System** | monoclinic |
| **Space Group** | $P2_1/c$ |
| **Unit cell dimensions:** | |
| **a [Å]** | 11.043(2) |
| **b [Å]** | 13.805(3) |
| **c [Å]** | 13.396(3) |
| **α [°]** | 90.00 |
| **β [°]** | 104.87(3) |
| **γ [°]** | 90.00 |
| **Volume [Å$^3$]** | 1973.8(8) |
| **Z** | 2 |
| **Crystal Description** | colourless needle |
| **Crystal Size [mm]** | 0.05 x 0.06 x 0.55 |
| **Density [g*cm$^{-3}$]** | 1.684 |
| **Absorption Coefficient [mm$^{-1}$]** | 7.532 |
| **θ range for data collection [°]** | 2.60 to 29.99 |
| **Reflections collected** | 88540 |
| **Independent reflections** | 5716 |
| **R(int)** | 0.0931 |
| **Completeness to θ [° (%)]** | 29.99 (99.2) |
| **Parameters** | 208 |
| **Goodness of fit** | 1.251 |
| **wR2** | 0.0669 |
| **Final R1 [I>2σ(I)]** | 0.0264 |

**Table 3** Crystal data and structure refinement for **L3**.

| Compound | L4 |
|---|---|
| **Empirical Formula** | $C_{104}H_{82}Au_4N_4O_1P_4$ |
| **Formula Weight [g/mol]** | 2315.58 |
| **Temperature [K]** | 173 |
| **Crystal System** | triclinic |
| **Space Group** | $P\bar{1}$ |
| **Unit cell dimensions:** | |
| **a [Å]** | 9.5773(7) |
| **b [Å]** | 13.0208(10) |
| **c [Å]** | 17.9136(13) |
| **α [°]** | 104.278(4) |
| **β [°]** | 90.541(4) |
| **γ [°]** | 92.994(4) |
| **Volume [Å$^3$]** | 2161.4(3) |
| **Z** | 1 |
| **Crystal Description** | colourless needle |
| **Crystal Size [mm]** | 0.06 x 0.07 x 0.23 |
| **Density [g*cm$^{-3}$]** | 1.779 |
| **Absorption Coefficient [mm$^{-1}$]** | 6.894 |
| **θ range for data collection [°]** | 2.13 to 32.965 |
| **Reflections collected** | 46687 |
| **Independent reflections** | 14247 |
| **R(int)** | 0.061 |
| **Completeness to θ [° (%)]** | 25.053 (94.2) |
| **Parameters** | 550 |
| **Goodness of fit** | 1.0433 |
| **wR2** | 0.0393 |
| **Final R1 [I>3σ(I)]** | 0.0474 |

**Table 4** Crystal data and structure refinement for **L4**.

| Compound | L5 |
|---|---|
| **Empirical Formula** | $C_{56}H_{48}Au_2N_2P_2$ |
| **Formula Weight [g/mol]** | 1204.84 |
| **Temperature [K]** | 173 |
| **Crystal System** | monoclinic |
| **Space Group** | $P2_1/n$ |
| **Unit cell dimensions:** | |
| **a [Å]** | 13.557(3) |
| **b [Å]** | 9.3786(19) |
| **c [Å]** | 18.139(4) |
| **α [°]** | 90.00 |
| **β [°]** | 94.63(3) |
| **γ [°]** | 90.00 |
| **Volume [Å$^3$]** | 2298.8(9) |
| **Z** | 2 |
| **Crystal Description** | colourless block |
| **Crystal Size [mm]** | 0.02 x 0.06 x 0.21 |
| **Density [g*cm$^{-3}$]** | 1.741 |
| **Absorption Coefficient [mm$^{-1}$]** | 6.485 |
| **θ range for data collection [°]** | 2.64 to 25.04 |
| **Reflections collected** | 29377 |
| **Independent reflections** | 4061 |
| **R(int)** | 0.1816 |
| **Completeness to θ [° (%)]** | 25.04 (99.9) |
| **Parameters** | 283 |
| **Goodness of fit** | 1.287 |
| **wR2** | 0.1641 |
| **Final R1 [I>2σ(I)]** | 0.0651 |

**Table 5** Crystal data and structure refinement for **L5**.

| Compound | L6 |
|---|---|
| **Empirical Formula** | $C_{60}H_{58}Au_2N_2O_1P_2$ |
| **Formula Weight [g/mol]** | 1279.01 |
| **Temperature [K]** | 123 |
| **Crystal System** | triclinic |
| **Space Group** | $P\bar{1}$ |
| **Unit cell dimensions:** | |
| **a [Å]** | 9.2636(7) |
| **b [Å]** | 10.3025(7) |
| **c [Å]** | 13.6906(10) |
| **α [°]** | 94.056(4) |
| **β [°]** | 97.201(4) |
| **γ [°]** | 92.625(4) |
| **Volume [Å$^3$]** | 1291.08(16) |
| **Z** | 1 |
| **Crystal Description** | colourless prism |
| **Crystal Size [mm]** | 0.08 x 0.13 x 0.32 |
| **Density [g*cm$^{-3}$]** | 1.645 |
| **Absorption Coefficient [mm$^{-1}$]** | 5.779 |
| **θ range for data collection [°]** | 1.985 to 41.530 |
| **Reflections collected** | 84925 |
| **Independent reflections** | 17279 |
| **R(int)** | 0.032 |
| **Completeness to θ [° (%)]** | 33.639 (99.5) |
| **Parameters** | 322 |
| **Goodness of fit** | 1.0467 |
| **wR2** | 0.0224 |
| **Final R1 [I>2σ(I)]** | 0.0236 |

**Table 6** Crystal data and structure refinement for **L6**.

| Compound | L7 |
|---|---|
| **Empirical Formula** | $C_{35}H_{25}AuN_3P$ |
| **Formula Weight [g/mol]** | 715.52 |
| **Temperature [K]** | 173 |
| **Crystal System** | monoclinic |
| **Space Group** | $P2_1/c$ |
| **Unit cell dimensions:** | |
| **a [Å]** | 19.658(4) |
| **b [Å]** | 8.3726(17) |
| **c [Å]** | 17.853(4) |
| **α [°]** | 90.00 |
| **β [°]** | 105.39(3) |
| **γ [°]** | 90.00 |
| **Volume [Å$^3$]** | 2833.0(10) |
| **Z** | 4 |
| **Crystal Description** | colourless plate |
| **Crystal Size [mm]** | 0.03 x 0.20 x 0.25 |
| **Density [g*cm$^{-3}$]** | 1.678 |
| **Absorption Coefficient [mm$^{-1}$]** | 5.279 |
| **θ range for data collection [°]** | 2.71 to 26.50 |
| **Reflections collected** | 44788 |
| **Independent reflections** | 5835 |
| **R(int)** | 0.0979 |
| **Completeness to θ [° (%)]** | 26.50 (99.2) |
| **Parameters** | 361 |
| **Goodness of fit** | 1.144 |
| **wR2** | 0.1087 |
| **Final R1 [I>2σ(I)]** | 0.0426 |

**Table 7** Crystal data and structure refinement for **L7**.

| Compound | L8 |
|---|---|
| **Empirical Formula** | $C_{121}H_{89}Au_4Cl_3N_{12}P_4$ |
| **Formula Weight [g/mol]** | 2729.16 |
| **Temperature [K]** | 173 |
| **Crystal System** | monoclinic |
| **Space Group** | *Pc* |
| **Unit cell dimensions:** | |
| **a [Å]** | 10.389(2) |
| **b [Å]** | 17.482(4) |
| **c [Å]** | 15.652(3) |
| **α [°]** | 90.00 |
| **β [°]** | 98.53(3) |
| **γ [°]** | 90.00 |
| **Volume [Å$^3$]** | 2811.2(10) |
| **Z** | 1 |
| **Crystal Description** | colourless needle |
| **Crystal Size [mm]** | 0.01 x 0.03 x 0.30 |
| **Density [g*cm$^{-3}$]** | 1.612 |
| **Absorption Coefficient [mm$^{-1}$]** | 5.384 |
| **θ range for data collection [°]** | 2.50 to 26.00 |
| **Reflections collected** | 49946 |
| **Independent reflections** | 10592 |
| **R(int)** | 0.1933 |
| **Completeness to θ [° (%)]** | 26.00 (99.9) |
| **Parameters** | 669 |
| **Goodness of fit** | 1.075 |
| **wR2** | 0.1525 |
| **Final R1 [I>2σ(I)]** | 0.0625 |

**Table 8** Crystal data and structure refinement for **L8**.

| Compound | L9 |
|---|---|
| **Empirical Formula** | $C_{38}H_{31}AuN_3P$ |
| **Formula Weight [g/mol]** | 757.60 |
| **Temperature [K]** | 173 |
| **Crystal System** | triclinic |
| **Space Group** | $P\bar{1}$ |
| **Unit cell dimensions:** | |
| **a [Å]** | 9.2574(9) |
| **b [Å]** | 17.6618(19) |
| **c [Å]** | 19.504(2) |
| **α [°]** | 107.172(8) |
| **β [°]** | 96.023(8) |
| **γ [°]** | 91.372(8) |
| **Volume [Å$^3$]** | 3024.9(5) |
| **Z** | 4 |
| **Crystal Description** | colourless plate |
| **Crystal Size [mm]** | 0.02 x 0.30 x 0.40 |
| **Density [g*cm$^{-3}$]** | 1.664 |
| **Absorption Coefficient [mm$^{-1}$]** | 4.949 |
| **θ range for data collection [°]** | 2.42 to 26.50 |
| **Reflections collected** | 67142 |
| **Independent reflections** | 12533 |
| **R(int)** | 0.1018 |
| **Completeness to θ [° (%)]** | 26.5 (99.9) |
| **Parameters** | 782 |
| **Goodness of fit** | 1.182 |
| **wR2** | 0.1379 |
| **Final R1 [I>2σ(I)]** | 0.0491 |

**Table 9** Crystal data and structure refinement for **L9**.

| Compound | C1 |
|---|---|
| **Empirical Formula** | $C_{35}H_{25.50}F_{12}N_{6.50}P_2Ru$ |
| **Formula Weight [g/mol]** | 928.13 |
| **Temperature [K]** | 223 |
| **Crystal System** | monoclinic |
| **Space Group** | $P2_1/c$ |
| **Unit cell dimensions:** | |
| **a [Å]** | 10.447(2) |
| **b [Å]** | 27.502(6) |
| **c [Å]** | 13.385(3) |
| **α [°]** | 90.00 |
| **β [°]** | 97.16(3) |
| **γ [°]** | 90.00 |
| **Volume [Å$^3$]** | 3815.8(13) |
| **Z** | 4 |
| **Crystal Description** | red block |
| **Crystal Size [mm]** | 0.03 x 0.22 x 0.55 |
| **Density [g*cm$^{-3}$]** | 1.616 |
| **Absorption Coefficient [mm$^{-1}$]** | 0.59 |
| **θ range for data collection [°]** | 2.13 to 29.00 |
| **Reflections collected** | 54897 |
| **Independent reflections** | 10109 |
| **R(int)** | 0.0891 |
| **Completeness to θ [° (%)]** | 29.00 (99.5) |
| **Parameters** | 574 |
| **Goodness of fit** | 1.102 |
| **wR2** | 0.1621 |
| **Final R1 [I>2σ(I)]** | 0.0587 |

**Table 10** Crystal data and structure refinement for **C1**.

# CURRICULUM VITAE

## PERSONAL INFORMATION:


**Name :** Marzena Kocik
**Date of birth:** 22.05.1982
**Address:** Mittlerestr. 33/11,
4056 Basel, Switzerland
**Tel:** + 41 78 770 77 51
**Email:** mkmarzenak@o2.pl
**Nationality :** Polish


## PROFILE:

Extensive experience in:

- Standard organic/inorganic techniques in synthesis, purification and characterisation
- Analytical techniques: NMR spectroscopy, UV-Vis spectroscopy, gamma spectroscopy, fluorescence spectroscopy and electrospray ionization (ESI) mass spectrometry
- Analysis of data and writing reports

## EMPLOYMENT:

**01.05 - 31.07.2008** Scientifics Limited (Harwell, England) as analyst *(*gamma spectroscopy)

## EDUCATION AND TRAINING:

| | |
|---|---|
| **2008 – present** | PhD studies in inorganic chemistry, University of Basel, Switzerland (supervisors: Prof. Dr. Catherine Housecroft and Prof. Dr. Edwin Constable) |
| **2006-2007** | Technical University of Wrocław (Chemical Technology), Poland |
| **2001-2006** | University of Wrocław (Chemistry), Poland |
| **1997-2001** | Secondary School in Dzierżoniów, Poland |

## PERSONAL AND SOCIAL SKILLS:

- Language skills: Polish (mother tongue), English (very good), German (basic)
- Effective scientific and technical problem-solving ability in a multi-disciplinary environment
- Effective organizational skills (project planning and time management)
- Strong writing and communication skills
- Providing technical support and training for students
- Very good interpersonal and teamwork skills

## HOBBIES:

cinema, power yoga, photography, reading books

## REFERENCES:

**Prof. Dr. Edwin Constable**
Department of Chemistry
University of Basel
Spitalstrasse 51
CH-4056 Basel
Switzerland
Tel: + 41 61 267 10 01
Email:
Edwin.Constable@unibas.ch

**Prof. Dr. Catherine Housecroft**
Department of Chemistry
University of Basel
Spitalstrasse 51
CH-4056 Basel
Switzerland
Tel. + 41 61 267 10 08
Email:
Catherine.Housecroft@unibas.ch

**Prof. Dr. Lechosław Latos-Grażyński**
Department of Chemistry
University of Wrocław
F. Joliot-Curie 14
50-383 Wrocław
Poland
Tel. + 48 71 375 72 56
Email:
lechoslaw.latos-grazynski@chem.uni.wroc.pl

**Dr. Natasza Spruta**
Department of Chemistry
University of Wrocław
F. Joliot-Curie 14
50-383 Wrocław
Poland
Tel. + 48 71 375 73 92
Email:
natasza.sprutta@chem.uni.wroc.pl

## PUBLISHED PAPERS:

N. Sprutta, S. Maćkowiak, M. Kocik, L. Szterenberg, T. Lis, and L. Latos-Grażyński *Angew. Chem. Int. Ed.*, **2009**, *48*, 3337-3341.

E. C. Constable , C. E. Housecroft , M. K. Kocik, M. Neuburger, S. Schaffner, J.A. Zampese, *Eur. J. Inorg. Chem.* **2009**, 4710 – 4717.

E. C. Constable , C. E. Housecroft , M. K. Kocik, J.A. Zampese, *Polyhedron*, **2011**, 30, 2704.